

From the Department of Neurology of the University of Lübeck

Director: Prof. Dr. Thomas F. Münte

Modulatory impact of metabolic states on the connectivity of the resting human brain

Dissertation for Fulfillment of Requirements for the Doctoral Degree of the University of Lübeck

from the Department of Natural Sciences

Submitted by:

Arkan Al-Zubaidi

from Baghdad (Iraq)

Lübeck 2019

First referee: Prof. Dr. med. Thomas F. Münte

Second referee: Prof. Karsten Specht

Date of oral examination: 10. September 2019

Approved for printing: Lübeck, 16. September 2019





Read in the name of your Lord who created. Created man from a clinging substance. Read, and your Lord is the most Generous. Who taught by the pen. Taught man that which he knew not. اقُرَأُ بِاسْمِ رَبِّكَ الَّذِي خَلَقَ خَلَقَ الْإِنْسَانَ مِنْ عَلَقِ اقْرَأُ وَرَبُّكَ الْأَكْرِم الَّذِي عَلَّمَ بِالْقُلَم عَلَّمَ الْانْسَانَ مَا لَمُ يَعْلِمَ عَلَّمَ الْانْسَانَ مَا لَمُ يَعْلِمَ

Contents

List of Figures	ix
List of Tables	xi
Acknowledgments	xiii
List of Abbreviations	XV
Abstract	xvii
Zusammenfassung	igures ix ables xi ledgments xiii abbreviations xv t xvii tenfassung xix 1: General introduction 1 Neuroimaging: Theoretical background 2 1.1 Basics principle of MRI 3 1.2 Correlation between BOLD and neural activity 13 1.3 Task fMRI vs. resting-state fMRI 15 Food Consumption 16 2.1 Neural mechanisms, metabolic state and glucose intake 18 2.2 Endocrine mechanisms 19 Aims and overview of chapters 20 2: Materials 25 Participants 25 Experimental design 26 Functional brain images 29 3.1 Acquisition 29 3.2 Preprocessing 29 3: Physiological and behavioral effects 35 Analysis 35 Results 36 Discussion 36
•	
1.1.1 Basics principle of MRI	3
1.1.2 Correlation between BOLD and neural activity	13
1.1.3 Task fMRI vs. resting-state fMRI	15
1.2 Food Consumption	16
1.2.1 Neural mechanisms, metabolic state and glucose intake	18
1.2.2 Endocrine mechanisms	19
1.3 Aims and overview of chapters	20
_	
2.2 Experimental design	26
2.3 Functional brain images	29
2.3.1 Acquisition	29
2.3.2 Preprocessing	29
<u> </u>	
3.2 Results	36
3.3 Discussion	38

Chapter 4	: Rs-fMRI connectivity-modeling	41
4.1]	Functional connectivity	42
4.1	1 Seed-based correlation analysis (SCA)	42
4.1	2 Independent component analysis (ICA)	43
4.1	3 Regional homogeneity (ReHo)	45
4.1	4 Degree of centrality (DC)	46
4.1	5 Fractional amplitude of low-frequency fluctuation (fALFF)	48
4.2	Effective connectivity	49
4.2	1 Spectral DCM (spDCM)	49
Chapter 5	: Influence of hunger, satiety and oral glucose on brain func	tional
_	ty	
	Introduction	
5.2 I	Materials and methods	58
5.2	1 Statistical analysis	58
5.3	Results	59
5.4	Discussion	63
5.5	Conclusions	67
Chapter 6	: Amplitude of brain signals classify hunger status based on	
_	earning in resting-state fMRI	
6.1]	Introduction	69
6.2 I	Materials and methods	74
6.2	1 Feature extraction from rs-fMRI data	75
6.2	2 Feature selection for hunger/satiety status classification	75
6.3	Results	78
6.4	Discussion	81
6.5	Conclusions	87

_	mpact of hunger, satiety, and oral glucose on the associa sma insulin and resting-state brain activity	
7.1 Int	roduction	89
7.2 Ma	aterials and methods	92
7.2.1	Statistical analysis	94
7.3 Re	sults	97
7.3.1	Resting state fMRI: hunger vs. satiety effects	97
7.3.2	Resting state fMRI: before vs. after glucose treatment	97
7.3.3	Correlations between physiological and neural effects	100
7.4 Dis	scussion	104
7.4.1	Resting-state fMRI: hunger vs. satiety effects	105
7.4.2	Resting state fMRI: before vs. after glucose treatment	106
7.4.3	Correlations between physiological and neural effects	107
7.5 Co	onclusions	108
8.1 Int	between hypothalamus and insular cortex troduction aterials and methods	111
	Participants	
	Preprocessing	
	Region-of-interest time-series extraction	
	Spectral DCM and model space selection	
	Parameter estimate of the winning model	
	Associations between DCM parameters, physiological and behavioral	l response
8.3 Re	sults	127
8.3.1	Bayesian model selection	127
8.3.2	Model parameters	128
8.3.3	Associations between DCM parameters, physiological and behavioral	-
8.4 Dis	scussion	135
8.4.1	Changes in endogenous connectivity related to metabolic conditions.	135
8.4.2	Associations between DCM parameters, physiological and behavioral	-

Chapter 9: General discussion	141
9.1 Addressing research questions	
9.1.1 First question: What is the effect of oral glucose administration on the brain activity during hunger and satiety conditions using rs-fMRI data?	_
9.1.2 Second question: What is a reliable marker of rs-fMRI signals to stu of hunger and satiety on the human brain?	
9.1.3 Third question: How can different metabolic states change whole br and how are these changes associated with hormonal signals	•
9.1.4 Fourth question: What is the impact of different metabolic states on tinteractions in a specific homeostasis hypothalamus-insula circuit?	
9.2 Methodological considerations	145
9.3 Caveats and future directions	147
9.4 Concluding remarks	150
References	153
Curriculum Vitae	173

List of Figures

Figure 1.1: Basic characteristics of hydrogen protons.	5
Figure 1.2: The change between states owing to absorption or transmission of energy.	7
Figure 1.3: T1, T2 and T2* relaxation.	9
Figure 1.4: Examples of different MRI image types.	12
Figure 1.5: A depiction of the three principal axes used in the standard coordinate space	e for MRI
from neurological views.	13
Figure 1.6: Schematic depiction of the functional neuroimaging analysis under for	od intake
modulation and the stage on which each of the chapters focused.	23
Figure 2.1: Time course of physiological parameters under hunger and satiety condition	ns 28
Figure 2.2: Summary of MCFLIRT estimated translation parameters for each exp	perimental
condition.	32
Figure 2.3: Summary of MCFLIRT estimated rotation parameters for each exp	perimental
condition.	33
Figure 3.1: Statistical differences in physiological and behavioral parameters under h	unger and
satiety conditions.	38
Figure 5.1: Influences of glucose treatment found with different brain connectivity ana	lyses 60
Figure 5.2: Changes of fALFF were obtained by two-way repeated measurements ANG	OVA 62
Figure 6.1: Full analysis procedure of hunger classification based on rs-fMRI data	74
Figure 6.2: Brain regions that provided relevant information to distinguish between h	unger and
satiety states in healthy lean participants.	80
Figure 6.3: Empirical distributions of incorrect classification generated via 10000 times	of random
label permutations for region sets selected by SFFS.	80
Figure 7.1: Time course of physiological parameters on the second day of the exper-	riment for
different metabolic states.	93
Figure 7.2: Hunger vs. satiety effects on brain activity.	98
Figure 7.3: Before vs. after glucose administration on brain activity	100
Figure 7.4: Glucose-associated low-frequency BOLD fluctuations.	102
Figure 7.5: Insulin-associated low-frequency BOLD fluctuations	103

Figure 7.6: Scatter plots illustrate the correlations between changes subjective feeling of hunger
with changes plasma glucose and insulin as well as with changes in brain activity (i.e. clusters that
survived the cluster-significance test)
Figure 8.1: Time course of physiological parameters on the second day of the experiment for
different metabolic states
Figure 8.2: Seeds superimposed on an average structural T1 image
Figure 8.3: Illustration of the hypothalamus-insula network and the results of the winning model
for a single subject
Figure 8.4: Different plausible hypotheses and Bayesian model selection
Figure 8.5: Percent variance explained (R^2) by the models for each experimental condition 124
Figure 8.6: Principal component analysis (PCA) on neuronal parameter estimates (NPEs; i.e. from
16 endogenous connections and 5 self-connections) for each of the four experimental conditions.
Figure 8.7: The winning model at the group level and its mean connectivity parameters (in Hz)
per experimental condition
Figure 8.8: Effective connectivity parameters that showed a significant main effect of the
metabolic state (hunger vs. satiety)
Figure 8.9: Multiple linear regression (MLR) analysis
Figure 8.10: Interactions between covariates in the linear mixed effects model predicting
individual physiological and behavioral responses

List of Tables

Table 1.1: List of relaxation times by brain tissue type and static magnetic field strength 10
Table 1.2: Comparison of rs-fMRI and task-based fMRI paradigms. 17
Table 5.1: Influences of oral glucose tolerance test treatment for different brain connectivity
parameters
Table 5.2: Brain regions showing differences in the fractional amplitude of low-frequency
fluctuations (fALFF)
Table 6.1: List of the anatomical regions (AAL atlas) of interest and their labels in the region
vector
Table 6.2: Confusion matrix 78
Table 6.3: Classification accuracy of rs-fMRI data using different models of brain
connectivity/activity and features selection algorithms with linear SVM classifier79
Table 7.1: Changes and associations of fALFF with food conditions and hormone levels
Table 7.2: Influences of oral glucose administration on brain activity under hunger and satiety
conditions
Table 8.1: Coordinates of the individual 5-mm ³ sphere clusters of the left and right ROIs of the
anterior and posterior insula, defined by Cauda et al. [398] and Wright et al. [66] 120
Table 8.2: Posterior estimates of effective connectivity (Hz) in the winning model (mean \pm SD)
per experimental condition

Acknowledgments

First and foremost, I would like to express my gratitude to my principal investigator Prof. Thomas F. Münte for his guidance, support and for believing in me, as well as all the opportunities I have received to meet and work together with other researchers, join international conferences, and spend an exciting and inspiring research stay in Zurich, Switzerland.

Special thanks to my second supervisor Prof. Alfred Mertins and his lab colleagues for their helpful comments and ideas throughout the duration of this research project.

I appreciate Prof. Kamila Jauch-Chara who offered me this research position and her management to prepare the hormonal data. Acknowledgment should be shown to all people involved in the data collection: Janis Nolde, Christian Erdmann, Susanne Schellbach and to the participants.

Additional thanks go to the management team of the GRK 1957 for providing the doctoral students with many interesting and instructive events, workshops and seminars throughout the doctoral phase.

A big thank you goes as well to my colleagues at the Department of Neurology and everyone else who helped me with advice and/or contributed any other means to my thesis: Dr. Marcus Heldmann, Dr. Macià Buades-Rotger, Dr. Norman Scheel, and Dr. Jenny Backhaus. I also thanks all the scientific collaborators named as co-authors in the articles arising from this work.

Moreover, I'm very grateful to Prof. Klaas Stephan and all the team members, especially Dr. Sandra Iglesias and Dr. David Cole, for the opportunity to join Translational Neuromodeling Unit research group in Zurich and to develop my Ph.D. project.

I thank my family, in particular, my parents for their ongoing support and enthusiasm. Moreover, finally, I would like to thank my wife (Lubna), daughter (Melak) and son (Mohammed) for their patience and allowing me to write this dissertation.

List of Abbreviations

ALL: Automated-Anatomical-Labeling K: number of voxel per cluster ACC: anterior cingulate cortex KCC: Kendall's coefficient concordance AD: LAINS: left anterior insula Alzheimer's; disease AINS: anterior insula LH: lateral hypothalamus **APCUNS: LPINS** anterior precuneus left posterior insula LME: B_0 : external magnetic field linear mixed-effects BMI: LOC: body mass index lateral occipital cortex LOOCV: BOLD: leave-one-out cross validation Blood-oxygen-level-dependent CA: classification accuracy M: mean CBF: cerebral blood flow M_0 : net magnetization CM: confusion matrix MRI: magnetic resonance imaging CSF: cerebrospinal fluid MCI: mild cognitive impairment CNS: GLM: general linear model central nervous system MLC: CSD: cross-spectra density machine learning classifier DARTEL: diffeomorphic anatomical registration through exponentiated Liealgebra Δ: delta=hunger-satiety MLRA: multiple linear regression analysis DC: MNI: degree of centrality Montreal Neurological Institute DCM: dynamic causal modeling MFG: middle frontal gyrus DMN: default mode network MVPA: multi-voxel pattern analysis DPARSFA: data processing assistant for resting-state fMRI advanced edition NPCs: EC: effective connectivity neuronal parameter components ER: NPEs: error rate neuronal parameter estimates fALFF: fractional amplitude of low-frequency fluctuations fMRI: functional magnetic resonance imaging FC: functional connectivity OLFC: olfactory cortex FSL: PCs: FMRIB Software Library principal components FEW: PCA: family-wise error principal component analysis PCC: HS: hippocampal structures posterior cingulate cortex ICA-AROMA: independent component analysis based strategy for automatic removal of motion artifacts IFG: inferior frontal gyrus PET: positron emission tomography IFGorb: PHG: orbital inferior frontal gyrus parahippocampal gyrus

IPG: inferior parietal gyrus

PoCG: postcentral gyrus

PreCG: precentral gyrus

RAINS: right anterior insula

RPINS: right posterior insula

PINS: posterior insula

ReHo: regional homogeneity

RF: radiofrequency ROI: region of interest

rm-ANOVA: repeated measures analysis of variance

rs-fMRI: resting-state functional magnetic resonance imaging

SD: standard deviation

SFS: sequential forward selection

SFFS: sequential forward floating selection

SVM: support vector machine

SPM: statitical parametic mapping

SFG: superior frontal gyrus

SMA: supplementary motor area

SCD: singular value decomposition

spDCM: spectral dynamic causal modeling

VAN: ventral attention network

VMN: ventromedial hypothalamus nucleus

Abstract

Food intake and energy homeostasis (the body's energy needs) are regulated by pathways of the central nervous system and by their bidirectional connections from and to peripheral organs. Understanding brain functions under different homeostatic conditions are of great importance. However, these functions remain incompletely characterized until now. Therefore, this dissertation investigates the effects of physical metabolic states (i.e. hunger and satiety) on brain functions as well as the association between brain activity and peripheral energy stores (i.e. insulin and glucose levels). This study outlines how to analyze human neuroimaging data (i.e. functional magnetic resonance imaging) to study the spontaneous (i.e. resting-state) brain activity in the context of metabolism and food intake to address these knowledge gaps.

Resting-state functional magnetic resonance imaging (rs-fMRI) and blood samples were obtained from 24 healthy normal-weight men in a repeated measurement design. Each participant was examined twice: once after 36 hours of fasting, i.e. hunger state, and once in a standard eating condition (three meals/day for 36 hours), i.e. satiety state. Rs-fMRI was recorded before and after the oral administration of 75 g of glucose for each metabolic state. Hunger ratings, plasma glucose levels and insulin levels data per condition were also collected.

First, functional connectivity (local and global) and activity (amplitude) approaches on the whole-brain level were applied to investigate the effects of glucose treatment on the resting brain's fluctuations during different metabolic states. We found that oral administration of glucose led to a reduction of brain connectivity as well as activity in the left supplementary motor area and increased local connectivity and amplitude of brain signals in the right middle and superior frontal gyri. In addition, the amplitude approach showed a significant interaction between metabolic state (hunger vs. satiety) and glucose treatment in the left thalamus. Second, functional connectivity and

activity modeling approaches were used to classifying two metabolic states depending on the observed rs-fMRI fluctuations by using feature selection algorithms with the objective function of a linear support vector machine classifier. The results revealed that the amplitude of rs-fMRI data is a more accurate parameter than local and global connectivity features in capturing the changes of the resting brain during states of hunger and satiety with a classification accuracy higher than 80%. Third, we tested whether changes in brain activity metrics are linked to hypoglycemia and whether they are modulated by peripheral signals. We observed a modulatory impact of fasting condition on intrinsic brain activity in the posterior cingulate cortex. Strikingly, differences in plasma insulin levels between hunger and satiety states after glucose administration at the time of the scans were negatively related to brain activity in the posterior insula and superior frontal gyrus, while plasma glucose levels were positively associated with activity changes in the fusiform gyrus. Finally, the effective (directed) interactions within a hypothalamus-posterior insula-anterior insula circuit under different metabolic states were investigated by using the dynamic causal modeling approach and Bayesian model selection. The strength of the connectivity parameter from posterior insula to anterior insula was increased in the fasting condition compared to satiety condition.

Overall, the findings presented here provide novel insights into brain activity patterns underlying energy homeostasis. Furthermore, the results extend the current understanding about how brain regions exchange information, thereby highlighting the impact of metabolic states on functional neural integration.

Zusammenfassung

Nahrungsaufnahme und Energiehomöostase werden durch Netzwerke im zentralen Nervensystem sowie durch deren bidirektionale Verbindungen zu peripheren Organen reguliert. Komplexe Veränderungen der Hirnfunktionen und der Homöostase des körpereigenen Stoffwechsels sind zugrundeliegende pathologische Mechanismen vieler körperlicher Erkankungen, wie zum Beispiel der Adipositas. Die Untersuchung des Zusammenhangs zwischen Metabolismus und Nahrungsaufnahme kann zur Verbesserung bestehender und zur Entwicklung neuer Ansätze in Diagnostik und Therapie führen. -Daher ist die Verwendung funktioneller Bildgebung zum besseren Verständnis der Veränderung von Hirnfunktionen unter verschiedenen homöostatischen Bedingungen von großer Bedeutung.

Im Kontext von Nahrungsaufnahme wurde bereits eine Vielzahl von aufgabenbasierten f-MRT Studien durchgeführt, die spezifische Hirnregionen und Aktivitätsmuster in Reaktion auf die Verarbeitung von lebensmittelassoziierten Reizen im Hunger- und Sättigungszustand identifizierten. Eine Einschränkung dieser Studien, die die gesamte Hirnaktivität untersuchen und bestimmte Hirnregionen und Netzwerke lokalisieren, ist, dass die verwendeten experimentellen Designs sich jeweils auf nur einen Aspekt (d.h. Stimulus bezogene Aktivität) beschränken. Bisher ist der Zusammenhang zwischen funktioneller neuronaler Integration, das heißt wie verschiedene Hirnregionen miteinander verbunden sind, und verschiedenen metabolischen Zuständen (Hunger und Sättigung) unzureichend verstanden. Vor allem in Humanstudien ist die Datenlage bislang uneindeutig. Die Untersuchung des Einflusses verschiedener metabolischer Zustände auf die Gehirnkonnektivität ist wichtig für ein tieferes Verständnis der Regulation Nahrungsaufnahme. In dieser Arbeit werden Ergebnisse von vier mathematischen Modellierungsansätzen präsentiert, die Hirnaktivität in Bezug zur Nahrungsaufnahme untersucht

haben, sowie den Zusammenhang zwischen Hirnaktivität und peripheren Signalen, die als Reaktion auf unterschiedliche homöostatische Zustände gebildet werden. Die vorliegende Arbeit beginnt mit einer allgemeinen Einführung (Kapitel 1), in der aktuelle Konzepte neuronaler bildgebenden Verfahren (insbesondere fMRT) sowie verschiedene Ernährungsmodelle und die Zielsetzungen der jeweiligen Kapitel dargestellt werden. Die Einleitung fasst bisherige Forschungsergebnisse zur Beziehung von Gehirnaktivität und Nahrungsaufnahme zusammen und verdeutlicht, dass insbesondere das Wechselspiel mit peripheren metabolischen Signalen, die in Reaktion auf Nahrungsaufnahme erzeugt werden, noch unterverstanden ist. Um diesen unverstandenen Aspekt zu untersuchen, wurde ein Experiment mit einem cross-over Design durchgeführt (Kapitel 2). In diesem Experiment wurden 24 gesunde und normalgewichtige Männer mehrfach untersucht. Eine erste Messung erfolgte nach 36-stündigem Fasten, eine zweite in einem gesättigten Zustand (drei Mahlzeiten/Tag für 36 Stunden). Am Ende jeder Sitzung wurde eine Ruhe-fMRT Messung (rs-fmrt) vor und nach oraler Verabreichung einer Glukoselösung angefertigt. Zusätzlich wurden 19 Blutproben pro Person und Bedingung zur Bestimmung des basalen Blutzucker-, Insulin- und Cortisolspiegels entnommen. Weiter werden in Kapitel 3 die Auswirkungen von Stoffwechselzuständen (Hunger vs. Sättigung) sowie von Nahrungsaufnahme (Glucoselösung) auf die Physiologie (Insulin- und Cortisolspiegels) und auf das Verhalten erläutert.

Da es keinen einheitlichen Ansatz zur Analyse der rs-fMRT Daten gibt und diese des Weiteren von der jeweiligen Fragestellung anhängig ist, werden in Kapitel 4 verschiedene Auswertungsmethoden zur Modellierung der Hirnaktivität und Konnektivität vorgestellt. In den darauffolgenden Abschnitten werden vier rs-fMRT Analysen dargestellt und analysiert die die zuvor genannten Auswertungsmethoden verwenden und damit den Zusammenhang zwischen homöostatischen Zuständen und der Aktivität relevanter neuronaler Netzwerke demonstrieren.

Die erste Analyse in Kapitel 5 wurde durchgeführt, um Informationen über die spontane neuronale Aktivität als Funktion des Stoffwechsels und der Glukoseaufnahme zu erforschen. Für die statistische Auswertung von drei datengesteuerten Ansätzen (lokale Konnektivität, globale Konnektivität und der Amplitude von rs-fMRT-Signalen) wurden separate, und Varianzanalysen für Wiederholungsmessungen (repeated-measurements-ANOVA) durchgeführt. Die Ergebnisse zeigen, dass diese drei Methoden angewandt auf rs-fMRT zur Aufklärung des Zusammenhangs zwischen Veränderungen in der Energiehomöostase und der Kalorienzufuhr betragen können. Darüber hinaus deuten die Ergebnisse darauf hin, dass die Amplituden von rs-fMRT den sensitivsten Messwert zur Erkennung des Effekts von metabolischen Zuständen auf die Ruhegehirnaktivität liefern.

Der zweite Teil dieser Arbeit zielt darauf ab, die Genauigkeit von drei datengesteuerten Ansätzen in der Klassifizierung von zwei Stoffwechselzuständen (Hunger vs. Sättigung) zu vergleichen. Alle drei Ansätze basierten auf Variablen aus rs-fMRT-Messungen. Für jeden Ansatz wurden Merkmalsparameter aus 90 Hirnregionen extrahiert, gefolgt von der Selektion von relevanten Parametern durch Merkmalsauswahlalgorithmen. Eine Klassifizierung mit einer linearen Support-Vector-Machine sollte zeigen, welcher Ansatz die gegensätzlichen homöostatischen Zustände (Hunger vs. Sättigung) anhand der vorher klassifizierten Merkmale unterscheiden kann. Die Ergebnisse zeigen, dass mithilfe von amplitudenbasierten rs-fMRT-Signalen zwischen Hunger und Sättigung mit einer Genauigkeit von bis zu 81% unterschieden werden kann. Diese Ergebnisse werden in Kapitel 6 präsentiert.

In einer dritten Analyse (Kapitel 7) wurde die multiple lineare Regressionsanalyse verwendet, um basierend auf den Ergebnissen der ersten und zweiten Studie die Interdependenz von amplitudenbasierten Ruhe-fMRT-Signalen und Insulin-/Glukosespiegeln im Plasma zu untersuchen. Unterschiede im Plasma-Insulinspiegel zwischen hungrigem und gesättigtem

Zustand nach der Glukoseverabreichung waren negativ mit amplitudenbasierten rs-fMRT-Signalen in der posterioren Insula und dem superioren frontalen Gyrus korreliert. Differenzen im Plasmaglukosespiegel waren positiv mit Aktivitätsänderungen im fusiformen Gyrus assoziiert.

In der vierten Analyse (Kapitel 8) wurden die Verfahren des dynamic causal modelling (DCM) und der Bayesian model selection verwendet, um die kausalen Wechselwirkungen innerhalb des Netzwerks aus Hypothalamus, posteriorer Insula und anteriorer Insula unter verschiedenen Stoffwechselzuständen zu untersuchen. Die Analysen ergaben, dass die Stärke der Verbindung zwischen posteriorer Insula und anteriorer Insula bei Hunger- im Vergleich zu Sättigungszustand erhöht war.

Die Arbeit schließt mit einer allgemeinen Diskussion (Kapitel 9) ab. Hier werden die Ergebnisse der vorliegenden Studien zusammengefasst, Rückschlüsse auf Hirnfunktionen nach der Nahrungsaufnahme gezogen und schließlich zukünftige Forschungsfragen aufgezeigt, die aus den vorgestellten Ergebnissen abgeleitet werden können.

Chapter 1: General introduction

Food intake is vital for any living organism to provide energy for the maintenance of all bodily processes from the absorbed nutrients such as carbohydrates, proteins and fats [1]. The control of food intake is remarkably complex, as it is determined by various endocrine signals and multiple interacting neural circuits [1-3]. The human brain uses two mechanisms to regulate food intake: The first non-homeostasic mechanism comprises factors which are not directly related to energy demands but instead are driven by external factors, such as food palatability, socioeconomic status, habits, social influence and emotional states [4–6]. The second homeostatic mechanism regulates food intake to keep the balance between energy supply and energy expenditure. For instance, after a period of energy expenditure or after fasting, hunger signals are generated, whereas, after a meal, these signals are inhibited [4]. One of the strategies to investigate homeostatic regulation and its changes in healthy participants is to predefine a fasting period in order to induce hunger and cause satiety after a predetermined standard meal or glucose administration [7]. Less is known about how metabolic energy is modulating brain functions, such as learning and memory or hypothalamic regulation of homeostasis. Neuroimaging has become an essential tool in obesity research to understand the neurobiological underpinnings of appetite and body weight homeostasis in humans.

This dissertation focuses on the impacts of the homeostatic mechanisms on brain functions. Here, we apply four approaches to analyze the data of participants. Each path is chosen to answer specific questions about the association between food intake and the brain's functions related to homeostatic balance/appetite. Readers who are familiar with the principles of generating functional brain imaging can skip the theoretical background section and proceed to Section 1.2,

where the related work that leads to the present dissertation is reviewed or Section 1.3 where the aims of this dissertation are presented.

1.1 Neuroimaging: Theoretical background

Over the past 25 years, cognitive neuroscientists have increasingly investigated brain functions by using functional neuroimaging techniques. Common neuroimaging approaches include positron emission tomography (PET) and functional magnetic resonance imaging (fMRI). PET imaging is based on the local quantification of concentrations of injected radioactive tracers. The resulting gamma ray emissions are detected and used as a measure for local functional changes in the brain, such as glucose metabolism or blood flow.

In contrast, in fMRI (describing the basic physics of MRI and fMRI in the next sub-section), the magnetic resonance imaging (MRI) technology is used to investigate brain function over time. Unlike PET, fMRI does not require any ionizing radiation and offers enhanced temporal resolution. For instance, fMRI acquires an image every few seconds while in PET needs a minute or even longer to measure the changes in brain activity [8]. Therefore, subjects can repeatedly participate without the cumulative health risks of emitted radiation. Indeed, fMRI can identify functional brain changes caused by experimental manipulations. These advantages contributed to the constantly increasing body of fMRI studies on brain functions.

In this dissertation, the fMRI technique is used to localize changes in brain activation patterns during controlled food intake modulations. In this section, the basic principles of MRI generation will firstly be presented [9–13]. Then the generation of the functional brain signal and its relation to neural activity are demonstrated [8,14].

1.1.1 Basics principle of MRI

The essential components of a MRI scanner are the external static magnetic field, radiofrequency coils and gradient coils. Fundamental ideas of using these compounds to create an image from an MRI scanner are described here.

The basic unit of all matter is called an atom. Each atom has an atomic nucleus and a cloud of electrons (negative charges). An atomic nucleus, in turn, has neutrons (neutral with no charges) and protons (positive charges). These atoms might have different magnetic properties among oft tissues in organisms. Human bodies are mainly composed of water molecules and fat where both of them contain an abundance of hydrogen atoms. Therefore MRI signals are generally derived from the behavior of hydrogen nuclei.

For a single hydrogen atom, the proton rotates (spins) around itself at a certain time point and with a certain number of rotations per second, these processes are known as the spinning phase and frequency, respectively, owing to thermal energy (Figure 1.1A). This spin motion generates an electric charge or current on its surface, which will cause a non-zero small magnetic source and a torque when there is no external magnetic field. A quantity that represents the strength of this magnetic source to make a magnetic field is called a magnetic moment. Meanwhile, the spin also results in a non-zero angular momentum because the hydrogen proton has an odd-numbered atomic number (i.e. a mass of one). Under normal conditions (absence of external magnetic field), the spin's axes of the protons are randomly oriented and this different orientation cause those magnetization moments to cancel with each other and lead to a very small net magnetization (Figure 1.1B), which is the vector sum of all spin vectors. To increase the net magnetization of the hydrogen atomic nucleus, a strong magnetic field must be applied to line up the axes of the spin

of the protons. Therefore, the MRI techniques do not measure a single atomic nucleus, but instead, measure the net magnetization of all protons in a volume.

In magnetic resonance (MR) examination, the subject is placed in a strong static magnetic field, usually referred to as B_0 and it is fixed in most devices to either 1.5 or 3 Tesla for clinical applications. The B_0 is a powerful magnetic field compared to the Earth's magnetic field, which is approximately 0.00005 Tesla. In this situation, the spinning proton of hydrogen nuclei will initiate a gyroscopic motion, which is known as precession (Figure 1.1C), where the spin axes of the proton rotate around a central axis of a magnetic field, like a spinning top. The speed of precession, which is how many times the hydrogen protons precess per second, is measured as the precession frequency, which is often called the Larmor frequency (w_0) in MHz, and is given

$$w_0 = \gamma_h B_0, \tag{1.1}$$

where γ_h is the constant gyromagnetic ration of hydrogen, which is the ratio of the magnetic moment (from the rotating charge of the proton) over the angular momentum (from the rotating mass of the proton) vector, $\gamma_h = 42.6 \, \text{MHz/Tesla}$. Also, the precession axis will align either parallel (i.e. the nuclei do not have enough energy to oppose the B_0 field, that is the low-energy state) or anti-parallel (i.e. the nuclei have enough energy to oppose the B_0 field, that is the high-energy state) to the magnetic field. The low-energy state is more stable than the high-energy state. Therefore more protons stay in the parallel state at the minimum energy level of the system, also the net magnetization will be parallel to the magnetic field, which is known as longitudinal magnetization. The magnitude of the longitudinal magnetization is proportional to the difference between a number of protons aligning parallel and anti-parallel to the B_0 , which ultimately depends on the temperature of the sample and the strength of the B_0 (Figure 1.1D). However, when an organism, like animal or human, is placed in the magnetic field of a MRI, the participant essentially acts as a magnet with a magnetic vector aligned with the external magnetic field. The net

magnetization of the subject cannot be measured when it is in the same direction as B_0 directly. To measure the net magnetization, the equilibrium of the protons must be disturbed and then detected how they are responding to the perturbation distortion.

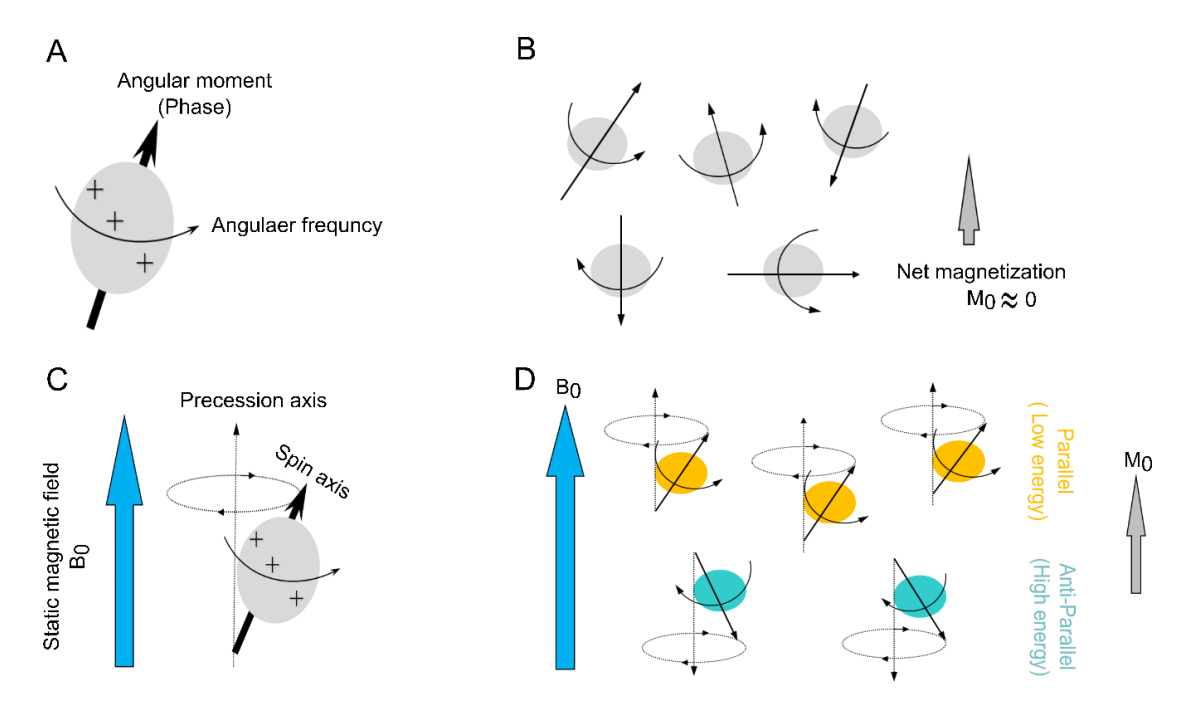


Figure 1.1: Basic characteristics of hydrogen protons.

(A) Spinning proton with angular momentum property, which is induced by the rotating charge. (B) In the absence of an external magnetic field, i.e. B_0 , protons are initially randomly oriented, which gives a total net magnetization (M_0) approximately equal to zero. (C) The motion of rotating proton (spin axis) around the main axis of B_0 is known as precession. (D) When B_0 is introduced, each proton's axis of spin aligns to the B_0 either parallel state, which has a lower energy level (shown in orange), or anti-parallel state, which has a high energy level (shown in green). In equilibrium condition, more protons align in a parallel state, resulting in an M_0 that is longitudinal, aligned with B_0 direction. Adapted from [8].

The MRI scanner uses a series of radiofrequency (RF) pulses to perturb the collection of protons at one spatial location, which is known as protons system. This perturbation happens through transference electromagnetic energy from RF coils to the anatomic nuclei of hydrogen and that leading to jump (flip) some protons from a low-energy state to a high-energy state, this process is called excitation (Figure 1.2A and B). Excitation occurs when RF coils send an electromagnetic wave that has the same frequency as the processional frequency of hydrogen nuclei within the

static magnetic field (i.e. Larmor frequency), in this situation the protons can take energy from the electromagnetic wave and this phenomenon is called resonance. The activation of a RF pulse has two primary influences in the protons. First, more protons will move from the parallel direction to the anti-parallel direction of B₀ and thus, the longitudinal magnetization decreases. Second, during RF pulse, precession protons will be flipped from the longitudinal direction, which is parallel to B₀, towards the transverse plane, which is orthogonal to B₀, and generate magnetization components called transverse magnetization. This transverse magnetization is created because the protons begin to process together in the same direction at the same time, which leads the protons to become in phase (together). The transverse magnetization vector is a rotating magnetic field at the Larmor frequency.

When the RF pulse is switched off and the excitation is over, the protons of hydrogen nuclei start to lose phase coherence and also return to a lower-energy state by emitting photons whose energy is equal to the difference between energy levels, i.e. high- and low-energy states (Figure 1.2C). During this reception period, this energy is a measurable MR signal and can be detected by receiver coils which are the same RF coils, because both excitation and reception have happened at Larmor frequency.

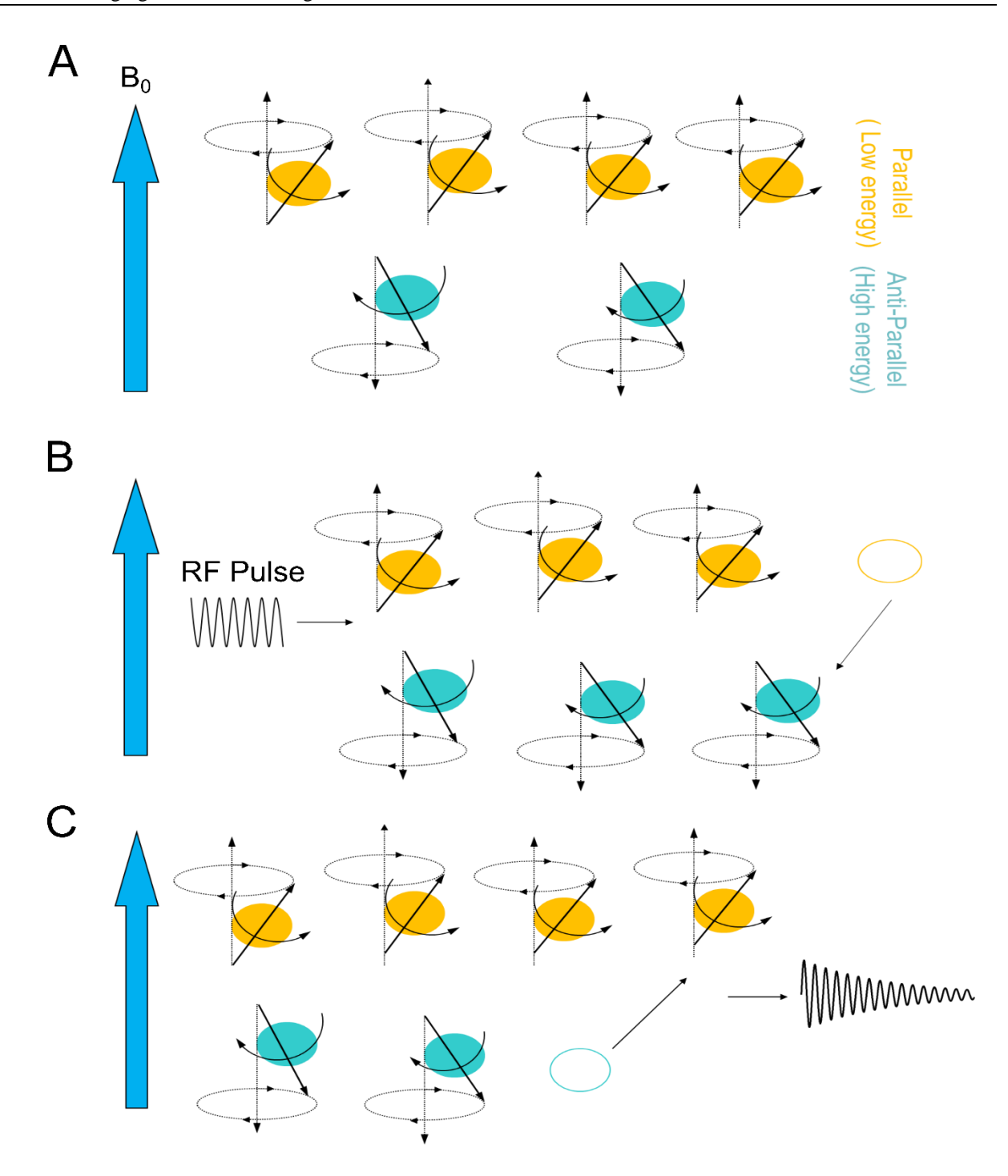


Figure 1.2: The change between states owing to absorption or transmission of energy.

(A) When protons are placed in a B_0 , more will be at the low-energy state (orange) than at the high-energy state (green). (B) If a radiofrequency (RF) pulse, which is an expatiation pulse, with the right amount of energy is applied, some protons will absorb that energy and jump to the high-energy state. (C) After the RF pulse is switched off, some of the protons in the high-energy state will relax and return to their low-energy state, releasing the absorbed energy as a radiofrequency wave with the same frequency of the RF pulse. Adapted from [8].

MR signals that are detected through RF coils following excitation and reception do not remain stable over time. Changes in MR signal (net magnetization) over time is referred to as protons relaxation. Relaxation of protons happens in two exponential processes. First, the transverse magnetization quickly loses phase coherence and begins to disappear. The time constant that describes the time taken for transverse magnetization to decay to approximately 37% of its original value, due to the accumulated phase difference is called T2 relaxation (T2 decay) or spinspin relaxation because it involves only the effects of internal inhomogeneity of spins (protons) with each other. However, in physiological tissue, the protons lose their phase coherence due to variations in local magnetic susceptibility, which is an essential characteristic of the tissue. Thus, the time constant that combines the effects of spin-spin relaxation, magnetic file inhomogeneity within the external magnetic field (B₀) and magnetic susceptibility to describe the decay signal of transverse magnetization is called T2* (star) relaxation or T2* decay. In the human head, magnetic susceptibility vibration that is seen in the blood vessels can be related to the neural activity in the brain. Therefore, T2* relaxation is more significant to fMRI [10]. The shape of T2 (Figure 1.3B) and T2* (Figure 1.3C) decay curves are similar but T2* is always faster (shorter) than T2. More details about associations between brain activity and T2* signals can be found in the next section.

The second exponential process that is describing the protons' return to the equilibrium state is known as longitudinal relaxation. The longitudinal relaxation occurs when the protons exchange energy with their surroundings or lattices to return to their lower-energy state. The time constant that describes the time taken for longitudinal magnetization to recovery/ return from zero to approximately 63% of its initial maximum value (M₀) parallel to B₀ is called T1 relaxation (T1 recovery) or spin-lattice relaxation (Figure 1.3A).

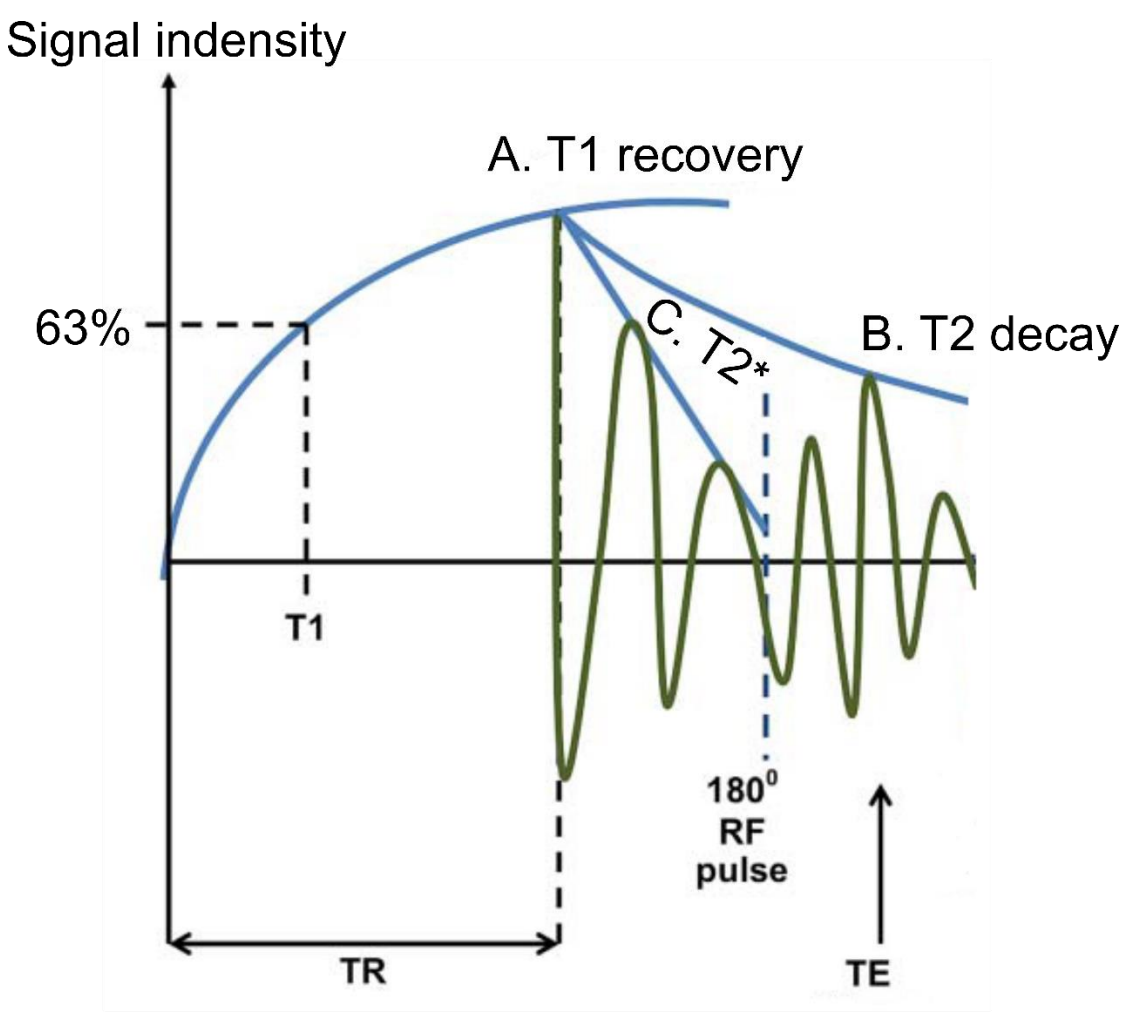


Figure 1.3: T1, T2 and T2* relaxation.

(A) T1 curve, the recovery of longitudinal magnetization over time following the switching off of a radiofrequency (RF) pulse. To recover most of the longitudinal magnetization, the repetition time (TR) has to be long enough. (B) T2 curve, the decay of transverse magnetization occurs over a period on milliseconds and a temporary gain in signal intensity at time echo (TE) due to accumulated phase differences caused by spin-spin interaction after 180° refocusing pulse. (C) T2* curve, this curve explains the time decay of transverse magnetization over time due to accumulated phase differences caused by both spin-spin interaction and local magnetic field inhomogeneity when a 180° refocusing pulse is not used. The T2* signal decays much faster than the T2 signal. Adapted from [13].

In contrast to longitudinal relaxation process, where energy is transferred from protons to the surrounding system, transverse relaxation may occur with or without overall energy loss. Moreover, T2 and T2* relaxation times are less dependent on the strength of the magnetic field, because they are more sensitive to languid molecular motions and not only to movements at the Larmor frequency. On the contrary, T1 relaxation times are dependent on the strength of the

magnetic field. From the Larmor equation, of the power of the B_0 field is increased the Larmor frequency will also increase, leading in longer T1 relaxation times for brain tissue. Generally, T1 relaxation times is approximately ten times longer than T2 relaxation. Table 1.1 provides T1, T2 and T2* relaxation values for different brain tissue.

Table 1.1: List of relaxation times by brain tissue type and static magnetic field strength. *Adapted from* [15].

Magnetic strength	Tissue	T1 (ms)	T2 (ms)	T2*(ms)
	White matter	510	67	78
	Gray matter	760	77	69
1.5 Tesla	CSF	2650	280	-
	Arterial blood	1441	290	55
3 Tesla	White matter	1080	70	50
	Gray matter	1820	100	50
	CSF	3817	1442	-
	Arterial blood	1932	275	46

The overall goal of MRI is to form an image that is a map of the spatial distribution of some property of the atomic nuclei within the sample. To capture this spatial information in three dimensions (3D) at least three gradients (G) coils are needed. These coils indicate how the strength of B₀ varies linearly in each of the x-,y- and z- directions. These gradients cannot turn all at the same time. Therefore, an MR image formation is sequentially separated into three steps: First, a spatial magnetic field gradient in the z-direction (Gz) is applied at the same time with an RF pulse to excite protons within a slice in order to select a particle slice of tissue in the brain or body volume. During this process, a two-dimensional (2D) slice of the tissue of interest is selected. Second, a phase-encoding gradient oriented in the y-direction (Gy) is activated and then quickly

turned off to change the protons phase and to process at different rates depending on their positions. Finally, a frequency-encoding gradient is turned on along the x-direction (Gx) to change the proton's frequency when the MR signals are read out. Each RF pulse fills a line in the k-space matrix, which reflects the Fourier transform of the image space, by repeating the process in the y-direction of k-space for the number of times equal to the number rows in an in-plane image. After a full k-space matrix is filled, a 2D inverse Fourier transform is applied to that matrix to convert the raw data from 2D k-space to 2D image space, thus completing a single slice image collection. Then the position of Gz is changed and the process mentioned above is repeated to create a 3D brain image, i.e. a complete brain volume. After k-space is filled, a 2D inverse Fourier transform is performed to convert raw data from k-space to image space, thus completing a single slice image collection. Then the position of Gz is changed and the above process is repeated to get a whole brain volume.

Different brain tissues have different MR relaxation times, as can see in Table 1.1. This allows creating different images that have high contrast among these tissues through adjusting the MRI sequences. The contrast of images in which the difference in signal intensity between tissues is derived from differences in T1, T2 or T2* relaxation times are called a T1-weighted, T2-weighted or T2*-weighted images, respectively. The T1-weighted image can be obtained by reducing the time between subsequent RF pulses, i.e. repetition time (TR), and it is used to study anatomical brain structures. For instance, cerebrospinal fluid (CSF) appears dark in the T1-weighted image, because it has long T1 and relaxes slowly. However, the T1 relaxation time of white matter is shorter than the relaxation time of CSF. Whereas, the gray matter has intermediate T1 value. Therefore, white matter, which has fast relaxation time, and gray matter, which has medium relaxation time, appear in a bright and gray contrast relative to CSF in the T1-weighted image, respectively. In contrast to the T1-weighted image, the T2-weighted image can be given by

increasing the time interval between the excitation and data acquisition, i.e. echo time (TE). The resulting T2-weighted image is darkest in voxels with short T2 values because those voxels will lose more signal (de-phases rapidly), such as white matter, and brightest in areas within long T2 values (de-phases slowly), such as CSF. Because T2-weighted scans have maximal signal in the CSF, it is essential for many clinical applications, such as tumors and arteriovenous malformations. The T2*-weighted image is more sensitive to changes in blood flow in the brain thus it is used to study brain functions over time. Both T2- and T2*-weighted images are provided by the pulse sequences with intermediate TE and long TR values. However, different sequences are used to create contrast images. For instance, spin-echo and gradient-echo sequences are most commonly used in T2- and T2*-weighted images, respectively [8]. Figure 1.4 shows examples of T1-, T2- and T2*-weighted images of the human brain.

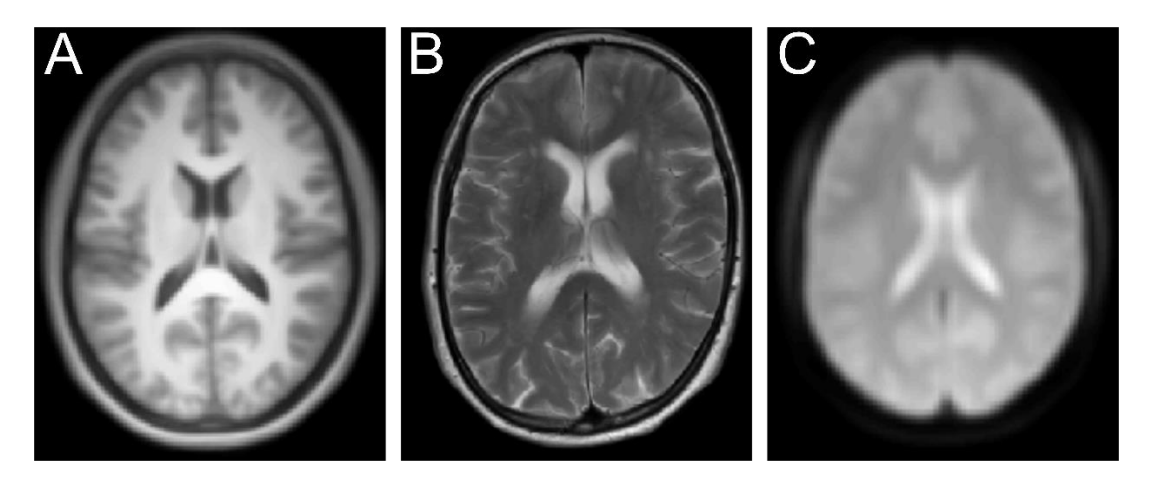


Figure 1.4: Examples of different MRI image types.
(A) The T1-weighted MRI. (B) The T2-weighted MRI. (C) The T2*-weighted fMRI. (A) and (C) are the average images of the collection of images that are obtained from the data that was used in this dissertation.

After collecting the MRI/fMRI images, these images are placed in a standard threedimensional Cartesian coordinate space. Thus, the points in the MRI/fMRI image are related to spatial locations and the different individuals are aligned. In this dissertation, we used the conventions and terminology of standard space, as shown in Figure 1.5, to describe the orientation when reporting the fMRI results.

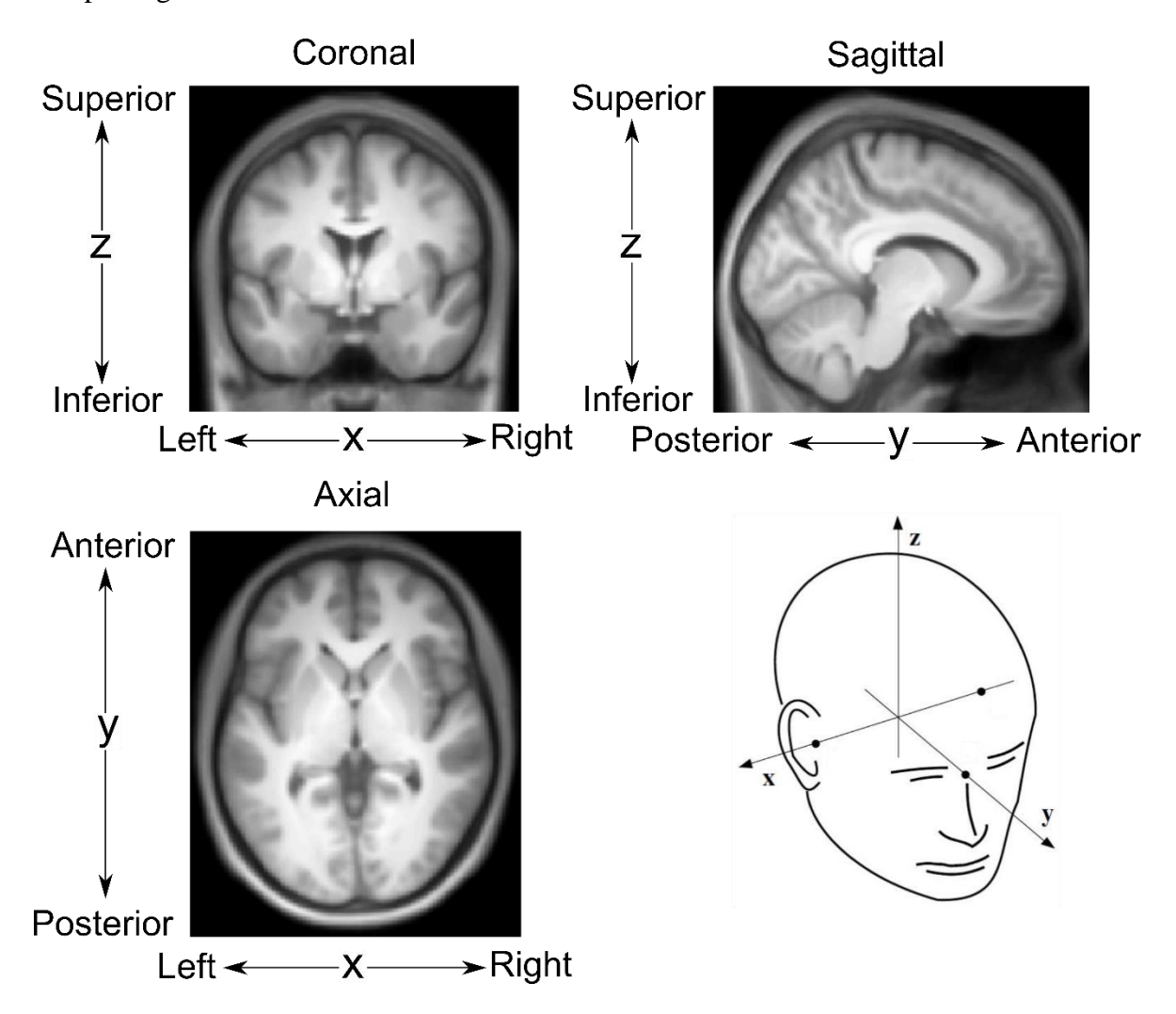


Figure 1.5: A depiction of the three principal axes used in the standard coordinate space for MRI from neurological views.

Adapted from [16] and

(http://www.fieldtriptoolbox.org/faq/how_are_the_different_head_and_mri_coordinate_systems_defined).

1.1.2 Correlation between BOLD and neural activity

As mentioned above, fMRI uses MRI scanners to investigate changes in brain function over time. The question that now arises is: how can the fMRI signals be related to the neural activity? In this section, the most important works are demonstrated to answer that question.

Active cells need energy, but the brain cells, so-called "neurons" do not store energy. They need glucose and oxygen supply by glial cells, which are supporting the activities in neurons and regulating their chemical environment around them. Both glucose and oxygen are provided by increases in blood flow, i.e. the volume of moving blood per unit time, to the active brain regions. Consequently, active neurons fulfill their functions. During this processing, oxygenated (oxygenrich) hemoglobin in the blood flow turns to deoxygenated hemoglobin (oxygen-poor). However, the vascular system supplies active brain regions with more blood that is rich in oxygen, which in turn leads to a decrease in deoxygenated hemoglobin in those regions. In 1936, Pauling and Coryell [17] detected that oxygenated and deoxygenated hemoglobin have different magnetic properties. Oxygenated hemoglobin is diamagnetic, which is weakly repulsing from a magnetic field and exerts little effects on the surrounding magnetic field. In contrast, deoxygenated hemoglobin is paramagnetic, which is weakly attracted to magnetic fields and in consequence distorts the local magnetic field. In 1990, Ogawa and colleagues [18] found that the gradient-echo brain images of rodents breathing pure oxygen were different from those of rodents breathing normal air (21%) oxygen), suggesting that signal differences on T2*-weighted images are a function of the amount of deoxygenated hemoglobin. This signal is called blood oxygenation level dependent (BOLD) contrast or signal. Maloney and Grinvald [19] showed a rising in the BOLD signal and reaching the peak (i.e. maximum amplitude) at approximately 5 seconds after stimulation onset. That result has been observed using high-resolution optical imaging in cat visual cortex.

To summarize, fMRI uses BOLD signals, which arise from the interplay of blood flow, blood volume and blood oxygenation, as an indirect approach to measure neural activity in the brain. When the neurons get activated, the fresh blood flow is oversupplied locally/specifically to the neural activity which gives rise to the relatively good spatial resolution of fMRI. This activity increases the local concentration of oxygenated hemoglobin and decreases the concentration of

deoxygenated hemoglobin. The reduction in the amount of deoxygenated hemoglobin corresponds with the decline in MR signal loss due to T2* effects and leads to increasing MR signals in the T2*-weighted image (i.e. a brighter MR image).

1.1.3 Task fMRI vs. resting-state fMRI

In classical fMRI experiments, the participants are instructed to perform a particular task, which is tailored to assess a defined function of the brain, for example, a motor task, vision, memory and language. The localization of the activated brain regions involved in solving the task is achieved by comparing the BOLD signal intensity during task performance to that at baseline conditions, i.e. when the respective task is not performed. This experimental paradigm is called "task-based fMRI" [20–23].

In contrast to the traditional fMRI described above, resting state fMRI (rs-fMRI) reflects the brain activity at rest when individuals are not requested to do a specific task [24,25]. The term "resting-state" is often used to denote this type of data, but other terms have been adopted as well, such as "intrinsic," "spontaneous" [26] and "model-free" analysis [27]. In this thesis, the term "resting-state" will be used because it is the conventional term within the field's literature. Rs-fMRI describes the natural low frequency (<0.1 Hz) of brain activity in the transient fluctuation of the BOLD baseline signal [28]. Analyses of the temporal coherence of spontaneous BOLD signals allow identification of brain regions that display a high degree of synchronicity, which is therefore considered as functionally connected. Although the BOLD contrast is the underlying phenomenon behind the rs-fMRI and task-based fMRI, some notable differences between these two techniques as contrasted in Table 1.2.

Biswal and coworkers [29,30] first introduced the concept of rs-fMRI by investigating the transfer function of the motor cortex in the brain. The rs-fMRI approach gained popularity when

Raichle and colleagues [31,32] identified the so-called default mode network (DMN). This network is activated during rs-fMRI and deactivated during task-based fMRI, when attention is oriented directly towards internal rather than towards external stimuli [33]. The DMN consists of the posterior cingulate cortex (PCC), precuneus, angular gyrus and medial prefrontal cortex. These regions have been identified to be involved in different functions including self-awareness and theory of mind [34,35]. In past years, rs-fMRI has become an established tool in clinical and drug development domains and also in the investigation of feeding behavior [26,36–46] to cite just a few studies.

1.2 Food Consumption¹

The brain is a major regulator of whole-body energy homeostasis. Fluctuations in brain activity are linked to changes in glucose metabolism and are a crucial influencing factor for whole-body energy homeostasis [47]. Homeostatic regulation in healthy participants can be investigated by comparing a "hunger condition" entailing a fasting period with a "satiety condition" after a predetermined standard meal [48]. Moreover, the common 75-g oral glucose tolerance test used clinically for the diagnosis of diabetes can be used to probe the brain's response to these different conditions. This approach has been used to study brain responses to food pictures after overnight fasting [7,48], and to explore brain connectivity at rest [46]. The brain is the only organ able to control its own energy supply, mainly via glucose, depending on its varying requirements [49]. In line with that, fluctuations in neural brain activity are linked to glucose metabolism and are a crucial influencing factor for whole body energy homeostasis [47].

¹ Portions of this section are adapted from the following publication: **Al-Zubaidi, A.**, Heldmann, M., Mertins, A., Jauch-Chara, K., & Münte, T. F. (2018). Influences of hunger, satiety and oral glucose on functional brain connectivity: A multimethod resting state fMRI study. *Neuroscience*. I participated in the experiment design and data collection. I analyzed the data and wrote the manuscript.

Table 1.2: Comparison of rs-fMRI and task-based fMRI paradigms. $Adapted\ from\ [50]$

	Rs-fMRI	Task-based fMRI
1	Analyses of spontaneous BOLD signal in the absence of any explicit task or input.	Analyses of spontaneous modulations in the BOLD signal in the presence of a particular (cognitive) task or activity.
2	60–80% of the brain's energy is consumed during the resting state.	Task-related increase in neuronal metabolism is less than 5%.
3	High contribution to overall brain activity.	Contribution to only a small fraction of overall brain activity.
4	Signals which are discarded as noise in task fMRI are taken as signals in rs-fMRI as they are the low-frequency spontaneous fluctuations in the BOLD signal.	The signal during a task-related activity is tiny compared to noise, i.e. 80% of the BOLD modulation is discarded as noise.
5	Improved SNR since it takes the overall spontaneous low-frequency fluctuations; spontaneous ongoing activity explains 50-80% of the BOLD variance.	Due to the discarding of the signal as noise, task fMRI has a low SNR; task-related modulation explains at maximum 20% of the BOLD variance.
6	Requires only one trial/session.	Requires a large number of trials which increase the time needed to measure the participants!
7	Acquired data of one session may be used to analyze several functions.	Each function of interest requires a separate task.
8	No consciousness and patient cooperation required. Rs-fMRI Allows investigation of pediatric, low IQ and vegetative or even comatose subpopulations.	Patient consciousness, cooperation and capability required.
9	No familiarity or repetition effects even in repeated measurements design. Therefore, rs-fMRI is comparable between sessions.	Familiarity and repetition effects to assess the disease prognosis, treatment, etc. Results are limited comparability between sessions due to interference with task performance.

1.2.1 Neural mechanisms, metabolic state and glucose intake

There is a large body of research that has used task-based fMRI in different metabolic states (hunger and satiety). Killgore and colleagues [51] were among the first to study fMRI activations in response to pictures of food of different caloric density. Killgore et al. [51] as well as other studies [52,53] reported a pattern of greater activation in medial and dorsolateral prefrontal areas, the anterior cingulate cortex (ACC), orbitofrontal cortex, striatum, amygdala, and insula in response to pictures depicting high caloric food. Further studies have shown that the reaction of these regions is modulated by the metabolic state, i.e. hunger vs. satiety [54–57]. Regarding the effect of sugar intake, Luo et al. [58], for example, have used fMRI while presenting food cues in conjunction with the ingestion of either fructose or glucose in a double-blinded, random-order cross-over design. Fructose relative to glucose resulted in greater activations to food cues in the visual and left orbital frontal cortex. One limitation of these studies is that task-related designs focus on one single aspect during the brain analysis to explain how the brain's overall activity is organized under food consumption. For example, the brain regions could appear statistically insignificant in response to a particular task. Thus, those regions cannot be investigated under food intake conditions, although they might carry some information related to eating behavior.

In contrast to task-based fMRI, human and animals resting-state studies have been shown that changes in the activity of hypothalamus and insula are associated with appetite and gastrointestinal signals [59–62]. For instance, the neurons of hypothalamus and insula belong to a homeostatic energy balance circuit and respond to orexigenic (i.e. appetite stimulant, e.g. hunger-inducing) and anorexigenic (i.e. loss of appetite, e.g. satiety-signaling) [63–66]. While hunger status increases the activity of hypothalamus and insula [59], satiety status as well as glucose or insulin administration have suppressive effects on the hypothalamic and insula signals [67–71].

This suggests that recording BOLD signals in the rs-fMRI design under hunger/ satiety conditions and analyzing them can indeed yield meaningful results.

1.2.2 Endocrine mechanisms

There is evidence that signals from the brain-gut axis constitute an integrated system which affects both food-related neural functions and behavioral aspects of food intake [72–74]. The hormones leptin and insulin have long been considered to play a particularly prominent role. Leptin and insulin provide signals to the brain about body adiposity and changes of metabolic status [1,75,76]. For instance, increasing both leptin and insulin, i.e. via direct administration, has been found to reduce food intake and to potentiate anorexia [77].

In the present thesis, we focus on insulin which has been hypothesized as a hunger-regulating hormone by researchers for more than 45 years, see [76]. Insulin is secreted by the pancreas to regulate blood glucose. Insulin receptors are distributed throughout body tissues (i.e. liver and muscle) and brain, where they can be activated by insulin after it passed the blood-brain barrier [78]. In animals and the human brain, insulin receptors are prominently expressed in the hypothalamus, prefrontal areas, limbic system and fusiform gyrus [79–83]. Insulin is one of the hormones that form a negative adiposity feedback loop ensuring balanced energy homeostasis [77,84–86] by signaling energy expenditure to the brain [83,87,88]. The function of insulin in the regulation of energy homeostasis was demonstrated by studies showing that intraventricular injections, as well as the intranasal administration of insulin to the central nervous system (CNS), decreases food intake and body weight in rodents [89,90] and humans [91].

In contrast, the inactivation of this hormone caused opposite effects [92,93]. Up to now, findings on insulin's impact on connections between brain regions are ambiguous. To gain further insights into that subject, we used rs-fMRI to reveal associations of insulin with the activation

amplitude of specific brain networks or brain sites that are modulated to the regulation of homeostatic states.

1.3 Aims and overview of chapters

The present work focuses on the analyses of rs-fMRI data under two metabolic conditions to investigate the integration of the neural processes, food intake and the fluctuations of hormone signals. This dissertation probes two general hypotheses:

The methods that are sensitive to the magnitude of the BOLD signals in the resting state are useful for assessing the brain regions that are involved in food intake and energy homeostasis circuits.

The metabolic state has modulatory effects on the endogenous (intrinsic) connections between brain regions that are involved in the energy homeostasis.

This doctoral dissertation aims to answer the following questions:

- i. What is the effect of oral glucose administration on the resting brain activity during hunger and satiety conditions using rs-fMRI data?
- ii. What is a reliable marker of rs-fMRI signals to study the effect of hunger and satiety on the human brain?
- iii. How can different metabolic states change whole brain activity and how are these changes associated with peripheral signals?
- iv. What is the impact of different metabolic states on the causal interactions in a specific homeostasis hypothalamus-insula circuit?

A schematic depiction of neuroimaging, biomarkers and behavior analyses, as well as the focus of each chapter of the present dissertation, are presented below and summarized in Figure 1.6.

Chapter 2: Describes the experimental design used in this thesis to investigate the effects of hunger and satiety on human brain signals as well as of MRI acquisition and preprocessing of rs-

fMRI data. Also, information about the handling of blood samples to measure hormone concentrations is documented.

Chapter 3: Reports and interprets the results of circulating glucose, insulin and cortisol levels and hunger ratings under different metabolic conditions.

Chapter 4: Explains the common modalities (methods) that have been developed to probe brain activity from BOLD signals. These modalities are applied to estimate the brain function from rs-fMRI as well to determine the causal interactions model from functional neuroimaging data. This chapter aims to provide details and methodological issues of rs-fMRI analysis.

Chapter 5: Investigates whether the metabolic states (hunger and satiety) and glucose administration (before and after treatment) have an impact on fluctuations of BOLD signals, and how these influences manifest in multimethod analyses of rs-fMRI data. Therefore, this chapter examines the interplay between spontaneous neural activity as a function of metabolic state and glucose intake.

Chapter 6: Compares the accuracy of three features, i.e. local connectivity, global connectivity and signal amplitude that can be extracted from rs-fMRI data to classify human metabolic states based on machine learning approaches. More specifically, we evaluate the different aspects of rs-fMRI fluctuations to find reliable markers for studying effects of hunger status on the human brain.

Chapter 7: Performs multiple linear regression analysis to find associations between the amplitude of rs-fMRI signals and both blood glucose and insulin concentrations under hunger and satiety conditions in response to glucose administration. This chapter investigates the links between changes in physiological biomarkers (glucose and plasma insulin levels), different homeostatic, states and resting brain activity.

Chapter 8: Investigates the impact of hunger and satiety conditions on the causal relationships between hypothalamus and insula. We specifically use dynamic causal modeling, a Bayesian approach allowing the estimation of direct connectivity on hidden neural states from measured brain data.

Chapter 9: Summarizes and discusses the findings of this thesis in terms of methods of rs-fMRI connectivity-modeling and establish directions for future work. The chapter then concludes the contributions of this thesis to extend the current understanding of brain functions under different metabolic states

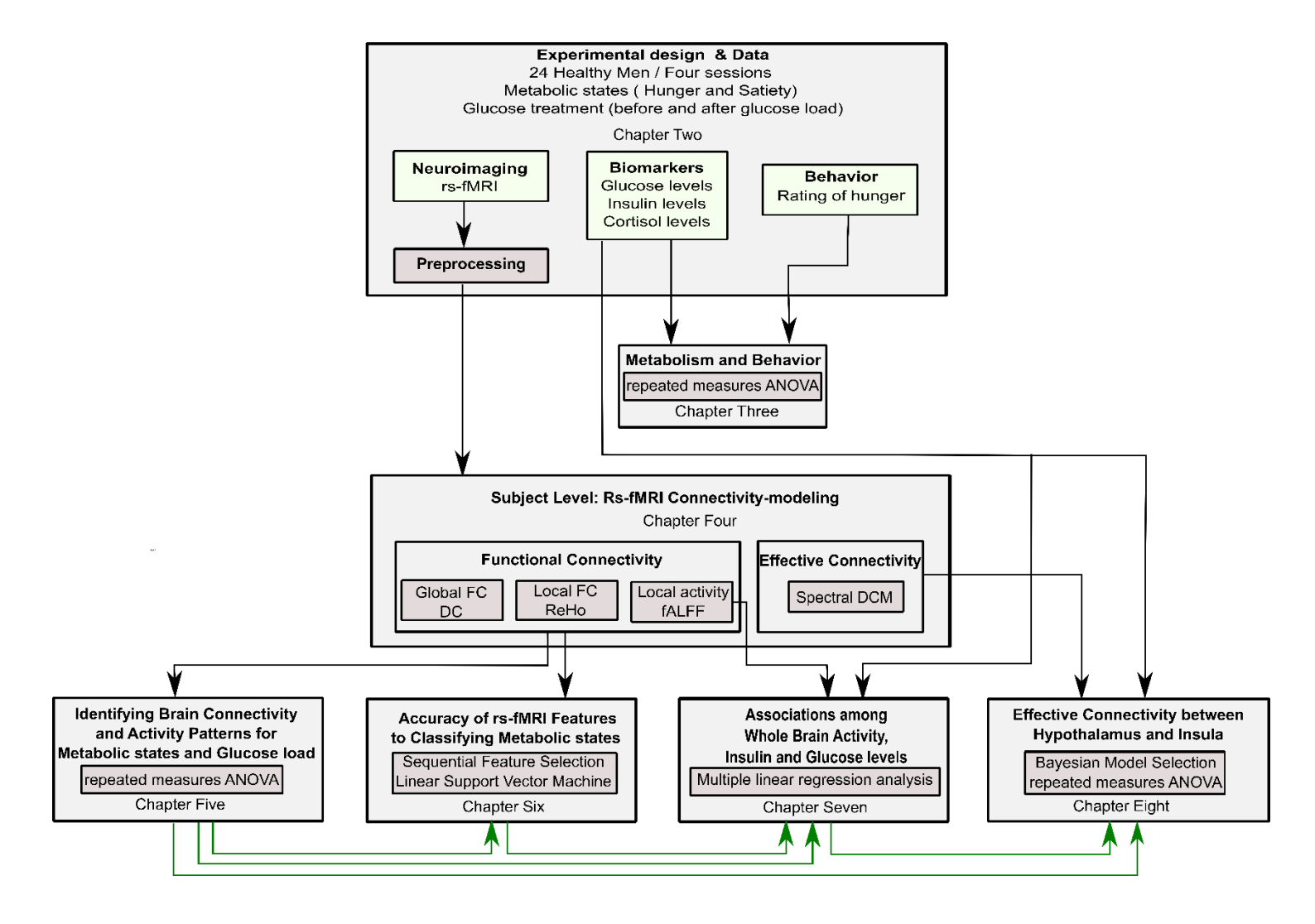


Figure 1.6: Schematic depiction of the functional neuroimaging analysis under food intake modulation and the stage on which each of the chapters focused.

Green arrows indicate which results are carried forward for subsequent analysis. Abbreviations: ANOVA, analysis of variance; DC, degree of centrality; fALFF, fractional amplitude of low-frequency fluctuations; FC, functional connectivity; ReHo, regional homogeneity; rs-fMRI, resting-state functional magnetic resonance imaging.

Chapter 2: Materials²

The four different analyses that will be explained later (Chapters 5, 6, 7 and 8) are based on the experimental design that is explained below. Furthermore, the preprocessing pipeline of rs-fMRI images is the same for all analyses (except the analysis of Chapter 8, will be mentioned later) and will be similarly detailed below.

2.1 Participants

Twenty-four normal weight healthy male volunteers (mean age: 25 years, range: 20-30 years, mean BMI: 22.5 kg/m², range: 20-25 kg/m²) were recruited from the local university community via e-mails and flyers. Female participants were not included to rule out any influences related to the hormonal cycle. All participants were subjected to a medical interview and examination assessing general health, medication, drug abuse, blood glucose concentration and cognitive disorders. Any regular medication, previous and current psychiatric, neurological (e.g. multiple sclerosis, previous head trauma), or metabolic disorders led to exclusion. Moreover, participants were required to have a BMI between 20 and 25. All participants were informed about the procedures and data handling. None of the participants from this all-male group reported any current or past periods of prolonged fasting. Within four weeks before and during the trials, subjects were instructed not to participate in other studies or to donate blood. All participants gave their informed consent before participation and received a small financial compensation. The study was carried

² This chapter corresponds largely to: **Al-Zubaidi**, **A**., Heldmann, M., Mertins, A., Jauch-Chara, K. and Münte, T. F. (2018). Influences of hunger, satiety and oral glucose on functional brain connectivity: A multimethod resting state fMRI study. *Neuroscience*. I participated in the experiment design and data collection. I analyzed the data and wrote the manuscript.

out in accordance with the Declaration of Helsinki (2002) and was approved by the ethics committee of the University of Lübeck, Germany.

2.2 Experimental design

Each subject was investigated twice, once while being in a hungry (36 hours fasting) and once while being in a satiated state (standardized eating, five meals over 36 hours). The order of the two sessions was counterbalanced across subjects and sessions were separated at least one week. Each session lasted two days. To control food intake and physical activity, participants were required to stay in the sleep laboratory of the Department of Psychiatry of the University Medical Campus Schleswig-Holstein (UKSH) for the entire 36 hours of the experiment. At the end of each 36 hours, the functional MRI was recorded.

In both conditions, participants abstained from eating and drinking from 23:00 hour the night before the experimental session and arrived fasted in the morning. In the hunger condition, participants stayed fasted (except water drinking) for 36 hours, while in the satiety condition participants got five standardized meals over the identical time span.

Standardized meals were served according to recommendations of the clinical diabetes counseling department at the UKSH: Breakfast (25% protein, 50% carbohydrate and 25% fat), lunch (20% protein, 63% carbohydrate and 17% fat) and dinner (22% protein, 60% carbohydrate and 18% fat) were provided at 09:00, 12:00 and 19:00 hours, respectively. For both sessions, participants arrived at the sleep lab at 08:00 hour. A cannula was inserted into a peripheral vein on the back of the hand to collect blood samples. The first blood samples for determining basal blood sugar, insulin and cortisol concentrations were drawn at 08:45 hour with subsequent blood samples drawn during the first day at 10:00, 12:45, 14:00, 16:00, 18:00, 18:45, 20:00 and 22:00 hours (Figure 2.1). All participants stayed and slept overnight in the sleep laboratory at UKSH. The next

morning, blood samples were taken at 08:45, 10:00, 11:45 and 13:05 hours. At the end of each experimental condition, functional MRI was obtained. Each MRI session started with the recording of resting state activity at 13:05 hour. Then, the participants were removed from the scanner and drank a solution containing the equivalent of 75 g of glucose at 13:25 hour (defined by a 300 ml mixture of mono and oligosaccharides; ACCU-CHEK® Dextro® O.G-T., Roche, Grenzach-Wyhlen, Germany). At 13:45 hour, another fMRI resting state was recorded and a blood sample was drawn. After the MRI measurements, participants returned to the sleep lab and provided blood samples every 30 minutes (14:15, 14:45, 15:15 and 15:45 hours) until 16:15 hour the same day. In total, 19 blood samples per subject and condition were collected, with 13 taken before administration of oral glucose and the remaining six samples thereafter. In each condition, participants rated their subjective hunger feeling 20 minutes before and 20 minutes after oral glucose intake on a visual analog scale ranging from 0 (not hungry at all) to 9 (very hungry).

For the resting state fMRI recording, participants were instructed to lie still inside the scanner with their eyes closed. They were instructed to not engage in any particular cognitive activity. The functional run's duration was six minutes.

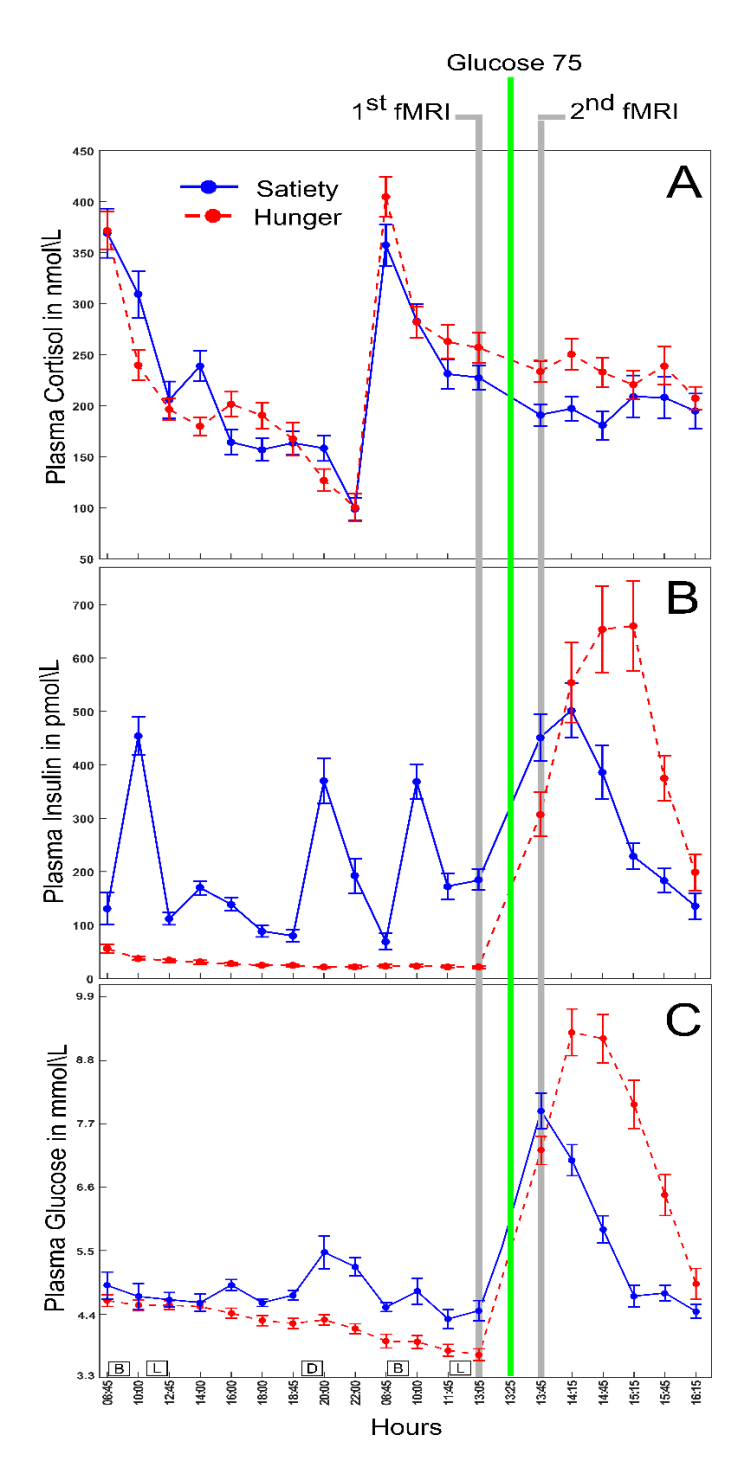


Figure 2.1: Time course of physiological parameters under hunger and satiety conditions.

Mean plasma concentrations of cortisol (A), insulin (B) and glucose (C) under hunger and satiety conditions before and after oral glucose treatment. Boxes on the bottom of the graph indicate the time points of meals in the satiety condition (B = breakfast, L = lunch and D = dinner at 09:00, 12:00 and 19:00 hours, respectively). In each condition, the first rs-fMRI was recorded 20 min before, the second rs-fMRI 20 min after the intake of oral glucose. The error bars represent the standard deviation.

2.3 Functional brain images

2.3.1 Acquisition

All structural and functional images were recorded with a 3-T Philips Achieva scanner (Philips Healthcare, the Netherlands). A standard eight-channel phased array head coil was used for radio frequency transmission and recording. The high-resolution structural T1 image consisted of 180 sagittal slices, by applying a T1-weighted 3D turbo gradient-echo sequence with SENSE (image matrix 240×240; field of view 240×240 mm²; slice thickness=1 mm; flip angle=9°). For functional resting state recording, 178 whole-brain functional images were acquired (T2*-weighted single-shot gradient-echo echo-planar imaging (EPI) sequence; repetition time TR= 2000 ms; echo time TE= 28 ms; isotropic 3 mm voxel size; field of view 192×192 mm²; flip angle= 80°; 40 slices, ascending interleaved slice order).

2.3.2 Preprocessing

Part of preprocessing on functional images was initially carried out using FSLv5.0 (available at http://fsl.fmrib.ox.ac.uk/fsl/) to implement independent component analysis (ICA)-based strategy for automatic removal of motion artifacts (ICA-AROMA) for head motion correction [94]. It has been shown that ICA-AROMA enhances the sensitivity and specificity of rs-fMRI activation and connectivity analyses [94]. To improve inter-subject alignment [95,96], the spatial preprocessing of the data were performed with the statistical parametric mapping 12b (SPM12b; available at http://www.fil.ion.ucl.ac.uk/spm/) in MATLAB (MathWorks, Natick, MA, USA) and data processing assistant for resting-state fMRI toolbox (DPARSF advanced edition, version 3.2, available at http://rfmri.org/DPARSF).

The rs-fMRI images were preprocessed as follows: (i) The first 7 volumes of each dataset were discarded to allow the signal to reach equilibrium and to allow the subjects to adjust to the

scanning noise; (ii) All images were manually reoriented in setting the origin to the anterior commissure; (iii) Head movement correction was performed during data acquisition by volumerealignment to the middle volume using MCFLIRT [97]; The MCFLIRT results in estimated realignment parameters for each experimental condition were summarized in Figure 2.2 and Figure 2.3 for motion translation and rotation parameters, respectively; (iv) We then submitted the data to ICA-AROMA [98] for identification and removing the independent components related to the head motion artifacts by three steps. The first step was running a probabilistic independent component analysis (PICA) using MELODIC (see Section 4.1.2) with automatic dimensionality estimation to find a set of components for each subject per session and per recording individually. Then, a predetermined classifier was applied on independent components to represent the motionrelated artifact components, which were identified at least by assessing each component to one of the following criteria: (1) maximum correlation with realignment parameters, (2) high-frequency temporal content > 35%, (3) spatial content in edge voxels and cerebrospinal fluid (CSF) > 10%. Finally, the regression of the motion-relevant components out of the data. Then the structural and denoised functional images were further preprocessed with DPARSF toolbox as follows [99]: (v) The T1 structural image was co-registered to the mean functional image; (vi) Gray matter, white matter and CSF segmentation, bias correction and spatial normalization of the T1 structural image were adjusted to the Montreal Neurological Institute (MNI) template using the DARTEL algorithm; (vii) Nuisance regression was performed to reduce the influence of unspecific physiological effects on BOLD signal. Nuisance variables included white matter and CSF; (viii) The functional images were spatially normalized to the MNI-template, by using the normalization parameters estimated by DARTEL algorithm with voxels size to 3 mm isotropic; (ix) Spatial smoothing was performed with a 6 mm full width at half maximum (FWHM) Gaussian kernel.

According to Zang et al. [100] fMRI signals were smoothed after calculating regional homogeneity not before (see Section 4.1.3); (x) Temporal band-pass filtering (0.01-0.08 Hz) was applied to the resting state fMRI signal to reduce the effect of low-frequency drift, e.g. respiratory, and high-frequency noise, such as heart activity. As suggested by Zou et al. [101] no further filters were applied when calculating the fractional amplitude of low-frequency fluctuations (see Section 4.1.5); (xi) All functional images were masked with a gray matter mask. The gray matter mask was calculated by averaging the grey matter images of all subjects. To generate the binary mask, we defined the common voxels between the average gray matter image and the gray matter template (without cerebellum lobules) derived from Automated-Anatomical-Labeling (AAL) atlas [102] by using the xjView toolbox. In some subjects, we were not able to measure the whole cerebellum. Therefore, cerebellum cortex was excluded from the gray matter mask and regions of interest (ROIs).

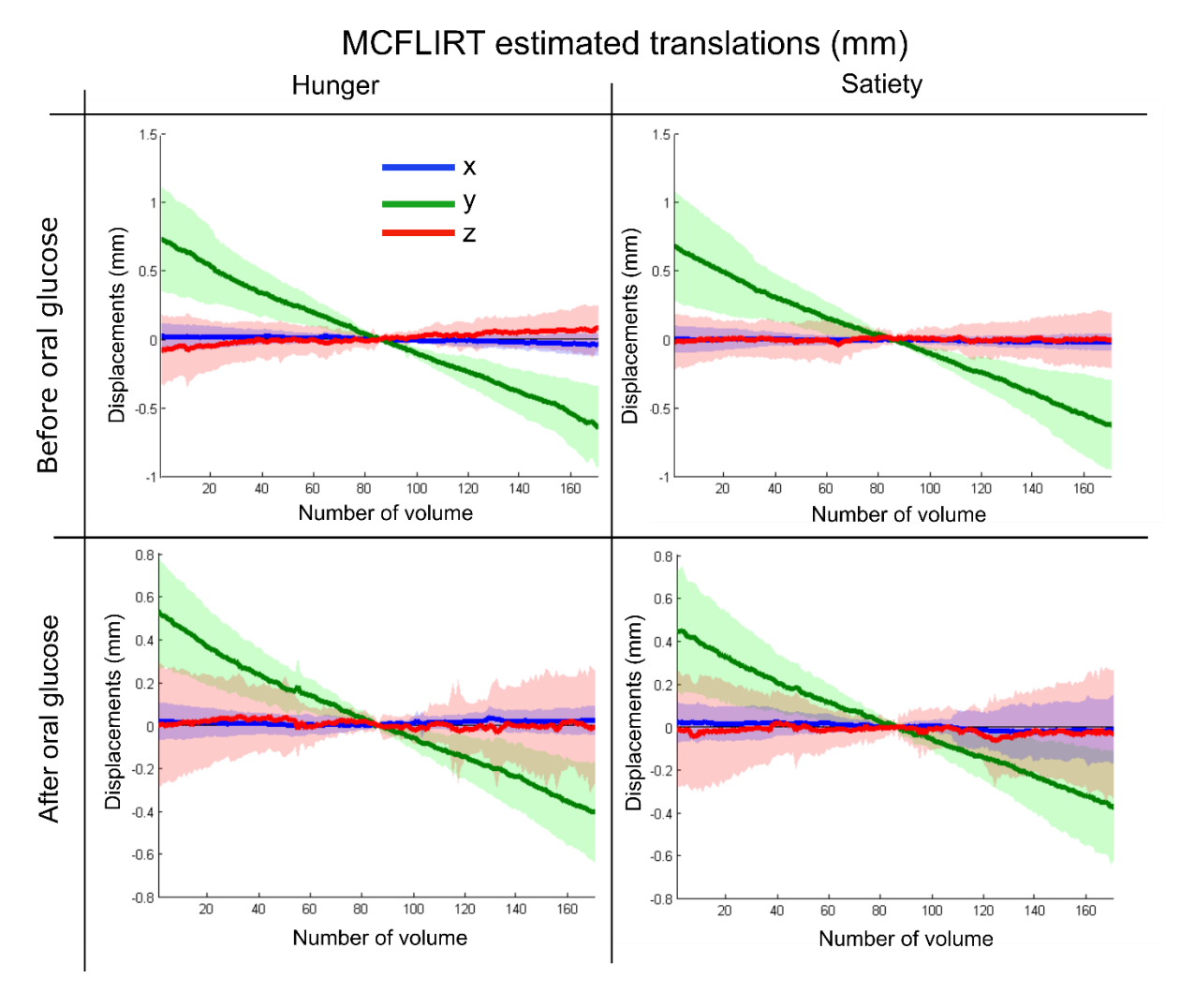


Figure 2.2: Summary of MCFLIRT estimated translation parameters for each experimental condition.

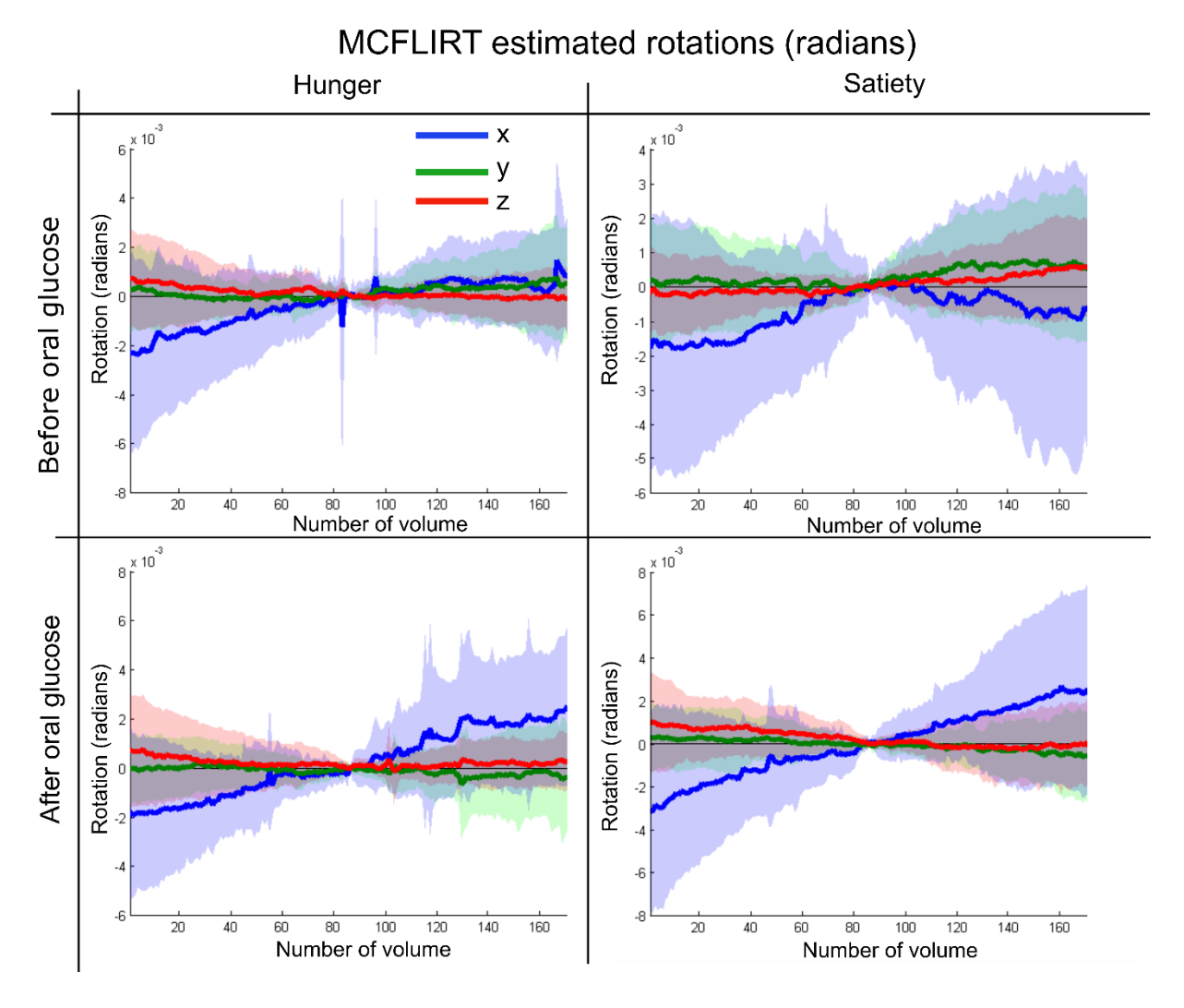


Figure 2.3: Summary of MCFLIRT estimated rotation parameters for each experimental condition.

Chapter 3: Physiological and behavioral effects³

Details regarding participants, the exact timing for obtaining blood samples and experimental design can be found in Chapter 2.

3.1 Analysis

Glucose concentrations were determined using the B-Glucose-Data-Management device (HemoCue GmbH, Grossostheim, Germany). For measuring the hormone levels, blood samples were centrifuged immediately. The supernatants were stored at -80° C until they were analyzed. Blood serum and plasma were used to measure the insulin and cortisol levels by commercial enzyme-linked immunoassay (Immulite DPC, Los Angeles, USA; insulin: intra-assay coefficient of variation (CV) < 1.5% and inter-assay CV < 4.9%; cortisol: intra-assay CV < 1.7% and inter-assay CV < 2.8%).

To investigate differences between the two experimental conditions (hunger and satiety) for plasma glucose, insulin and cortisol levels before and after glucose administration (oral glucose intake) two averages across the relevant samples of the second day were calculated for each participant and condition: one before and one after the oral glucose intake.

To test for differences two-way repeated measures ANOVAs (rm-ANOVA) with factors metabolic state (levels: hunger, satiety) and glucose administration (levels: before, after glucose intake) were performed for each of the dependent variables, i.e. hunger rating, plasma glucose,

³ Portions of this Chapter are adapted from the following publication: **Al-Zubaidi, A.**, Heldmann, M., Mertins, A., Jauch-Chara, K. and Münte, T. F. (2018). Influences of hunger, satiety and oral glucose on functional brain connectivity: A multimethod resting state fMRI study. *Neuroscience*. I participated in the experiment design and data collection. I analyzed the data and wrote the manuscript.

insulin, and cortisol levels, separately. All analyses were performed using SPSS software Version 22.0. Values are reported as mean (M) and standard deviation (± SD).

3.2 Results

The analysis of plasma glucose (Figure 3.1A) concentrations resulted in significant main effects of metabolic state ($F_{(1,23)}$ =25, p<0.0001) and glucose administration ($F_{(1,23)}$ =187, p<0.0001) and a significant metabolic state * glucose administration interaction ($F_{(1,23)}$ =72, p<0.0001). Post hoc t-tests performed to reveal the interaction driving effects indicated that the glucose level before the glucose administration was significantly higher in the satiated (M=4.8 mmol/L, SD=1.5) compared to the hunger state (M=4.2 mmol/L, SD=1.4). After glucose administration, this effect reversed and a significantly higher glucose level was seen in the hungry (M=7.5 mmol/l, SD=2.9) compared to the satiated state (M=5.8 mmol/l, SD=1.5). This effect indicates reduced responsiveness to the circulating glucose during the satiated state.

The analysis of plasma insulin (Figure 3.1B) concentrations revealed a significant main effect of glucose administration ($F_{(1,23)}$ =106, p<0.0001) and a significant metabolic state * glucose administration interaction ($F_{(1,23)}$ =102, p<0.0001), but no significant main effect of the metabolic state ($F_{(1,23)}$ =0.65, p=0.4). The post hoc analysis showed significantly higher insulin concentrations in the satiated state (M=198.8 pmol/L, SD=65.2) compared to the hunger state (M=22.5 pmol/L, SD=10.1) before the administration of glucose. After glucose administration, this effect reversed and significantly higher insulin concentrations were observed in the hunger state (M=457.9 pmol/L, SD=185.6) than in the satiated state (M=314.6 pmol/L, SD=123.5) indicating reduced responsiveness to circulating insulin. Due to the fasting-induced insulin resistance, the body secretes more insulin to overcome this resistance.

Furthermore, for plasma cortisol (see Figure 3.1C) significant main effects of metabolic state $(F_{(1,23)}=9.1,\ p=0.006)$ and glucose administration $(F_{(1,23)}=7,\ p=0.01)$ were revealed with no significant interaction $(F_{(1,23)}=0.03,\ p=0.9)$. Before glucose treatment, the plasma cortisol level for the hunger state (M= 260 nmol/L, SD=68.2) was higher compared to the satiated state (M=229.2 nmol/L, SD=56.4). A similar effect was found after glucose treatment, the plasma cortisol level was greater in the hunger (M=230.6 nmol/L, SD=44.4) compared to a satiated state (M=169.6 nmol/L, SD=61.2). This result demonstrates that glucose treatment had no impact on how the metabolic states affected the plasma cortisol levels.

Finally, with regard to subjective hunger ratings (Figure 3.1D) a main effect of metabolic state ($F_{(1,23)}$ =28.9, p<0.001) with higher hunger ratings in the hunger state (M=5.3, SD=2.6) compared to the satiated state (M=2.7, SD=2.1) was obtained but neither the main effect of glucose administration or a metabolic state * glucose administration interaction. These findings confirm the success of our fasting treatment.

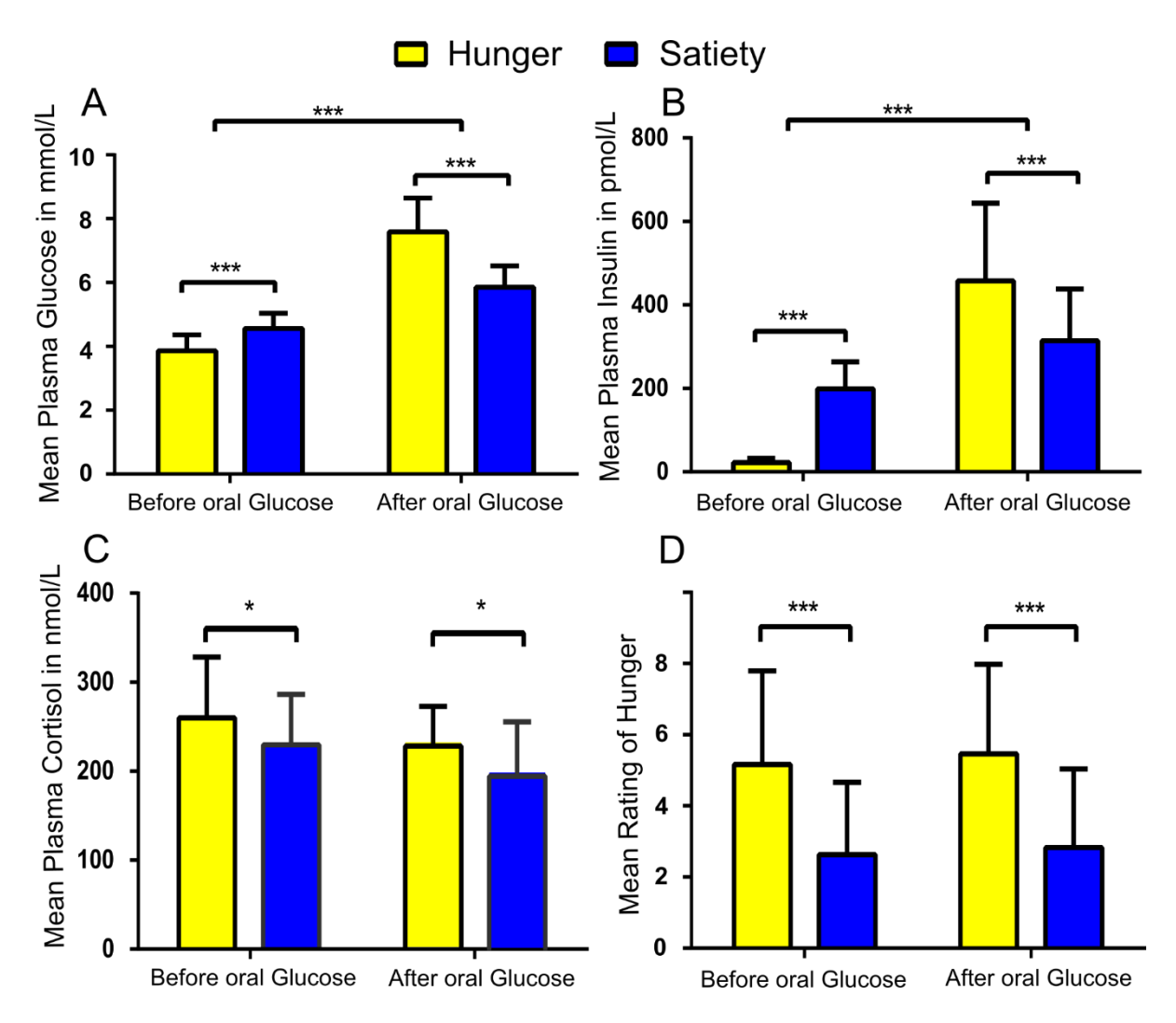


Figure 3.1: Statistical differences in physiological and behavioral parameters under hunger and satiety conditions.

Mean of (A) plasma glucose, (B) plasma insulin, (C) plasma cortisol levels, and (D) hunger ratings per factor: metabolic states (two levels: hunger and satiety) and oral glucose administration (two levels: before, and after treatment) across participants. The error bars represent the standard deviation. * and *** represent the significant differences between conditions, at a threshold of p < 0.01 and p < 0.0001, respectively.

3.3 Discussion

Expectedly, plasma glucose and insulin levels differed between hunger and satiety conditions and were also differentially influenced by glucose administration (Figure 3.1A and B). In the satiety condition, a major peak in insulin and glucose levels around 3 hours before glucose ingestion is related to the breakfast consumed in this condition. Generally, before glucose administration,

insulin and glucose levels are higher in the satiety compared to fasting condition, which is in quality and quantity the expected result [103]. After ingestion of glucose, there is a massive rise of both insulin and glucose levels as expected. This curve (Figure 2.1 B and C) is higher and wider for both parameters in the fasting condition, which can be explained by post-fasting glucose intolerance [103]. Furthermore, the delay in the time until the maximum is reached in the fasting condition compared to the satiety condition can be explained with a delayed gastric emptying time for fasted individuals [104]. In addition, a meta-analysis showed that high insulin levels in response to a meal suppress appetite [105]. Therefore, glucose and insulin may act as biomarkers of the satiety [106]. Hunger ratings have been shown to increase with a blood glucose concentration of 4.4 mmol/L (85 mg/dL) or lower [107]. In our study, the mean blood glucose level was 3.6 mmol/L under hunger condition (Figure 2.1C), and the feeling of hunger was higher under hunger relative to satiety condition before the fMRI scans (Figure 3.1D). These findings suggest that the experimental manipulation was successful allowing us to place our rs-fMRI findings into the context of fundamental metabolic regulations.

Finally, blood cortisol concentrations increased as expected during the fasting relative to the satiety condition (Figure 3.1C) pointing to higher stress during periods of food deprivation. Previous studies have shown a direct relationship between increases in cortisol levels and dieting or starvation due to changes in biological functioning such as freeing of energy and psychological influences like resisting food temptation [108,109].

To conclude, our study shows differential effects in response to glucose ingestion of three investigated physiological markers, glucose, insulin and cortisol, during different metabolic states, namely hunger and satiation, in healthy normal weight man.

Chapter 4: Rs-fMRI connectivity-modeling

Researchers in imaging neuroscience assume that human brain function needs to be characterized in terms of synchronization, functional segregation and integration processes [110–112]. Functional segregation refers to specific brain areas and networks that are involved in particular, separated brain functions. For example, Broca's and Wernicke's areas are known to be involved in language processing, whereas the supplementary motor area (SMA) and preSMA support motor processing. In contrast, functional integration, also called brain connectivity, concerns how different brain areas interact or connect to create specific functions within individual networks. In terms of functional neuroimaging, brain connectivity analyses can be organized into three different categories to explore brain connections, as follows:

- 1- Anatomical or structural connectivity depends on measurement of structural links between neurons and neural populations based on axonal connections, i.e. fiber tracks of white matter, or synaptic contacts. To identify the fiber tracks between brain areas, diffusion-weighted MRI (DWI) techniques are used to quantify the motion of water molecules in a voxel into directional components [8].
- 2- Functional connectivity (FC) reflects statistical dependencies or relationships between time series (i.e. BOLD signals) to remote neurophysiological events. Usually, FC is based on a statistical measure like correlation, covariance or spectral coherence. In rs-fMRI studies, this type of connectivity is a mechanism-free model and is used to identify synchronous BOLD signals from different brain areas. Thus, changes in resting-state functional connectivity are thought to characterize certain intrinsic processes of the brain [8].

3- Effective connectivity (EC) refers to *directed* functional connectivity between brain regions. In fMRI studies, EC describes the direct influence of BOLD signal activation of one brain area to directly cause changes (i.e. activation or depression) of the signals in another brain area based on a specific statistical model.

In this chapter, typical common models or approaches to assess functional and effective connectivity from rs-fMRI signals will be explained.

4.1 Functional connectivity

4.1.1 Seed-based correlation analysis (SCA)

SCA is a straightforward method to compute the time course models of FC from rs-fMRI data. In SCA, typically, the strength of the FC is estimated by calculating the linear correlation coefficients between time series vectors. These time series vectors may be either extracted from any voxel in the brain or by averaging the time series of voxels within a particular brain region of interest (ROI). To generate the FC map, the linear correlation is estimated by calculating the Pearson correlation coefficient (ρ) between the time series of ROI and other voxels within the brain mask [29,113], as follows:

$$\rho_{A,X_{j}} = \frac{\sum_{t=1}^{T} \left[(A[t] - \overline{A}) (X[t]_{j} - \overline{x}_{j}) \right]}{\sqrt{\sum_{t=1}^{T} \left[(A[t] - \overline{A})^{2} (X[t]_{j} - \overline{x}_{j})^{2} \right]}}, j = 1, \dots N, t = 1, \dots T,$$
(4.1)

where A is the average of the time series of voxels within a ROI and X_j is the time series of voxel jth. \overline{A} and \overline{X}_j are the mean of the A and X_j , respectively. N is the number of voxels within the brain mask and T is the length of the time series. Then, the ρ values are usually normalized into a normal distribution by using Fisher's z-score transformations:

$$Z_{A,X_j} = 0.5 \ln \left(\frac{1 + \rho_{A,X_j}}{1 - \rho_{A,X_j}} \right)$$
 (4.2)

The main advantage of adopting an SCA approach is that it provides a direct answer to a direct question, for instance how the FC pattern of a specific region might change across participants or experimental conditions. An essential disadvantage of SCA that its results are sensitive to the prior selection of size, location and shape of ROI. Furthermore, SCA results become more complex and not practical when utilizing more than a few simultaneous ROIs. Due to that complexity, using SCA alone is usually not possible to provide a general picture regarding the association between brain networks [50,114].

4.1.2 Independent component analysis (ICA)

ICA has been developed to determine unknown (i.e. hidden) source signals from a set of measurements or observed data [115,116]. In the ICA approach, the observed data (e.g. fMRI data) are assumed to be a linear mix of different source signals or physical processes (e.g. different neural processes in fMRI). Thus, those source signals are statistically independent [115]. Statistical independence implies that obtaining the value of one source signal does not provide any information about the value of the others. Furthermore, the histogram of each source signal is more non-Gaussian (e.g. peaky) than the histogram of the observed data [115]. The goal of ICA is to estimate an un-mixing matrix by searching for non-Gaussian signals in the data and thus enable a good approximation of source signals [117].

The application of the ICA approach to rs-fMRI data allows recovering spatial components that are independent over space [118–121]. The spatial ICA approach has been widely used by neuroimaging researchers to identify maps of brain networks that represent independent spatial patterns (i.e. stationery sets of voxels that have minimal spatial redundancy in the maps of the

resting-state connectivity) and different time courses from measured rs-fMRI data [8,16]. Each brain network consists of a set of voxels, these voxels could be from different brain regions but with similar BOLD signal fluctuations over rs-fMRI recording time [8]. Notably, the standard ICA model is noise-free and has a certain risk of overfitting the data [122]. Beckmann and Smith [123] suggested a new model called probabilistic ICA to avoid overfitting. Probabilistic ICA model is performed as the multivariate exploratory linear optimized decomposition into independent components (MELODIC) toolbox in FMRIB Software Library (FSL) [120,124]. It has the following mathematical representation for rs-fMRI data:

$$\mathbf{X} = \mathbf{AS} + \mathbf{E},$$

$$\mathbf{X} = \begin{bmatrix} x_{11} x_{12} & \cdots & x_{1(N-1)} & x_{1N} \\ x_{21} x_{22} & \cdots & x_{2(N-1)} & x_{2N} \\ \vdots & \vdots & \ddots & \vdots & & \vdots \\ x_{T1} x_{T2} & \cdots & x_{T(N-1)} & x_{TN} \end{bmatrix}, \mathbf{A} = \begin{bmatrix} a_{11} & \cdots & a_{1P} \\ a_{12} & \cdots & a_{2P} \\ \vdots & \ddots & \vdots \\ a_{T1} & \cdots & a_{TP} \end{bmatrix},$$

$$\mathbf{S} = \begin{bmatrix} s_{11} & s_{12} & \cdots & s_{1(N-1)} & s_{1N} \\ \vdots & \vdots & \ddots & \vdots & & \vdots \\ s_{P1} & s_{P2} & \cdots & s_{P(N-1)} & s_{PN} \end{bmatrix}, \mathbf{E} = \begin{bmatrix} e_{11} x_{12} & \cdots & e_{1(N-1)} & e_{1N} \\ e_{21} x_{22} & \cdots & e_{2(N-1)} & e_{2N} \\ \vdots & \vdots & \ddots & \vdots & & \vdots \\ e_{T1} x_{T2} & \cdots & e_{T(N-1)} & e_{TN} \end{bmatrix},$$

$$(4.3)$$

where N, T and P(<T) represent some voxels, dimensional of time series observations and independent spatial components (spatial maps), respectively. X is the rs-fMRI data that we are trying to decompose. Each row vector in matrix X denotes rs-fMRI data from a 3D volume at a time point t, i.e. $X=[x_1,x_2,...,x_N]^{t}$. A is the unknown linear mixing matrix that combines a set of unknown spatial components, which is S matrix, to obtain the rs-fMRI data. Each column vector in matrix A, i.e. $A=[a_1;a_2;...;a_T]^p$, comprises the contributions of all P spatial independent components to the rs-fMRI volume at the corresponding time point. Each row vector in S matrix refers to an independent spatial component, i.e. a brain network. E matrix represents the Gaussian noise. Using Gaussian noise as an explicit background in probabilistic ICA reduces the influence of noisy parts of the rs-fMRI data when estimating the number of spatial components by assessing

the statistical significance of the estimated sources [120,122,125]. For a given number of sources, the set of the spatial independent components and time courses can be estimated using the FastICA algorithm [117,123].

The advantage of using ICA over SCA approaches on rs-fMRI data is that ICA can provide brain networks as well as noise components without including any specific time series in the analysis model. Therefore, ICA-based approaches can be used to clean up the rs-fMRI data by determining noise from a wide variety of sources, such as head motion effects, physiological noise and MRI artifacts. In this dissertation, the ICA-AROMA approach was used to identify and remove the noise components from the data; more details about that technique are explained in Section 2.3.2, prepossessing section. One limitation of classical or even probabilistic ICA is that the results are not unique when analyzing the same data multiple times with an ICA procedure. For instance, the order of extracted components and also the component parameters may change slightly because of the method used to optimize ICA solutions.

4.1.3 Regional homogeneity (ReHo)

ReHo describes the local connectivity within brain regions and is a measure of the temporal homogeneity among brain voxels and the neighboring brain voxels within the low-frequency range of rs-fMRI signals [100]. ReHo is based on the assumption that the BOLD signal has characteristics that depend on neuronal activities and therefore the time series of neighboring voxels in a functional brain area will be highly similar or synchronized when that area supports specific goals or representations [126]. The ReHo index for a particular voxel is calculated by using Kendall's coefficient concordance (*KCC*) approach. In this study, the *KCC* was calculated using the following formula [100]:

$$KCC = \frac{\sum_{i=1}^{n} (R_i)^2 - n(\bar{R})^2}{\frac{1}{12} K^2(n^3 - n)}$$
(4.4)

where KCC is the ranging coefficient, from 0 to 1 (no to maximal coherence), of a given voxel in relation to its nearest neighbors, R_i represents the rank sum of ith time point as $R_i = \sum_{j=1}^k r_{ij}$ and r_{ij} is the rank of the ith time point of the jth voxel. \bar{R} refers to the average of the R_i and n represents the length of the time series (here n=170 time points). K is the number of voxels within the targeted clusters (here K=27, the given voxel (which is the center voxel) plus its 26 immediate neighbors). Then, the KCC value is assigned to the center voxel of the respective cluster. From the KCC of all voxels, the so-called ReHo map can be constructed. In order to reduce the effect of individual variability, a z-scores normalization was applied, by subtracting the ReHo mean value of each individual ReHo map and dividing by the standard deviation.

Relative to other methods (e.g. SCA), ReHo does not require prior selection of ROI to estimate FC. Because ReHo is looking at the homogeneity of local FC, the boundaries between brain regions that are functionally inhomogeneous emerge [114,126,127]. In contrast to the ICA method, ReHo does not need an assumption regarding the spatial independence of identified maps to estimate the measure of the local FC [100,114]. However, it is highly sensitive to different levels of spatial smoothing because it is fundamentally driven by the local neighborhood [114,122].

4.1.4 Degree of centrality (DC)

According to graph theory [128], a network (graph) is defined as a set of objects and the lines between them. Each object (voxel or anatomical area) in the network is called a node, and the lines that connect some pairs of objects (voxels) are called edges [129]. DC is used to investigate the global connectivity of brain regions, which is defined as the number of connections of one voxel in the brain to the voxels of the entire brain [130]. This measure depends on graph theoretical

approaches. The individual DC map was generated by correlating the time course of each voxel in the brain with all other voxels in the brain and calculating the number of connections above a definite threshold [130]. The temporal relationship between two voxels is defined by Pearson's correlation coefficient (r) approach. The individual correlation coefficients are then used to generate a correlation matrix $=\begin{bmatrix} r_{11} & \cdots & r_{1j} \\ \vdots & \ddots & \vdots \\ r_{i1} & \cdots & r_{ij} \end{bmatrix}$, $1 \le i, j \le N$, where N is the number of voxels

within the whole-brain mask and r_{ij} is the temporal Pearson's correlation of time series between the *i*th and *j*th voxels measuring the similarity between two voxels. The correlation matrix was thresholded at 0.25 to build a binary undirected and unweighted network matrix d_{ij} as follows:

$$d_{ij} = \begin{cases} 0, \ r_{ij} < 0.25 \\ 1, \ r_{ij} \ge 0.25 \end{cases}$$
 (4.5)

The binary connectivity matrix d_{ij} was used to define the degree centrality of voxel D_i by the following:

$$D_{i} = \sum_{j=1}^{N} d_{ij}. \tag{4.6}$$

The voxel degree maps were transformed to z-score to ensure they were comparably scaled and to prepare them for comparing across subjects. The z-scores standardization is:

$$Z_i = \frac{D_i - \overline{D}}{\sigma_D} (i = 1 \dots N), \qquad (4.7)$$

where \overline{D} and σ_D are mean the and standard deviation of the degree voxel maps within the brain mask, respectively.

DC is an efficient method to summarize complex networks. It calculates how each voxel, from a specific network, is correlated with other networks' voxels and then yields a single value to each participant. However, thresholding the correlation matrix into a binary matrix removes a

lot of potentially relevant information from the original data. Accordingly, it can be difficult to understand how the changes in the DC index are associated with changes in brain states [122].

4.1.5 Fractional amplitude of low-frequency fluctuation (fALFF)

To quantify spontaneous local brain activity, the amplitude of the BOLD signals has been used. This can be assessed by the amplitude of low-frequency fluctuations (ALFF) and its derivative fALFF [101,131]. While ALFF describes the local spontaneous brain activity across the whole brain by assessing the amplitude in a given voxel or brain area in the low-frequency range (0.01-0.08 Hz), fALFF is a normalized derivation of ALFF representing the ratio of low-frequency range amplitudes (0.01-0.08 Hz) relative to the entire frequency range (e.g. 0-0.25 if TR=2 seconds) amplitudes. To calculate the individual fALFF map, a fast Fourier transform (FFT) is performed on the time series of each voxel without temporal band-pass filtering. Then, the amplitude of each frequency is estimated by calculating the square root of the power spectrum. Finally, the total amplitude of the low-frequency range (0.01-0.08 Hz) is divided by that of the entire frequency range 0-0.25 Hz (TR=2s). For standardization purposes, the individual fALFF map is transformed to z-scores by subtracting its mean and dividing it by the standard deviation.

Both ALFF and fALFF have high temporal stability [132] and test-retest reliability [133]. In contrast to ALFF, fALFF has been reported to have higher specificity in detecting local spontaneous brain activity, especially in the gray matter [101,134]. Moreover, fALFF is recommended to be used instead of ALFF [45] since it is more robust against nonspecific signal components, such as physiological noise [134]. In the present study, the fALFF on rs-fMRI data was performed to describe the local spontaneous brain activities.

4.2 Effective connectivity

Several methods have been used to estimate effective connectivity (EC). For instance, Granger causality (GC) has been applied to test whether a BOLD signal extracted from a certain region Z has a direct effect of causing a BOLD signal from another region X [135,136]. Similarly, structural equation modeling (SEM) is another method to test hypotheses regarding the influences among interacting a set of independent and dependent variables [137,138]. GC and SEM are not suitable to capture the dynamic change in the fMRI because both of them are excluding the temporal infraction, i.e. history of an experimental task or imaging data, and ignore the hemodynamic convolution [139–144]. In contrast, multivariate autoregressive modeling (MAR) uses temporal information in terms of the historical influence to measure the inferior causality among BOLD time series. However, the MAR model cannot estimate the hidden neuronal states.

Friston and colleges [145] proposed a method to estimate at the neuronal level the causal effects of one region over another called dynamic causal modeling (DCM). DCM allows inferring effective (directed) connectivity on latent (hidden) neural states from measured brain data using predefined models [145]. Furthermore, DCM can be used to gather evidence favoring one model (hypothesis) over another to understand how brain regions communicate and influence each other [146]. With a DCM based algorithm called spectral DCM (spDCM) it is now possible to reveal the intrinsic connectivity in resting-state fMRI data [147]. Spectral DCM uses a Bayesian procedure to estimate the likeliest strength of endogenous causality.

4.2.1 Spectral DCM (spDCM)

SpDCM uses a Bayesian model inversion procedure to infer from the measured cross-spectra density (CSD) of BOLD signals on parameters of connections that link neural states in pre-defined networks of regions. The inverse Fourier transform of CSD corresponds to a cross-correlation

function over time, which is the measure of the FC (Pearson's correlation) at zero lag [147–149]. In other words, inverting a probabilistic forward model (from hidden neural states to observed CSD of BOLD signals), spDCM estimates the directed connectivity among hidden neuronal states that best explains the measured FC between brain regions.

In DCM for fMRI, the dynamic changes in regional- and time-dependent activity (i.e. $\dot{x} = \frac{dx}{dt}$) are modeled using a system of differential equations [145,150]. Furthermore, the DCM for rs-fMRI has two components [151]: The first component is a state space model with linear differential equations, which is used to describe neural dynamics (neuronal states) of a system of distributed brain regions. The second one is a nonlinear differential equation model (hemodynamic model) that is based on the Balloon/Windkessel model [152], which is used to translate the predicted neural dynamics into region-wise blood oxygen level dependent (BOLD) signals. The basic form of DCM for rs-fMRI (in the absence of external inputs) comprises two sets of differential equations modeling the neuronal dynamics and hemodynamics, respectively:

$$\dot{x} = Ax(t) + v(t),$$

$$y(t) = h(x(t), \theta_h) + e(t),$$
(4.8)

where A is a matrix repesenting the endogenous connectivity among the regions, $A \subset \theta$. The column vector $x(t) = [x_1(t), ..., x_n(t)]^T$ represents a hidden neural states of n brain regions at time t. The endogenous neuronal fluctuations are denoted by v(t). The observed BOLD fMRI data y(t) are modeled as a nonlinear hemodynamic response function h of the neuronal state x(t) as well as the hemodynamic parameters of the model $\theta_h \subset \theta$ [153] and an additional measurement error e(t).

In spDCM, the nature of the endogenous fluctuations underlying neuronal activity and observed noise are modeled with a free scale power-law form with a spectral density of "pink"

noise [154–156]. In the absence of any external stimulus, i.e. a resting state, the v(t) and e(t) can be modeled as:

$$g_v(w,\theta) = \alpha_v w^{-\beta v},$$

$$g_e(w,\theta) = \alpha_e w^{-\beta e}.$$
(4.9)

Here, g(w) represents the complex cross-spectra, where α and β , $\{\alpha, \beta\} \subset \theta$, are the parameters controlling the amplitude and exponents of the spectral density of the neuronal fluctuation, respectively, w is the angular frequency $(2\pi f)$. In summary, the likelihood model is specified by considering the probability of observing some data features given the model parameters $\theta = \{A, \alpha, \beta, \theta_h\}$. These parameters are used to generate the expected cross-spectra $\hat{g}(w, \theta)$ of the BOLD signals using Fourier transform

$$\hat{g}(w,\theta) = K(w) \cdot g_v(w,\theta) \cdot K(w)^* + g_e(w,\theta),$$
 (4.10)

where K(w) is the Fourier transform of a function of the Jacobian or EC. By using linear systems theory in frequency space, the observed sample cross-spectra of the BOLD signal g(w) can then be considered as the predicted cross-spectra $\hat{g}(w,\theta)$ plus some Gaussian sampling error N(w) such that

$$g(w) = \hat{g}(w, \theta) + N(w). \tag{4.11}$$

By specifying the relationship between the sample and the expected cross-spectra, one can assess the likelihood function $p(g(w)|\theta, m)$, which descibes the probability of the observied cross spectra g(w) data to be generated from model m given a set of parameters θ . The product of the likelihood function $p(g(w)|\theta,m)$ and the prior beliefs distribution of the model parameters $p(\theta|m)$ is called a generative model. The word "generative" refers to the fact that one can generate or simulate synthetic data points by sampling parameter values from the prior and inserting them into the likelihood function. In spDCM, this generative model defines the joint probability

distribution $p(g(w), \theta|m)$ over the observed cross spectra g(w) and model parameters θ , given the model m:

$$p(g(w), \theta|m) = p(g(w)|\theta, m) p(\theta|m). \tag{4.12}$$

This generative modal can be understood as a probabilistic forward mapping from latent (hidden) parameter values to the observed cross spectra. Usually, a main goal of the generative models is to infer on the most likely latent (hidden) parameter values of the system given the observed data [157,158]. This is known as "model inversion" and basically corresponds to computing the probability (i.e. conditional posterior density) of a set of model parameters given the observed cross spectra $p(\theta|g(w), m)$ according to Bayesian inversion of the generative model:

$$p(\theta|g(w),m) = \frac{p(g(w)|\theta,m)p(\theta|m)}{p(g(w)|m)},\tag{4.13}$$

where p(g(w)|m) refers to model evidence or marginal likelihood, which represents the probability to obtain the data under model m. Since the conditional posterior distribution $p(\theta|g(w),m)$ is computationally exorbitant to compute, it is approximated using variational Bayes under the Laplace approximation (VBL) [159]. Briefly, VBL for DCM provides an approximation to guess the true conditional posterior density $p(\theta|g(w),m)$ by assuming a mean field assumption to split between parameters and hyperparameters and uses variational or proposal densities $q(\theta)$ under a fixed-form Laplace (i.e. Gaussian) approximation. Importantly, this approximation is optimized by maximising model log-evidence, which can be expressed mathematically as:

$$ln p(g(w)|m) = F(g(w),q) + DKL[q(\theta)||p(\theta|g(w),m),$$

$$F(g(w),q) = ln p(g(w)|m) - DKL[q(\theta)||p(\theta|g(w),m),$$
(4.14)

where F(g(w), q) represents negative free-energy and DKL refers to the Kullback–Leibler divergence between the approximated posterior density $q(\theta)$ and the true posterior $p(\theta|g(w), m)$.

Due to the fact that the DKL divergence is always positive or zero when the densities are identical [160,161], the negative free-energy provides the lower bound or becomes equal (when $q(\theta)$ is equal to true posterior) to the model evidence. Furthemore, minimizing DKL divergence can be done by maximizing the negative free energy. The F(g(w),q) depends on the approximate posterior but does not depend on the true unknown posterior $p(\theta|g(w),m)$. Thus, estimating this negative free-energy is feasible. In other words, maximizing negative free-energy concerning VBL assumptions by using a gradient ascent provides two things: First, the variational density becomes posterior density over θ parameters, $q(\theta) \approx p(\theta|g(w),m)$, which is needed for model identification. The second one is the negative free-energy that becomes an approximation to the lower bound of the log model evidence, $F(g(w),q) \leq ln p(g(w)|m)$, which is needed to measure the model "goodness", and which takes into account both the accuracy and complexity of the model [162]. The negative free-energy is a metric for comparing different models (alternative hypotheses) and for selecting the most plausible model (hypothesis) of how the data were generated [163,164].

Chapter 5: Influence of hunger, satiety and oral glucose on brain functional connectivity⁴

5.1 Introduction

In contrast to the task-related fMRI, resting state fMRI (rs-fMRI) reflects the brain activity at rest, i.e. when individuals are not requested to perform a particular task [24], more details can be found in Section 1.1.3. Fluctuations of rs-fMRI have been considered to reflect rates of glucose oxidation in the gray matter [165]. Rs-fMRI lends itself to functional connectivity (FC, see Chapter 4) analyses by a number of techniques that analyze temporal correlations between spatially remote neurophysiological events [8,166]. In response to glucose uptake, the relationship between spatial metabolic information, which was provided by fluorodeoxyglucose- PET (FDG-PET), and FC, which was derived from rs-fMRI metrics, has been observed in the hypothalamus, thalamus and within the DMN [167,168]. Thereby, changes in FC of rs-fMRI signals can be considered as a biomarker for baseline shifts of resting state activity and have also been used to assess glucose metabolism in the brain [169].

Correspondingly, Bolo et al. [170] showed increased FC of the posterior cingulate cortex with the default mode network (DMN) and decreased FC of the inferior/ superior frontal gyrus with the cerebellum/ basal ganglia and temporal networks in hypoglycemia. Consistent with that, DMN activity was positively correlated with hunger ratings [171].

⁴ This chapter corresponds largely to: **Al-Zubaidi, A.**, Heldmann, M., Mertins, A., Jauch-Chara, K. and Münte, T. F. (2018). Influences of hunger, satiety and oral glucose on functional brain connectivity: A multimethod resting state fMRI study. *Neuroscience*. I participated in the experiment design and data collection. I analyzed the data and wrote the manuscript.

Glucose administration decreases the hypothalamic BOLD signal [67,68] and increases functional connectivity (FC) between the hypothalamus, thalamus, caudate and putamen within the limbic network after overnight fasting [46,172]. However, these studies did not investigate the responses and connectivity patterns to oral glucose on the whole brain level. To address this research gap, we investigated the interaction of metabolic state (hungry vs. satiated) and glucose administration (before vs. after administration of 75 g of oral glucose) with regard to rs-fMRI activity. The study of rs-fMRI is a relatively new field with rapid methodological developments. To encompass different aspects of the resting fMRI activity, we employed three methods that assess local and global FC as well as amplitude fluctuations of the BOLD response: First, regional homogeneity (ReHo) was determined, which describes the local connectivity of brain regions [100,126]. The ReHo method is termed after its property to reflect the coherence of spontaneous neuronal activity in a brain region [173]. It describes the similarity or synchronization of time series of a given voxel and its nearest neighbors at the low-frequency fluctuations of the BOLD signal [100]. The ReHo analysis revealed altered local connectivity of the brain in Alzheimer's disease [174], schizophrenia [175], attention deficit hyperactivity disorder [176], autism spectrum disorders [177] and Parkinson's disease [178]. Second, the degree of centrality (DC) measures the global connectivity of brain regions [128–130] in the sense of 'global functional connectivity density' [179]. The DC measures the connectedness of a node (here a voxel) within the entire brain network, by calculating the number of connections of a voxel to the other voxels in the brain above a certain threshold [128–130]. Nodes with high DC are considered to function as "hubs". Recently, the DC approach has been used as a marker for altered connectivity in Alzheimer's disease [130], obsessive-compulsive disorder [180,181], Parkinson's disease (PD) [182], attention deficit disorders and autism spectrum disorder [183] among others. In one study of PD [182], for example,

it was suggested that PD leads to a disconnection syndrome, i.e. a reduction of connectivity, which was most apparent in the visual network module. On the other hand, a higher connectedness within the sensorimotor module in PD patients was interpreted in terms of a compensation mechanism in order to overcome the functional deficit of the striato-cortical motor loops. Similar functional interpretations have been made for the other conditions mentioned above.

The third approach utilized here is the fractional amplitude of low-frequency fluctuations (fALFF). The fALFF provides information about the amplitude of spontaneous brain activity of each brain region within a network based on the magnitude of the BOLD signal in the low-frequency range [101]. The fALFF approach has been shown to efficiently suppress non-specific signal components, such as physiological noise [101,184]. Recently, studies have observed that fALFF can be related to emotion processing [185], differences in behavior [186] and social decision-making [187]. For example, in the [186] study, the amplitude of spontaneous low-frequency oscillations during rest predicted task-related fMRI activations and behavior in an Eriksen flanker task taxing executive control. In particular, low-frequency oscillations in the cingulate cortex predicted the magnitude of the behavioral congruency effect typically measured in the flanker task. These results support the notion that the brain's intrinsic functional architecture as measured in the resting state constrains behavior in tasks. Furthermore, the fALFF method has been shown to reflect aspects of depression [188,189] and attention deficit disorders with hyperactivity [173].

A multimethod approach of rs-fMRI has been used before to investigate brain disorders such as autism spectrum disorder and Granulin mutations [190,191]. One important question of the present study is, whether or not the different approaches are equally sensitive to changes in metabolic state. One previous investigation by Aiello et al. [168] showed there is a high inter-

correlation between these metrics after glucose uptake. Also, these parameters have been shown to correlate with regional glucose metabolism as measured by PET [167,168].

5.2 Materials and methods

Details regarding samples and preprocessing pipeline of rs-fMRI images can be found in Chapter 2. Calculating of ReHo, DC and fALFF maps for each subject per experimental condition are done as explanted in Chapter 4.

5.2.1 Statistical analysis

To investigate the effects of metabolic states, glucose treatment and the interaction between them on FC matrices, we performed a separate fixable factorial model in SPM 12 for each connectivity matrix (fALFF, ReHo and DC). We designed rm-ANOVA in the fixable factorial model by including three factors, see [192]: subject (to control for the repeated measures), metabolic state (two levels: hunger, satiety) and glucose treatment (two levels: before, and after treatment). The statistical results of whole-brain analyses were inspected at an initial threshold of p<0.001, which is the liberal primary threshold to avoid type I error [193]. Then the main effects of hunger vs. satiety and before vs. after glucose were reported statically from T-values at a cluster-defining threshold of p<0.016, corrected for multiple comparisons according to the FWE (Family Wise Error) method and adjusted for the number of FC analyses (0.05/3, Bonferroni corrected for multiple comparisons). For the interaction between factors, we inspected the F contrast corresponding to the two-way interaction; the interaction result was as well thresholded at peaklevel p<0.001, the number of voxel per cluster (K) >10. As a post-hoc test, the paired-sample ttest was used. Significant clusters were anatomically labeled according to the AAL atlas [102] included in the xjView toolbox (http://www.alivelearn.net/xjview8). The MNI-template Morel Atlas of the thalamus was applied to identify the substructure of the thalamic nuclei [194]. To visualize the spatial overlap among increases and decreases in multimethod rs-fMRI approaches, we projected the significant clusters as overlays on a structural brain image and determined the common voxels for all approaches. The xjView toolbox was used to identify the interaction among significant results

5.3 Results

Main effects of glucose treatment for the multimethod rs-fMRI (fALFF, ReHo, and DC) from rm-ANOVA are shown in Figure 5.1 and summarized in Table 5.1. There were some common effects for the different analyses: Significantly decreased fALFF, ReHo, and DC after glucose treatment were found in the left supplementary motor area (SMA) while increased fALFF and ReHo were observed in the right superior and middle frontal gyri (SFG, MFG; Figure 5.1D). There were also effects that were found only in one of the analysis approaches: Reduced fALFF was found in the right precentral gyrus (PreCG) and the right postcentral gyrus after glucose administration (PoCG; Figure 5.1A, Table 5.1). The ReHo analysis showed an increased after glucose treatment in the right parahippocampal gyrus (PHG) and hippocampal structures (HS), while a reduced ReHo was evident in the left inferior parietal gyrus (IPG) and the left PoCG (Figure 5.1B, Table 5.1). Finally, a reduction of DC after glucose treatment was seen in the left orbital inferior frontal gyrus (IFGorb) and the left anterior insula (AINS; Figure 5.1C, Table 5.1).

For the main effect of hunger, fALFF was increased in the posterior cingulate cortex (PCC) and the anterior precuneus (APCUN; Figure 5.2A and Table 5.2). Otherwise, we found no significant main effect on the satiety condition. For ReHo and DC analyses we observed no significant interaction between metabolic state and glucose treatment, and the main effect of metabolic state did not survive the correction for multiple comparisons.

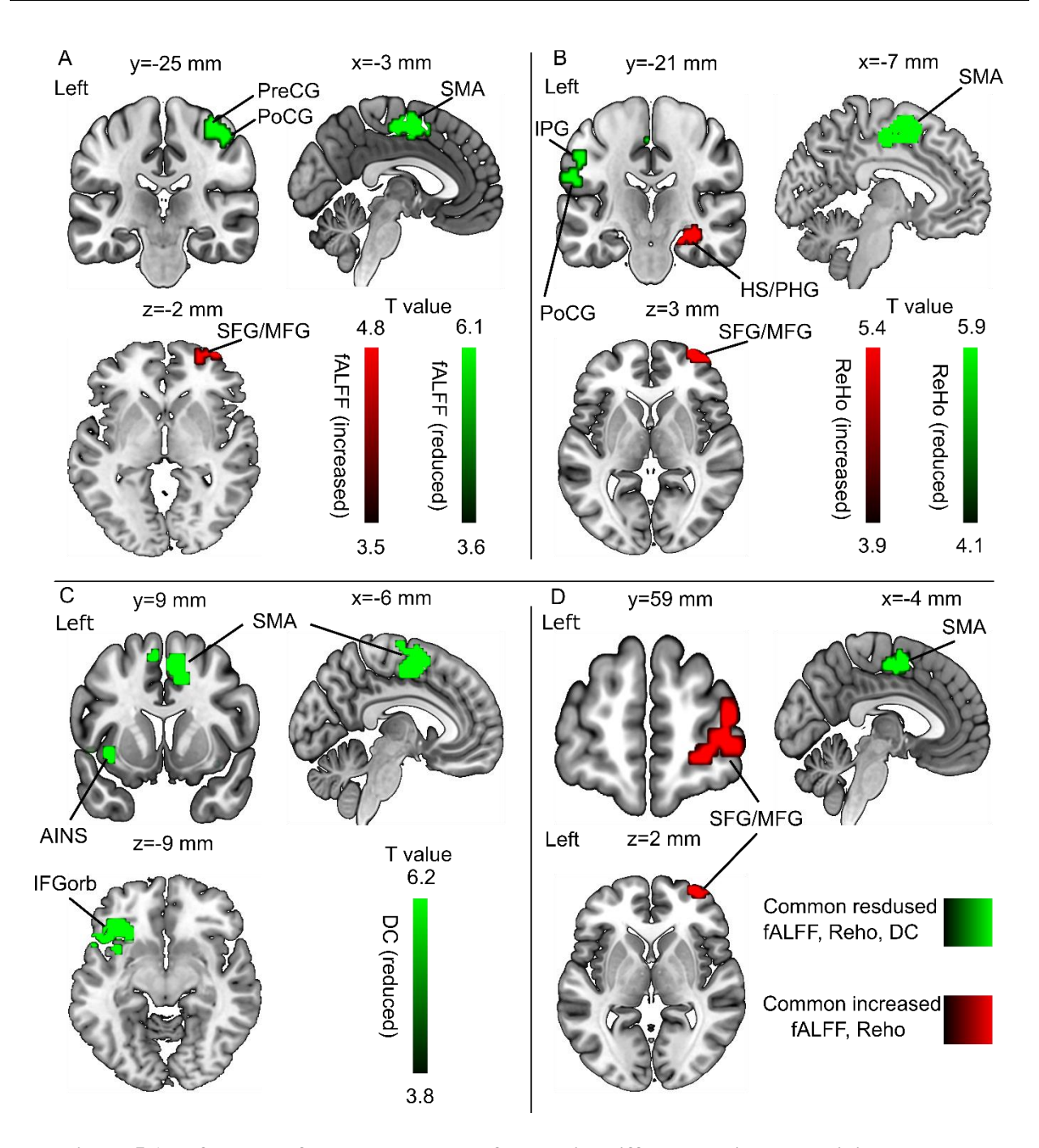


Figure 5.1: Influences of glucose treatment found with different brain connectivity analyses.(A) Fractional amplitude of low-frequency fluctuation (fALFF). (B) Regional homogeneity (ReHo). (C) Degree centrality (DC). (D) Common regions of multimethod brain approach. All statistical images were assessed for cluster-wise significance using a cluster defining threshold P<0.001, 0.016 FWE corrected at the cluster level. Abbreviations: PreCG: precentral gyrus; PoCG: postcentral gyrus; SMA: supplementary motor area; SFG: superior frontal gyrus; MFG: middle frontal gyrus; IFGorb: orbital inferior frontal gyrus; AINS: anterior insula; PHG: parahippocampal; HS: hippocampal structures.

Table 5.1: Influences of oral glucose tolerance test treatment for different brain connectivity parameters

Regions	Hes.	p(adj.)	K	T value	Local maxima (x y z) (m		y z) (mm)
fALFF (increased)		1 (3 /					, , , ,
Sup. orbital frontal gyrus	R	0.007	48	4.78	24	57	-6
Middle frontal gyrus	R			4.38	39	60	0
Sup. frontal gyrus	R			4.33	36	60	12
fALFF (reduced)							
Supplementary motor area	L	0.000	323	6.08	-3	-3	54
Supplementary motor area	R			4.39	12	3	45
Precentral gyrus	R	0.000	125	5.09	39	-15	57
Postcentral gyrus	R			4.32	45	-24	57
Postcentral gyrus	R			3.59	39	-33	69
ReHo (increased)							
Middle frontal gyrus	R	0.006	130	5.36	39	60	12
Middle frontal gyrus	R			4.64	36	63	3
Sup. orbital frontal gyrus	R			4.49	21	60	-6
Hippocampus	R	0.010	116	5.13	33	-24	-15
Parahippocampal gyrus	R			4.01	33	-39	-9
Hippocampus	R			3.83	30	-30	-6
ReHo (reduced)							
Supplementary motor area	R	0.000	377	5.97	9	3	48
Supplementary motor area	L			5.96	0	-6	54
Supplementary motor area	R			5.81	-3	6	54
Postcentral gyrus	L	0.005	135	5.06	-60	-15	24
Inferior parietal gyrus	L			4.06	-54	-21	39
DC (reduced)							
Inf. orbital frontal gyrus	L	0.000	221	6.23	-33	27	-12
Anterior insula	L			4.18	-36	12	-9
Supplementary motor area	L	0.000	363	5.28	-9	3	60
Supplementary motor area	R			4.68	12	3	48

Notes: The table shows three local maxima (MNI coordinates) more than 8.0 mm, the adjusted p-values are reported at p<0.001 (height threshold) and cluster-level FEW corrected p<0.016 (0.05/3). T=peak of T values. K=cluster size. Hes. =hemisphere. fALFF= fractional amplitude of low-frequency fluctuations. ReHo= regional homogeneity. DC= degree of centrality.

For fALFF, a significant interaction between metabolic state and glucose treatment in the left thalamus was observed (Figure 5.2B, Table 5.2). The z-score of the left thalamus were extracted and are shown in Figure 5.2C to illustrate the direction of this interaction. Before glucose treatment, the fALFF of the thalamus in hunger and satiety conditions did not differ; however,

after glucose treatment, the fALFF increased in hunger and decreased in satiety. Post-hoc comparisons of hunger vs. satiety after glucose treatment are shown in Figure 5.2D.

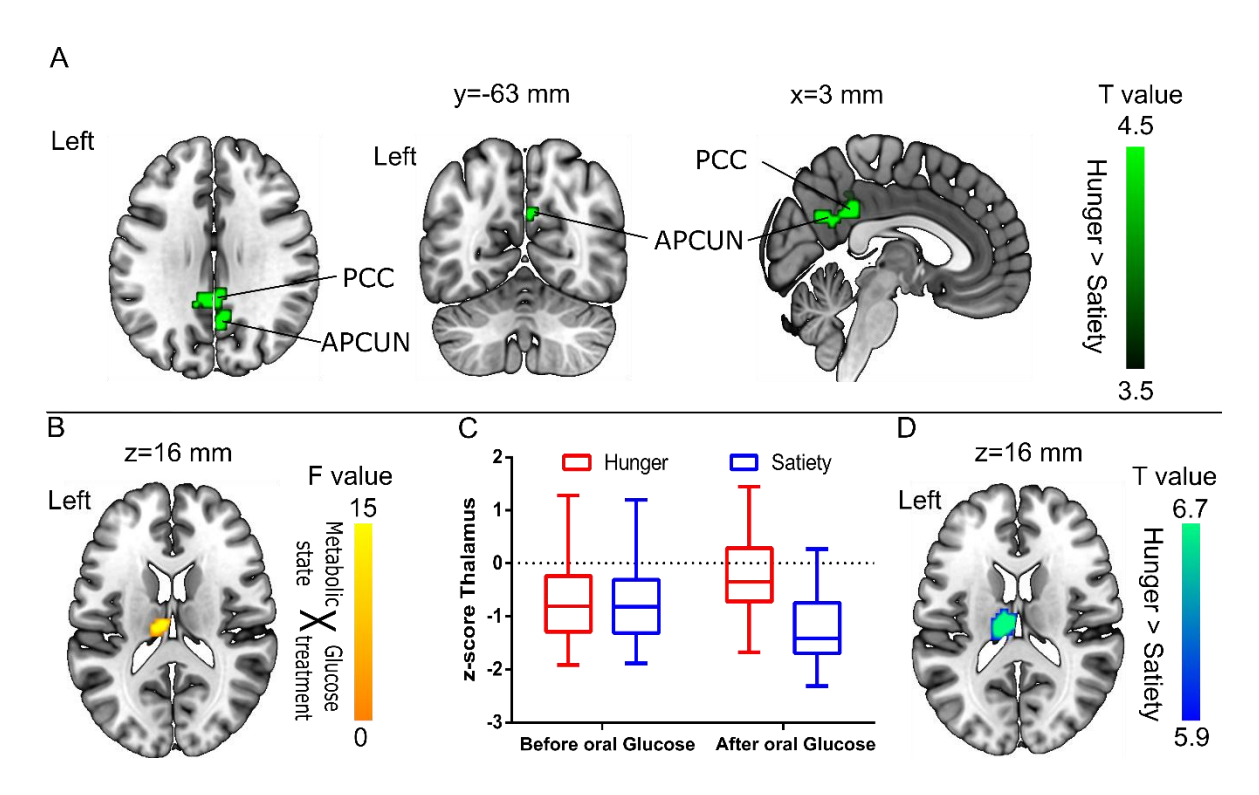


Figure 5.2: Changes of fALFF were obtained by two-way repeated measurements ANOVA. (A) The main effect of hunger versus satiety. (B) A significant interaction of metabolic state and glucose in the left thalamus (peak-level of P < 0.001, K > 10). (C) Interaction of metabolic state and glucose treatment in the left thalamus. (D) fALFF in the left thalamus in hunger vs. satiety after glucose (post-hoc test). Statistical images were assessed for cluster-wise significance using a cluster defining threshold p < 0.001, 0.016 FWE corrected at the cluster level. Abbreviations: PCC: posterior cingulate cortex; APCUN: anterior precuneus.

Table 5.2: Brain regions showing differences in the fractional amplitude of low-frequency fluctuations (fALFF)

Regions	Hes.	p(adj.)	K	T value	Local maxima (x y z) (mn		y z) (mm)		
Main effect: hunger > satiety									
Posterior cingulate cortex	L	0.001	67	4.47	-6	-42	33		
Anterior precuneus	R			3.91	3	-63	30		
Anterior precuneus	R			3.63	6	-54	27		
$ \begin{array}{cccccccccccccccccccccccccccccccccccc$									
Post-hoc paired t-test after glucose: hanger > satiety									
Thalamus	L	0.000	62	6.67	-3	-21	15		
Thalamus	L			5.34	-12	-21	15		
Thalamus	L			5.05	-9	-33	6		

Notes: The table shows three local maxima (MNI coordinates) more than 8.0 mm, the adjusted p-values are reported at p<.001 (height threshold) and p<0.016 (FWE extent threshold for cluster levels, 0.05/3). . 4 is the p-value (p<0.001) at peak level. T=peak of T values, except ε is the peak of F value. K=cluster size. Hes. =hemisphere.

5.4 Discussion

This Chapter explored whether the metabolic state (fasted vs. satiated states) and fluctuations in blood glucose levels might be reflected in changes of resting-state connectivity in the brain. Therefore, we used data-driven approaches to assess hemodynamic changes related to neuronal activity (BOLD signal). In Chapter 3, we showed that blood sugar levels were differentially affected by metabolic state and administration of glucose. In this Chapter, after glucose treatment, we found a significant decrease of fALFF, ReHo, and DC in the left SMA, while a significant increase of fALFF and ReHo was observed in the right MFG and SFG. Third, hunger relative to satiety increased the amplitude (intensity) of spontaneous brain activity in the PCC and the anterior PCUN. Fourth, we observed a significant interaction between metabolic state and glucose treatment in the left thalamus using fALFF analysis.

In the main effects of glucose treatment, a decreased of fALFF, ReHo, and DC was found in the left SMA after glucose treatment. This region is important for motor planning and programming [195,196] and action observation [197]. While our data were obtained during rest without a task, the effect of glucose treatment on SMA might indicate suppressed action planning or initiation, because the energy requirements of the brain and body are met. Thus, we propose that different levels of circulating glucose differentially affect activity in brain regions involved in attention, motor planning, and food evaluation, thereby providing a background signal that might modulate activities such as foraging.

Apart from subcortical structures we also found increased fALFF and ReHo in the right SFG and MFG when we evaluated the main effects of glucose treatment. Activation in both regions is positively correlated in healthy participants using whole brain correlation analysis [198]. The SFG is activated in response to appetitive stimuli in fasting participants [199,200]. The right MFG is active during attention shifts towards unexpected stimuli [201,202] or reorienting attention from exogenous to endogenous foci [198] and is part of a ventral attention network (VAN) [203,204].

We identified further differences in brain responses after glucose. First, we found it decreased fALFF in the right PreCG and the right PoCG. The PreCG is a primary motor area, and the PoCG is a primary sensory area and both regions are part of the sensorimotor network [120,205]. For this network, we furthermore found decreased amplitudes of the BOLD signal after glucose administration pointing to overall reduced activation of that network. Supporting our findings, a study using ICA showed increased FC of the PreCG and PoCG regions in the sensorimotor network during hypoglycemia [170]. Secondly, we found increased ReHo in the right PHG and HS, regions that figure prominently in memory processes. Reduced ReHo was evident in the left IPG and the left PoCG. Finally, suppression of DC was marked in the left IFGorb and AINS which harbors the primary gustatory cortex and contains neurons that respond to different tastes and food textures [206,207]. Furthermore, a meta-analysis by Kelley and colleagues [208]

affirmed participation of the left insula in the processing of appetite and food stimuli. In addition, the AINS is connected with the anterior cingulate cortex, the middle and inferior frontal cortex, and the temporoparietal cortex within the resting state network [134]. This network is mostly related to limbic regions that play a role in emotion processing [129]. Our observations suggest that sensing the arrival of energy supply from oral glucose, probably via signaling from sweet taste receptors, suppresses connectivity in AINS to interrupt the resting state network as proposed by Zou et al. [129] and switch to a state of increased activity.

For the main effect of metabolic state, DC and ReHo analyses failed to identify differential connectivity patterns according to hunger vs. satiety after correction for multiple comparisons. Thus, the global and local connectivity of the brain appears to be largely independent of metabolic changes in perceived hunger, at least with regard to the extent seen in the present experiment. By contrast, fALFF analysis revealed that the amplitude of the BOLD signal was increased in PCC and APCUN during hunger (Figure 5.2A and Table 5.2). As has been shown before, the insula, PCC, and the precuneus are activated during food choice versus non-food choice in hunger conditions [209]. Moreover, PCC, APCUN are core hubs of the default mode network (DMN) [23,35] which is activated in rs-fMRI when attention is oriented towards internal rather than towards external stimuli [33,34]. The PCC has been shown to be involved in self-referential processes [210] and APCUN in self-centered mental imagery strategies [211]. In an FC study on overweight/obese participants, the reduction of DMN activity was associated with a decrease in fat mass and hunger ratings after six months of exercise [171]. In the current experiment, the increased BOLD amplitude in PCC independent of glucose administration appears to be related to the metabolic state [107]. DMN activity has previously been shown to be positively correlated

with hunger ratings [171] and with lower blood glucose levels [170]. The enhanced activation of DMN under hunger conditions leads to the hypothesis that this indicates an increase in self-focus.

In addition to the main effects of metabolic state, we found a significant interaction between metabolic state and glucose level on the activation of the left thalamus (mediodorsal). This interaction was driven by a fALFF increase after glucose treatment in the hunger and a fALFF decrease after glucose in the satiety condition. In agreement with our findings, it has been shown before, that hunger is associated with increased amplitude of BOLD signals and cerebral blood flow in the thalamus [212,213]. By contrast, ghrelin application [214] as well as glucose infusion decreased the BOLD signals in the thalamus [70,215]. Kroemer et al. [48] found that fasting levels of ghrelin correlated positively with brain responses to food pictures in the thalamus but did not find an effect of standardized glucose intake. The thalamus plays a central role in the processing of food-related sensory information as well as the integration of information from the gastrointestinal (GI) tract [70,216]. In particular, a spinothalamic pathway conveys afferent information from the GI tract to thalamus via the vagus nerve [217]. Rolls [207,218] has identified the role of the mediodorsal thalamus in the short-term regulation of food intake. We therefore suggest that the altered activity of the mediodorsal thalamus region after glucose treatment is dependent on the perception of hunger or satiety, and related to the glucose level.

In summary, we found that changes in the metabolic state, i.e. hunger vs. satiety affected the amplitude of the BOLD signal, but did not influence local and global connectivity. By contrast, we did observe significant alterations in amplitude as well as local and global connectivity after glucose treatment. This indicates that local and global brain connectivity remained stable after 36 hours of fasting or standardized meals, whereas they were acutely modulated after glucose. It has previously been stressed that the brain has a unique capacity to control its own energy supply [49]

even under conditions of hunger and the stable connectivity pattern between satiated and hungry state might reflect this control function.

5.5 Conclusions

The fALFF method proved to be a sensitive and reliable marker to measure changes in the homeostasis of the resting brain. While fALFF is an index for the power of the BOLD signal in the low-frequency ranges, ReHo and DC measure local and global connectivity, respectively. We found indications of VAN and DMN activation as reflected by corresponding increases in signal intensities of SFG, MFG, PCC, and APUCN. Both networks serving different functions are involved in attention shifts between internal and external stimuli (VAN) and feeding-related behavior (DMN), suggesting that the changes in blood sugar levels lead to changes in brain activity which may be important to initiate behaviors such as foraging and food intake. The current findings suggest that examining the effect of oral glucose under different metabolic states by a multimethod approach for rs-fMRI analysis can contribute to the delineation of the relationship between metabolism, brain, and behavior. Particularly, the results indicated a rather stable pattern of connectivity in both metabolic states, suggesting that the brain's energy supply is kept stable. Glucose administration on the other hand led to an acute modulation of the connectivity pattern which might indicate the need to adjust behaviors in the face of ample energy supply.

Chapter 6: Amplitude of brain signals classify hunger status based on machine learning in resting-state fMRI⁵

6.1 Introduction

Resting-state functional magnetic resonance imaging (rs-fMRI) has been increasingly applied to study activity and connectivity of the resting brain and involves the recording of the blood-oxygen-level-dependent (BOLD) signal without imposing a task [45,219]. This approach can be used to assess intrinsic and spontaneous brain activity. Analysis techniques of rs-fMRI have evolved rapidly over the past few years and are based on correlation methods [128,220–222], partial correlation [223–225], graph theory based analysis [128,226] and sparse representation methods [227,228], among others. Because of its simplicity (short scan time, no stimulation equipment needed, no task requirements, see Section 1.1.3), the rs-fMRI method has become particularly popular for the characterization of clinical conditions, for example pinpointing to differences between healthy participants and patients with Parkinson's disease [182,229], Alzheimer's disease [230,231], bilateral vestibular failure [232], schizophrenia [233,234], obsessive-compulsive disorder [235,236] to name but a few targeted neuropsychiatric conditions.

In neuroimaging, machine learning classifier (MLC) methods are applied to fMRI data to detect model-free brain activity and to use these brain activity patterns to differentiate between groups or conditions [237,238]. The application of MLC to fMRI data is often referred to as multivoxel (i.e. analyzing more than one voxel at once) pattern analysis (MVPA). MVPA is a helpful

⁵ This chapter corresponds largely to: **Arkan Al-Zubaidi**, Alfred Mertins, Marcus Heldmann, Kamila Jauch-Chara and Thomas F. Münte (2019). Machine learning based classification of resting-state fMRI features exemplified by metabolic state (hunger/satiety). *Frontiers in human neuroscience*. I participated in the experiment design and data collection. I analyzed the data and wrote the manuscript.

tool to investigate how a pattern of brain activity is related to different cognitive state [239–241]. The process of applying the MVPA approach to fMRI data can be broken down into three stages [16,238]. First, feature extraction, which converts the BOLD fMRI signals to the relevant variables, i.e. features, which will be used to train and to test the classifier. Second, feature selection, which determines features that have to be included in the classifier analysis in order to improve the classification. Third, cross-validation methods that divide the data into training and testing samples and determine the accuracy of the classifier in generalization to new data.

Support vector machine (SVM) [242,243] is a powerful method available to perform MVPA. In contrast to alternative MVPA methods (such as linear discriminant analyses), SVM provides better prediction accuracy, having the advantage of being relatively insensitive to the sample size of the training dataset [244,245]. Furthermore, SVM has additional advantages regarding efficiency, simplicity, robustness and is less susceptible to noise [245,246].

The application of SVM to fMRI data at the group level has several advantages over traditional univariate (i.e. individual) voxel-based methods, like the general linear model (GLM). For instance, SVM allows to identify voxels or brain regions of interest that are informative for classifying groups by accumulating the information in an efficient way across many spatial locations, while in GLM analysis, these voxels or brain regions could appear statistically insignificant, although they might carry some information about differences between states or groups [239,240]. Thus, SVM provides insight into the defining differences between the two states or groups [237,247].

In many cases, fMRI data have a small number of samples and a large number of variables or features. This often leads to overfitting in classification, which in turn leads to deceptive diagnostic results and poor generalization performance [238,248]. To avoid the danger of

overfitting, most of the MVPA-based fMRI studies applied both methodologies, feature-selection algorithms to remove redundant information and MLC methods that are less sensitive to high dimensionalities, such as linear SVM. Finally, cross-validation analyses are performed to evaluate the classification accuracy and generalizability for unseen data [237,249–251].

Rs-fMRI yields data comprise multiple data points per subject and/or condition among other things raising the question of whether it might be possible to distinguish between different conditions (e.g. disease present or not) using classification algorithms from the realm of machine learning. Indeed, several recent publications have tackled this question. For example, Abós et al. [252] obtained functional connectomes from the rs-fMRI in healthy controls (HC) and 70 Parkinson's disease patients (of which one third had a mild cognitive impairment (MCI)). Using a SVM trained on features selected through randomized logistic regression with leave-one-out crossvalidation (LOOCV) they could separate patients with MCI from those not having MCI with an accuracy of about 83% in the training sample. In a smaller validation sample of 25 Parkinson patients (8 MCI), classification accuracy with regard to MCI was 80% using the features found in the training sample [252]. This suggests that SVM classification based on metrics obtained from rs-fMRI can indeed yield meaningful results. Likewise, applying a graph theoretical approach to rs-fMRI to characterize functional connectivity in patients with MCI, Alzheimer's disease (AD) and age-matched HC (total sample n=168) followed by SVM based classification, Khazaee et al. [253] were able to accurately classify the subjects into three groups (HC, MCI, AD) with 88.4% accuracy. The same research group [254] tried to distinguish patients with MCI who later converted to an AD from MCI patients who did not. Again a SVM using features derived from local and global graph measures was used. This approach yielded a specificity of 91.4% and sensitivity of 83.2% regarding the conversion to the AD. Bi et al. [255] attempted to classify patients with autism spectrum disorder (ASD) from HC using random SVM cluster and reported classification accuracy based on the optimal feature to be 96%. These are just a few examples illustrating that rs-fMRI derived features can be used for classification of conditions using machine learning algorithms. What it is less clear, however, is which method of rs-fMRI analysis delivering the most discriminating features might be best in distinguishing different metabolic states (hunger vs. satiety).

In the present investigation, we therefore sought to compare the accuracies of three different connectivity parameters or features (the predictor variables used for classification) extracted from rs-fMRI fluctuations. These features assess local and global functional connectivity as well as changes in the brain activity as indicated by the amplitude of the BOLD signal, i.e. regional homogeneity (ReHo), degree of centrality (DC) and fractional amplitude of low-frequency fluctuations (fALFF), respectively (see Chapter 4). Briefly, ReHo characterizes the local connectivity of a brain voxel to its nearest neighboring brain voxels [100,126] by determining the coherence among spontaneous BOLD signals that might reflect spontaneous neuronal activity ReHo has been applied to widely differing neuropsychiatric conditions [173]. [174,175,178,256,257]. DC is derived from graph theory based analysis and describes the global connectivity (global connectedness) of a given voxel with the voxels in the entire brain, by computing the number of connections above a certain threshold [128–130]. Again, DC has seen widespread application in neuropsychiatric conditions [130,180,181,183,232]. Finally, to quantify spontaneous local brain activities, the amplitude or intensity of the BOLD signals is used as a marker. We performed fALFF on rs-fMRI datasets to describe the local spontaneous brain activities.

The aim of feature selection algorithms is to reduce the dimensionality of feature space and computation time as well as to enhance the accuracy of optimization methods by ignoring redundant, irrelevant or noisy features [258,259]. In general, the feature selection algorithms are classified into two categories, according to the type of objective functions that one chooses to work with: filter methods and wrapper methods [238,260]. Filter methods select the feature subsets based on statistical properties (such as interclass distance, mutual information, entropy or statistical independence) of the features to filter out poorly informative ones without employing any classification algorithm. In contrast, wrapper methods rate the feature subsets based on their predictive accuracy to improve the performance of classification when applying a particular classifier (such as SVM or the k-nearest neighbor). Filter methods are advantageous because they perform quickly, afford a more general solution and tend to select large feature subsets. Wrapper methods are expensive because they need more time to train the classifier of each subject many times (i.e. cross-validation), but often do not deteriorate from the problem of overfitting [261] and provide more accurate results comparable to filter methods [262,263].

There are several strategies to apply wrapper methods [260]. For instance, sequential forward selection (SFS) and sequential forward floating selection (SFS) are easy to execute and are assumed to provide useful results. Although the SFFS strategy requires massive computational resources, it performs better and is more effective for solving small- and medium-scale problems than simpler strategies like SFS [264]. However, the SFS strategy reduces the computational costs for the feature subset selection. Accordingly, Burrell and colleagues [261] concluded that SFS was a reasonable alternative to select a small subset of features for fMRI data. In this work, we compared between SFS and SFFS strategies for creating feature subsets to distinguish different metabolic states.

The emphasis of the present work is on the ability to classify the metabolic states (hunger vs. satiety) by MVPA approach. Therefore, we first estimate and compare the prediction accuracy of classification (hunger vs. satiety) based on different features of rs-fMRI data (ReHo, DC and fALFF). Second, we identify brain regions containing discriminating information between different metabolic states. To this end, we apply support linear SVM as classifier and two feature selection strategies (SFS and SFFS) to identify those brain regions that most efficiently differentiate between hungry and satiated states based on rs-fMRI data. Finally, we employ a cross-validation scheme and permutation tests to validate the reliability of classifier and significance testing, respectively (see Figure 6.1 for classification procedure).

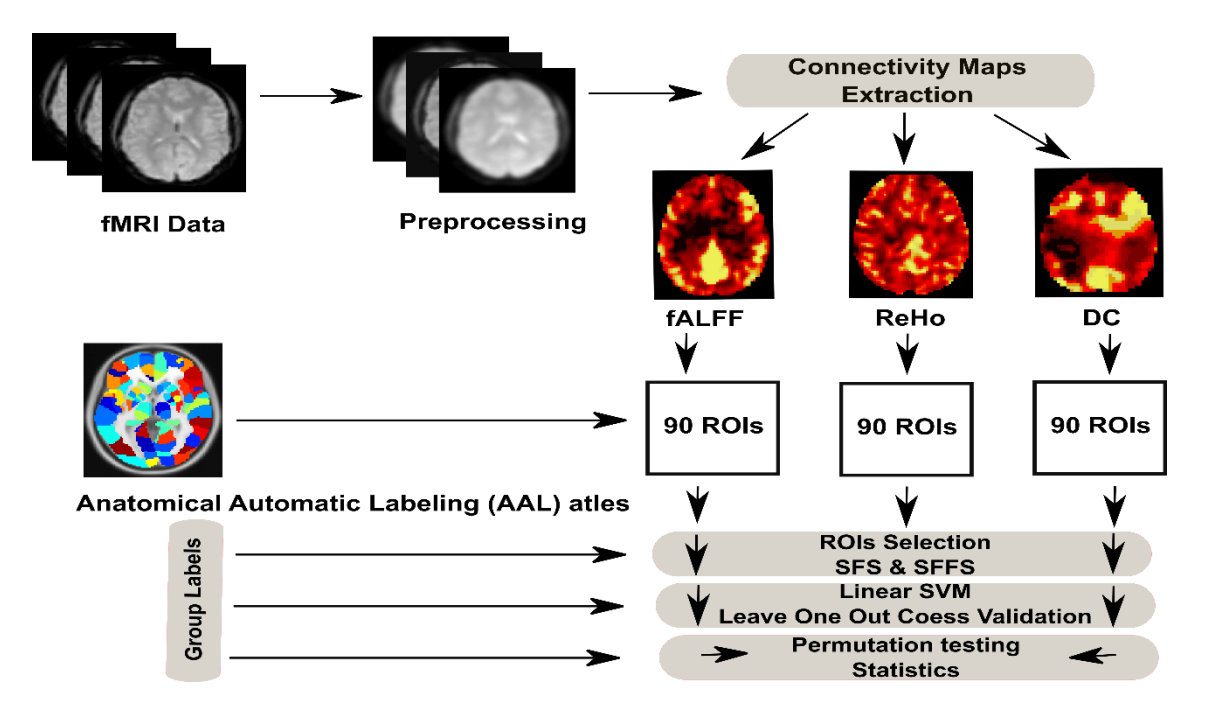


Figure 6.1: Full analysis procedure of hunger classification based on rs-fMRI data.

6.2 Materials and methods

Twenty-four lean, healthy male volunteers (age 25 ± 5 years) were recruited from the University and the local population of Lübeck city. Each subject was measured under two metabolic states, once under fasting (36 hours fasting) and once under the standardized eating condition with a break

of one week between conditions. At the end of each session, structural and functional images were recorded. More details on the experimental design, image acquisition and preprocessing of rs-fMRI data can be found in Chapter 2.

6.2.1 Feature extraction from rs-fMRI data

Feature extraction is used to reduce the dimension of the original data space to a new feature space. This new feature space helps to minimize the training time taken by the classifier [265]. To encompass different aspects of rs-fMRI fluctuations, we extracted and compared three of the most common features according to their accuracy to select those brain regions that best distinguish different metabolic states by using linear SVM together with feature selection strategies. In the beginning, we submitted the preprocessed data to the DPARSF toolbox [99] and extracted three features (DC, ReHo and fALFF) from each subject per section as described in Chapter 4. Then, those features were analyzed as explained in Section 6.2.2.

6.2.2 Feature selection for hunger/satiety status classification

After generating ReHo, DC and fALFF maps from rs-fMRI data for each subject per condition, we used the AAL atlas to define the ROIs. The AAL atlas is a well-established anatomical parcellation of the brain into 45 ROIs per hemisphere when excluding the cerebellar lobules (see Chapter 2, Section preprocessing). Mean values of ReHo, DC and fALFF were calculated for each ROI and used to create a feature (region) vector, i.e. R [1,...,90], with 90 dimensions for each map. Those features are listed in Table 6.1.

Table 6.1: List of the anatomical regions (AAL atlas) of interest and their labels in the region vector.

Label	Anatomical	Label	Anatomical	Label	Anatomical
1	L. Amygdala	31	R. Sup. Frontal Med.	61	L. Sup. Parietal Gyrus
2	R. Amygdala	32	L. Sup. Frontal Orbital	62	R. Sup. Parietal Gyrus
3	L. Angular Gyrus	33	R. Sup. Frontal Orbital	63	L. Postcentral Gyrus
4	R. Angular Gyrus	34	R. Superior Frontal	64	R. Postcentral Gyrus
5	L. Calcarine Fissure	35	L. Fusiform Gyrus	65	L. Precentral Gyrus
6	R. Calcarine Fissure	36	R. Fusiform Gyrus	66	R. Precentral Gyrus
7	L. Caudate Nucleus	37	L. Heschl Gyrus	67	L. Precuneus
8	R. Caudate Nucleus	38	R. Heschl Gyrus	68	R. Precuneus
9	L. Ant. Cingulate Cort.	39	L. Hippocampus	69	L. Putamen
10	R. Ant. Cingulate Cort.	40	R. Hippocampus	70	R. Putamen
11	L. Mid. Cingulate Cort.	41	L. Insula	71	L. Rectus gyrus
12	R. Mid. Cingulate Cort.	42	R. Insula	72	R. Rectus gyrus
13	L. Pos. Cingulate Cort.	43	L. Lingual Gyrus	73	L. Rolandic Operculum
14	R. Pos. Cingulate Cort.	44	R. Lingual Gyrus	74	R. Rolandic Operculum
15	L. Cuneus	45	L. Inf. Occipital Gyrus	75	L. Supplementary Motor Area
16	R. Cuneus	46	R. Inf. Occipital Gyrus	76	R. Supplementary Motor Area
17	L. Inf. Frontal Oper.	47	L. Mid. Occipital Gyrus	77	L. Supramarginal Gyrus
18	R. Inf. Frontal Oper.	48	R. Mid. Occipital Gyrus	78	R. Supramarginal Gyrus
19	L. Inf. Frontal Orbital	49	L. Sup. Occipital Gyrus	79	L. Inf. Temporal Gyrus
20	R. Inf. Frontal Orbital	50	R. Sup. Occipital Gyrus	80	R. Inf. Temporal Gyrus
21	L. Inf. Frontal Triang.	51	L. Olfactory Cortex	81	L. Mid. Temporal Gyrus
22	R. Inf. Frontal Triang.	52	R. Olfactory Cortex	82	R. Mid. Temporal Gyrus
23	L. Med. Frontal Orbital	53	L. Pallidum	83	L. Mid. Temporal Pole Gyrus
24	R. Med. Frontal Orbital	54	R. Pallidum	84	R. Mid. Temporal Pole Gyrus
25	L. Frontal Middle	55	L. Paracentral Lobule	85	L. Sup. Temporal Pole Gyrus
26	L. Frontal Mid. Orbital	56	R. Paracentral Lobule	86	R. Sup. Temporal Pole Gyrus
27	R. Mid Frontal Orbital	57	L. Parahippocampal	87	L. Sup. Temporal Gyrus
28	R. Middle Frontal	58	R. Parahippocampal	88	R. Sup. Temporal Gyrus
29	L. Superior Frontal	59	L. Inf. Parietal Gyrus	89	L. Thalamus
30	L. Frontal Sup. Med.	60	R. Inf. Parietal Gyrus	90	R. Thalamus

Abbreviations: AAL: Automated-Anatomical-Labeling. Ant: Anterior; Cort: Cortex; Inf: Inferior; L: Left; Med: Medial; Mid: Middle; Oper: Opercular; Pos: Posterior; R: Right; Sup: Superior; Triang: Triangular;

In the classification problem, the goal of feature selection is to automatically search and select the best feature subset for the classification purpose. Here, we applied sequential feature selection algorithms to select the optimal feature subset (region subset) that best captured differences between hunger and satiety. This type of selection algorithm contains two components. The first element is a sequential search strategy to select and establish the best future subset, which evaluates additional features by a criterion function. In this study we used two strategies, namely

sequential forward selection (SFS) and sequential forward floating selection (SFS). The SFS procedure starts by identifying the first feature with the highest classification rate and feeds it to a new empty candidate set. Other features are selected sequentially by adding a local feature to the first feature or the last subset of features in the candidate set, and testing a new feature combination until the highest classification rate (objective function) is achieved. The processing continues until further features do not enhance the objective function. However, the SFS algorithm is suboptimal and suffers from the "nesting effect" [266], while SFFS offers the flexibility to discard features that were earlier selected and to re-evaluate features that had been discarded previously. This theoretical advantage notwithstanding, Burrell and colleagues [261] showed that the computationally less demanding SFS could provide a reasonable alternative to SFFS to select features for discriminating between epileptic and non-epileptic activity of epileptic patients, indicating that both strategies had similar difficulties to separate patterns of functional and dysfunctional brain activities in epileptic patients. In this study, we compared SFS and SFFS strategies in order to figure out if SFS already provides near-optimal results. SFS and SFFS strategies were performed using the "sequentialfs" function in MATLAB and sequential floating feature selection toolbox (http://splab.cz/en/download/software/software-pro-sekvencni-selekcipriznaku), respectively.

The second component in the feature selection strategy is an objective (criterion) function to evaluate over all possible feature subsets. In this work, the misclassification rate of the linear SVM classifier was set as an objective function [262]. The combination of SFFS and SVMs has previously been used, for example, to assess Gabor features for classification of Parkinson's disease risk assessment based on transcranial sonography images [267]. To evaluate the feature subset, the data were divided into test and training samples using a leave-one-out cross-validation

(LOOCV) scheme. Accordingly, independent samples were used for training and testing. For each LOOCV loop, the training samples were submitted to train an SVM model, and the test sample was applied to that model to evaluate the feature subset. In the end, the average of the values returned by LOOCV loops was calculated and used to assess each candidate's feature subset [268].

The classification accuracy (CA) was derived by using a LOOCV strategy with confusion matrix (CM) and calculation of classification error rate (ER). In our study, the CM comprises information about the actual and predicted classifications generated by linear SVM. By comparing the results of the SVM classifier (hunger or satiety) with the reference data, we documented the outcomes of the CM in the present study as given in Table 6.2. For significance testing [238], we estimated the empirical distribution by calculating the error rate 10000 times for random label permutations in a cross-validation procedure. P < 0.05 implies that classification results differ significantly from chance.

Table 6.2: Confusion matrix

		Referer	Reference data			
		Hunger	Satiety			
Classified	Hunger	[TP	FP]			
	Satiety	LFN	TNJ			

True positive (TP): The number of participants that were correctly classified in hunger condition False positive (FP): The number of participants that were incorrectly classified in hunger condition False negative (FN): The number of participants that were incorrectly classified in satiety condition True negative (TN): The number of participants that were correctly classified in satiety condition

6.3 Results

The experiments showed that fALFF was marginally better than ReHo and DC in distinguishing between hunger and satiety states in the healthy brain (Table 6.3). The region subset obtained by SFFS resulted in higher classification accuracy than SFS, both higher than no feature selection (90).

regions). Using a linear SVM classifier with a LOOCV strategy, we observed that the fALFF region subset selected by SFFS identified the hunger state with the highest classification accuracy of 81%. In our SFFS results (Table 6.3), the regions 45 and 46 are the left and right inferior occipital lobe (Table 6.1), respectively, and region 50 is the right superior occipital lobe. Also, regions 5 and 35 are medial (Calcarine) and inferior (Fusiform) surfaces of the occipital lobe, respectively. Furthermore, regions 17 and 18 are left and right frontal gyrus, respectively, region 52 is the right Olfactory cortex, region 56 is the right Paracentral lobule and region 73 is the left Rolandic operculum. SFFS-identified brain regions which distinguished best between hunger and satiety for each rs-fMRI feature are shown in Figure 6.2. Furthermore, SFFS fALFF (Figure 6.3) was most stable in the permutation test (ER=0.19 / p=0.0001) closely followed by DC (ER=0.21 / p=0.0004) and ReHo (ER=0.29 / p=0.0068).

Table 6.3: Classification accuracy of rs-fMRI data using different models of brain connectivity/activity and features selection algorithms with linear SVM classifier

D (0.15)	90	regio	ns	Region se	ets by S	SFS		Regions sets by SFFS			
Rs-fMRI features	CA	C	M	R[1,,90]	CA	A CM		R[1,,90]	CA	СМ	
ReHo	50%	$\begin{bmatrix} 12 \\ 12 \end{bmatrix}$	12 12	R[22,61]	69%	$\begin{bmatrix} 17 \\ 7 \end{bmatrix}$	8 16	R[45,17]	71%	$\begin{bmatrix} 20 \\ 4 \end{bmatrix}$	10 14
DC	54%	[16 8	$\begin{bmatrix} 14\\10 \end{bmatrix}$	R[50,55,4,68]	71%	[¹⁹ ₉	9 15]	<i>R</i> [50,4,5,35]	79%	$\begin{bmatrix} 22 \\ 2 \end{bmatrix}$	8 16]
fALFF	58%	$\begin{bmatrix} 16 \\ 8 \end{bmatrix}$	12 12]	R[61,77,35,6,1]	73%	$\begin{bmatrix} 17 \\ 7 \end{bmatrix}$	6 18	R[56,73,46,52,18]	81%	$\begin{bmatrix} 19 \\ 5 \end{bmatrix}$	$\begin{bmatrix} 4 \\ 20 \end{bmatrix}$

Abbreviations: SFS: sequential forward selection; SFFS: sequential forward floating selection; CA: classification accuracy; CM: confusion matrix.

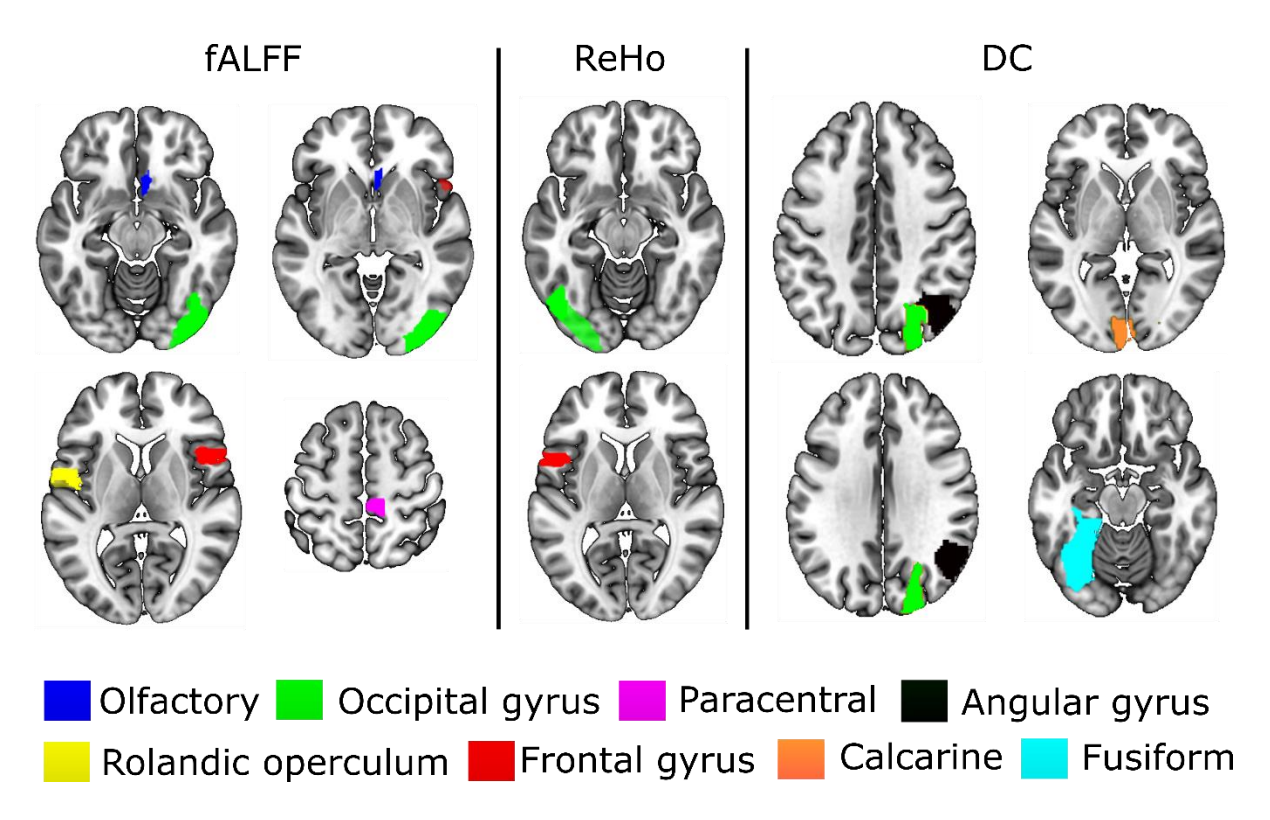


Figure 6.2: Brain regions that provided relevant information to distinguish between hunger and satiety states in healthy lean participants.

The performance of these regions was evaluated by linear SVM classifier and SFFS algorithm. All images are in neurological orientation, i.e. right = right and left = left.

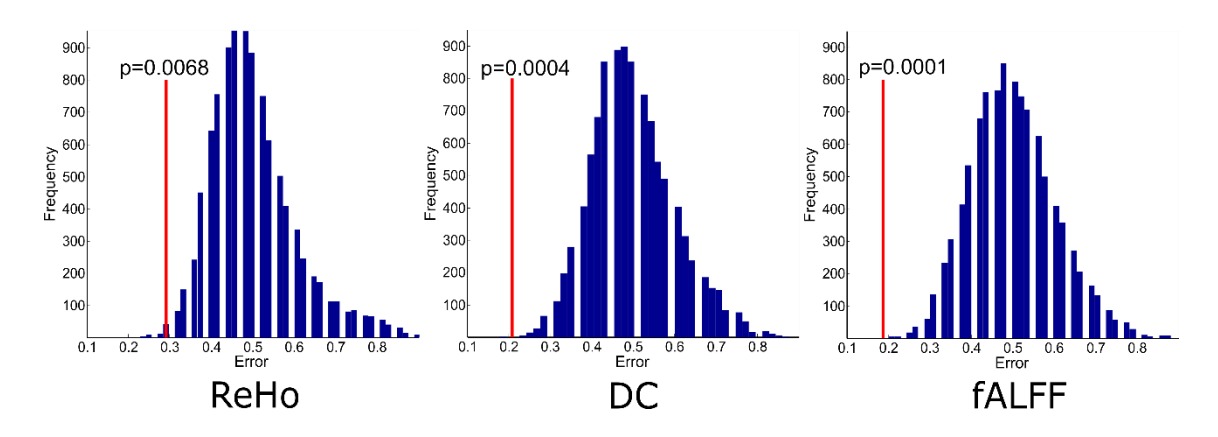


Figure 6.3: Empirical distributions of incorrect classification generated via 10000 times of random label permutations for region sets selected by SFFS.

Red line shows the actual classification error.

6.4 Discussion

The primary goal of the present chapter was to assess the ability to classify different brain states by applying a MVPA approach, i.e. feature selection strategies and linear SVM, on various features, i.e. connectivity parameters, derived from rs-fMRI data. This approach was carried out on a data set comprising two conditions (hungry and satiated) in a repeated measures design. As the two metabolic states, i.e. hunger and satiety, were induced for a rather long time (36 hours), experimental conditions can be treated as the ground truth to compare and evaluate the classification scheme.

An advanced preprocessing, including ICA-AROMA, was carefully applied (see Section 2.3.2), ensuring the removal of motion artifacts and other structured noise from the data (e.g. cardiac pulsation artifacts [98]). Thus, classification in the current case is deemed to reflect true brain differences rather than extracerebral differences (e.g. motion) between the conditions.

A critical question with regard to classification is the selection of the best approach for feature selection. The inclusion of all possible features and the computation of all possible combinations of features is computationally not feasible at present. Therefore, sequential search techniques have gained some popularity. These work by choosing the best individual feature and then adding a second feature that yields the best classification accuracy in combination with the first feature. This procedure is repeated for a third and any subsequent features until the addition of further features does not yield in an improvement of classification rates. Alternatively, the user can predetermine the maximum number of features. The SFFS method tries to optimize feature selection by adding an elimination step to this sequential search process. Concretely, at each level, it is examined whether the classification rates improve if any of the selected features are eliminated. If this happens, the feature set is reduced by this feature. Then, the search continues

based on the new set. Jain and Zongker [269], for example, compared 14 different methods for feature selection applying them to the problem of handwriting recognition. In this case, the SFFS method outperformed other feature selection schemes. It has to be pointed out, however, that conventional feature selection approaches, including SFS and SFFS as well as filter approaches [270,271], have recently been supplemented by metaheuristic methods for feature selection. In this regard, Zhu et al. [272] have suggested a genetic algorithm combined with local search in a hybrid wrapper and filter feature selection algorithms. Others like Neshatian and Zhang [273] and Gu et al. [274] proposed new optimizations methods including such advanced feature selection procedures. Applying genetic algorithms and new optimization functions on rs-fMRI data are beyond the scope of this study and will be considered in future work.

In the present analysis, the subset of regions obtained by the SFFS algorithm provided the highest classification rate for all rs-fMRI maps (Table 6.3). Using fALFF, SFFS and SVM classification, we were able to demonstrate that patterns of amplitude BOLD signals in five brain regions (paracentral lobule, Rolandic operculum, olfactory cortex, lateral occipital (inferior division) gyrus, and inferior frontal (opercular) gyrus; Figure 6.2) can distinguish between metabolic states (hunger vs. satiety) with 81% accuracy.

The Rolandic operculum, which belongs to somatosensory regions, is activated during the anticipation and consumption of food [275,276], in response to palatable food receipt [277] and has been associated with the processing of high- and low-caloric food pictures [278]. Among many functions, paracentral gyrus is known to response to highly rewarding stimuli [276]. A study using independent component analysis to estimate functional connectivity (FC) parameters showed that the connectivity strength of the paracentral gyrus in the sensorimotor network was increased during hypoglycemia relative to euglycemia [170]. Furthermore, Van Duinkerken and colleagues [279]

reported that the change of sensorimotor FC was associated with basal glycemic levels in type 1 diabetes mellitus patients. Thus, the paracentral lobule seems to be part of the reward system and the sensorimotor network. The olfactory cortex (OLFC), whose activity was modulated by metabolic states as well, is involved in the experience and processing of negative affective states, including anxiety and depression [280]. Consistent with that, a rs-fMRI study in rodents demonstrated that ReHo of the OLFC is increased in stress-exposed rats compared to a control group [281]. In our study, the fasting for 36 hours might have led to a stress increase which might be reflected in an increased OLFC activity. Moreover, the satiety state might have reduced peripheral hunger signals compared to the hunger state and accordingly might have influenced brain regions related to somatosensory processes, such as Rolandic operculum, and parts of the sensorimotor network like the paracentral lobule.

The inferior frontal gyrus (IFG) has been suggested to be involved in cognitive control [282,283]. IFG activation during response inhibition has been associated with a reduced desire for food and with successful impulse regulation [284–286]. In addition, stronger IFG activity in response to orosensory stimulation was found in successful weight loss maintainers compared to people who were obese or normal weighted [287]. In our experiment, participants had to refrain from eating during the hunger state and from overfeeding during the satiety state, which may have contributed to the finding that the IFG is partially important for classifying between different metabolic states.

The lateral occipital cortex (LOC) is part of the visual association cortex and is activated in response to the perception of emotionally salient stimuli, such as food, which is thought to be a correlate of heightened attention [288,289]. For instance, a recent rs-fMRI study using SVM on graph theory analysis indicates that the LOC is partly important for classification between high-

caloric (potato chips) vs. low-caloric (zucchini) food ingestion on the brain of healthy subjects [290]. Furthermore, it has been suggested that the processing of visual salience of a stimulus depends on the affective state of the individual and the motivational value of a stimulus [288]. Considering the general role of the LOC in the visual processing of food stimuli, this region might potentially facilitate the detection/perception of such cues in a deprived state. Note that these interpretations are based on reverse inference of resting-state data and should thus be taken with caution.

However, some studies have used rs-fMRI to investigate changes in baseline brain activity of lean or obese participants during both hunger and satiety states. For instance, Lohmann et al. [27] showed increased centrality, which was measured by eigenvector centrality analysis, of anterior precuneus (APCUN) during the hunger relative to the satiety state of 22 normal volunteers. Consistent with that, our previous analysis (Chapter 5) revealed that the fALFF was increased in the APCUN and posterior cingulate cortex (PCC) when comparing hunger against satiety state. Additionally, Wright and colleagues [66] used seed-based connectivity analysis to estimate the FC parameters of 19 healthy participants. They reported that the FC between the posterior insula and superior frontal gyrus and between the hypothalamus and IFG were enhanced during the hunger state. Furthermore, it has been found that both 20 lean and 20 obese subjects had increased ReHo connectivity from hunger to the satiety state in the orbitofrontal cortex and inferior temporal lobe [291]. These studies reported different brain regions that might be related to the changes in the metabolic state compared to the results of the current study, except IFG. These inconsistencies here might be associated with the different experimental paradigms and neuroimaging modalities.

Importantly, the statistical analysis at group levels of the studies mentioned above was computed by using GLM approaches to define the significant brain regions at baseline activity that

are sensitive to changes in metabolic state. In GLM approaches, the p-values are the successful statistical tests to represent significant brain regions that show different brain activities in the average sense of one or more brain features when compare between different groups and/or experimental conditions. On the other hand, SVM classifier aims to automatically classify each subject into one of the groups or experimental design in the study. Thus, the overall classification accuracy is usually used to measure the success of the studies. In general, it is easier to demonstrate group or experimental condition differences compared to predict a single subject [292]. Furthermore, the significant variables or features that show the difference between group or experiment do not necessarily have high classification accuracy and vice versa [292,293]. Hence, brain regions that showed significant differences between hunger and satiety states in previous studies do not necessarily mean that these regions can predict the subject class with high accuracy and vice versa.

Furthermore, our results indicate that fALFF analysis is more informative than ReHo and is slightly more precise than DC for classification of resting brain changes during hunger and satiety, probably because fALFF is an index of the power of the BOLD signal. Against this, ReHo and DC parameters refer to dynamics of BOLD connectivity, either with some (in this case, 26) neighboring voxels (ReHo) or with all voxels (DC) in the gray matter of the brain.

One other important question is, whether SFFS based classification is superior to simply trying to classify states using statistically significant group differences. Baker et al. [294] answered this question on an EEG data set from AD patients, MCI patients and HC. They used an SFFS algorithm and a t-test to classify patients and found that the SFFS technique resulted in improved classification rates compared to the t-test for four feature types (average power, coherence,

correlation, and phase synchrony). They conclude that the SFFS algorithm selects reliable features for classification where statistically significant features fail in classification.

The sample size of most fMRI studies is often relatively small due to the high costs of scanning time and subject stamina [295]. However, sample size impacts the trade-off between accuracy and generalizability [296]. For instance, in the context of rs-fMRI features and SVM classification methods, several studies reported high classification accuracies (92±9%) with relatively small sample sizes (20±5 subjects per group) when classifying groups of brain disease patients and healthy subjects [253,297–302]. Here, the high classification accuracy is driven by the heterogeneity between groups [292,296]. In contrast, studies with large sample sizes are assumed to result in classification models with a higher degree of generalizability, allowing for a better prediction in samples drawn from other populations. Their classification models capture a complete picture of disease patterns but at the cost of lower accuracy, which is likely due to the within-group heterogeneity [292,296,303–305].

One limitation of the present analysis is the ability to generalize since the sample size of 24 subjects is relatively small. Accordingly, larger samples are needed to confirm our findings. However, we would like to argue that our results are not driven by the heterogeneity between samples, because we have chosen a within-subject design in a well-controlled experimental setting. Also, we evaluated whether the rs-fMRI features in conjunction with sequential feature selection strategies were sufficiently reliable to predict the subject's metabolic state by using the LOOCV scheme. Thus, independent training and testing samples were used to estimate the SVM model parameters and to validate the classification model. In this case, the CA was derived by averaging the resulting classification accuracies over all samples. All in all, the homogeneity of our samples

and the high CA results in an increased validity of our findings determining brain patterns that can discriminate between different metabolic states.

6.5 Conclusions

As rs-fMRI has received widespread attention over the past ten years, the possibility of reliable classification of disease conditions or subject states (e.g. sleep stages) paves the way for using rs-fMRI as a diagnostic tool on an individual patient/subject level. In addition, the applications mentioned in the introduction, such as the prediction of conversion of MCI to AD [254], many other diagnostic and research questions lend themselves to this approach, e.g. the differentiation of typical Parkinson's disease from atypical Parkinsonian syndromes (c.f., Tang et al. [306]). From our data, we conclude that fALFF in combination with SFFS based feature selection is a useful and straightforward way to proceed in tackling such research questions.

Chapter 7: Impact of hunger, satiety, and oral glucose on the association between plasma insulin and resting-state brain activity⁶

7.1 Introduction

Food ingestion and energy homeostasis are regulated by central nervous pathways [307–309] and modulated by endocrine signals [310]. Insulin is one of the hormones that is part of a negative feedback loop that ensures balanced energy homeostasis [84,86,311]. Of note, both intraventricular injection and intranasal administration of insulin decreases food intake and body weight in rodents [89,90] and humans [91]. In contrast, inactivation of insulin leads to opposite effects [92,93].

Task-based fMRI has been used to study the impact of insulin and glucose on brain responses to food-related stimuli under different homeostatic conditions on the network level [312,313] linking plasma glucose [7] and fasting insulin levels [314] to neural activity changes in the hypothalamus, thalamus, amygdala, insula, and superior frontal cortex, brain sites assumed to regulate appetite-related eating behavior [315]. According to Smitha et al. [50], task-based designs focus on a small fraction of the brain's overall activity only. To avoid these disadvantages in the present investigation, we used resting-state fMRI in order to reveal potential links between whole brain activity and insulin and glucose levels in different metabolic states.

Resting-state fMRI (rs-fMRI) is a task-free paradigm in which participants do not perform any specific task [29,316,317], more details can be found in Section 1.1.3. Several studies using

⁶ This chapter corresponds largely to: **Arkan Al-Zubaidi**, Marcus Heldmann, Alfred Mertins, Georg Brabant, Janis Marc Nolde, Kamila Jauch-Chara and Thomas F. Münte (2019). Impact of hunger, satiety, and oral glucose on the association between insulin and resting-state human brain activity. *Frontiers in human neuroscience*. I participated in the experiment design and data collection. I analyzed the data and wrote the manuscript.

rs-fMRI revealed associations of insulin or glucose levels with the functional connectivity (FC) of particular brain networks or brain sites that are related to homeostatic regulation but not without contradictions. Some studies reported an increase of resting-state FC within the limbic system in response to the administration of 75 g oral glucose after overnight fasting. This increase in FC was positively correlated with plasma insulin levels [46,318]. Conflicting results were found by Page et al. [172] using MRI-CBF (cerebral blood flow) during rest: here, changes of insulin levels were negatively associated with changes of CBF signals in the caudate and the putamen in response to glucose administration. Similarly, changes in plasma insulin levels in response to a meal after overnight fasting were negatively correlated with changes of CBF signals in the insula and prefrontal cortex [212]. Additionally, the FC between the posterior insula (PINS) and superior frontal gyrus (SFG) under hunger conditions was partially moderated by the plasma glucose levels, indicating that the PINS connectivity depends on the homeostatic energy deficit caused by fasting [66]. Furthermore, a study with experimentally induced hypoglycemia reported increased FC of the default mode network (DMN) with the posterior cingulate cortex (PCC) and decreased FC of the insula, superior and inferior frontal gyri with temporal networks, basal ganglia, and cerebellum in healthy subjects [170]. The inconsistencies reported here might be related to the different experimental paradigms and neuroimaging modalities. In most of these studies, FC parameters were computed by using seed-based analysis or independent component analysis (ICA) to define brain networks of interest or to decompose the brain into multiple networks, respectively. This means that FC studies rely on the correlations and ignore the changes in regional brain activity under different metabolic conditions. However, it has been shown that there is a linear relationship between the amplitude of the BOLD signal and brain metabolism [179]. Therefore, in our study, we used the amplitude of the rs-fMRI signal to investigate the sensitivity of resting-state brain

activity [101] to changes in metabolic states. A critical question of the present search is, whether or not the changes in the amplitude of the BOLD signal of specific brain regions are associated with changes in hormonal signals, such as insulin.

To clarify some of the issues discussed in the previous paragraph, we investigated (i) whether changes in brain regions linked to hypoglycemia, such as the default mode network, are modulated by insulin and glucose or different metabolic states and (ii) whether changes in activity of specific brain regions, such as hypothalamus and insula, are modulated by changes of blood insulin or glucose levels after glucose administration. In the present investigation, we used a voxel-wise frequency-domain approach to measure whole brain activity by using amplitude (intensity) values of BOLD signals called fractional amplitude of low-frequency fluctuation (fALFF) for each individual per condition [101]. The fALFF allow us to study the local spontaneous brain activity across the whole brain based on the magnitude of the BOLD signal in the low-frequency range [101,319] which is higher in gray than in white matter [134]. The fALFF approach efficiently suppresses non-specific signal components, such as physiological noise [101,184]. Other studies have observed that fALFF is associated with body mass index (BMI) after intranasal insulin application [315].

In Chapter 5, we examined the activity and connectivity brain responses to the interaction of metabolic state (hungry vs. satiated) and glucose administration (before vs. after administration of 75 g of oral glucose). In that Chapter, we used multimethod rs-fMRI approaches to identify brain activation patterns that are associated with changes in metabolic states and caloric intake. We showed that in contrast to other voxel-wise analyses like regional homogeneity or degree of centrality, fALFF is a more sensitive metric for identifying differences in the resting brain activity, for example, the amplitude of the SFG and PCC were increased after oral glucose treatment and

in hunger conditions, respectively. However, Chapter 5 focused on the effect of glucose treatment solely on brain activity and connectivity without taking the impact of plasma glucose and insulin levels into account when analyzing neuroimaging data. To get a better insight into hormone-dependent brain activity at rest, in the present analysis we used multiple linear regression analysis (MLRA) with covariates (plasma insulin and glucose levels) to investigate the dependencies between brain activities, measured as the amplitude of the BOLD signal, and hormone levels. By manipulating metabolic state (hunger/satiety) and glucose administration (before and after 75 g of oral glucose) in a factorial design, we tested the hypothesis that brain areas involved in homeostatic regulation are modulated by peripheral circulating insulin and glucose levels [3,320,321].

7.2 Materials and methods

To study the interplay of metabolic state (hungry vs. satiated) and glucose administration (including hormonal modulation) on brain function, rs-fMRI and blood samples were obtained in 24 healthy normal-weight men in a repeated measurement design. Participants were measured twice: once after a 36 hours fast (except water) and once under satiation (three meals/day for 36 hours). During each session, rs-fMRI and hormone concentrations were recorded before and after a 75 g oral dose of glucose. As reported in Chapter 2, nine blood samples on the first day and ten blood samples on the second day per subject and condition were collected. The blood samples of the second day were potentially a valuable source of information because they were taken before and after glucose administration. Figure 7.1 shows the time course of the mean concentrations of plasma glucose and insulin on the second day of the experiment for hunger and satiety states.

Details on the exclusion criteria of participants, the exact timing for obtaining blood samples and the preprocessing pipeline of rs-fMRI images can be found in Chapter 2. Furthermore, fALFF maps of each subject per experimental condition were calculated as mentioned in Chapter 4.

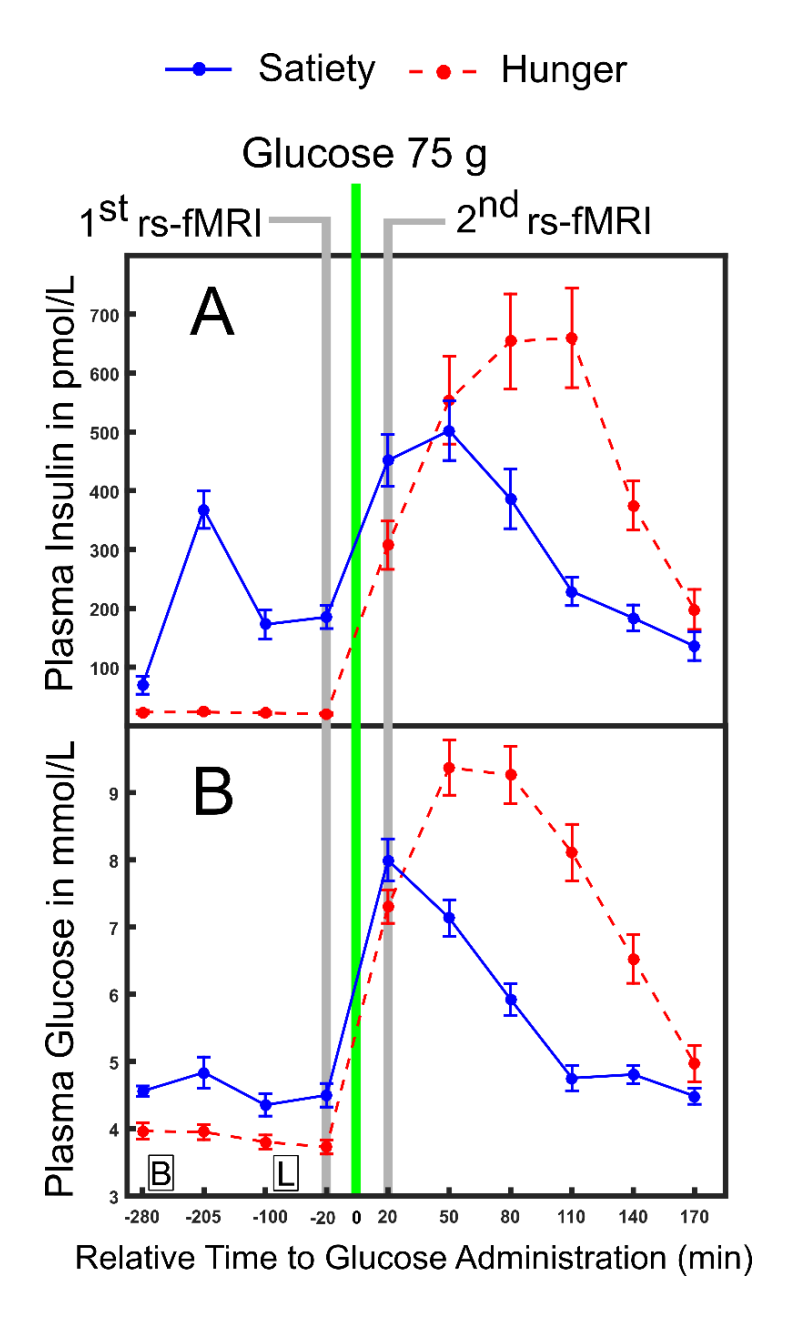


Figure 7.1: Time course of physiological parameters on the second day of the experiment for different metabolic states.

Mean plasma concentration of insulin (A) and glucose (B) under hunger and satiety conditions. Glucose administration was ingested at time point 0. The time-points of the first and second fMRI investigations are marked in gray. Boxes on the bottom of the graph indicate the time points of meals on the second day (B = breakfast, L = lunch at 09:00 am and 12:00 pm, respectively). The error bars represent the standard deviation.

7.2.1 Statistical analysis

To capture the modulatory impact of glucose administration on the association between the activity of brain regions and plasma insulin or glucose levels under different metabolic states, we performed two multiple linear regression analyses (MLRA) using SPM12, the first "before" and the second "after" oral glucose treatment. Each MLRA was designed with two covariates (plasma insulin and glucose levels). Briefly, MLRA is used to describe how a 'linear combination' of multiple variables, called independent or explanatory variables, to predict a single response variable, referred to as the dependent or target variable. The contribution of each independent variable to the model is assessed by looking at the regression coefficients [322].

In this Chapter, we used MLRA to figure out the contribution of plasma insulin (an independent variable) to the prediction of brain activity (the dependent variable) when taking the effect of plasma glucose (another independent variable) into account [323,324], and vice versa. Accordingly, our multiple linear regression model is:

$$Y_j = \mu + x_{j1}\beta_1 + x_{j2}\beta_2 + \epsilon_j, \tag{7.1}$$

where Y_j is a dependent variable (such as fALFF at a particular voxel) and j=1,...,J indexes the observation. The regression coefficient μ represents a constant term (the mean of the dependent variable when all predictors are zero), while β_1 represents the regression slope, which quantifies the association of Y with x_1 (such as plasma insulin), adjusting for the effect of x_2 (plasma glucose) on Y and vice versa for β_2 and ϵ is the error associated with the regression (the variance of the dependent variable from its mean when all predictors are zero). The parameters were estimated by using the least squares method. To find significant voxels whose activity was affected by hunger vs. satiety or by glucose or insulin, we used one-sample t-tests for each regression coefficient on the voxel level per MLRA (see the section below). The resulting statistics indicate whether the

regression coefficient of a particular voxel is significantly different from the error in that estimate [324]. To correct for multiple comparisons, the topological false discovery rate (FDR) q=0.05 was employed with a cluster defining threshold of p<0.001 for the t-tests [325].

In the 1st MLRA (before glucose administration), we contrasted hunger vs. satiety states while controlling the moderating fluctuation of glucose and insulin. We calculated differences (delta (Δ) =hunger-satiety) of fALFF maps before oral glucose treatment. For glucose and insulin, the area under the concentration-time curve (AUC) of the first four samples (Figure 7.1A and B) was calculated and the Δ of the AUC was obtained. The AUC has been used as an index to assess the regulation of glucose and insulin [326,327]. It was calculated using the standard trapezoid method, which is computing the AUC with respect to ground, see Formula 2 in [328]. The group level analysis was performed using Δ AUC of glucose and insulin as covariates (independent variables) and the Δ fALFF maps as the dependent variable in the MLRA. Notably, the Δ AUC of glucose and insulin were not significantly correlated (|r|=0.3, p=0.1). To check whether the AUC of plasma glucose and insulin influence our findings, we also recomputed the 1st MLRA by including the Δ plasma glucose and insulin based on the value 20 min before glucose ingestion (Figure 7.1) as independent variables. The results of this model were similar to the results of the model with AUC (see Table 7.1 and Figure 7.2). The AUC provides an overview of plasma glucose and insulin level profiles under diet or standard meal versus time [103]. Also, we believe that the changes in brain activity before glucose ingestion may be related to profile change more than single glucose and insulin values. Therefore, we will report the AUC model results only.

The 2^{nd} MLRA (after glucose administration) had a similar design as first MLRA. Differences (Δ) of amplitude rs-fMRI signals were calculated by subtracting the fALFF maps of hunger condition from satiety condition. The Δ calculated for glucose and insulin was based on

the value 20 min after glucose ingestion (Figure 7.1) only to keep the temporal association of endocrine and functional imaging data as clear as possible. Δ glucose and Δ insulin were used as covariates in the MLRA. Again, glucose and insulin were not significantly correlated (|r|=0.14, p=0.5). Additional glucose and insulin samples collected after oral glucose intake were not included in this analysis, because they were taken after the second rs-fMRI recording.

To ensure that the correlation between specific brain regions and glucose or insulin values is not biased [329], we extracted fALFF values by averaging across voxels in each cluster that survived the cluster-significance test. Then, we performed the leave-one-out cross-validation (LOOCV) of Pearson correlation to evaluate the relationship between averaged Δ fALFF values of each brain region with Δ of the plasma glucose and insulin. Finally, we performed full and partial correlation analyses between clusters linked to plasma insulin levels to investigate the association between them and the effects of glucose and insulin values on that association.

Finally, to investigate the acute effect of glucose administration on the interaction between brain activity and physiological changes, we performed two additional MLRA. The 3rd and 4th MLRAs estimate the correlations between changes in fALFF (Δ fALFF= pre-post glucose ingestion) and changes in plasma glucose/insulin (Δ of plasma glucose/insulin were calculated based on the value of 20 min before and after glucose ingestion; Figure 7.1) under satiety and hunger conditions separately, respectively.

We used the automated anatomical labeling (AAL) atlas [102] included in the xjView toolbox (http://www.alivelearn.net/xjview8) to label the anatomical location of significant clusters. Thalamic nuclei were identified by applying the MNI-based Morel Atlas [194].

We also ran a Pearson correlation analysis to investigate the associations between changes of the subjective feeling of hunger with changes plasma glucose and insulin as well as with changes brain activity (i.e. clusters that survived the cluster-significance test).

7.3 Results

7.3.1 Resting state fMRI: hunger vs. satiety effects

The 1st MLRA (before glucose administration) revealed differences of resting brain activity as a function of hunger in the posterior cingulate cortex (PCC) and the left anterior precuneus (PCUN), as well as in the left inferior parietal gyrus (IPG; Figure 7.2A and B, Table 7.1). The 2nd MLRA (after glucose administration) showed an increase of the fALFF signal in the hunger compared to the satiety condition in the left thalamus and the left PCC (Figure 7.2C and D, Table 7.1).

7.3.2 Resting state fMRI: before vs. after glucose treatment

The 3rd (under satiety condition) and 4th (under hunger condition) MLRA results showed that the resting brain activity of supplementary motor area (SMA) was significantly decreased after glucose ingestion (Figure 7.3A and B, Table 7.2). In the hunger condition (4th MLRA), a reduced resting brain activity was evident in the precentral gyrus (PreCG) and the postcentral gyrus (PoCG) after glucose administration (Figure 7.3B, Table 7.2).

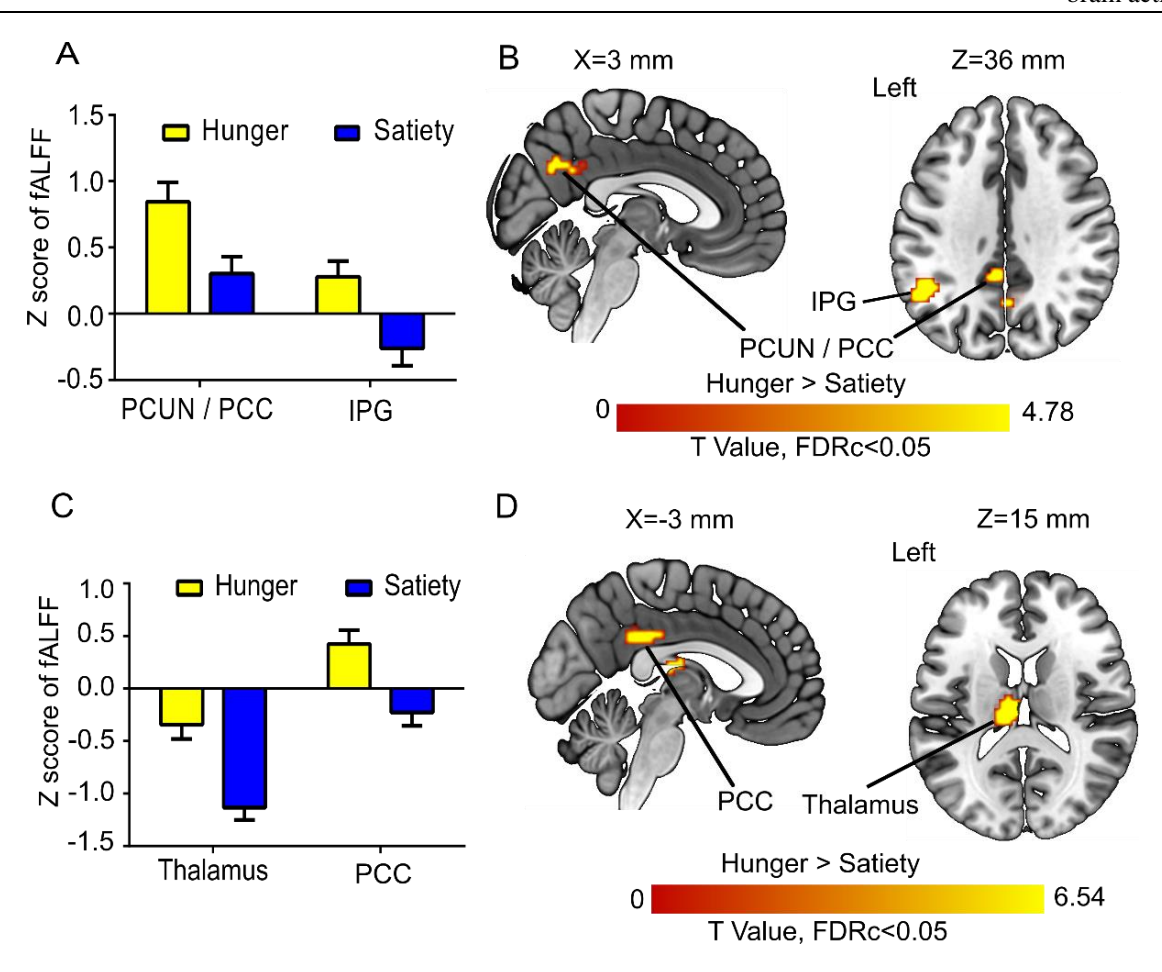


Figure 7.2: Hunger vs. satiety effects on brain activity.

(A) Mean fALFF value of all voxels of a significant cluster per condition across participants. (B) Results of the first model (before glucose administration). (C) Mean fALFF value of all voxels of a significant cluster per condition across participants. (D) Results of the second model (after glucose administration). Abbreviations: PCC: posterior cingulate cortex; PCUN: precuneus. IPG: inferior parietal gyrus.

Table 7.1: Changes and associations of fALFF with food conditions and hormone levels.

Regions	Hes.	p(adj.)	K	T value	Local maxima (x y z) (mm)					
Before glucose administration: hunger > satiety										
Inferior parietal gyrus	L	0.03	24	4.78	-45	-51	36			
Inferior parietal gyrus	L			4.51	-51	-57	36			
Posterior cingulate cortex	L	0.01	34	4.70	-6	-45	36			
Posterior cingulate cortex	L			4.16	0	-48	30			
Precuneus	R			4.04	9	-54	30			
After glucose administration: hunger > satiety										
Thalamus	L	0.001	55	6.54	-3	-21	15			
Thalamus	L			5.18	-12	-21	15			
Thalamus	L			4.86	-9	-33	5			
Posterior cingulate cortex	L	0.002	45	5.68	0	-33	33			
Posterior cingulate cortex	L			4.42	-9	-33	33			
Correlations between changes in physiological and neural of metabolic										
states(hunger-satiety), after glucose administration										
Positive correlation with plasma glucose levels										
Fusiform gyrus	L	0.04	25	4.07	-42	-63	-12			
Fusiform gyrus	L			4.05	-27	-72	-15			
Fusiform gyrus	L			3.39	-33	-66	-15			
Negative correlation with plasma insulin levels										
superior frontal gyrus	L	0.04	19	5.50	-12	21	63			
superior frontal gyrus	L			4.47	-15	15	57			
superior frontal gyrus	L			3.99	-6	33	57			
Posterior insula	L	0.004	19	4.39	-33	-9	9			
Posterior insula	L			4.31	-36	-21	9			

Notes: The table shows three local maxima (MNI coordinates) more than 8.0 mm, the adjusted (adj.) p-values are reported at p<0.001 (height threshold) and q<0.05 (FDR extent threshold). T=peak of T values. K=cluster size. Hes. =hemisphere. L=left. R=right.

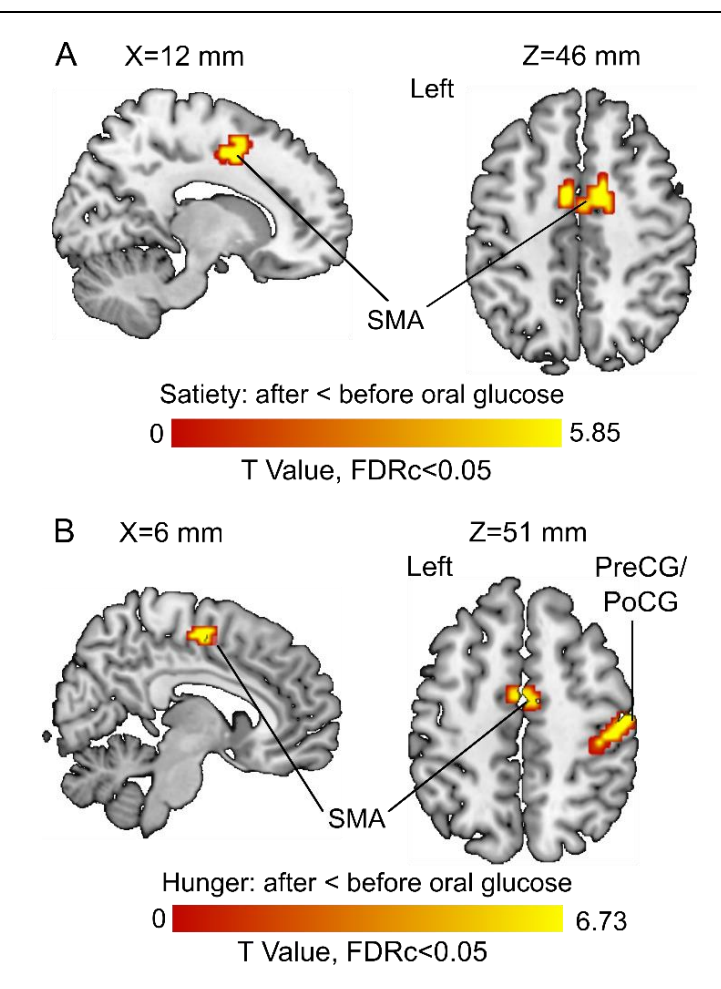


Figure 7.3: Before vs. after glucose administration on brain activity.
(A) Results of the third model (under satiety condition). (B) Results of the fourth model (under hunger condition). Abbreviations: SMA: supplementary motor area; PreCG: precentral gyrus. PoCG: postcentral gyrus.

7.3.3 Correlations between physiological and neural effects

For the 1st, 3rd and 4th MLRAs, we found no correlation between changes in resting brain activity and changes in glucose and insulin passing the correction for multiple comparisons.

For 2nd MLRA (i.e. hunger-satiety), after glucose administration and while controlling for effects of Δ insulin we found a correlation between Δ fALFF and Δ plasma glucose in the left fusiform gyrus (Figure 7.4A and B, Table 7.1). A LOOCV between the average Δ fALFF values of the

fusiform cluster and Δ plasma glucose after data being adjusted for Δ plasma insulin level (Figure 7.4C) revealed a significant positive correlation (r=0.75).

Table 7.2: Influences of oral glucose administration on brain activity under hunger and satiety conditions

Regions	Hes.	p(adj.)	K	T value	Local maxima (x y z) (mm)					
Satiety condition: after oral glucose < before oral glucose										
Supplementary motor area	L	0.003	39	5.85	-3	-18	54			
Supplementary motor area	R	< 0.001	86	4.77	12	3	45			
Supplementary motor area	L			4.63	-6	3	48			
Hunger condition: after oral glucose < before oral glucose										
Postcentral gyrus	R	< 0.001	136	6.73	51	-18	51			
Precentral gyrus	R			5.61	30	-6	69			
Precentral gyrus	R			5.49	36	-15	66			
Precentral gyrus	L	< 0.001	51	6.60	-24	-12	69			
Supplementary motor area	L	< 0.001	58	5.52	-3	-6	54			
Supplementary motor area	R			4.88	6	-15	54			

Notes: The table shows three local maxima (MNI coordinates) more than 8.0 mm, the adjusted (adj.) p-values are reported at p<0.001 (height threshold) and q<0.05 (FDR extent threshold). T=peak of T values. K=cluster size. Hes. =hemisphere. L=left. R=right

Next, when controlling for Δ plasma glucose we found a connection between Δ fALFF and Δ plasma insulin after glucose administration in the left posterior insula and superior frontal gyrus (SFG; Figure 7.5A and B). A significant negative correlation (r=-0.7) was found between average Δ fALFF of the posterior Insula cluster and Δ plasma insulin (Figure 7.5C; red dots and line), as well as a significant negative correlation (r=-0.8) between average Δ fALFF SFG and Δ plasma insulin (Figure 7.5C; blue dots and line).

A potential influence of plasma insulin and plasma glucose on the association between Δ fALFF posterior insula and Δ fALFF SFG was tested by using the average Δ fALFF in these clusters and revealed a significant positive correlation (r=0.5, p=0.004, Figure 7.5D) which

survived when adjusting for Δ plasma glucose(r=0.5, p=0.004, Figure 7.5E) but not when adjusting for Δ plasma insulin level (r=-0.06, p=0.7, Figure 7.5F).

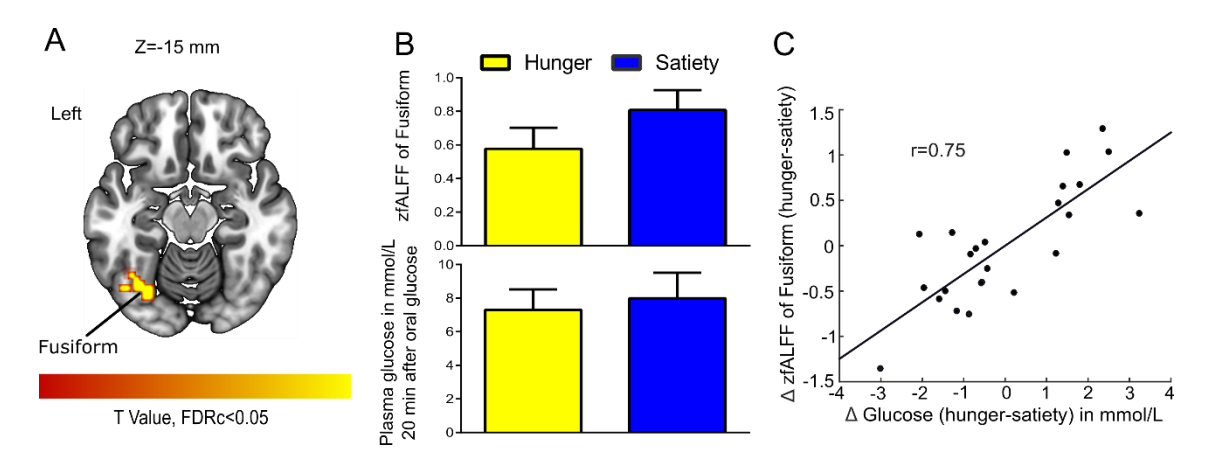


Figure 7.4: Glucose-associated low-frequency BOLD fluctuations.

(A) The Δ (hunger-satiety) of fALFF in Fusiform connected with Δ glucose plasma after glucose administration. The statistical image was assessed for cluster-wise significance using a cluster defining threshold p<0.001, 0.05 FDR corrected at the cluster level. (B) Amplitude of BOLD signal in the fusiform gyrus and plasma glucose levels in the hunger and satiety states. (C) The LOOCV showed that a positive correlation (r=0.75) between the average Δ fALFF value of fusiform cluster and Δ plasma glucose, adjusted for Δ plasma insulin level. LOOCV: leave-one-out cross-validation.

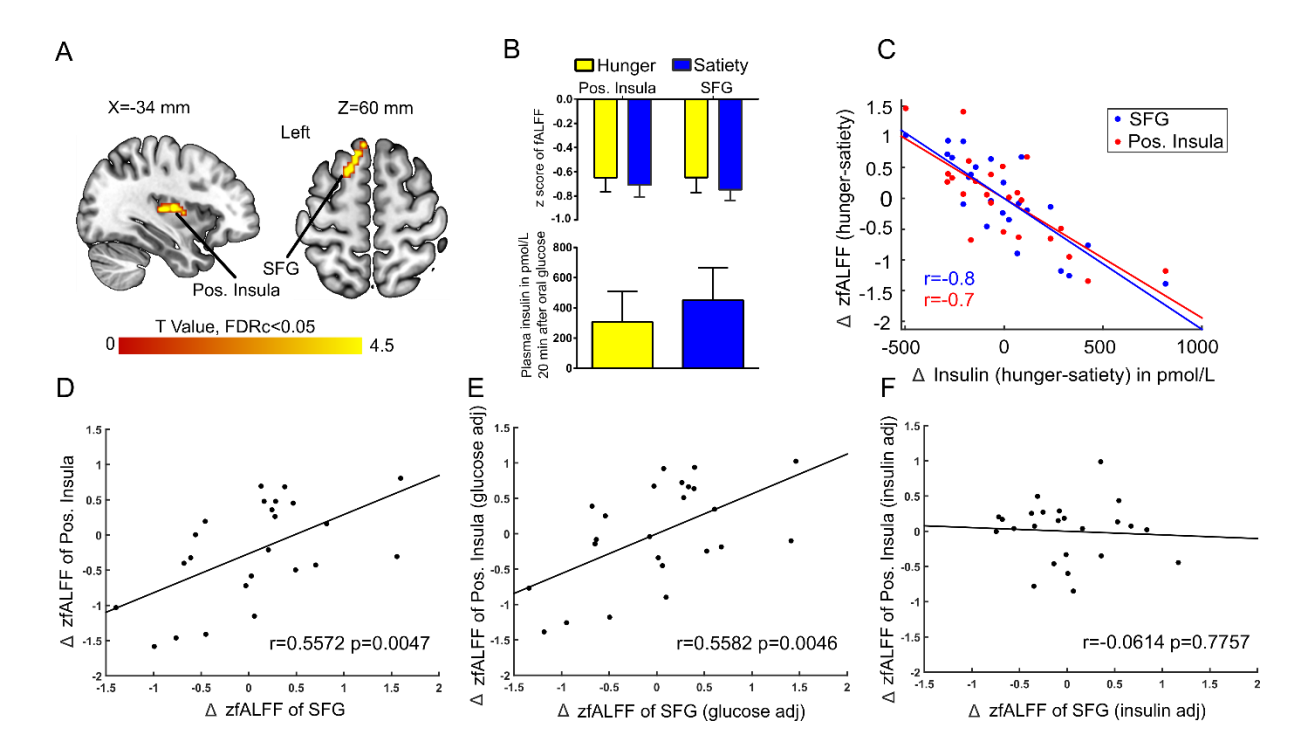


Figure 7.5: Insulin-associated low-frequency BOLD fluctuations.

(A) The Δ (hunger-satiety) of fALFF in the left posterior (pos.) insula and superior frontal gyrus (SFG) connected with Δ plasma insulin after glucose administration. The results were assessed for clusterwise significance using a cluster defining threshold p<0.001, 0.05 FDR corrected at the cluster level. (B) SFG and pos. insula amplitude values of the BOLD signal and plasma insulin levels in the hunger and satiety states. (C) Scatter plot of the correlation between Δ plasma insulin and average Δ fALFF value of left pos. Insula (LOOCV of r=0.7; red dots and line) and left SFG (LOOCV of r=0.8; blue dots and line), adjusted for Δ plasma glucose level. (D and E) Represent a significant positive correlation between the average Δ fALFF values of left pos. Insula and left SFG when the data was either not adjusted or adjusted for Δ plasma glucose, respectively. (F) The correlation between the average Δ fALFF value of left posterior Insula and left SFG was no longer significant when the data were adjusted for Δ plasma insulin level, which suggests the effects were driven by plasma insulin. LOOCV: leave-one-out cross-validation.

In addition, we found no significant correlations between subjective feeling of hunger with changes plasma glucose and insulin as well as with changes brain activity (i.e. clusters that survived the cluster-significance test). These results are shown in Figure 7.6.

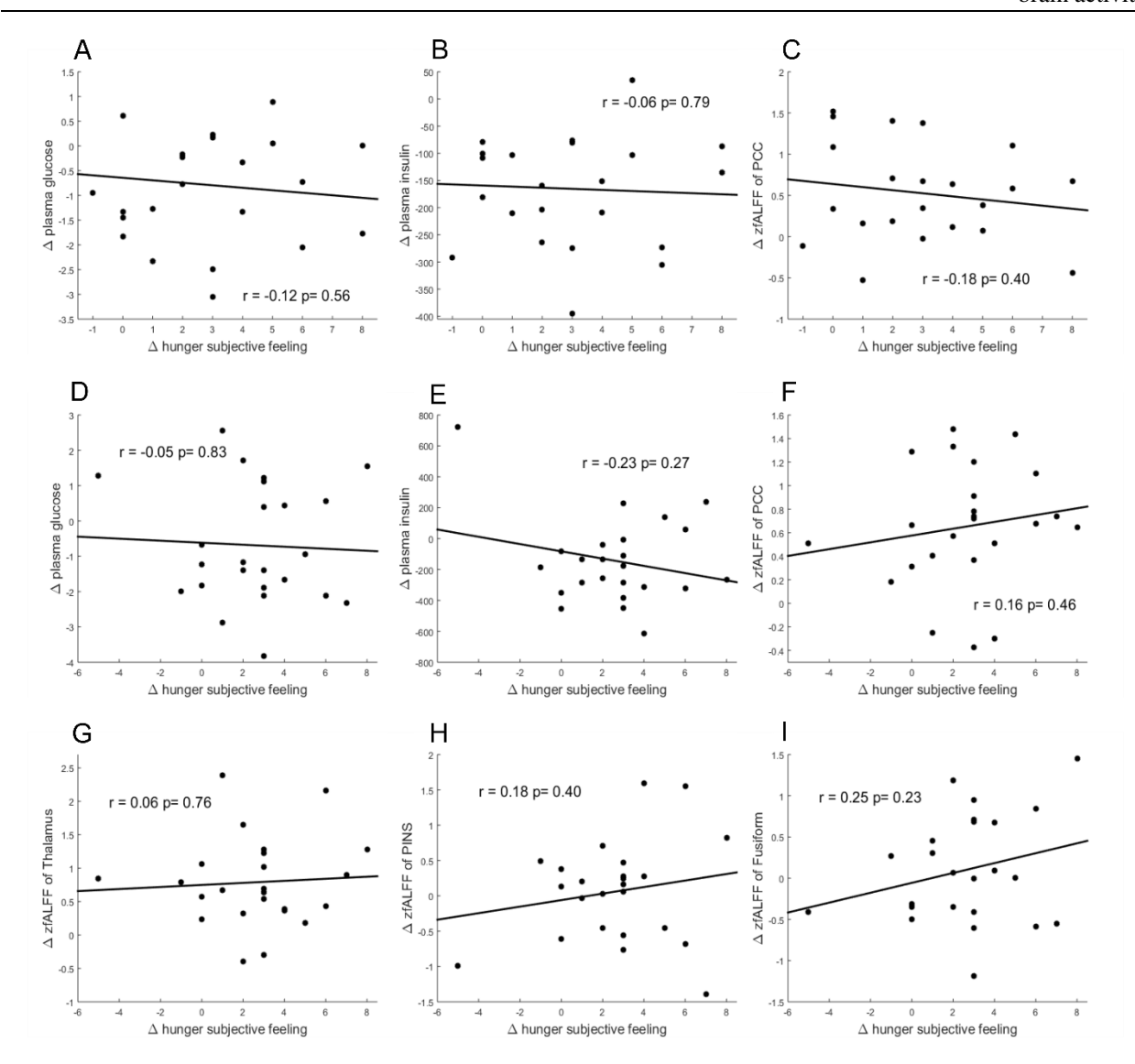


Figure 7.6: Scatter plots illustrate the correlations between changes subjective feeling of hunger with changes plasma glucose and insulin as well as with changes in brain activity (i.e. clusters that survived the cluster-significance test).

(A)-(C) represent the associations before glucose administration. (D)-(I) represent the associations after glucose administration. Δ refers to the difference between hunger and satiety.

7.4 Discussion

As mentioned in Chapter 3, plasma glucose and insulin levels differed between hunger and satiety conditions and were also differentially influenced by glucose administration (Figure 3.1).

In the present chapter, we investigated the interaction of hunger and satiety with plasma glucose and plasma insulin levels before and after glucose administration and explored this interaction's impact on changes in resting state fMRI. We used fALFF, a measure reflecting the temporal fluctuation of the BOLD signal, to study neural activity and connectivity. Multiple linear regressions analyses (MLRA) with two covariates (glucose, insulin) was used to assess the moderating influence of these covariates on the differences between hunger and satiety conditions.

The analyses of the fALFF data revealed an increased BOLD signal amplitude in the posterior cingulate cortex in hunger relative to satiety that was independent of glucose and insulin plasma levels. Brain activity reflecting the difference between hunger vs. satiety was modulated by changes in glucose and insulin plasma levels in fusiform and PINS after oral glucose intake, respectively.

7.4.1 Resting-state fMRI: hunger vs. satiety effects

The amplitude of the rs-fMRI signal was increased for hunger vs. satiety in the left inferior parietal gyrus (IPG) before oral glucose treatment and in the posterior cingulate cortex (PCC) before and after oral glucose treatment (Figure 7.2). Several studies using visual stimuli showed the enhanced activity of IPG,PCC, precuneus and insula during food choice vs. non-food choice under hunger conditions [209,330]. Moreover, PCC and precuneus are core hubs of the default mode network (DMN) [91,211]. The DMN is activated during the rs-fMRI paradigm and deactivated during task-based fMRI, when attention is oriented towards internal rather than external stimuli [34,331]. In line with that, the DMN, especially in the PCC, has been shown to be involved in self-referential processes [210]. A study using ICA approach to investigate the FC of obese/overweight subjects found a reduction of DMN activity associated with a decrease in hunger ratings and fat mass after six months of exercise [171]. In the current experiment, the increased fALFF in PCC region seems to be driven by metabolic state (hunger vs. satiety; Figure 7.2) independently of changes in the plasma glucose and insulin levels. Consistent with our results, DMN activity has been shown to

be positively correlated with lower blood glucose levels [170] and with hunger ratings [171]. Our findings in the current and previous chapter about increased activation of the DMN (i.e. PCC) under hunger condition might be indicative of increased self-focus during food deprivation.

We found a significant increase of fALFF in the left mediodorsal thalamus under hunger conditions and a decrease in satiety after (but not before) glucose treatment indicating an interaction between metabolic state and glucose administration in this region. Thalamic brain activity has been reported to vary as a function of hunger [212,213], ghrelin application [214] and glucose infusion [70,215]. A previous study [48] reported a positive correlation between fasting levels of ghrelin and thalamic reactivity to food images, though this effect was not further modulated by glucose intake (75 g glucose). The thalamus is central for the integration of proprioceptive information stemming from the gastrointestinal (GI) tract [70,216]. Specifically, afferent information from this tract reaches the thalamus via the vagus nerve [217]. Consistent with this observation, Rolls [207,218] postulated that the mediodorsal thalamus impacts short-term eating behavior. Our results agree with these proposals in that mediodorsal thalamus activity is partly dependent on metabolic state and associated with glucose metabolism.

7.4.2 Resting state fMRI: before vs. after glucose treatment

FALFF was lower in the left SMA after glucose ingestion (Figure 7.3). The SMA is crucial for planning movements [195,196] and observation of actions [197]. The response to glucose ingestion in the form of lower activity in the SMA could potentially lead to suppressed action planning or initiation because of an alteration in the available energy resources of the body. Therefore, plasma glucose might affect brain regions controlling attention, food evaluation and motor planning. Further research is needed to back up this interpretation in the form of task-related

fMRI or behavioral studies that show such functional differences in dependency of blood glucose levels.

7.4.3 Correlations between physiological and neural effects

We observed that changes in plasma insulin levels (hunger vs. satiety) after oral glucose administration were negatively associated with changes in the amplitude of the BOLD signal in the left PINS and the left SFG). Furthermore, we found a significant positive correlation between left PINS and left SFG when the Δ fALFF values were adjusted for the Δ plasma glucose, while this relationship disappeared when the Δ fALFF values were adjusted for the Δ plasma insulin (Figure 7.5). In contrast, changes in plasma glucose levels were positively correlated with changes in the fALFF in the left fusiform after oral glucose administration (Figure 7.4). The PINS is involved in sensory, motor and interoception taste intensity [208,332–334] but is also activated during hunger [212], during food craving [335], and on receiving an appetitive drink [336]. The SFG is activated in response to appetitive stimuli in fasted subjects [199,200], and it is frequently involved in inhibiting approach behavior towards food [337–339]. The fusiform gyrus harbors high-level visual processes (e.g. face recognition [340]) but has been shown to be activated in the response of food cues after glucose administration [341], to high vs. low caloric food pictures in lean subjects [7], and as a function of increasing hunger [213].

Our data showed that oral glucose administration modulates the insulin-dependent association between PINS and SFG, as well as the association between left fusiform gyrus activity with plasma glucose. Our results suggest that the fusiform, PINS, and SFG activity is modulated by an intricate interplay of glucose and insulin levels, most likely to regulate ingestive behavior by differential engagement of attentional, executive and effective processes.

These findings dovetail nicely with results from rs-fMRI studies demonstrating that body weight and insulin levels influence the functional connectivity within and between cognitive and homeostatic brain regions [315,318].

One limitation of the current analysis is the correlation analysis after glucose administration was only performed with endocrine data narrowly associated with the fMRI data collection to keep this connection as clear as possible. This Chapter focused on revealing correlations between plasma insulin and glucose concentrations and brain activity under different metabolic states. To strengthen these results, future studies might employ a longitudinal design with multiple fMRI sessions during the course of the fasting and control conditions and collection of the endocrine data. If the shown correlations persist or build up in a sensible way over time, these results would be a strong contribution to the correlational findings of this study. As this study was designed to confirm findings of other studies and show the validity of these potential correlations in a physiological setting with an oral glucose intake intervention we only performed two fMRI sessions. To establish a causal relationship in contrast to our correlational findings, an experimental manipulation using insulin clamp and/or glucose clamp techniques is needed.

7.5 Conclusions

Our results suggest that plasma glucose and insulin respond similarly to oral glucose intake (Chapter 3) depending on metabolic states (hunger vs. satiety) and that these responses are related to different neural processing in the brain (Chapter 7). Changes in plasma glucose were associated with changes of activation patterns in the fusiform gyrus, while changes in plasma insulin enhanced connectivity between the posterior insula and superior frontal gyrus when added as a covariate in the multiple linear regression analysis, indicating that changes in plasma insulin levels were at least partially responsible for the augmented connectivity. This connectivity appears to be

related to alleviating an acute hemostatic energy deficit. This connectivity appears to be related to alleviating an acute hemostatic energy deficit. These results contribute to identifying the neural mechanisms through which insulin regulates food intake [38]. All in all, our findings expand existing neural models of homeostatic energy and highlight the complex nature of food intake and hormone-relationships in humans.

Chapter 8: Effect of hunger, satiety and oral glucose on the effective connectivity between hypothalamus and insular cortex⁷

8.1 Introduction

Food intake in humans is determined and affected by non-homeostatic (i.e. external) factors, such as the social situation and time, and homeostatic (i.e. internal) factors related to the body's energy needs, such as hunger and starvation [1,342,343]. However, controlling food intake and energy homeostasis under different metabolic states (hunger vs. satiety) is remarkably complex in humans, since it is influenced by the interaction of the endocrine system and brain structures involved in monitoring proprioceptive signals [1,4,64]. Interactions between brain function and body energy homeostasis can be further altered by various pathophysiological conditions such as increased blood lipids in obesity [344–346]. For instance, in overweight subjects, body mass index (BMI) and insulin levels are associated with variations in neural of resting-state functional connectivity (FC) after an overnight fast [318]. Furthermore, FC imbalance between brain regions associated with impulsivity (i.e. inferior parietal lobe), response inhibition (i.e. frontal pole) and reward (i.e. nucleus accumbens) is correlated with increased food approach behaviors and obesity in children [347]. Nevertheless, FC captures purely correlational relationships between the two regions and does not yield information with regard to the direction of influences. Therefore, studying how the directed connectivity within brain networks involved in homeostatic regulation

⁷ This chapter corresponds largely to: **Arkan Al-Zubaidi**, Sandra Iglesias, Klaas E. Stephan, Macià Buades-Rotger, Marcus Heldmann, Janis Marc Nolde, Henriette Kirchner, Alfred Mertins, Kamila Jauch-Chara and Thomas F. Münte. Effects of hunger, satiety and oral glucose on effective connectivity between hypothalamus and insular cortex. *In revision at NeuroImag*. I participated in the experiment design and data collection. I analyzed the data and wrote the manuscript.

is modulated by physiological (metabolic) states would constitute an important step forward to understanding the neural control of food intake.

The hypothalamus was identified as a core node of homeostatic networks many decades ago [348–351]. It is linked, at both the structural and functional levels, with brain regions, such as the insula, thalamus, prefrontal cortex and brainstem, which are involved in controlling the homeostatic energy balance [352–357].

The insular cortex is a heterogeneous and complex area that has been linked to diverse processes including motivation, reward and emotion [333,358,359]. However, its functions also include the processing of external sensory (e.g. gustatory) information [360,361], and is therefore thought to represents an interface between homeostatic and hedonic processes controlling food intake [351,362,363]. The insula is also proposed to be a hub linking multiple large-scale brain systems [358]. Macroscopically, it is divided into the anterior/agranular insula (AINS) and the posterior/granular insula (PINS) in humans [333,364], rats [358,365] and non-human primates [366,367].

Both hypothalamus and insular cortex respond to hunger- and satiety-inducing signals [63–66]. For instance, whilst hunger increases activity of the hypothalamus [59], satiety exerts suppressive effects on the hypothalamic signal, as occurs after exogenous glucose or insulin administration, [67–71]. However, most of brain imaging studies used a typical resting-state fMRI (rs-fMRI) approach to investigate the FC between seeds (i.e. hypothalamus, AINS and PINS) and brain areas involved in appetite regulation [60,66,368,369] and thus cannot clarify the directionality of connections between these regions. For example, a study using seed-based analysis to investigate the effect of fasting and satiation on FC of healthy subjects found an

enhancement of FC between the posterior insula and superior frontal gyrus, and between the hypothalamus and inferior frontal gyrus after overnight fasting [66].

Much of our understanding on how the central nervous system governs ingestive behavior is based on experiments in rodents, which has proven especially fruitful to uncover functional sub specializatzions within the hypothalamus [370]. However, the markedly larger and more gyrified neocortex observed in humans [371] complicates direct comparisons in cortical processing between humans and rodents. Non-human primates offer a more valid animal model with which to delineate the neural architecture of appetite regulation. Indeed, convergent evidence from studies in non-human and human primates suggests a highly conserved architecture underlying the neural processing of food. Specifically, the AINS -which contains the primary gustatory cortexappears to code for the physical properties of food (i.e. texture, temperature), whereas the orbitofrontal cortex (OFC) tracks the subjective pleasantness of flavors and smells [207]. Subcortical areas such as the hypothalamus or the brain stem do not seem to be involved in these evaluative processes to the same degree. Rather, these structures receive interoceptive information signaling hunger and satiety [207,372,373]. This information is then relayed through the PINS towards the AINS and from there to orbitofrontal areas, where subjective valuation of the organisms' metabolic state presumably takes place [374–376].

There is thus a hierarchical structure by which proprioceptive information reaches the hypothalamus and becomes increasingly elaborated in the insular cortex, where it is integrated with external inputs and forwarded to the OFC. Despite the similarity of this circuit between apes and humans, the enlarged relative size and folding of frontal and temporal lobes in humans intrinsically limits generalization across species [377]. Moreover, human ingestive behavior is more strongly governed by non-homeostatic (i.e. external) factors, and thus animal models might

not suffice to capture complex processes that go beyond rudimentary affective states such as joy or fear [378].

Finally, it is unclear how metabolic states affect the effective connectivity (EC), between these regions. To fill this research gap, we applied dynamic causal modeling (DCM) to infer effective (directed) connectivity on latent (hidden) neuronal states from measured brain data using predefined models [145] in a study that manipulated metabolic state (hunger vs. satiety) and energy availability (before and after glucose administration) in healthy young men. DCM can be used to gather evidence favoring one network model (hypothesis) over other models and to understand how nodes (i.e. brain regions) might influence each other [146]. With a DCM variant called spectral DCM (spDCM) it has become possible to examine the intrinsic connectivity in rs-fMRI data [147]. Spectral DCM uses a Bayesian procedure to estimate the strengths of endogenous connectivity in the absence of (known) external perturbations like tasks or stimuli.

In a previous analysis of the same data set, we observed reduced FC in AINS after glucose application during both hunger and satiety, see Chapter 5. Furthermore, we found that increases in plasma insulin levels between hunger and satiety were negatively related to PINS activity after glucose administration, see Chapter 7.

In the present investigation, we first used spDCM to estimate the EC parameters for each participant and experimental condition (hunger vs. satiety, before vs. after glucose administration) using rs-fMRI data. Subsequently, we applied Bayesian model selection (BMS) [163] to determine the most plausible model in each condition from a set of competing hypotheses (i.e. models). Finally, we performed an analysis of variance (ANOVA) on estimated neural parameters to test whether the estimated connection strengths between hypothalamus, PINS and AINS are affected by the metabolic states and glucose treatment. We hypothesized increased forward information

flow in the hypothalamus-PINS-AINS network during fasting relative to satiety, in line with studies showing enhanced hypothalamic activity [59] and coupling with frontal structures [66] in a hunger state. We further speculated that glucose administration would act as a transient satiety signal [67–71] and hence reduce the strength of these forward connections. We were however agnostic regarding the effect of prandial state and glucose administration on backward connections due to the absence of previous studies on the topic.

8.2 Materials and methods

8.2.1 Participants

Twenty-four healthy male participants of normal weight were twice measured: once after 36 hours of fasting (except water consumption) and once under satiated conditions. During each session, rs-fMRI and hormone concentrations were recorded before and after glucose administration. Furthermore, the only plasma cortisol, glucose and insulin levels narrowly associated with the rs-fMRI data collection (i.e. at 20 min before and after glucose; see Figure 8.1) were used to associate the EC parameters with endocrine signals.

In four participants, we were not able to obtain a sufficient normalization of the functional individual brain image into standard space. Accordingly, these subjects were excluded from the analyses (see section "Region-of-interest time-series extraction" for further explanation). Details on the exclusion criteria of participants and the exact timing for obtaining blood samples can be found in Chapter 2.

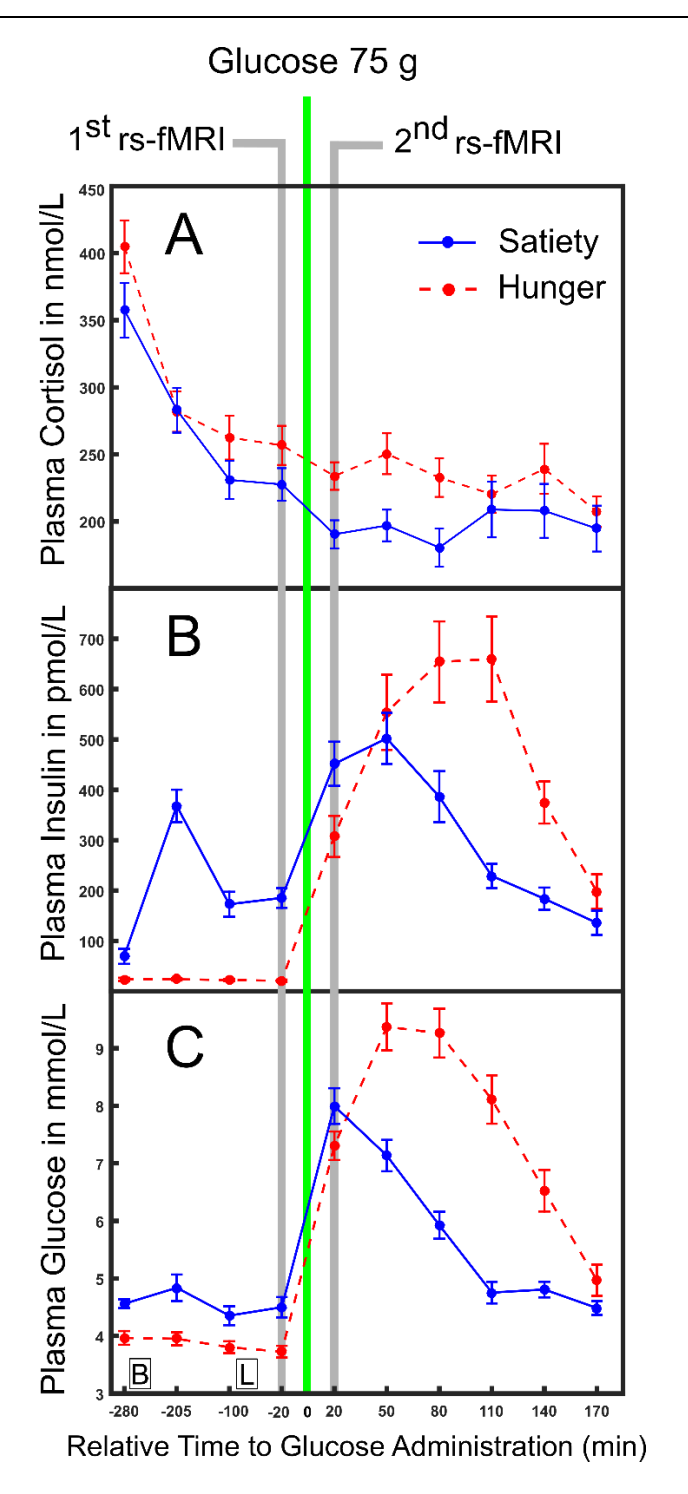


Figure 8.1: Time course of physiological parameters on the second day of the experiment for different metabolic states.

Mean blood plasma concentrations for cortisol (A), insulin (B) and glucose (C) under hunger and satiety conditions before and after oral glucose treatment (time point 0). Boxes on the bottom of the graph indicate the time points of meals on the second day (B = breakfast, L = lunch at 09:00 am and 12:00 pm., respectively). In each condition, the first rs-fMRI was recorded 20 min before, the second rs-fMRI 20 min after the intake of oral glucose. The error bars represent the standard deviation.

8.2.2 Preprocessing

All structural and functional images were recorded using a 3-T Philips Achieva scanner (Philips Healthcare, the Netherlands). More information regarding the image acquisition can be found in Chapter 2

Preprocessing of the data was performed with the "data processing assistant for resting-state fMRI" toolbox (DPARSF advanced edition, version 3.2, available at http://rfmri.org/DPARSF). DPARSF uses a subset of functions provided by SPM (SPM12, available at http://www.fil.ion.ucl.ac.uk/spm/). The rs-fMRI images were preprocessed as follows: (i) The first 7 volumes of each dataset were discarded to allow the signal to reach equilibrium and to allow the subjects to adjust to the scanning noise; (ii) The origins of structural and functional images were manually set to the anterior commissure and reoriented to enable a better alignment to the SPM template in order to prevent from normalization artifacts and to optimize between-subject alignment; (iii) Functional images were slice-time corrected to the middle slice by means of Fourier phase shift interpolation [379]. Head movement correction was performed on data by volume-realignment to the mean volume using a rigid body spatial transform to estimate the realignment parameters; (iv) Then, the T1 structural image was co-registered to the mean functional image of each subject; (v) Gray matter, white matter and cerebrospinal fluid (CSF) segmentation, bias correction and spatial normalization of the T1 structural image were adjusted to the Montreal Neurological Institute (MNI) template using the DARTEL algorithm [380]; (vi) The functional images were spatially normalized to the MNI-template by using the normalization parameters estimated by the DARTEL algorithm with voxels size to 3 mm isotropic; (vii) Spatial smoothing was performed with a 6 mm full width at half maximum (FWHM) Gaussian kernel.

8.2.3 Region-of-interest time-series extraction

As regions of interest (ROI), we defined four ROIs located in the insula (two insula ROIs per hemisphere) and one within the hypothalamus (Figure 8.2). For each insula ROI, we determined several coordinates (Table 8.1) to cover the functional differentiation within human insula [66]. These coordinates were chosen based on FC studies that provided the association of the specific ROIs of the insula with other brain areas [368] and which investigated the effect of hunger and satiety on the insular cortex [66]. Subsequently, each coordinate was used to generate a 5 mm³ sphere cluster (Figure 8.2A) by using the SPM Marsbar toolbox. Then, we summed up these clusters to create one combined seed for every subregion of the insula (i.e. anterior and posterior insula ROI). To avoid an overlap of the insula seed regions and other anatomical brain regions (i.e. regions outside the insula), we defined the final insula ROIs by finding common voxels between the insula ROIs and the corresponding insula masks from the Neuromorphometrics atlas provided by SPM12. The middle insula was not defined in order to avoid any overlap between the anterior and posterior insula ROIs.

The hypothalamus is notoriously difficult to examine in fMRI experiments as multiple factors can cause interference due to its anatomical position and size [376]. Even though the hypothalamus is very extensively subdivided with functional subcenters, we focused our analysis on the whole hypothalamus as it would have been unrealistic to achieve more spatially detailed results without running unique measurements adapted to the hypothalamus, which was not the primary goal of this study. The bilateral hypothalamus ROI (Figure 8.2B) was based on the SPM Wake Forest University (WFU) Pickatlas toolbox (http://www.fmri.wfubmc.edu/cms/software, version 3.0; [381]).

The preprocessed rs-fMRI data for each subject per condition were entered into the general linear model (GLM) with a constant term, the confound regressors of the CSF signal, the white matter signal and 24 head motion parameters (six standard realignment parameters, their derivative and the quadratic terms of these 12 realignment parameters; [382]). The applied temporal high pass filter of 1/100 Hz was included in the GLM model to remove slow frequency components caused by scanner drift. After estimation of the GLM model, we extracted time series from our ROIs, removing any signal that could be explained as a linear mixture of our 26 confound regressors. The time series was extracted using a singular value decomposition (SVD) procedure implemented in SPM12 and the first principal eigenvector was retained to represent the ROI time series (Figure 8.3B). Figure 8.3C and D show the predicted cross-spectral density of the BOLD signals and the hidden neuronal states, respectively, of the winning model for a single subject. In four subjects, we were not able to calculate the time series of the bilateral hypothalamus ROI correctly because some of the voxels within the hypothalamus ROI belonged to the CSF (normalization artifact). Accordingly, these subjects were excluded from further analyses.

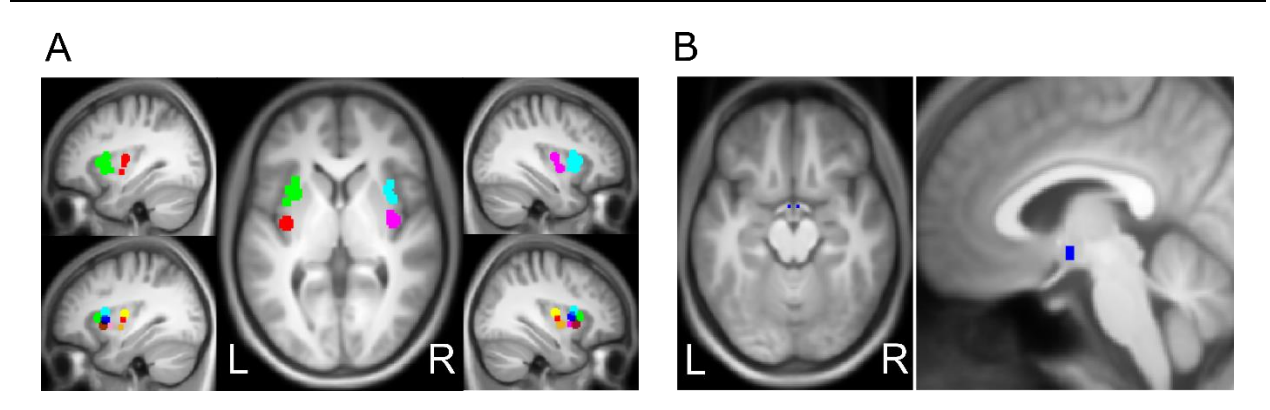


Figure 8.2: Seeds superimposed on an average structural T1 image.

(A) Middle picture and upper row: left and right anterior insula (green and cyan) and posterior insula (red and magenta) ROIs. Lower row: individual seeds in the right and left insula. (B) Hypothalamus (blue) ROI. L, left; R, right.

Table 8.1: Coordinates of the individual 5-mm³ sphere clusters of the left and right ROIs of the anterior and posterior insula, defined by Cauda et al. [383] and Wright et al. [66]. K represents the number of voxels that are common between the insula ROIs and the insula masks from the Neuromorphometrics atlas provided by SPM12.

Seeds	Clusters	Left He	ems. MN	VI (x,y,z)	ROI(K)	Right H	ems. MN	I(x,y,z)	ROI(K)
Ant. Ins.	1	-34.5	12.5	-2.5		34.5	12.5	-2.5	
	2	-36.5	4.5	-3		38.5	5.5	-2.5	
	3	-30.5	18.5	5.5	- 59	35.5	16.5	5.5	- 62
	4	-32.5	9	11.5		36.5	7	5	
	5	-30.5	9	4.5		32.5	9	11.5	
Post. Ins.	1	-36.5	-7.5	-3.5		36.5	-4.5	-3	
	2	-36.5	-10	4	- 24	38.5	-8	4	- 25
	3	-34.5	-13	10		34.5	-11	10.5	

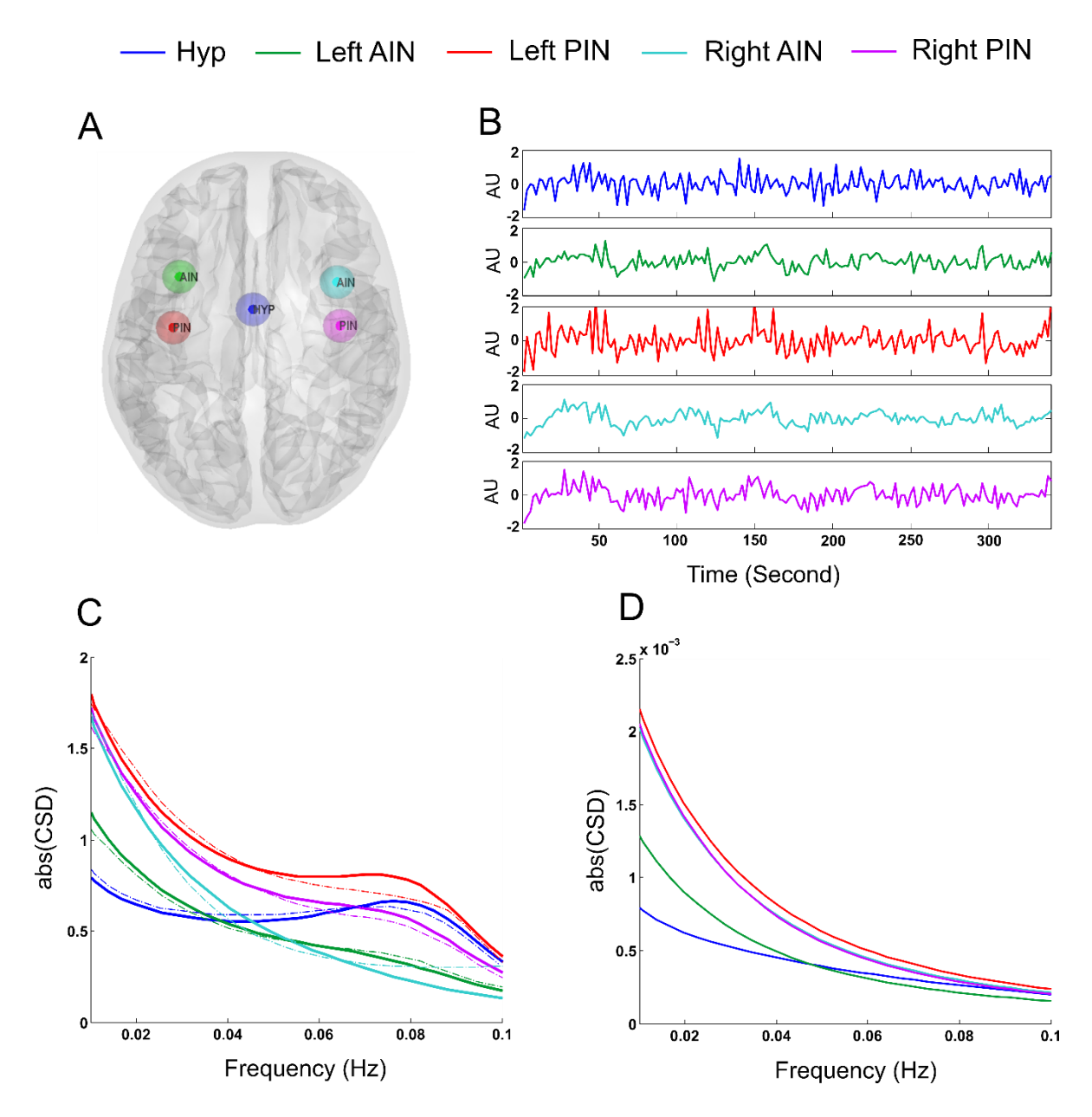


Figure 8.3: Illustration of the hypothalamus-insula network and the results of the winning model for a single subject.

The five spheres in (A) denote the five ROIs used in the spDCM analysis. The time series (B) from the five regions are the principle eigenvariates of the regions identified using a conventional SPM analysis. The observed (dashed lines) and predicted (solid lines) CSD of BOLD signals (C) by the winning model in the five ROIs. The underlying CSD predicted for the hidden neural states (D). Hyp = Hypothalamus; $AIN = anterior\ Insula$; $PIN = posterior\ Insula$; $AU = arbitrary\ units$; $CSD = cross-spectral\ density$; abs = absolute.

8.2.4 Spectral DCM and model space selection

The spDCM analyses (more details can be found in Section 4.2.1 regarding spDCM) were specified for each subject in each experimental condition (satiety-before, satiety-after, hungerbefore and hunger-after oral glucose) separately using DCM12 (revision 7196) implemented in SPM12 (revision 7219). For each condition and participant, the average EC between the ROIs was modeled using different models. These different models varied in their directed connections between the five ROIs and were specified in order to explore alternative hypotheses of insulahypothalamus network interactions. To limit the number of possible models, we assumed that during rs-fMRI measurements connectivity patterns are symmetric for the left-right hemisphere. The connections between hemispheres were supposed to take place either via hypothalamus, PINS and AINS (Figure 8.4A: models 1-4) or via hypothalamic connections alone (Figure 8.4A: models 5-8). Endocrine signaling of gut peptides that are related to promote meal initiation (e.g. ghrelin) or to promote meal cessation (e.g. insulin and leptin) reach specialized neurons within the hypothalamus and achieve their consequences by influencing brain regions involved in food intake regulation [3,64,384,385]. Therefore, we abstained from calculating models without any hypothalamic connections. The models in Figure 8.4A display eight possible connections (parallel, i.e. models 1,2,5 and 6, forward, i.e. models 3 and 7, and backward, i.e. models 4 and 8) between the hypothalamus, PINS and AINS. After inverting and estimating the models, we used BMS to determine the most accurate model structure to describe the measured fMRI data [163]. The optimal model is determined by selecting the model with the best balance between data fitting (i.e. accuracy) and model complexity, as defined by the free energy bound on the model evidence [386]. Random-effects BMS calculates the posterior model probability (that a specific model generated the data of a randomly chosen subject) and the protected exceedance probability (that a given

model is more likely than any other model considered). Treating the model as a random variable in the population renders the method capable of dealing with population heterogeneity whilst being robust to outliers, or equivalent [163].

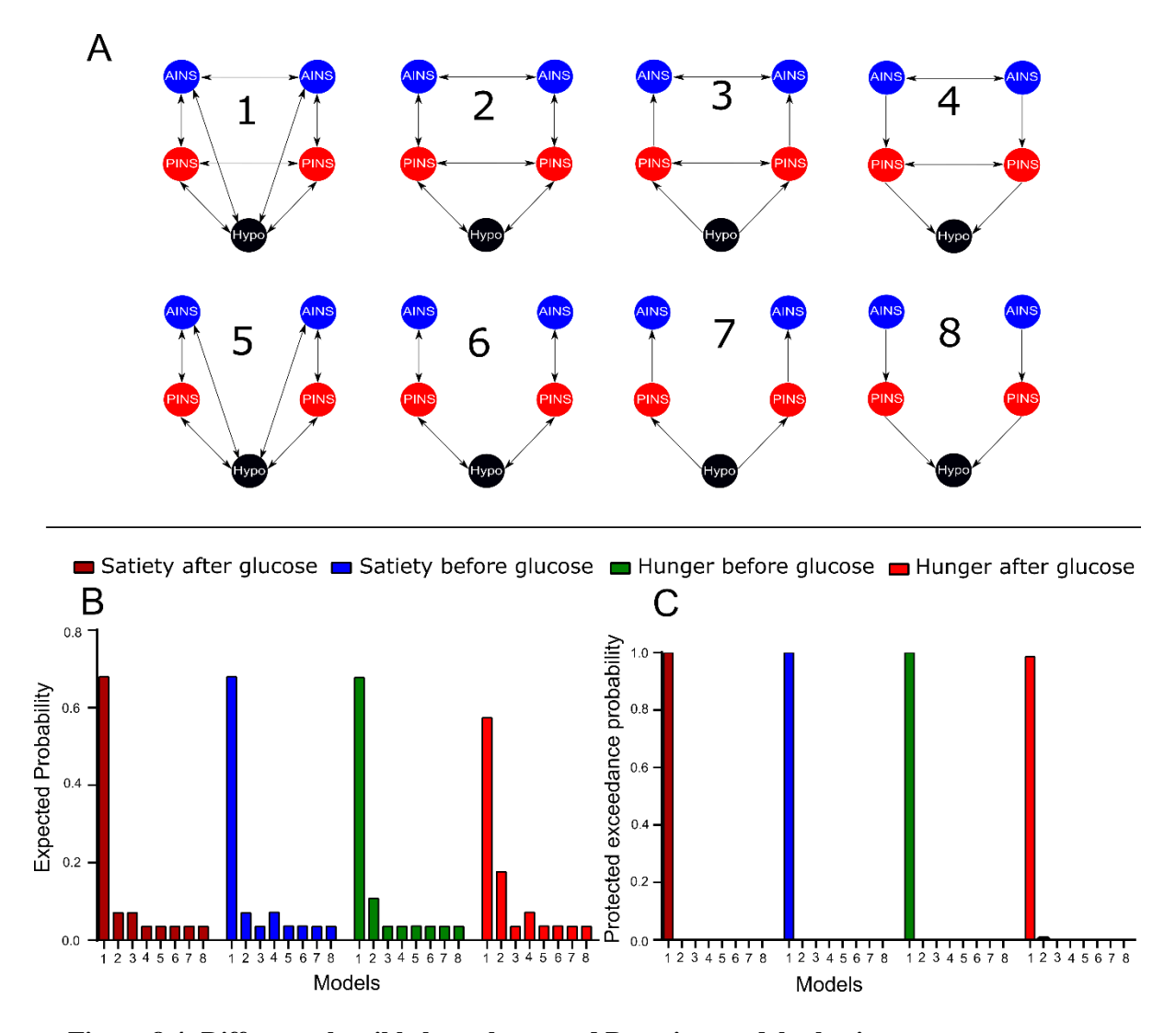


Figure 8.4: Different plausible hypotheses and Bayesian model selection.

(A) Possible connections among the five ROIs to explain the effective connectivity in the hypothalamus-insula network. Note that double arrow means reciprocal connections between two regions. (B) and (C) denote Bayesian model selection results per experimental condition for expected and protected exceedance probability in 8 models compared using RFX BMS, respectively. Hypo = Hypothalamus; AINS= anterior Insula; PINS = posterior Insula.

To evaluate the success of model inversion or fit, the percent variance explained (or R2) by the models for each experimental condition and subject were calculated using $spm_dcm_fmri_check.m$, see Figure 8.5.

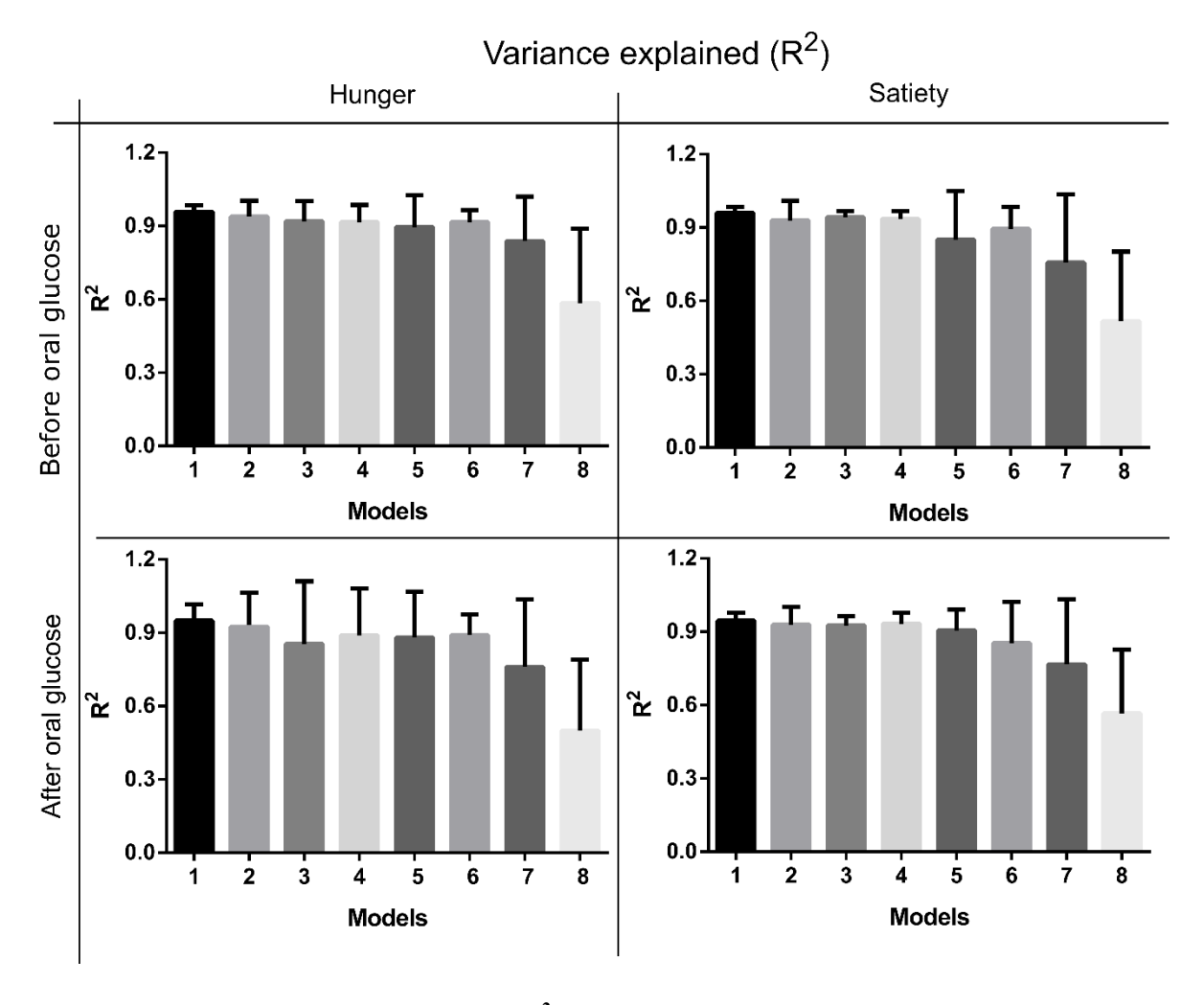


Figure 8.5: Percent variance explained (\mathbb{R}^2) by the models for each experimental condition. The bars show mean of \mathbb{R}^2 across subjects and the error bars represent the standard deviation.

8.2.5 Parameter estimate of the winning model

The random-effects BMS procedures were used to determine the "winning model" for each metabolic state condition (hunger or satiety) and glucose treatment (before or after glucose administration), separately. Then, we evaluated the endogenous connectivity parameters of the winning model in each condition using a second-level frequentist test. [387]. One-sample t-tests

(p<0.05/16, Bonferroni corrected for multiple comparisons) were applied to test whether the parameters of interest deviated significantly from zero. We reported the strength of the connections in Hz across participants (mean \pm SD) and the corresponding p-value.

The winning model of each condition resulted in the same model (see results section). Thus, we can examine the influence of conditions on the connections between ROIs. In the next step, the endogenous connectivity parameters of the winning model were submitted to rm-ANOVA with factors metabolic state (levels: hunger, satiety) and glucose administration (levels: before, and after treatment).

8.2.6 Associations between DCM parameters, physiological and behavioral responses

We tested whether the participant's physiological (plasma cortisol, glucose and insulin levels) and behavioral (rating of hunger) responses could be predicted by the neuronal parameter estimates (NPEs; i.e. from 16 endogenous connections and 5 self-connections) of the winning model. We used multiple linear regression (MLR) analysis to test for a statistically significant relationship between components of NPEs (independent variables) and the respective dependent variable. First, we performed principal component analysis (PCA) on NPEs to reduce the dimensionality of the independent variables and to provide principal components (PCs), which are the linear combination of the NPEs. Separate PCA analyses were applied to 21 parameters for each of the four experimental conditions to determine the number of components (Figure 8.6). Approximately 87±2% of the variance was explained by the remaining the first six neuronal parameter components (NPCs; Figure 8.6). Therefore, six NPCs were extracted from the NPEs per experimental conditions. Next, these NPCs were used as independent variables in the MLR model [388] to predict participants' plasma glucose, plasma insulin, plasma cortisol and hunger ratings. Each of the MLR analysis was performed four times to cover all experimental conditions. To keep the

temporal association of endocrine and functional imaging data as clear as possible, the physiological data at 20 min before and after glucose ingestion only (Figure 8.1) were used as dependent variables for MLR analysis.

The rm-ANOVA on the NPEs (see Results 8.3.2 and Figure 8.8), resulted in a significant main effect of the metabolic state on the endogenous connection estimates from the right posterior to the right anterior insula (RPINS \rightarrow RAINS) and from the right anterior to the right posterior insula (RPINS \(\in \)RAINS). To investigate whether the changes in these connections were associated with physiological and behavioral responses, we used linear mixed-effects (LME) analysis which allows us to perform multiple regression while taking into account the repeated measures design of our subjects [389]. The LME model identifies the linear relationships between a dependent variable (e.g. cortisol) and independent variables (NPEs), with coefficients that explain variation in respect to one or more grouping variables (e.g. experimental conditions). To this end, separate LME analyses were carried out for each of the four dependent variables (i.e. plasma cortisol, glucose and insulin levels as well as hunger ratings). Furthermore, the only plasma cortisol, glucose and insulin levels narrowly associated with the rs-fMRI data collection were used as dependent variables (Figure 8.1). For each of these four models, we entered the metabolic state (levels: hunger vs. satiety) and glucose administration (levels: before vs. after glucose administration) as well as EC of RPINS→RAINS and RPINS←RAINS as a fixed effect with the intercepts for subjects as a random effect. As post-hoc tests, a set of LME was used to further analyze the interaction driving factor levels. All continuous variables were z-scored. LME analyses were performed using the "lmer" function in the lme4 package [390] with R [391] and siPlot [392]. For significant slopes, we reported the regression coefficient parameter estimate (β) .

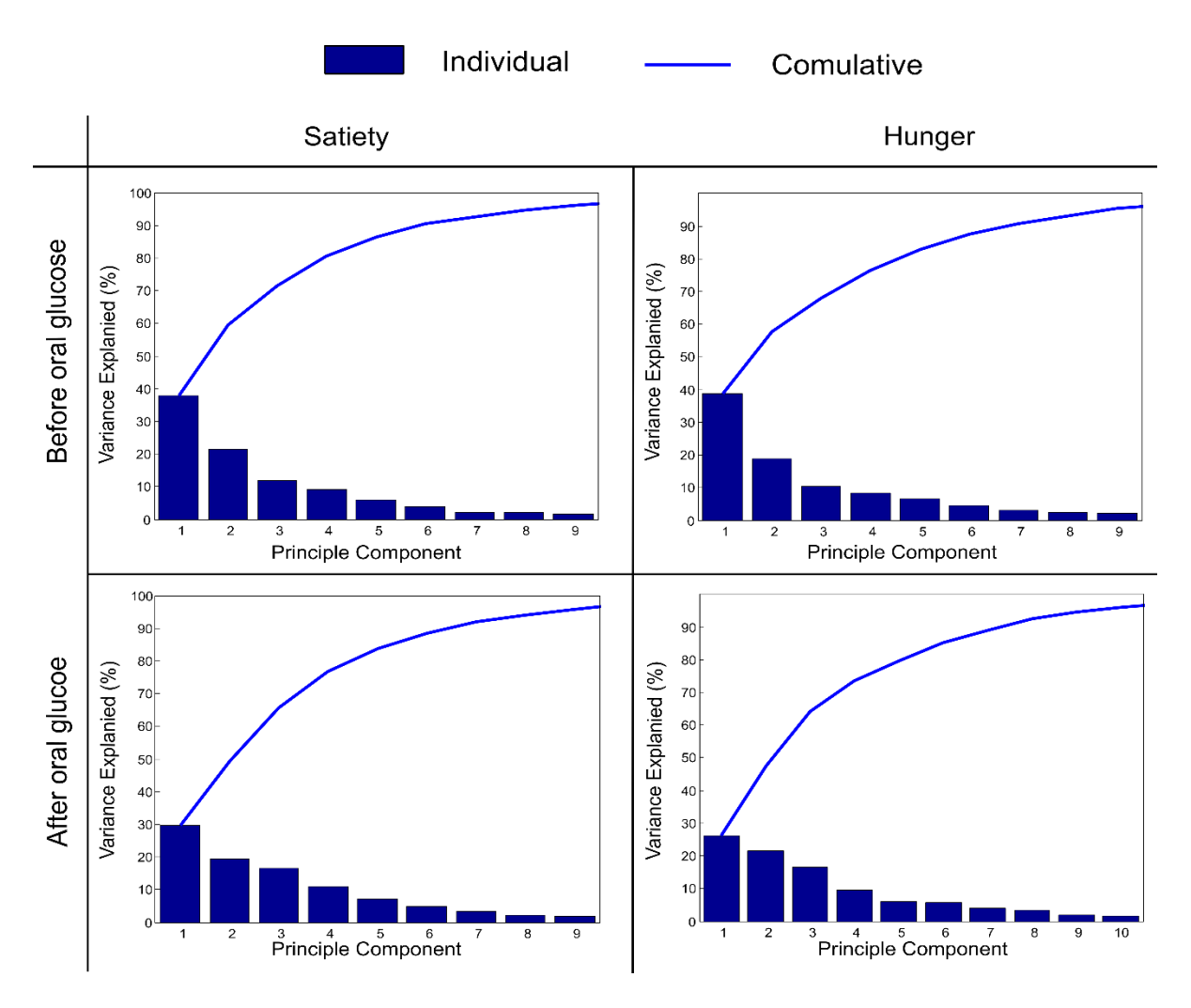


Figure 8.6: Principal component analysis (PCA) on neuronal parameter estimates (NPEs; i.e. from 16 endogenous connections and 5 self-connections) for each of the four experimental conditions.

The bars show the proportion of variance represented by each component and the solid line represents the cumulative variance. Approximately 87±2% of NPEs information (variance) was explained by remaining the first six neuronal parameter components.

8.3 Results

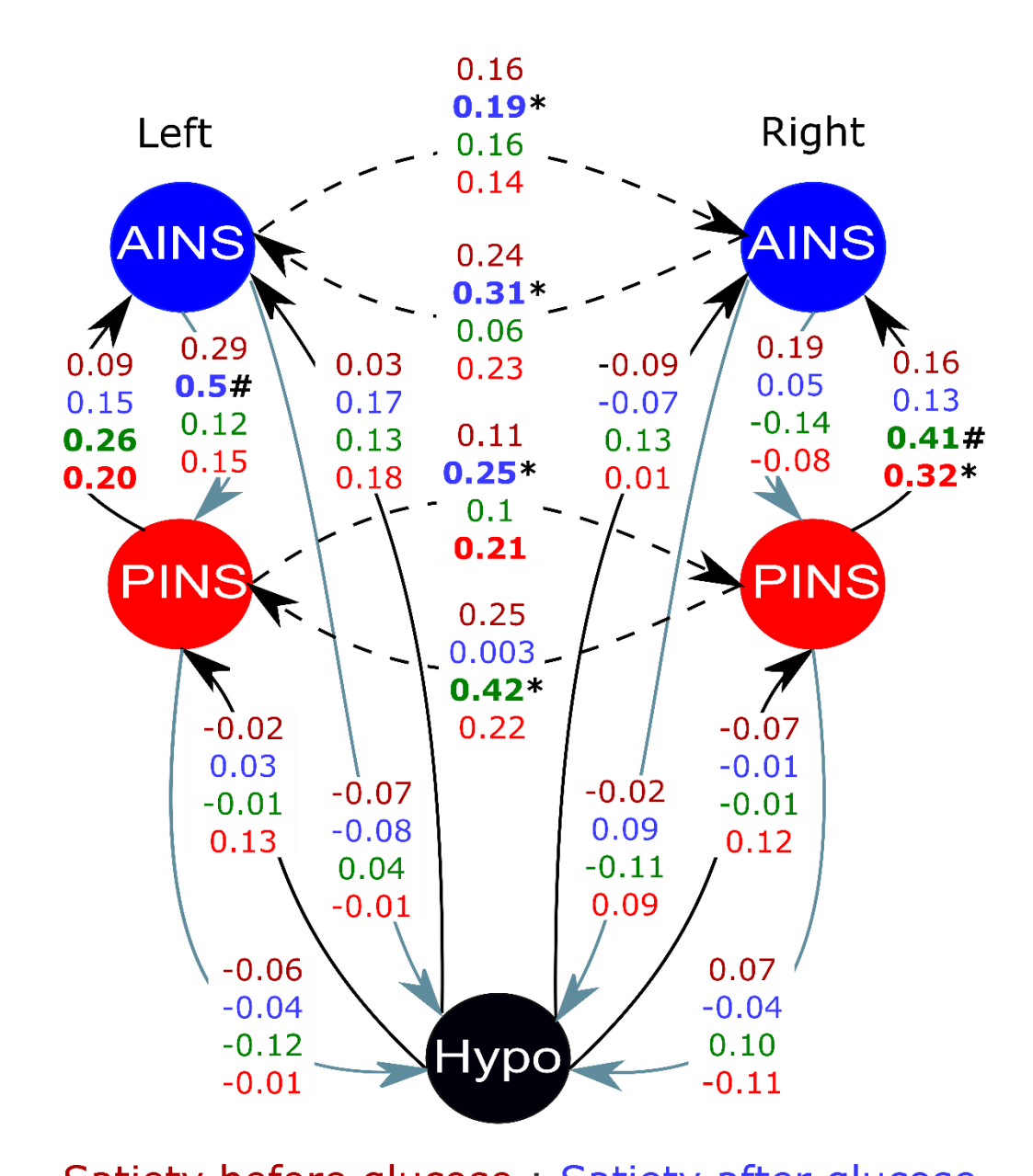
8.3.1 Bayesian model selection

When testing for the model structure that explains the rs-fMRI data best by using RFX BMS, model 1 (Figure 8.4B) had the highest protected exceedance probability (PXP= 0.99) at the group level for each experimental condition (shown in Figure 8.4C). The lower evidence of models

without interhemispheric connections (models 5-8) indicates that lack of inter-hemispheric connectivity led to a worse explanation of the participants' network activity. This result suggests that the reciprocal connections, both within hemispheres (i.e. hypothalamus-PINS-AINS) and between hemispheres were necessary network features.

8.3.2 Model parameters

We investigated whether the EC among the ROIs estimated using the winning model were significantly non-zero separately for each condition. In Table 8.2 and Figure 8.7 we show the mean connection strength (in Hz) and the results from the one-sample t-tests. For simplicity, self-connections are not included in the table and graph. To sum up, in the satiety condition after oral glucose intake we found that the connection strength from left anterior insula (LAINS) to left posterior insula (LPINS) was significantly different from zero (p=0.002, surviving Bonferroni correction). Furthermore, in the hunger condition before oral glucose intake, we found that the connection from the right posterior insula (RPINS) to the right anterior insula (RAINS) was significantly different from zero in satiety (p=0.001, surviving Bonferroni correction), too. Finally, we did not find any significant connections from or to the hypothalamus.



Satiety before glucose; Satiety after glucose
Hunger before glucose; Hunger after glucose

Forward
Backward -
Interhemisphere

Forward ← Backward − → Interhemispheric
Figure 8.7: The winning model at the group level and its mean connectivity parameters (in Hz)

per experimental condition.The significant (p<0.05) connections are shown in bold. The * and # represent significance at p<0.01 and after Bonferroni correction (p<0.05), respectively.

Two-way rm-ANOVA was conducted to determine the influence of two independent variables (metabolic state and glucose administration) on endogenous connection estimates of the winning model. Both metabolic state (hunger and satiety) and administration (before and after glucose intake) consisted of two levels. There were no significant effects of glucose administration and interactions between both factors on all endogenous connection estimates. We found a significant (p<0.05) main effect of metabolic state on the endogenous connections from RPINS to RAINS (forward connection, RPINS \rightarrow RAINS) (F_(1,19)=8.8, p=0.008), indicating significant stronger connectivity during hunger (M=0.37 Hz, SD=0.49) compared to satiety (M=0.15 Hz, SD=0.54). Also, we observed a significant main effect of metabolic state on the endogenous connections from RAINS to RPINS (backward connection, RPINS \leftarrow RAINS) (F_(1,19)=4.7, p=0.04) indicating that the satiated state (M=0.12 Hz, SD=0.49) showed higher connectivity strength compared to the hunger state (M=-0.11 Hz, SD=0.55), as shown in Figure 8.8.

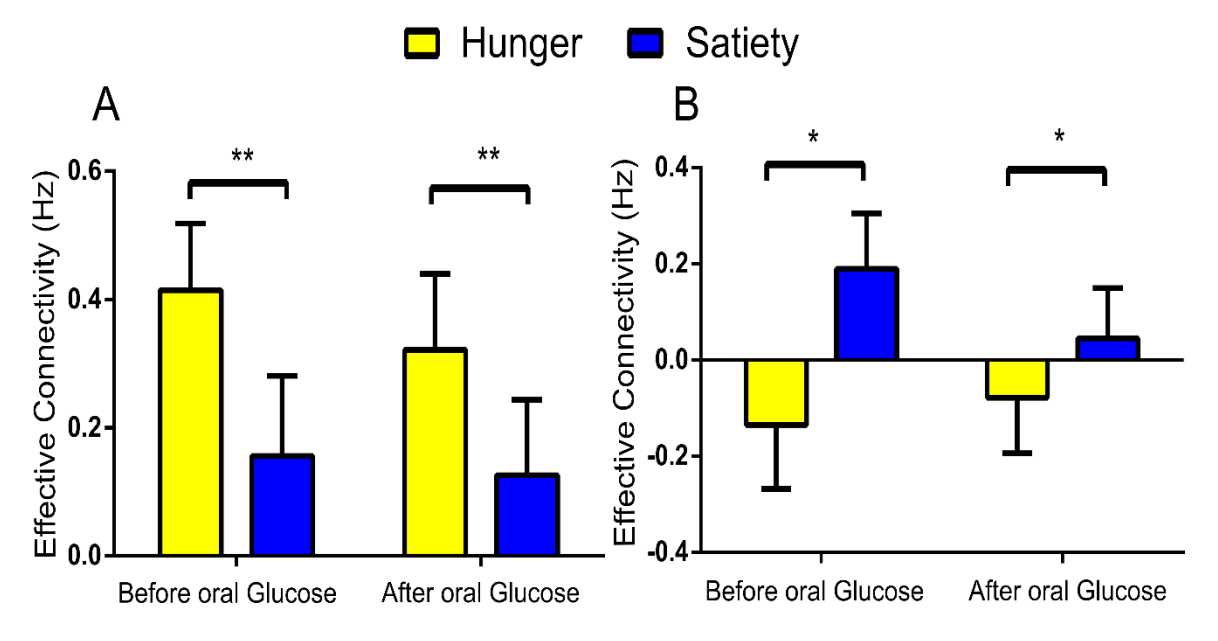


Figure 8.8: Effective connectivity parameters that showed a significant main effect of the metabolic state (hunger vs. satiety).

(A) Strength of the forward connections from RPINS to RAINS (RPINS \rightarrow RAINS). (B) Strength of the backward connections from RAINS to RPINS (RPINS \leftarrow RAINS). * and ** represent the significant differences between conditions, p < 0.05 and p < 0.01, respectively.

Table 8.2: Posterior estimates of effective connectivity (Hz) in the winning model (mean \pm SD) per experimental condition. Using one-sample t-tests, we tested whether effective connectivity was significantly different from zero.

Connections		Satiety				Hunger			
		Before Glucose		After Glucose		Before Glucose		After Glucose	
		Strength (HZ)	P-Value						
LAINS -	→ Нуро	-0.07 ± 0.61	0.8	-0.08 ± 0.37	0.15	0.04 ± 0.68	0.35	-0.01 ± 0.44	0.21
LPINS -	→ Нуро	-0.06 ± 0.29	0.9	-0.04 ± 0.28	0.85	-0.12 ± 0.41	0.85	-0.01 ± 0.23	0.5
RAINS -	→ Нуро	-0.02 ± 0.72	0.32	0.09 ± 0.64	0.85	-0.11 ± 0.51	0.07	0.09 ± 0.51	0.92
RPINS -	→ Нуро	0.07 ± 0.56	0.46	-0.04 ± 0.38	0.95	0.1 ± 0.44	0.91	-0.11 ± 0.42	0.26
Hypo \rightarrow	→ LAINS	0.03 ± 0.61	0.62	0.17 ± 0.51	0.34	0.13 ± 0.62	0.77	0.18 ± 0.61	0.89
LPINS -	→ LAINS	0.09 ± 0.43	0.16	0.15 ± 0.53	0.46	0.26 ± 0.35	0.03	0.2 ± 0.39	0.04
RAINS -	→ LAINS	0.24 ± 0.59	0.16	0.31 ± 0.51	0.008*	0.06 ± 0.85	0.21	0.23 ± 0.73	0.11
Hypo \rightarrow	→ LPINS	-0.02 ± 0.68	0.37	0.03 ± 0.67	0.57	-0.01 ± 0.68	0.2	0.13 ± 0.83	0.87
LAINS -	→ LPINS	0.29 ± 0.89	0.35	0.5 ± 0.25	0.002#	0.12 ± 0.72	0.07	0.15 ± 0.63	0.06
RPINS -	→ LPINS	0.25 ± 0.73	0.12	0.003 ± 0.72	0.43	0.42 ± 0.75	0.006*	0.22 ± 0.58	0.05
Hypo - 2	→ RAINS	-0.09 ± 0.38	0.91	-0.07 ± 0.45	0.55	0.13 ± 0.32	0.36	0.01 ± 0.38	0.43
· ·	→ RAINS	0.16 ± 0.47	0.08	0.19 ± 0.39	0.009*	0.16 ± 0.55	0.78	0.14 ± 0.37	0.17
RPINS -	→ RAINS	0.16 ± 0.56	0.11	0.13 ± 0.52	0.67	0.41 ± 0.46	0.001#	0.32 ± 0.53	0.004*
Hypo \rightarrow	→ RPINS	-0.07 ± 0.43	0.58	-0.01 ± 0.59	0.65	-0.01 ± 0.47	0.33	0.12 ± 0.47	0.24
LPINS -	→ RPINS	0.11 ± 0.35	0.14	0.25 ± 0.36	0.006*	0.1 ± 0.54	0.11	0.21 ± 0.42	0.02
RAINS -	> RPINS	0.19 ± 0.52	0.23	0.05 ± 0.46	0.29	-0.14 ± 0.59	0.72	-0.08 ± 0.52	0.82

The significant (p<0.05) connections are shown in **bold**. The * and # represent significance at p<0.01 and after Bonferroni correction (p<0.05), respectively. Abbreviations: LAINS, left anterior insula; LPINS, left posterior insula; Hypo, hypothalamus; RAINS, right anterior insula; RPINS, right posterior insula.

8.3.3 Associations between DCM parameters, physiological and behavioral responses

MLR analysis was applied to explain the physiological or behavioral responses of participants based on their NPEs (i.e. six NPCs). We found a significant regression equation for the prediction of plasma cortisol levels before oral glucose intake for both satiety ($F_{(6,13)}=3$, p=0.04 with an $F_{(6,13)}=3$ and hunger conditions ($F_{(6,13)}=2.8$, p=0.05 with an $F_{(6,13)}=3.8$ hown in Figure 8.9 no other regression became significant.

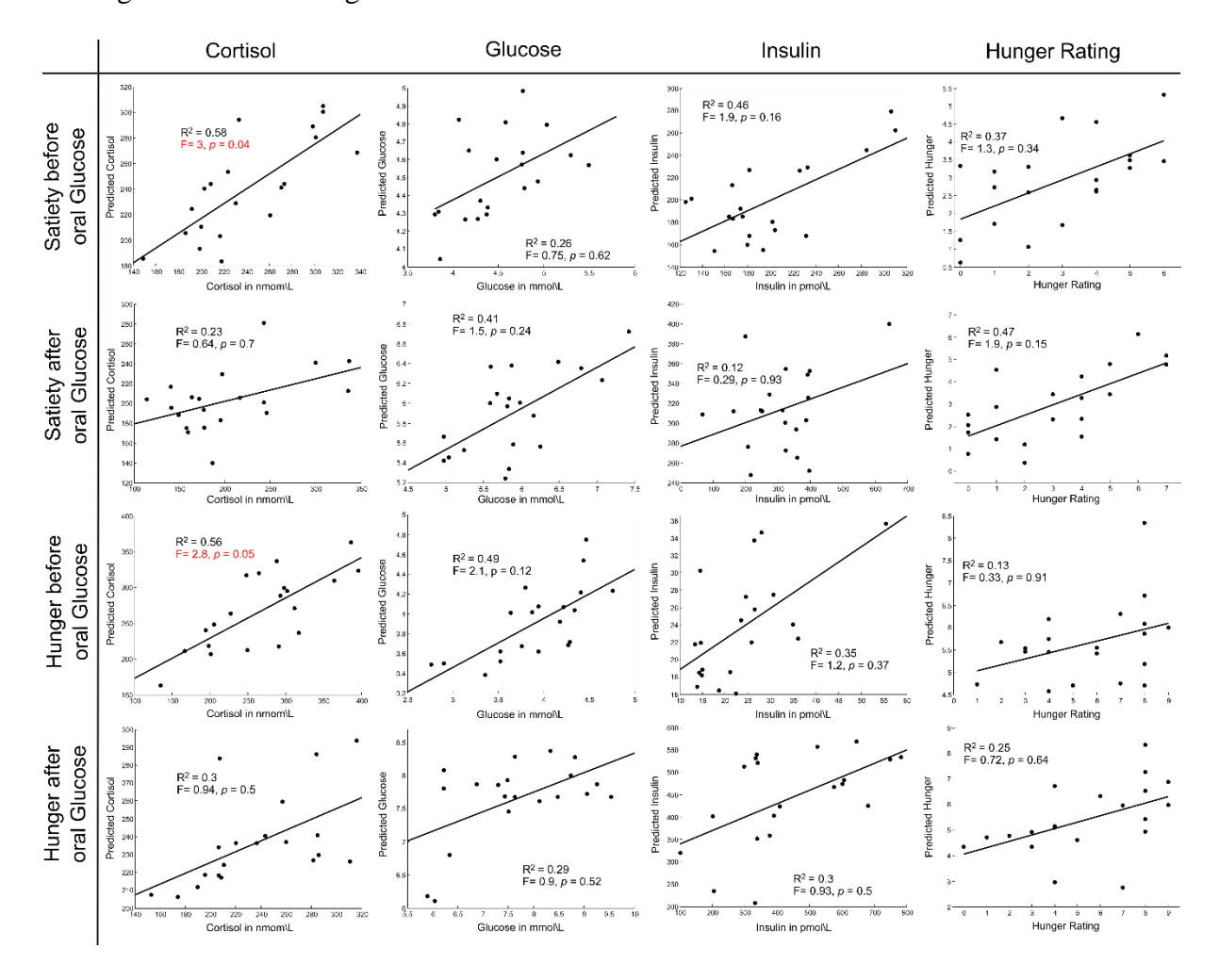


Figure 8.9: Multiple linear regression (MLR) analysis.

The expression of significant regression equations to predict physiological (plasma glucose, insulin and cortisol levels) and behavioral responses (rating of hunger) of participants based on their six principal components computed from the spDCM neuronal parameter estimates (for every experimental condition separately). The red color represents the significant results.

Critically, LME analyses revealed significant interactions (β =-0.8, p=0.007) between RPINS \rightarrow RAINS connection (forward connection) strength, metabolic state and glucose administration in explaining cortisol levels (Figure 8.10A). To further analyze the interaction-driving factor, we performed LME analyses per glucose treatment condition separately, as post-hoc tests. We found that the interactions between RPINS \rightarrow RAINS and metabolic state predicting the cortisol levels was significant (β =0.9, p=0.01) before, but not (β =-0.5, p=0.2) after oral glucose. More precisely, before oral glucose treatment, the forward RPINS \rightarrow RAINS connectivity showed a strong positive (β =-0.7, p=0.03) and negative (β =-0.5, p=0.06) relation to cortisol levels in hunger and satiety conditions, respectively. Whereas, after oral glucose treatment, the relationship between RPINS \rightarrow RAINS strength and cortisol disappeared for both the hunger (β =-0.4, p=0.08) and satiety (β =-0.03, p=0.9) conditions.

Finally, the interactions between the RPINS \leftarrow RAINS connection strength (backward connection) and metabolic state significantly predicted cortisol levels (Figure 8.10B; β =-0.7, p=0.02) and the hunger ratings (Figure 8.10C; β =-0.6, p=0.03). More precisely, the backward RPINS \leftarrow RAINS connection strength showed positive relations to both, the cortisol levels (β =0.5, p=0.1) and hunger ratings (β =0.7, p=0.007) in the satiety condition. In contrast, in the hunger condition, the RPINS \leftarrow RAINS connection strength was negatively and non-significantly associated with cortisol levels (β =-0.3, p=0.2) and hunger ratings (β =-0.5, p=0.08). In addition, we observed no significant relations between the glucose or insulin levels and the forward RPINS \rightarrow RAINS or backward RPINS \leftarrow RAINS connection strengths.

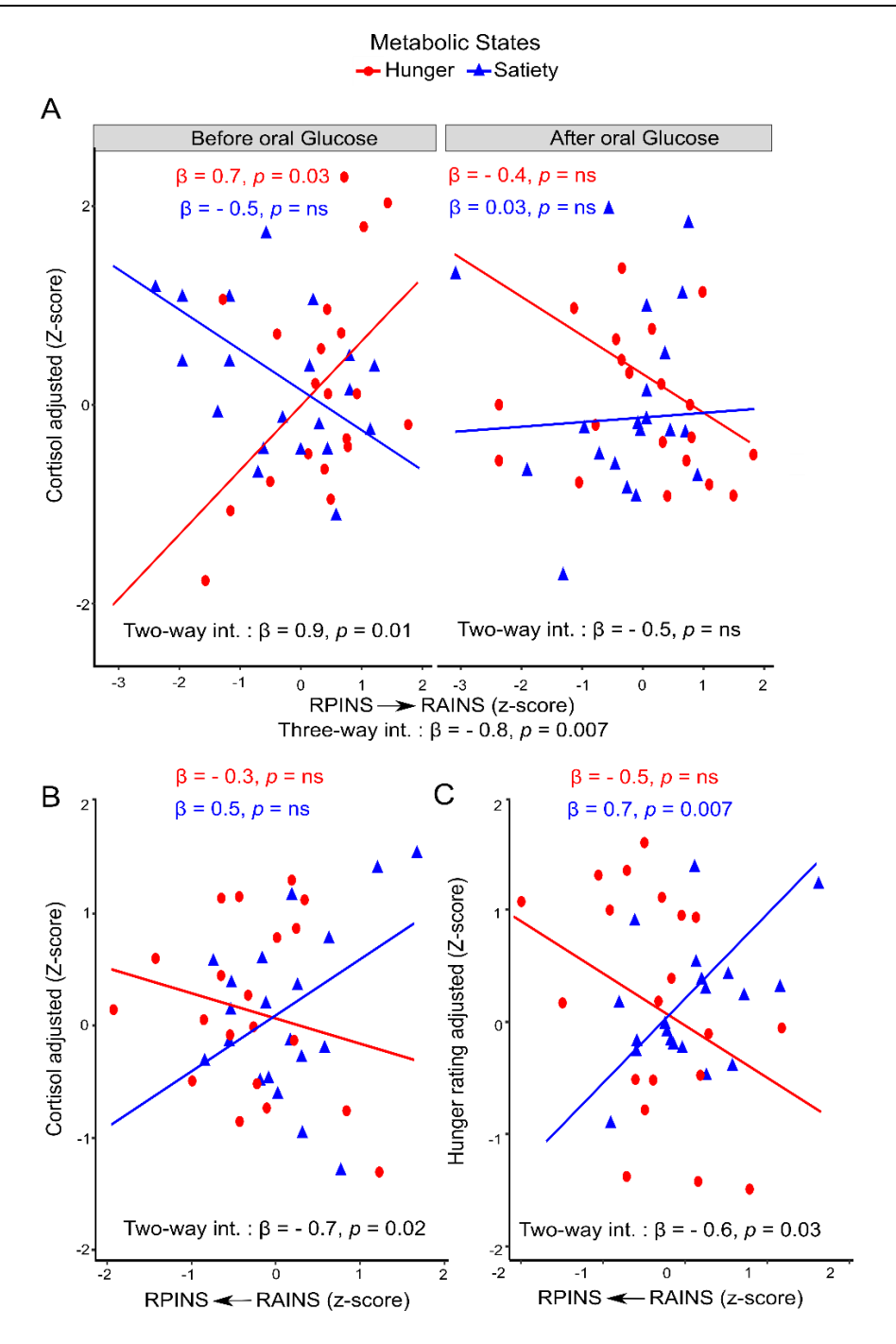


Figure 8.10: Interactions between covariates in the linear mixed effects model predicting individual physiological and behavioral responses.

(A) Interaction of RPINS \Rightarrow RAINS connectivity (forward connection) with the metabolic state (levels: hunger vs. satiety) and glucose administration (levels: before vs. after glucose administration). (B) and (C) interaction of RAINS \Rightarrow RPINS connectivity (backward connection) with metabolic state predicting cortisol levels and hunger ratings, respectively. Solid lines indicate linear regression fit between the dependent variables (y-axis) and covariates (x-axis). int.: interaction. RAINS: right anterior insula. RPINS: right posterior insula. β : slope coefficient parameter estimate resulting from linear mixed-effects models. ns: represent no significance.

8.4 Discussion

The purpose of this study was to investigate the influence of prandial state (hunger vs. satiety) and glucose administration on EC patterns between the hypothalamus, PINS and AINS as core components of the neural network supporting ingestive behavior. Applying spDCM to rs-fMRI data, we were able to estimate the directed connectivity between brain regions of interest at neuronal states. Our results suggest that the strength of the EC was modulated by changes in prandial states, but not glucose administration. Specifically, during the hunger condition, the strength of endogenous connectivity was increased from right PINS to the right AINS, while it was decreased from right AINS to right PINS (Figure 8.8). Connectivity strength from AINS to PINS was further related to enhanced hunger ratings during the satiety condition, suggesting that EC changes in the homeostasis regulation network might partly underlie subjective hunger perceptions and thereby impact food intake.

8.4.1 Changes in endogenous connectivity related to metabolic conditions

Spectral DCM analysis is a framework to model the effective connectivity between ROIs based on the FC in rs-fMRI data as well as make inferences about specific parameter changes [147]. BMS reveals the most likely model (i.e. possible way of connections) among a set of different models to explain the data by taking into account the balance between complexity and goodness-of-fit [386,393,394]. In this work, BMS suggested that the fully connected model (model 1 in Figure 8.4A) was the best model in all experimental conditions (Figure 8.4C).

Regarding the endogenous connectivity, we observed that inter-hemispheric connections between left-right AINS and between left-right PINS were positive in both directions for all experimental conditions, i.e. left and right insula exerted a mutual positive influence on each other; this could be regarded as 'baseline' reciprocal activation. Lateralization of emotional and

homeostatic processing in the insula has been suggested to be associated with differential autonomic inputs (sympathetic/parasympathetic) to this structure [395–397]. For instance, Oppenheimer et al. [398] demonstrated that direct stimulation of the right insular cortex results in changes in sympathetic functions, which are needed in hunger, avoidance behavior and negative affect [374], while the left insular cortex has been reported to be involved in parasympathetic functions, which are required in feeding, approach behavior and positive affect [374]. Furthermore, a recent meta-analytical study demonstrated asymmetrical information processing in the insular cortex in response to hunger-inducing food stimuli [399]. Our results suggest continuous cross-communication between homologous insula regions, which could serve to integrate sympathetic and parasympathetic signals.

After fasting, we observed a strong positive connection in the right hemisphere from PINS to AINS (RPINS→RAINS; Figure 8.7 and Figure 8.8A) which suggests a more intense influence of interoceptive inputs represented in PINS on AINS function [397,400–402]. In the same condition, a negative connection from right AINS to right PINS (RPINS←RAINS; Figure 8.7 and Figure 8.8B) indicated an inhibitory influence of the anterior insula on posterior insula during hunger. These findings can be interpreted in the context of recent theories of interoception that we describe below.

According to meta-analyses [403,404], PINS receives information about the physiological and homeostatic conditions of the body. For instance, PINS is activated in response to hunger, receiving an appetitive drink, thirst, sensual touch, gastric distention without actual food intake, itch and temperature changes [208,333,334,401,405–411]. Also, the PINS is linked to the posterior cingulate cortex, supplementary motor area, sensory-motor and part of occipital areas. This network is mainly related to environmental monitoring, response selection and body orientation

[332,395,405,412–414]. It thus subserves the objective representation of physical body conditions [415,416].

In contrast to PINS, AINS is of particular significance for food intake and corresponding primary gustatory signals [207,417]. For example, right AINS is activated in response to different tastes, smells and food textures [332,334]. In addition, the right AINS is proposed as a primary cortical area for awareness of and attention shift to internal body signals, for instance in the perception of pain and heartbeat [415,416,418–423]. Furthermore, the AINS is anatomically and functionally connected to the middle and inferior temporal cortex, anterior cingulate cortex (ACC) and orbitofrontal cortex. This network is mostly concerned with attention and executive functioning as well as salience detection [368,383,424–429]. The AINS is therefore regarded as one of the main brain areas for multimodal integration and has been proposed to represent subjective emotional states [415,416].

Craig [430] suggested a pathway that maps objective representations of body conditions onto a subjective representation of the physical self, via posterior-to-anterior pathways within the right insula. Our results demonstrate that the connection strength from the right PINS to the right AINS is increased in hunger by 22% relative to satiety conditions. This finding indicates that the connectivity within the right posterior-to-anterior insula pathway (RPINS→RAINS) can be altered by food intake because those changes were only observed in response to changes in metabolic states, but not in glucose treatment. Our observations suggest that changes within this pathway, which is related to subjective hunger feelings, could be caused by increasing the perceived salience of internal bodily states [397,430]. In contrast, we observed a decreased strength of backward connections from right AINS to right PINS (RPINS←RAINS) during hunger conditions. One could assume that the reduced strength of EC from RAINS to RPINS might be the result of bodily

signals forwarded from posterior to anterior insula (RPINS → RAINS), which may become more salient in the hunger condition. An alternative (and equally tentative) interpretation refers to recent theories that PINS, AINS, and ACC are part of a hierarchical system for inference on bodily states (interoception) and homeostatic/allostatic regulation [431,432]. These theories view interoception as a "predictive coding" [433,434] process in which inference is mediated by transmitting predictions via backward connections and prediction errors via forward connections. Predictions represent previously learned and expected bodily states, whereas (interoceptive) prediction errors signal the mismatch between the actual bodily state and the expectation. Therefore, interoceptive prediction errors signal changes in the AINS, thereby triggering homeostatic regulation [435]. Thus, the strengthening of forwarding connections from PINS to AINS during hunger states could be potentially interpreted as the reflection of tonically increased prediction error signals, while the negative (inhibitory) connection could reflect the effect of predictions (which, in predictive coding, are subtracted from actual states).

8.4.2 Associations between DCM parameters, physiological and behavioral responses

Only blood cortisol levels before glucose administration could be predicted by the six neuronal PCs (Figure 8.9). Furthermore, the relationship between the strength of RPINS→RAINS connection (i.e. forward connection) and plasma cortisol levels was modulated by metabolic states before oral glucose intake (Figure 8.10A). However, the modulation of the association between the strength of RPINS←RAINS connection (i.e. backward connection) and both, plasma cortisol levels and hunger ratings, depended only on the metabolic states and were therefore independent of glucose treatment (Figure 8.10B and C, respectively).

After glucose stimulation, the insulin and cortisol levels of fasted and non-fasted subjects responded differentially, namely insulin increased and cortisol remain stable. Variability in insulin

and cortisol responsivity is nonetheless influenced by a complex interplay of the glucose absorption-rate, fasting-induced insulin resistance and gastrointestinal hormone secretion[436,437]; this may have decreased our ability to explain physiological states as a function of connectivity estimates. Especially the onset of fasting-induced insulin resistance and the associated increase in inflammatory markers [436,437] that, in turn affect, cortisol levels may have confounded the relation between connectivity estimates and physiological states that was visible before glucose administration.

One limitation of the current analysis, due to the rather small sample size we could not directly investigate the relation between all NPEs and hormone variables (i.e. plasma glucose, insulin and cortical levels) using standard multiple linear regression. We used principal component regression instead. To establish a direct relationship between NPEs and hormonal data, a replication of the current study with a larger sample would be desirable.

8.5 Conclusions

Hypothalamic and insular cortex activation has previously been found to reflect changes in the homeostatic energy balance. By applying spDCM and BMS analyses to rs-fMRI data, we examined whether the metabolic state (hunger vs. satiety) and glucose administration (before vs. after) would modulate the EC between brain regions involved in ingestive behavior. Our most plausible model in all metabolic and glucose conditions comprised intra- and interhemispheric connections within a bilateral the hypothalamus-PINS-AINS network model. EC was significantly increased for the forward connection RPINS→RAINS but decreased for the backward connection RPINS←RAINS under hunger compared to satiety, with no influence of glucose treatment. Furthermore, the strength of RPINS→RAINS connectivity was positively associated with plasma cortisol levels in the hunger condition, particularly before glucose administration. Overall, these

results illustrate how connections among brain regions involved in interoception and homeostatic regulation change between hunger and satiety and provide a basis for future investigations of hypothalamic-insular networks in the context of food intake

Chapter 9: General discussion

The overarching goal of the current dissertation was to investigate and understand the impact of varying metabolic states (hunger vs. satiety) on the human brain's functional connectivity by using different approaches to analyze rs-fMRI data. Each approach was chosen to answer a specific question and also to carry the results forward from one analysis to subsequent analyses.

Rs-fMRI was used to investigate the neural correlates of changing hunger and satiety states as well as glucose intake. Therefore, the basic principles of MRI recording and the link of fMRI signals to neural activity were outlined in the introduction (Chapter 1). Also, the recent literature on the impact of food consumption on brain functions has been summarized. From this literature review, there are open questions regarding the relationship of brain activity to food intake, in particular pertaining to the link between brain activity and peripheral hormonal and metabolic signals. To fill this gap, an experiment was designed to examine the role of modulations of metabolic states on human brain function as explained in Chapter 2. This study examined 24 healthy normal-weight men twice: once after 36 hours of fasting (except water) and once in satiated (five meals/day for 36 hours) conditions. At the end of each session, rs-fMRI was recorded before and after glucose administration (75 g of oral glucose). Furthermore, 19 blood samples per subject and condition were drawn to assess hormonal and metabolic measures. In Chapter 3, the effects of metabolic states and glucose treatment on physiological and behavioral data were explained. As the results of Chapter 3 met our expectations and corresponded with the literature, this experimental design allowed us to interpret our rs-fMRI findings appropriately concerning fundamental metabolic regulations.

There is no ideal approach to analyze rs-fMRI signals. Instead, the selection of a specific analysis technique depends on the specific questions that the researchers wish to answer from the rs-fMRI data. Therefore, in Chapter 4, a methodological review and comparison of several common methods to analyze rs-fMRI data were provided.

As mentioned in the introduction, this work was particularly interested in answering four different, non-redundant questions from one experimental design but different analysis procedures. In the next paragraphs, these questions will be recalled and the methods and results to answer them will be summarized. Moreover, methodological considerations supporting the results of this project will be discussed. Finally, relevant caveats will be addressed and future directions to continue this work will be suggested. In the end, this work will close with some concluding remarks that support our primary two hypotheses mentioned in the introduction of this dissertation.

9.1 Addressing research questions

9.1.1 First question: What is the effect of oral glucose administration on the resting brain activity during hunger and satiety conditions using rs-fMRI data?

In Chapter 5, a multi-method rs-fMRI analysis approach was used to investigate the effect of glucose administration on the brain's resting functional connectivity and activity during different metabolic states. We found that glucose administration reduced these measures selectively in the left supplementary motor area, indicating reduced synchronization between a target voxel within that region with its neighbor voxels or all voxels in the brain as well as reduced the resting state activity in that region, and increased fALFF and ReHo in the right middle frontal gyrus. For fALFF, we observed a significant interaction between metabolic states and glucose in the left thalamus. This interaction was driven by a fALFF increase after glucose treatment in the hunger relative to the satiety condition. The findings of Chapter 5 suggest that even when there is less

energy in the body, the brain can flexibly allocate the energy to regions of higher needs, as indicated by the changes in local (ReHo) and global (DC) connectivity after glucose administration, owing to the brain's unique capacity to control its own energy supply [49].

The results of Chapter 5 show that using local and global connectivity as well as the amplitude of rs-fMRI signals can contribute to the delineation of the relationship between changes in energy homeostasis and caloric intake.

9.1.2 Second question: What is a reliable marker of rs-fMRI signals to study the effect of hunger and satiety on the human brain?

In Chapter 6, we compared the accuracy of ReHo, DC and fALFF approaches for the classification of two metabolic states (hunger vs. satiety) depending on the observed rs-fMRI fluctuations. Therefore, we reanalyzed the obtained data but focused on the brain activity of both experimental conditions before glucose administration. After extracting the associated connectivity parameters of 90 brain regions for each method, we used feature selection algorithms with the objective function of linear SVM classification and permutation tests to investigate which method differentiates best between hunger and satiety. We observed that the fALFF region subset selected by the sequential forward floating selection algorithm identified the hunger state with the highest classification accuracy of 81%, while the classification accuracy based on ReHo and DC was 79% and 70%, respectively.

Our results indicate that the amplitude of rs-fMRI signals serves as a suitable basis for machine learning based classification of brain activity. This opens up the possibility to apply this combination of algorithms to similar research questions, such as the characterization of brain states (e.g. sleep stages) or disease conditions (e.g. Alzheimer's disease, minimal cognitive impairment).

9.1.3 Third question: How can different metabolic states change whole brain activity and how are these changes associated with hormonal signals?

In Chapter 7 we studied the interplay of metabolic state (hungry vs. satiety) and glucose administration (including hormonal modulation) on brain activity. We used fALFF as an index that shows changes of brain activity because the results of Chapters 5 and 0 indicate that the fALFF of the BOLD rs-fMRI signal was the most sensitive measure to identify spontaneous brain activity associated with changes in homeostasis and caloric intake. To answer the above questions, multiple linear regression analysis was used to investigate the interdependence of amplitude of rs-fMRI signals, plasma insulin as well as glucose levels. We observed a modulatory impact of the fasting state on intrinsic brain activity in the posterior cingulate cortex. Strikingly, differences in plasma insulin levels between hunger and satiety states after glucose administration at the time of the scan were negatively related to brain activity in the posterior insula and superior frontal gyrus, while plasma glucose levels were positively associated with activity changes in the fusiform gyrus. Furthermore, we could show that changes in plasma insulin enhanced the connectivity between the posterior insula and superior frontal gyrus.

Our results suggest that hormonal signals like insulin alleviate an acute hemostatic energy deficit by modifying the homeostatic and frontal circuitry of the human brain.

9.1.4 Fourth question: What is the impact of different metabolic states on the causal interactions in a specific homeostasis hypothalamus-insula circuit?

Both the hypothalamus and insular cortex play an essential role in the regulation of homeostasis by responding to hunger- and satiety-related signals. Rs-fMRI studies showed that alterations in FC of these sites are associated with the fluctuation of metabolic states and caloric intake (see Chapter 8). However, FC captures purely correlational dependencies between the neurovascular

signaling of two regions. Accordingly, FC cannot provide any information regarding the modulatory impact of metabolic states on the directed or effective connectivity between the hypothalamus, posterior insula (PINS) and anterior insula (AINS). To overcome this limitation, we used spectral DCM to estimate effective connectivity between brain regions at the neural rather than vascular levels [147]. Specifically, we investigated whether effective connectivity within this network varies as a function of the metabolic state (hunger vs. satiety) and energy availability (e.g. glucose levels).

Using a Bayesian model selection, we observed that the same model was identified as the most likely model for each rs-fMRI recording. Compared to satiety, the hunger condition enhanced the strength of the forward connections from PINS to AINS and reduced the strength of backward connections from AINS to PINS. Furthermore, the strength of connectivity from PINS to AINS was positively related to plasma cortisol levels in the hunger condition, mainly before glucose administration. However, there was no direct relationship between glucose treatment and effective connectivity.

Our findings suggest that metabolic states modulate connectivity between PINS and AINS and relate to theories of interoception and homeostatic regulation that invoke hierarchical relations between posterior and anterior insula.

9.2 Methodological considerations

For the present work various approaches for analyzing rs-fMRI data were applied, which require some methodological considerations:

First of all, we minimized frequently discussed limitations related to fMRI approaches such as artifacts and noise. Because we applied an ICA-AROMA strategy on the data, which in addition to motion artifacts also removes other structured noise from the data (e.g. cardiac pulsation

artifacts; Pruim et al. 2015b), we argue that the results of this work are not caused by motion artifacts and non-specific physiological effects. Also, we regressed out the time-series for WM and CSF from the data to remove and reduce residual (non-motion related) physiological noise.

Regarding voxel-based connectivity modeling, we applied three data-driven approaches to study the effect of glucose on local and global of brain FC as well as on the amplitude of brain activity. Of those three, fALFF index appeared to be the most sensitive measure for the detection of homeostatic changes in the resting brain. This might result from fALFF's property as an index of the power of the BOLD signal in the low-frequency range. Whereas fALFF measures the overall BOLD fluctuations of a single voxel without evaluating the relationship between voxels, ReHo and DC analyses calculate the state-dependent dynamics of BOLD connectivity, either with the 26 neighboring voxels (ReHo) or with the entire brain (DC). Overall, using multimethod rs-fMRI analyses provided additional insights into underlying network changes, which were crucial for interpreting our results

In terms of statistical models, we used rm-ANOVAs to study the changes in brain activity over experimental conditions except for the functional connectivity analyses described in Chapter 4. In short, ANOVA is a univariate approach, applied on a voxel-by-voxel basis, and hence a special case of the general linear model (GLM) [438]. One critical limitation of GLM approaches is the fact that covariance across neighboring voxels is not informative about the combination of voxels or brain regions to study differences between groups or experimental conditions [238,241].

In contrast, multivariate approaches provide a complete realistic design which is better suited for complex research problems [439,440], such as associations between brain networks [241,441]. To address this issue, we additionally applied a linear SVM method (Chapter 6) to investigate the

as the amplitude of rs-fMRI signals. The results of both univariate and multivariate approaches pointed to the amplitude of the BOLD signal as the most informative index to investigate the effects of metabolic states on brain functions, rather than local and global connectivity.

9.3 Caveats and future directions

Although the current study led to novel findings on mechanisms changing spontaneous brain activity under different metabolic states, some limitations need to be addressed.

First, although the hypothalamus is a central region for the regulation of energy homeostasis, food intake and glucose sensing [442,443], we did not find its activity modulated in each of our investigations (Chapters 5 and 7), which may be due to insufficient resolution of this small structure in fMRI imaging [4] and the use of cluster-level correction (number of voxels per cluster; [193]). This shortcoming might be overcome by performing specific scanning protocols targeted at subcortical structures (e.g. by reducing voxel size to 1 x 1 x 1 mm, see [444]) in combination with region-of-interest analyses to detect hypothalamic effects. Furthermore, we were not able to show a significant effect of hunger on connections from the hypothalamus to AINS or PINS and vice versa (see Chapter 8). It has been shown that nuclei of the hypothalamus stimulate feeding (lateral hypothalamus, LH) or inhibit feeding behavior (ventromedial hypothalamus nucleus, VMN) [445,446]. This dual function of hypothalamic nuclei, as well as their small size, might have led to a canceling of the two opposing signals [4]. Moreover, the acquisition parameters of the fMRI were not optimized to differentiate between different nuclei in such a small subcortical structure. Additionally, the SNR of BOLD signals from subcortical nuclei is generally lower than in cortex.

Second, to limit the influence of the hormonal cycle, we only included healthy young male participants in the current study. Therefore, the results of this dissertation may not be readily generalizable to other populations such as women. However, functional neuroimaging studies have shown differences in response to food taste (e.g. sweet, liquid meals) and even to odors of sweet (e.g. Abu Afif Baklava) under hunger and satiety conditions in several sexually dimorphic and BMI-sensitive brain regions [372,447–449]. Also, the effects of insulin signaling on the human brain show sex differences [91,450]. Future studies could address this question by also including women and overweight participants and thus discuss the relationship between changes in brain activity under different metabolic states and sex or BMI.

Finally, as mentioned in the introduction of Chapter 8, the hypothalamus and insular cortex are involved in a variety of functions related to interoception and homeostatic regulation in response to different metabolic states. Here, we investigated a particular set of models comprising five brain regions to address specific questions about relationships among connectivity in this network and physiological states. It is important to keep in mind that the models we examined are (necessarily) wrong in that they are enormously simplified compared to the real neural system and only consider a small number of potentially relevant regions. Including additional regions and connections (e.g. hypothalamic subnuclei) could change the input structure to (some or all) regions and may alter the results. This "missing region" problem — and other caveats of effective connectivity analyses with DCM (and other methods) — are well known and have been discussed previously (e.g. [451]). It is therefore important to establish the "utility" of the particular model we identified, for example, whether the inferred connection strengths relate to independent variables (e.g. physiological states) and whether these connectivity estimates allow for out-of-

sample predictions. While the former has been examined in this study, the latter will be investigated in future work.

There are still many questions arising from the results of this dissertation worth to be explored in the future in order to enhance the understanding of food intake and its impact on brain activity and connectivity. For instance, from the method's point of view, dynamic fluctuation of adipocyte-dependent (e.g. leptin and adiponectin) and gut-dependent (e.g. ghrelin and insulin) hormones together with their relationships to resting state brain networks under different metabolic conditions have not been studied yet. To investigate this issue, an experimental paradigm that collects both rs-fMRI measurements and hormone levels over multiple time points under fasting and eating conditions appears suitable, together with a multivariate approach for instance, such as parallel ICA [452–454], to investigate the relationship between the time-variations in resting state brain networks and hormone time-courses.

Another interesting question is how the changes in homeostasis and caloric intake affect the organization and the effective connectivity of large-scale networks, namely: the salience network (SN), dorsal attention network (DAN) and DMN. While the DMN is involved in self-related processes and future-oriented thinking during resting brain functions, the DAN is engaged in externally directed tasks, such as cognitive control of emotion and behavior. The SN is proposed as a switching network between DMN and DAN to allocate behavior with the goal of maintaining homeostasis [455]. Therefore, re-analysis of the data obtained by this project by using group ICA analysis to specify the ROIs for each network and spectral DCM models to find the direct connectivity between the networks could help to understand the causal processes among resting state networks in response to the interactions between metabolic states and glucose treatment [456].

9.4 Concluding remarks

The present dissertation investigated whether changes in physiological metabolic states (i.e. hunger and satiety) together with the availability of energy (e.g. glucose administration) can affect the resting state brain activity in healthy normal-weight male participants. Additional physiological and behavioral responses of fasting and standard meal conditions were determined to gain insights into the underlying regulatory mechanism between hormonal levels (e.g. insulin and cortisol levels) and metabolic states.

The current project shows for the first time that the amplitude of BOLD signals is a reliable and accurate marker rather than local (ReHo) and global (DC) connectivity to localize brain functions and to find patterns of brain networks related to metabolic states. For localizing brain function the metabolic state of hunger increased the amplitude of BOLD signals or the activity of brain regions in the PCC and thalamus. Furthermore, the changes in the amplitude of brain signals, reflecting the difference between hunger vs. satiety, were associated negatively with changes in plasma insulin levels in the posterior insula after glucose administration. Regarding brain activation patterns, combinations of amplitude BOLD signals in five brain regions (Olfactory, Occipital, Paracentral, Rolandic operculum and Frontal gyri) can accurately distinguish between metabolic states (hunger vs. satiety) with 81% accuracy.

The second important finding of the current work is that changes in metabolic states, not oral glucose administration, have effects on the strength of the endogenous (intrinsic) connections within the insular cortex. Our results seem to be consistent with other research which found that the transfer information from posterior to anterior insula is associated with awareness of bodily and homeostatic perceptions [397,430]. Furthermore, our findings indicate that spDCM provides helpful insights into the brain mechanisms involved in homeostatic regulation.

Overall, the hunger and satiety states not only modulate brain activity but also have influences on the direction of information flow. Using multi-method rs-fMRI to investigate the brain connectivity provides an unbiased approach to identify spontaneous brain activity associated with changes in homeostasis and caloric intake. Taken together, this work provides new insights into the interaction of food intake and CNS activity that may be used for further investigations of metabolic dysfunction, for instance, obesity.

References

- Begg DP, Woods SC. The endocrinology of food intake. Nature Reviews Endocrinology. 2013. pp. 584–597. doi:10.1038/nrendo.2013.136
- 2. Kaur J. A comprehensive review on metabolic syndrome. Cardiol Res Pract. Hindawi; 2014;2014.
- 3. Zanchi D, Depoorter A, Egloff L, Haller S, Mählmann L, Lang UE, et al. The impact of gut hormones on the neural circuit of appetite and satiety: A systematic review. Neurosci Biobehav Rev. Elsevier; 2017;
- 4. De Silva A, Salem V, Matthews PM, Dhillo WS. The use of functional MRI to study appetite control in the CNS. Exp Diabetes Res. 2012;2012. doi:10.1155/2012/764017
- 5. Vartanian LR, Spanos S, Herman CP, Polivy J. Modeling of food intake: a meta-analytic review. Soc Influ. 2015;10: 119–136. doi:10.1080/15534510.2015.1008037
- 6. Darmon N, Drewnowski A. Contribution of food prices and diet cost to socioeconomic disparities in diet quality and health: A systematic review and analysis. Nutr Rev. 2015;73: 643–660. doi:10.1093/nutrit/nuv027
- 7. Kroemer NB, Krebs L, Kobiella A, Grimm O, Vollstädt-Klein S, Wolfensteller U, et al. (Still) longing for food: Insulin reactivity modulates response to food pictures. Hum Brain Mapp. 2013;34: 2367–2380. doi:10.1002/hbm.22071
- 8. Huettel SA, Song AW, McCarthy G. Functional magnetic resonance imaging. Sinauer Associates Sunderland; 2004.
- 9. Schilds H. MRI made easy [Internet]. (...Well Almost). Berlin: Schering AG; 1991. doi:10.1017/CBO9781107415324.004
- 10. Jezzard P, Clare S. Principle of nuclear magnetic resonance and MRI. Functional MRI an introduction to methods. Oxford University Press; 2002. pp. 67–92.
- 11. Pooley RA. Fundamental physics of MR imaging. Radiographics. Radiological Society of North America; 2005:25: 1087–1099.
- 12. Hashemi H, Bradley WG, J. L. MRI: the basics. 3rd ed. Philadelphia: Lippincott Williams & Wilkins; 2011.
- 13. Currie S, Hoggard N, Craven IJ, Hadjivassiliou M, Wilkinson ID. Understanding MRI: basic MR physics for physicians. Postgrad Med J. The Fellowship of Postgraduate Medicine; 2013;89: 209–223.
- 14. Logothetis NK, Wandell BA. Interpreting the BOLD Signal. Annu Rev Physiol. 2004;66: 735–769. doi:10.1146/annurev.physiol.66.082602.092845
- 15. MacIntosh BJ, Graham SJ. Magnetic resonance imaging to visualize stroke and characterize stroke recovery: A review. Front Neurol. 2013;4 MAY. doi:10.3389/fneur.2013.00060
- 16. Poldrack R a, Mumford JA, Nichols TE. Handbook of functional MRI data analysis. Russell The Journal Of The Bertrand Russell Archives. 2011.
- 17. Pauling L, Coryell CD. The Magnetic Properties and Structure of Hemoglobin, Oxyhemoglobin and Carbonmonoxyhemoglobin. Proc Natl Acad Sci. 1936; doi:10.1073/pnas.22.4.210
- 18. Ogawa S, Lee TM, Kay AR, Tank DW. Brain magnetic resonance imaging with contrast dependent on blood oxygenation. Proc Natl Acad Sci U S A. 1990; doi:http://dx.doi.org/10.1073/pnas.87.24.9868
- 19. Malonek D, Grinvald A. Interactions Between Electrical Activity and Cortical Microcirculation Revealed by Imaging Spectroscopy: Implications for Functional Brain Mapping. Science (80-). 1996; doi:10.1126/science.272.5261.551
- 20. Heeger DJ, Ress D. What does fMRI tell us about neuronal activity? Nature Reviews Neuroscience. 2002. pp. 142–151. doi:10.1038/nrn730
- 21. Linden DE, Prvulovic D, Formisano E, Völlinger M, Zanella FE, Goebel R, et al. The functional neuroanatomy of target detection: an fMRI study of visual and auditory oddball tasks. Cereb cortex. 1999;9: 815–823. doi:10.1093/cercor/9.8.815
- Worsley KJ. An overview and some new developments in the statistical analysis of PET and fMRI data. Hum Brain Mapp. 1997;5: 254–258. doi:10.1002/(SICI)1097-0193(1997)5:4<254::AID-HBM9>3.0.CO;2-2
- 23. Worsley KJ, Friston KJ. Analysis of fMRI time-series revisited Again. Neuroimage. 1995;2: 173–181. doi:10.1006/nimg.1995.1023
- 24. Greicius M. Resting-state functional connectivity in neuropsychiatric disorders. Curr Opin Neurol. 2008;21: 424–30. doi:10.1097/WCO.0b013e328306f2c5
- 25. Greicius MD, Supekar K, Menon V, Dougherty RF. Resting-state functional connectivity reflects structural connectivity in the default mode network. Cereb Cortex. 2009; doi:10.1093/cercor/bhn059

- Fox MD, Snyder AZ, Vincent JL, Raichle ME. Intrinsic Fluctuations within Cortical Systems Account for Intertrial Variability in Human Behavior. Neuron. 2007;56: 171–184. doi:10.1016/j.neuron.2007.08.023
- 27. Lohmann G, Hoehl S, Brauer J, Danielmeier C, Bornkessel-Schlesewsky I, Bahlmann J, et al. Setting the frame: The human brain activates a basic low-frequency network for language processing. Cereb Cortex. 2010;20: 1286–1292. doi:10.1093/cercor/bhp190
- 28. Auer DP. Spontaneous low-frequency blood oxygenation level-dependent fluctuations and functional connectivity analysis of the "resting" brain. Magn Reson Imaging. 2008;26: 1055–1064. doi:10.1016/j.mri.2008.05.008
- 29. Biswal B, FZ Y, VM H, JS H. Functional connectivity in the motor cortex of resting human brain using. Magn Reson Med. 1995;34: 537–541. doi:10.1002/mrm.1910340409
- 30. Biswal BB. Resting state fMRI: A personal history. NeuroImage. 2012. pp. 938–944. doi:10.1016/j.neuroimage.2012.01.090
- 31. Raichle ME, MacLeod AM, Snyder AZ, Powers WJ, Gusnard DA, Shulman GL. A default mode of brain function. Proc Natl Acad Sci U S A. 2001;98: 676–82. doi:10.1073/pnas.98.2.676
- 32. Fox MD, Raichle ME. Spontaneous fluctuations in brain activity observed with functional magnetic resonance imaging. Nature Reviews Neuroscience. 2007. pp. 700–711. doi:10.1038/nrn2201
- 33. Greicius MD, Krasnow B, Reiss AL, Menon V. Functional connectivity in the resting brain: a network analysis of the default mode hypothesis. Proc Natl Acad Sci U S A. 2003;100: 253–8. doi:10.1073/pnas.0135058100
- 34. Buckner RL, Andrews-Hanna JR, Schacter DL. The brain's default network: Anatomy, function, and relevance to disease. Ann N Y Acad Sci. 2008;1124: 1–38. doi:10.1196/annals.1440.011
- 35. Raichle ME. The Brain's Default Mode Network. Annu Rev Neurosci. 2015;38: 433–447. doi:10.1146/annurev-neuro-071013-014030
- 36. Greicius MD, Srivastava G, Reiss AL, Menon V. Default-mode network activity distinguishes Alzheimer's disease from healthy aging: evidence from functional MRI. Proc Natl Acad Sci U S A. 2004;101: 4637–42. doi:10.1073/pnas.0308627101
- 37. Hogenkamp PS, Zhou W, Dahlberg LS, Stark J, Larsen AL, Olivo G, et al. Higher resting-state activity in reward-related brain circuits in obese versus normal-weight females independent of food intake. Int J Obes. 2016;40: 1687–1692. doi:10.1038/ijo.2016.105
- 38. Kullmann S, Heni M, Veit R, Scheffler K, Machann J, Häring H-U, et al. Intranasal insulin enhances brain functional connectivity mediating the relationship between adiposity and subjective feeling of hunger. Sci Rep. Nature Publishing Group; 2017;7.
- 39. Castellanos FX, Margulies DS, Kelly C, Uddin LQ, Ghaffari M, Kirsch A, et al. Cingulate-precuneus interactions: a new locus of dysfunction in adult attention-deficit/hyperactivity disorder. Biol Psychiatry. Elsevier; 2008;63: 332–337.
- 40. Fleisher AS, Sherzai A, Taylor C, Langbaum JBS, Chen K, Buxton RB. Resting-state BOLD networks versus task-associated functional MRI for distinguishing Alzheimer's disease risk groups. Neuroimage. 2009;47: 1678–1690. doi:10.1016/j.neuroimage.2009.06.021
- 41. Varoquaux G, Baronnet F, Kleinschmidt A, Fillard P, Thirion B. Detection of brain functional-connectivity difference in post-stroke patients using group-level covariance modeling. Lecture Notes in Computer Science (including subseries Lecture Notes in Artificial Intelligence and Lecture Notes in Bioinformatics). 2010. pp. 200–208. doi:10.1007/978-3-642-15705-9 25
- 42. Murphy SE, Mackay CE. Using MRI to measure drug action: caveats and new directions. J Psychopharmacol. Sage Publications Sage UK: London, England; 2011;25: 1168–1174.
- 43. Khalili-Mahani N, Zoethout RMW, Beckmann CF, Baerends E, de Kam ML, Soeter RP, et al. Effects of morphine and alcohol on functional brain connectivity during "resting state": A placebo-controlled crossover study in healthy young men. Hum Brain Mapp. 2012;33: 1003–1018. doi:10.1002/hbm.21265
- 44. García-García I, Jurado MÁ, Garolera M, Segura B, Sala-Llonch R, Marqués-Iturria I, et al. Alterations of the salience network in obesity: A resting-state fMRI study. Hum Brain Mapp. 2013;34: 2786–2797. doi:10.1002/hbm.22104
- 45. Zuo X-N, Xing X-X. Test-retest reliabilities of resting-state FMRI measurements in human brain functional connectomics: A systems neuroscience perspective. Neurosci Biobehav Rev. 2014; doi:10.1016/j.neubiorev.2014.05.009
- 46. Wölnerhanssen BK, Meyer-Gerspach AC, Schmidt A, Zimak N, Peterli R, Beglinger C, et al. Dissociable Behavioral, Physiological and Neural Effects of Acute Glucose and Fructose Ingestion: A Pilot Study. PLoS One. 2015;10: e0130280. doi:10.1371/journal.pone.0130280
- 47. Göbel B, Oltmanns KM, Chung M. Linking neuronal brain activity to the glucose metabolism. Theor Biol

- Med Model. 2013;10: 50. doi:10.1186/1742-4682-10-50
- 48. Kroemer NB, Krebs L, Kobiella A, Grimm O, Pilhatsch M, Bidlingmaier M, et al. Fasting levels of ghrelin covary with the brain response to food pictures. Addict Biol. 2013;18: 855–862. doi:10.1111/j.1369-1600.2012.00489.x
- 49. Peters A, Langemann D. Build-ups in the supply chain of the brain: on the neuroenergetic cause of obesity and type 2 diabetes mellitus. Front Neuroenergetics. 2009;1: 2. doi:10.3389/neuro.14.002.2009
- 50. Smitha KA, Raja KA, Arun KM, Rajesh PG, Thomas B, Kapilamoorthy TR, et al. Resting state fMRI: A review on methods in resting state connectivity analysis and resting state networks. 2017; doi:10.1177/1971400917697342
- 51. Killgore WDS, Young AD, Femia LA, Bogorodzki P, Rogowska J, Yurgelun-Todd DA. Cortical and limbic activation during viewing of high-versus low-calorie foods. Neuroimage. Elsevier; 2003;19: 1381–1394.
- 52. Cornier M-A, Von Kaenel SS, Bessesen DH, Tregellas JR. Effects of overfeeding on the neuronal response to visual food cues—. Am J Clin Nutr. Oxford University Press; 2007;86: 965–971.
- 53. Frank S, Laharnar N, Kullmann S, Veit R, Canova C, Hegner YL, et al. Processing of food pictures: Influence of hunger, gender and calorie content. Brain Res. 2010;1350: 159–166. doi:https://doi.org/10.1016/j.brainres.2010.04.030
- 54. Führer D, Zysset S, Stumvoll M. Brain activity in hunger and satiety: an exploratory visually stimulated FMRI study. Obesity. Wiley Online Library; 2008;16: 945–950.
- 55. Goldstone AP, Prechtl de Hernandez CG, Beaver JD, Muhammed K, Croese C, Bell G, et al. Fasting biases brain reward systems towards high-calorie foods. Eur J Neurosci. Wiley Online Library; 2009;30: 1625–1635.
- 56. Siep N, Roefs A, Roebroeck A, Havermans R, Bonte ML, Jansen A. Hunger is the best spice: an fMRI study of the effects of attention, hunger and calorie content on food reward processing in the amygdala and orbitofrontal cortex. Behav Brain Res. Elsevier; 2009;198: 149–158.
- 57. Mehta S, Melhorn SJ, Smeraglio A, Tyagi V, Grabowski T, Schwartz MW, et al. Regional brain response to visual food cues is a marker of satiety that predicts food choice—. Am J Clin Nutr. Oxford University Press; 2012;96: 989–999.
- 58. Luo S, Monterosso JR, Sarpelleh K, Page KA. Differential effects of fructose versus glucose on brain and appetitive responses to food cues and decisions for food rewards. Proc Natl Acad Sci. National Acad Sciences; 2015;112: 6509–6514.
- 59. Lizarbe B, Benitez A, Peláez Brioso GA, Sánchez-Montañés M, López-Larrubia P, Ballesteros P, et al. Hypothalamic metabolic compartmentation during appetite regulation as revealed by magnetic resonance imaging and spectroscopy methods. Front Neuroenergetics. 2013; doi:10.3389/fnene.2013.00006
- 60. Frank S, Kullmann S, Veit R. Food related processes in the insular cortex. Front Hum Neurosci. 2013;7: 1–6. doi:10.3389/fnhum.2013.00499
- 61. Dagher A. Functional brain imaging of appetite. Trends in Endocrinology and Metabolism. 2012. doi:10.1016/j.tem.2012.02.009
- 62. Kenny PJ. Reward Mechanisms in Obesity: New Insights and Future Directions. Neuron. Elsevier Inc.; 2011;69: 664–679. doi:10.1016/j.neuron.2011.02.016
- 63. Valassi E, Scacchi M, Cavagnini F. Neuroendocrine control of food intake. Nutr Metab Cardiovasc Dis. 2008; doi:10.1016/j.numecd.2007.06.004
- 64. Mayer EA. Gut feelings: the emerging biology of gut-brain communication. Nat Rev Neurosci. Nature Publishing Group; 2011;12: 453.
- 65. Schloegl H, Percik R, Horstmann A, Villringer A, Stumvoll M. Peptide hormones regulating appetite—focus on neuroimaging studies in humans. Diabetes Metab Res Rev. Wiley Online Library; 2011;27: 104–112.
- 66. Wright H, Li X, Fallon NB, Crookall R, Giesbrecht T, Thomas A, et al. Differential effects of hunger and satiety on insular cortex and hypothalamic functional connectivity. Eur J Neurosci. 2016;43: 1181–1189. doi:10.1111/ejn.13182
- 67. Smeets PAM, De Graaf C, Stafleu A, Van Osch MJP, Van Der Grond J. Functional MRI of human hypothalamic responses following glucose ingestion. Neuroimage. 2005;24: 363–368. doi:10.1016/j.neuroimage.2004.07.073
- 68. Smeets P a M, Vidarsdottir S, de Graaf C, Stafleu A, van Osch MJP, Viergever M a, et al. Oral glucose intake inhibits hypothalamic neuronal activity more effectively than glucose infusion. Am J Physiol Endocrinol Metab. 2007;293: E754–E758. doi:10.1152/ajpendo.00231.2007
- 69. Kullmann S, Frank S, Heni M, Ketterer C, Veit R, Häring H-U, et al. Intranasal insulin modulates intrinsic reward and prefrontal circuitry of the human brain in lean women. Neuroendocrinology. Karger Publishers; 2012;97: 176–182.

- 70. Little TJ, McKie S, Jones RB, D'Amato M, Smith C, Kiss O, et al. Mapping glucose-mediated gut-to-brain signalling pathways in humans. Neuroimage. Elsevier B.V.; 2014;96: 1–11. doi:10.1016/j.neuroimage.2014.03.059
- 71. Thomas JM, Higgs S, Dourish CT, Hansen PC, Harmer CJ, McCabe C. Satiation attenuates BOLD activity in brain regions involved in reward and increases activity in dorsolateral prefrontal cortex: An fMRI study in healthy volunteers. Am J Clin Nutr. 2015; doi:10.3945/ajcn.114.097543
- 72. Broberger C. Brain regulation of food intake and appetite: Molecules and networks. Journal of Internal Medicine. 2005. pp. 301–327. doi:10.1111/j.1365-2796.2005.01553.x
- 73. Gómez-Pinilla F. Brain foods: The effects of nutrients on brain function. Nature Reviews Neuroscience. 2008. pp. 568–578. doi:10.1038/nrn2421
- 74. Kim KS, Seeley RJ, Sandoval DA. Signalling from the periphery to the brain that regulates energy homeostasis. Nature Reviews Neuroscience. 2018. pp. 185–196. doi:10.1038/nrn.2018.8
- 75. Benoit SC, Clegg DJ, Seeley RJ, Woods SC. Insulin and leptin as adiposity signals. Recent Prog Horm Res. 2004; doi:10.1210/rp.59.1.267
- 76. Hillebrand JJG, Geary N. Do leptin and insulin signal adiposity? Frontiers in Eating and Weight Regulation. 2009. pp. 111–122. doi:10.1159/000264399
- 77. Schwartz MW, Woods SC, Porte D, Seeley RJ, Baskin DG. Central nervous system control of food intake. Nature. 2000;404: 661–671. doi:10.1038/35007534
- 78. Banks WA, Lim WS. Insulin and the Blood-Brain Barrier. Blood-Brain Barriers: From Ontogeny to Artificial Interfaces. 2007. pp. 265–285. doi:10.1002/9783527611225.ch12
- 79. Havrankova J, Roth J, Brownstein M. Insulin receptors are widely distributed in the central nervous system of the rat. Nature. 1978. pp. 827–829. doi:10.1038/272827a0
- 80. Hill JM, Lesniak MA, Pert CB, Roth J. Autoradiographic localization of insulin receptors in rat brain: Prominence in olfactory and limbic areas. Neuroscience. 1986;17: 1127–1138. doi:10.1016/0306-4522(86)90082-5
- 81. Hopkins DFC, Williams G. Insulin receptors are widely distributed in human brain and bind human and porcine insulin with equal affinity. Diabet Med. 1997;14: 1044–1050. doi:10.1002/(SICI)1096-9136(199712)14:12<1044::AID-DIA508>3.0.CO;2-F
- 82. Kullmann S, Heni M, Veit R, Scheffler K, Machann J, Haring HU, et al. Selective insulin resistance in homeostatic and cognitivecontrol brain areas in overweight and obese adults. Diabetes Care. 2015;38: 1044–1050. doi:10.2337/dc14-2319
- 83. Heni M, Kullmann S, Preissl H, Fritsche A, Häring H. Impaired insulin action in the human brain: causes and metabolic consequences. Nat Publ Gr. Nature Publishing Group; 2015; doi:10.1038/nrendo.2015.173
- 84. Obici S, Zhang BB, Karkanias G, Rossetti L. Hypothalamic insulin signaling is required for inhibition of glucose production. Nat Med. Nature Publishing Group; 2002;8: 1376.
- 85. Obici S, Feng Z, Karkanias G, Baskin DG, Rossetti L. Decreasing hypothalamic insulin receptors causes hyperphagia and insulin resistance in rats. Nat Neurosci. Nature Publishing Group; 2002;5: 566.
- 86. Schwartz MW. Brain pathways controlling food intake and body weight. Exp Biol Med. SAGE Publications Sage UK: London, England; 2001;226: 978–981.
- 87. Gerozissis K, Kyriaki G. Brain insulin: regulation, mechanisms of action and functions. Cell Mol Neurobiol. 2003;23: 1–25. doi:10.1023/A:1022598900246
- 88. Kleinridders A, Ferris HA, Cai W, Kahn CR. Insulin action in brain regulates systemic metabolism and brain function. Diabetes. 2014;63: 2232–2243. doi:10.2337/db14-0568
- 89. Chavez M, Kaiyala K, Madden LJ, Schwartz MW, Woods SC. Intraventricular insulin and the level of maintained body weight in rats. Behav Neurosci. American Psychological Association; 1995;109: 528.
- 90. Brown LM, Clegg DJ, Benoit SC, Woods SC. Intraventricular insulin and leptin reduce food intake and body weight in C57BL/6J mice. Physiol Behav. Elsevier; 2006;89: 687–691.
- 91. Benedict C, Kern W, Schultes B, Born J, Hallschmid M. Differential sensitivity of men and women to anorexigenic and memory-improving effects of intranasal insulin. J Clin Endocrinol Metab. Oxford University Press; 2008;93: 1339–1344.
- 92. McGowan MK, Andrews KM, Kelly J, Grossman SP. Effects of chronic intrahypothalamic infusion of insulin on food intake and diurnal meal patterning in the rat. Behav Neurosci. American Psychological Association; 1990;104: 373.
- 93. Brüning JC, Gautam D, Burks DJ, Gillette J, Schubert M, Orban PC, et al. Role of brain insulin receptor in control of body weight and reproduction. Science (80-). American Association for the Advancement of Science; 2000;289: 2122–2125.

- 94. Pruim RHR, Mennes M, Buitelaar JK, Beckmann CF. Evaluation of ICA-AROMA and alternative strategies for motion artifact removal in resting state fMRI. Neuroimage. Elsevier Inc.; 2015; doi:10.1016/j.neuroimage.2015.02.063
- 95. Klein A, Andersson J, Ardekani BA, Ashburner J, Avants B, Chiang M-C, et al. Evaluation of 14 nonlinear deformation algorithms applied to human brain MRI registration. Neuroimage. Elsevier; 2009;46: 786–802.
- 96. McLaren DG, Kosmatka KJ, Kastman EK, Bendlin BB, Johnson SC. Rhesus macaque brain morphometry: a methodological comparison of voxel-wise approaches. Methods. Elsevier; 2010;50: 157–165.
- 97. Jenkinson M, Bannister P, Brady M, Smith S. Improved optimization for the robust and accurate linear registration and motion correction of brain images. Neuroimage. 2002;17: 825–841. doi:10.1016/S1053-8119(02)91132-8
- 98. Pruim RHR, Mennes M, van Rooij D, Llera A, Buitelaar JK, Beckmann CF. ICA-AROMA: A robust ICA-based strategy for removing motion artifacts from fMRI data. Neuroimage. Elsevier Inc.; 2015;112: 267–277. doi:10.1016/j.neuroimage.2015.02.064
- 99. Yan. DPARSF: a MATLAB toolbox for "pipeline" data analysis of resting-state fMRI. Front Syst Neurosci. 2010;4: 1–7. doi:10.3389/fnsys.2010.00013
- Zang Y, Jiang T, Lu Y, He Y, Tian L. Regional homogeneity approach to fMRI data analysis. Neuroimage. 2004;22: 394–400. doi:10.1016/j.neuroimage.2003.12.030
- 101. Zou QH, Zhu CZ, Yang Y, Zuo XN, Long XY, Cao QJ, et al. An improved approach to detection of amplitude of low-frequency fluctuation (ALFF) for resting-state fMRI: Fractional ALFF. J Neurosci Methods. 2008;172: 137–141. doi:10.1016/j.jneumeth.2008.04.012
- 102. Tzourio-Mazoyer N, Landeau B, Papathanassiou D, Crivello F, Etard O, Delcroix N, et al. Automated anatomical labeling of activations in SPM using a macroscopic anatomical parcellation of the MNI MRI single-subject brain. Neuroimage. 2002;15: 273–289. doi:10.1006/nimg.2001.0978
- 103. Johnson NA, Stannard SR, Rowlands DS, Chapman PG, Thompson CH, O'Connor H, et al. Effect of short-term starvation versus high-fat diet on intramyocellular triglyceride accumulation and insulin resistance in physically fit men. Exp Physiol. 2006;91: 693–703.
- 104. Corvilain B, Abramowicz M, Fery F, Schoutens A, Verlinden M, Balasse E, et al. Effect of short-term starvation on gastric emptying in humans: relationship to oral glucose tolerance. Am J Physiol Liver Physiol. 1995;269: G512–G517.
- 105. Flint A, Gregersen NT, Gluud LL, Møller BK, Raben A, Tetens I, et al. Associations between postprandial insulin and blood glucose responses, appetite sensations and energy intake in normal weight and overweight individuals: a meta-analysis of test meal studies. Br J Nutr. Cambridge University Press; 2007;98: 17–25.
- 106. Graaf C De, Blom WAM, Smeets PAM, Stafleu A, Hendriks HFJ. Biomarkers of satiation and satiety 1, 2. 2004; 946–961.
- 107. Ciampolini M, Bianchi R. Training to estimate blood glucose and to form associations with initial hunger. Nutr Metab (Lond). 2006;3: 42. doi:10.1186/1743-7075-3-42
- Johnstone AM, Faber P, Andrew R, Gibney ER, Elia M, Lobley G, et al. Influence of short-term dietary weight loss on cortisol secretion and metabolism in obese men. Eur J Endocrinol. 2004; doi:10.1530/eje.0.1500185
- 109. Tomiyama AJ, Mann T, Vinas D, Hunger JM, Dejager J, Taylor SE. Low calorie dieting increases cortisol. Psychosom Med. 2010; doi:10.1097/PSY.0b013e3181d9523c
- 110. Friston KJ. Imaging neuroscience: Principles or maps? Proc Natl Acad Sci. 1998; doi:10.1073/pnas.95.3.796
- 111. Friston KJ. Functional and effective connectivity: a review. Brain Connect. 2011;1: 13–36. doi:10.1089/brain.2011.0008
- 112. Lang EW, Tomé AM, Keck IR, Górriz-Sáez JM, Puntonet CG. Brain connectivity analysis: A short survey. Computational Intelligence and Neuroscience. 2012. doi:10.1155/2012/412512
- Joel SE, Caffo BS, Van Zijl PCM, Pekar JJ. On the relationship between seed-based and ICA-based measures of functional connectivity. Magn Reson Med. 2011; doi:10.1002/mrm.22818
- 114. Cole DM, Smith SM, Beckmann CF. Advances and pitfalls in the analysis and interpretation of resting-state FMRI data. 2010;4: 1–15. doi:10.3389/fnsys.2010.00008
- 115. Stone J V. Independent Component Analysis A Tutorial Introduction. London: Cambridge University Press; 2004.
- 116. Shlens J. A tutorial on independent component analysis. arXiv Prepr arXiv14042986. 2014;
- 117. Hyvärinen A, Oja E. Independent component analysis: Algorithms and applications. Neural Networks. 2000. doi:10.1016/S0893-6080(00)00026-5
- 118. McKeown MJ, Makeig S, Brown GG, Jung T, Kindermann SS, Bell AJ, et al. Analysis of fMRI data by blind separation into independent spatial components. Hum Brain Mapp. 1998;6: 160–188.

- doi:10.1002/(SICI)1097-0193(1998)6:3<160::AID-HBM5>3.0.CO;2-1
- 119. Calhoun VD, Adali T, Pearlson GD, Pekar JJ. A method for making group inferences from functional MRI data using independent component analysis. HumBrain Mapp. 2001;14: 140–151. doi:10.1016/S1053-8119(01)91431-4
- 120. Beckmann CF, DeLuca M, Devlin JT, Smith SM. Investigations into resting-state connectivity using independent component analysis. Philos Trans R Soc L B Biol Sci. 2005;360: 1001–1013. doi:10.1098/rstb.2005.1634
- 121. Calhoun VD, Adali T. Unmixing fMRI with independent component analysis. IEEE Eng Med Biol Mag. 2006;25: 79–90. doi:10.1109/MEMB.2006.1607672
- 122. Bijsterbosch JD, Smith S, Beckmann CF. Introduction to Resting State fMRI Functional Connectivity. Oxford: Oxford University Press; 2017.
- 123. Beckmann CF, Smith SM. Probabilistic Independent Component Analysis for Functional Magnetic Resonance Imaging. IEEE Trans Med Imaging. 2004;23: 137–152. doi:10.1109/TMI.2003.822821
- 124. Beckmann CF, Smith SM. Tensorial extensions of independent component analysis for multisubject FMRI analysis. Neuroimage. 2005;25: 294–311. doi:10.1016/j.neuroimage.2004.10.043
- 125. Cordes D, Nandy R. Independent component analysis in the presence of noise in fMRI. Magn Reson Imaging. Elsevier; 2007;25: 1237–1248.
- 126. Jiang L, Zuo X-N. Regional Homogeneity: A Multimodal, Multiscale Neuroimaging Marker of the Human Connectome. Neurosci. 2015; 1–20. doi:10.1177/1073858415595004
- 127. Zuo XN, Xu T, Jiang L, Yang Z, Cao XY, He Y, et al. Toward reliable characterization of functional homogeneity in the human brain: Preprocessing, scan duration, imaging resolution and computational space. Neuroimage. 2013; doi:10.1016/j.neuroimage.2012.10.017
- 128. Bullmore E, Sporns O. Complex brain networks: graph theoretical analysis of structural and functional systems. Nat Rev Neurosci. 2009;10: 186–198. doi:10.1038/nrn2575
- 129. Zuo XN, Ehmke R, Mennes M, Imperati D, Castellanos FX, Sporns O, et al. Network centrality in the human functional connectome. Cereb Cortex. 2012;22: 1862–1875. doi:10.1093/cercor/bhr269
- 130. Buckner RL, Sepulcre J, Talukdar T, Krienen FM, Liu H, Hedden T, et al. Cortical Hubs Revealed by Intrinsic Functional Connectivity: Mapping, Assessment of Stability, and Relation to Alzheimer's Disease. J Neurosci. 2009;29: 1860–1873. doi:10.1523/JNEUROSCI.5062-08.2009
- 131. Zang Y-F, He Y, Zhu C-Z, Cao Q-J, Sui M-Q, Liang M, et al. Altered baseline brain activity in children with ADHD revealed by resting-state functional MRI. Brain Dev. 2007;29: 83–91. doi:10.1016/j.braindev.2006.07.002
- 132. Küblböck M, Woletz M, Höflich A, Sladky R, Kranz GS, Hoffmann A, et al. Stability of low-frequency fluctuation amplitudes in prolonged resting-state fMRI. Neuroimage. 2014; doi:10.1016/j.neuroimage.2014.09.038
- 133. Zuo XN, Xing XX. Test-retest reliabilities of resting-state FMRI measurements in human brain functional connectomics: A systems neuroscience perspective. Neuroscience and Biobehavioral Reviews. 2014. doi:10.1016/j.neubiorev.2014.05.009
- 134. Zuo XN, Di Martino A, Kelly C, Shehzad ZE, Gee DG, Klein DF, et al. The oscillating brain: Complex and reliable. Neuroimage. Elsevier Inc.; 2010;49: 1432–1445. doi:10.1016/j.neuroimage.2009.09.037
- 135. Sato JR, Fujita A, Cardoso EF, Thomaz CE, Brammer MJ, Amaro E. Analyzing the connectivity between regions of interest: An approach based on cluster Granger causality for fMRI data analysis. Neuroimage. 2010; doi:10.1016/j.neuroimage.2010.05.022
- 136. Gates KM, Molenaar PCM, Hillary FG, Ram N, Rovine MJ. Automatic search for fMRI connectivity mapping: An alternative to Granger causality testing using formal equivalences among SEM path modeling, VAR, and unified SEM. Neuroimage. 2010; doi:10.1016/j.neuroimage.2009.12.117
- 137. McLntosh AR, Gonzalez-Lima F. Structural equation modeling and its application to network analysis in functional brain imaging. Hum Brain Mapp. 1994; doi:10.1002/hbm.460020104
- Büchel C, Friston KJ. Modulation of connectivity in visual pathways by attention: cortical interactions evaluated with structural equation modelling and fMRI. Cereb Cortex. 1997;7: 768–78. doi:10.1093/cercor/7.8.768
- 139. Penny WD, Stephan KE, Mechelli A, Friston KJ. Modelling functional integration: A comparison of structural equation and dynamic causal models. NeuroImage. 2004. doi:10.1016/j.neuroimage.2004.07.041
- 140. Friston KJ. Statistical Parametric Mapping: The Analysis of Functional Brain Images. Functional neuroimaging: Technical. 2006.
- 141. Seth AK, Chorley P, Barnett LC. Granger causality analysis of fMRI BOLD signals is invariant to

- hemodynamic convolution but not downsampling. Neuroimage. 2013; doi:10.1016/j.neuroimage.2012.09.049
- Wen X, Rangarajan G, Ding M. Is Granger Causality a Viable Technique for Analyzing fMRI Data? 2013;8. doi:10.1371/journal.pone.0067428
- 143. Friston K. Dynamic causal modeling and Granger causality Comments on: The identification of interacting networks in the brain using fMRI: Model selection, causality and deconvolution. Neuroimage. 2009; doi:10.1016/j.neuroimage.2009.09.031
- Deshpande G, Sathian K, Hu X. Effect of hemodynamic variability on Granger causality analysis of fMRI. Neuroimage. 2010; doi:10.1016/j.neuroimage.2009.11.060
- 145. Friston KJ, Harrison L, Penny W. Dynamic causal modelling. Neuroimage. 2003;19: 1273–1302. doi:https://doi.org/10.1016/S1053-8119(03)00202-7
- 146. Friston KJ, Li B, Daunizeau J, Stephan KE. Network discovery with DCM. Neuroimage. Elsevier Inc.; 2011;56: 1202–1221. doi:10.1016/j.neuroimage.2010.12.039
- 147. Friston K, Kahan J, Biswal B, Razi A. A DCM for resting state fMRI. Neuroimage. 2014;94: 396–407. doi:https://doi.org/10.1016/j.neuroimage.2013.12.009
- 148. Razi A, Kahan J, Rees G, Friston KJ. Construct validation of a DCM for resting state fMRI. Neuroimage. Elsevier; 2015;106: 1–14.
- 149. Razi A, Friston KJ. The connected brain: causality, models, and intrinsic dynamics. IEEE Signal Process Mag. IEEE; 2016;33: 14–35.
- 150. Stephan KE. On the role of general system theory for functional neuroimaging. 2004; 443–470.
- 151. Friston K, Kahan J, Razi A, Stephan KE, Sporns O. On nodes and modes in resting state fMRI. Neuroimage. Elsevier B.V.; 2014;99: 533–547. doi:10.1016/j.neuroimage.2014.05.056
- 152. Buxton RB, Wong EC, Frank LR. Dynamics of blood flow and oxygenation changes during brain activation: the balloon model. Magn Reson Med. Wiley Online Library; 1998;39: 855–864.
- 153. Stephan KE, Weiskopf N, Drysdale PM, Robinson PA, Friston KJ. Comparing hemodynamic models with DCM. Neuroimage. Elsevier; 2007;38: 387–401.
- Bullmore E, Long C, Suckling J, Fadili J, Calvert G, Zelaya F, et al. Colored noise and computational inference in neurophysiological (fMRI) time series analysis: Resampling methods in time and wavelet domains. Hum Brain Mapp. 2001; doi:10.1002/1097-0193(200102)12:2<61::AID-HBM1004>3.0.CO;2-W
- 155. Shin CW, Kim S. Self-organized criticality and scale-free properties in emergent functional neural networks. Phys Rev E Stat Nonlinear, Soft Matter Phys. 2006; doi:10.1103/PhysRevE.74.045101
- 156. Stam CJ, De Bruin EA. Scale-free dynamics of global functional connectivity in the human brain. Hum Brain Mapp. 2004; doi:10.1002/hbm.20016
- 157. Iglesias S, Tomiello S, Schneebeli M, Stephan KE. Models of neuromodulation for computational psychiatry. 2016; 1–22. doi:10.1002/wcs.1420
- 158. Frässle S, Yao Y, Schöbi D, Aponte EA, Heinzle J, Stephan KE. Generative models for clinical applications in computational psychiatry. 2018; 1–21. doi:10.1002/wcs.1460
- 159. Friston KJ, Mattout J, Trujillo-Barreto N, Ashburner J, Penny W. Variational free energy and the Laplace approximation. Neuroimage. Elsevier; 2007;34: 220–234.
- 160. MacKay DJC, Mac Kay DJC. Information theory, inference and learning algorithms. Cambridge university press; 2003.
- 161. Frässle S, Lomakina EI, Razi A, Friston KJ, Buhmann JM, Stephan KE. Regression DCM for fMRI. Neuroimage. 2017; doi:10.1016/j.neuroimage.2017.02.090
- 162. Bishop CM. Pattern recognition and machine learning. New York: Springer; 2006.
- 163. Stephan KE, Penny WD, Daunizeau J, Moran RJ, Friston KJ. Bayesian model selection for group studies. Neuroimage. Elsevier; 2009;46: 1004–1017.
- 164. Penny WD. Comparing dynamic causal models using AIC, BIC and free energy. Neuroimage. Elsevier; 2012;59: 319–330.
- 165. Hyder F, Herman P, Bailey CJ, Møller A, Globinsky R, Fulbright RK, et al. Uniform distributions of glucose oxidation and oxygen extraction in gray matter of normal human brain: No evidence of regional differences of aerobic glycolysis. J Cereb Blood Flow Metab. 2016;36: 903–916.
- 166. Friston KJ, Frith CD, Liddle PF, Frackowiak RS. Functional connectivity: the principal-component analysis of large (PET) data sets. [Internet]. Journal of cerebral blood flow and metabolism: official journal of the International Society of Cerebral Blood Flow and Metabolism. 1993. pp. 5–14. doi:10.1038/jcbfm.1993.4
- 167. Nugent AC, Martinez A, D'alfonso A, Zarate CA, Theodore WH. The relationship between glucose metabolism, resting-state fMRI BOLD signal, and GABAA-binding potential: a preliminary study in healthy subjects and those with temporal lobe epilepsy. J Cereb Blood Flow Metab. SAGE Publications Sage UK:

- London, England; 2015;35: 583-591.
- 168. Aiello M, Salvatore E, Cachia A, Pappatà S, Cavaliere C, Prinster A, et al. Relationship between simultaneously acquired resting-state regional cerebral glucose metabolism and functional MRI: A PET/MR hybrid scanner study. Neuroimage. Elsevier Inc.; 2015;113: 111–121. doi:10.1016/j.neuroimage.2015.03.017
- 169. Thompson GJ, Riedl V, Grimmer T, Drzezga A, Herman P, Hyder F. The whole-brain "global" signal from resting state fMRI as a potential biomarker of quantitative state changes in glucose metabolism. Brain Connect. 2016; doi:10.1089/brain.2015.0394
- 170. Bolo NR, Musen G, Simonson DC, Nickerson LD, Flores VL, Siracusa T, et al. Functional Connectivity of Insula, Basal Ganglia, and Prefrontal Executive Control Networks during Hypoglycemia in Type 1 Diabetes. J Neurosci. 2015;35: 11012–11023. doi:10.1523/JNEUROSCI.0319-15.2015
- 171. McFadden KL, Cornier M-A, Melanson EL, Bechtell JL, Tregellas JR. Effects of exercise on resting-state default mode and salience network activity in overweight/obese adults. Neuroreport. 2013;24: 866–71. doi:10.1097/WNR.000000000000013
- 172. Page K a, Chan O, Arora J, Belfort-Deaguiar R, Dzuira J, Roehmholdt B, et al. Effects of fructose vs glucose on regional cerebral blood flow in brain regions involved with appetite and reward pathways. JAMA. 2013;309: 63–70. doi:10.1001/jama.2012.116975
- 173. Sato JR, Hoexter MQ, Fujita A, Rohde LA. Evaluation of pattern recognition and feature extraction methods in ADHD prediction. Front Syst Neurosci. 2012;6: 68. doi:10.3389/fnsys.2012.00068
- 174. He Y, Wang L, Zang Y, Tian L, Zhang X, Li K, et al. Regional coherence changes in the early stages of Alzheimer's disease: A combined structural and resting-state functional MRI study. Neuroimage. Elsevier Inc.; 2007;35: 488–500. doi:10.1016/j.neuroimage.2006.11.042
- 175. Liu H, Liu Z, Liang M, Hao Y, Tan L, Kuang F, et al. Decreased regional homogeneity in schizophrenia: a resting state functional magnetic resonance imaging study. Neuroreport. 2006;17: 19–22. doi:00001756-200601230-00005 [pii]
- 176. Cao Q, Zang Y, Sun L, Sui M, Long X, Zou Q, et al. Abnormal neural activity in children with attention deficit hyperactivity disorder: a resting-state functional magnetic resonance imaging study. Neuroreport. 2006;17: 1033–6. doi:10.1097/01.wnr.0000224769.92454.5d
- 177. Paakki JJ, Rahko J, Long X, Moilanen I, Tervonen O, Nikkinen J, et al. Alterations in regional homogeneity of resting-state brain activity in autism spectrum disorders. Brain Res. 2010;1321: 169–179. doi:10.1016/j.brainres.2009.12.081
- Wu T, Long X, Zang Y, Wang L, Hallett M, Li K, et al. Regional homogeneity changes in patients with parkinson's disease. Hum Brain Mapp. 2009;30: 1502–1510. doi:10.1002/hbm.20622
- Tomasi D, Wang G, Volkow N. Energetic cost of brain functional connectivity. Proc Natl Acad Sci. 2013;110: 13642–13647. doi:10.1073/pnas.1303346110/-/DCSupplemental.www.pnas.org/cgi/doi/10.1073/pnas.1303346110
- 180. Beucke JC, Sepulcre J, Talukdar T, Linnman C, Zschenderlein K, Endrass T, et al. Abnormally high degree connectivity of the orbitofrontal cortex in obsessive-compulsive disorder. JAMA psychiatry. 2013;70: 619–29. doi:10.1001/jamapsychiatry.2013.173
- 181. Hou JM, Zhao M, Zhang W, Song LH, Wu WJ, Wang J, et al. Resting-state functional connectivity abnormalities in patients with obsessive-compulsive disorder and their healthy first-degree relatives. J Psychiatry Neurosci. 2014;39: 130220. doi:10.1503/jpn.130220
- 182. Göttlich M, Münte TF, Heldmann M, Kasten M, Hagenah J, Krämer UM. Altered Resting State Brain Networks in Parkinson's Disease. PLoS One. 2013;8. doi:10.1371/journal.pone.0077336
- 183. Di Martino A, Zuo XN, Kelly C, Grzadzinski R, Mennes M, Schvarcz A, et al. Shared and distinct intrinsic functional network centrality in autism and attention-deficit/hyperactivity disorder. Biol Psychiatry. Elsevier; 2013;74: 623–632. doi:10.1016/j.biopsych.2013.02.011
- 184. Cole MW, Pathak S, Schneider W. Identifying the brain's most globally connected regions. Neuroimage. Elsevier Inc.; 2010;49: 3132–3148. doi:10.1016/j.neuroimage.2009.11.001
- 185. Cox CL, Uddin LQ, Di Martino A, Castellanos FX, Milham MP, Kelly C. The balance between feeling and knowing: affective and cognitive empathy are reflected in the brain's intrinsic functional dynamics. Soc Cogn Affect Neurosci. Oxford University Press; 2011;7: 727–737.
- 186. Mennes M, Zuo XN, Kelly C, Di Martino A, Zang YF, Biswal B, et al. Linking inter-individual differences in neural activation and behavior to intrinsic brain dynamics. Neuroimage. Elsevier Inc.; 2011;54: 2950–2959. doi:10.1016/j.neuroimage.2010.10.046
- 187. Fujino J, Tei S, Jankowski KF, Kawada R, Murai T, Takahashi H. fMRI Study using Fractional Amplitude of Low-frequency FluctuationsRole of Spontaneous Brain Activity in Explicit and Implicit Aspects of Cognitive

- Flexibility under Socially Conflicting Situations: A Resting-state. Neuroscience. 2017;367: 60–71. doi:https://doi.org/10.1016/j.neuroscience.2017.10.025
- 188. Guo W, Liu F, Zhang J, Zhang Z, Yu L, Liu J, et al. Dissociation of regional activity in the default mode network in first-episode, drug-naive major depressive disorder at rest. J Affect Disord. 2013;151: 1097–1101. doi:10.1016/j.jad.2013.09.003
- 189. Argyelan M, Lencz T, Kaliora S, Sarpal DK, Weissman N, Kingsley PB, et al. Subgenual cingulate cortical activity predicts the efficacy of electroconvulsive therapy. Transl Psychiatry. Nature Publishing Group; 2016;6: e789.
- 190. Di Martino a, Yan C-G, Li Q, Denio E, Castellanos FX, Alaerts K, et al. The autism brain imaging data exchange: towards a large-scale evaluation of the intrinsic brain architecture in autism. Mol Psychiatry. 2014;19: 659–67. doi:10.1038/mp.2013.78
- 191. Premi E, Cauda F, Gasparotti R, Diano M, Archetti S, Padovani A, et al. Multimodal fMRI resting-state functional connectivity in Granulin mutations: The case of fronto-parietal dementia. PLoS One. 2014;9. doi:10.1371/journal.pone.0106500
- 192. Glascher J, Gitelman D. Contrast weights in flexible factorial de sign with multiple gr oups of subjects. Unpubl Tutor. 2008; Available: http://www.sbirc.ed.ac.uk/cyril/download/Contrast_Weighting_Glascher_Gitelman_2008.pdf
- 193. Woo CW, Krishnan A, Wager TD. Cluster-extent based thresholding in fMRI analyses: Pitfalls and recommendations. Neuroimage. Elsevier Inc.; 2014;91: 412–419. doi:10.1016/j.neuroimage.2013.12.058
- 194. Blanc R, Bere EL. Generation of Individualized Thalamus Target. Ajnr. 2012;33: 1-7.
- 195. Cunnington R, Windischberger C, Deecke L, Moser E. The Preparation and Execution of Self-Initiated and Externally-Triggered Movement: A Study of Event-Related fMRI. Neuroimage. 2002;15: 373–85. doi:10.1006/nimg.2001.0976
- 196. Nachev P, Kennard C, Husain M. Functional role of the supplementary and pre-supplementary motor areas. Nat Rev Neurosci. 2008;9: 856–869. doi:10.1038/nrn2478
- 197. Grèzes J, Decety J. Does visual perception of object afford action? Evidence from a neuroimaging study. Neuropsychologia. 2002;40: 212–222. doi:10.1016/S0028-3932(01)00089-6
- 198. Japee S, Holiday K, Satyshur MD, Mukai I, Ungerleider LG. A role of right middle frontal gyrus in reorienting of attention: a case study. Front Syst Neurosci. 2015;9: 23. doi:10.3389/fnsys.2015.00023
- Malik S, McGlone F, Dagher A. State of expectancy modulates the neural response to visual food stimuli in humans. Appetite. Elsevier Ltd; 2011;56: 302–309. doi:10.1016/j.appet.2011.01.005
- 200. Martens MJI, Born JM, Lemmens SGT, Karhunen L, Heinecke A, Goebel R, et al. Increased sensitivity to food cues in the fasted state and decreased inhibitory control in the satiated state in the overweight. Am J Clin Nutr. 2013;97: 471–479.
- 201. Shulman GL, Astafiev S V, Franke D, Pope DLW, Snyder AZ, McAvoy MP, et al. Interaction of stimulus-driven reorienting and expectation in ventral and dorsal fronto-parietal and basal ganglia-cortical networks. J Neurosci. 2009;29: 4392–4407. doi:10.1523/JNEUROSCI.5609-08.2009
- 202. Doricchi F, MacCi E, Silvetti M, MacAluso E. Neural correlates of the spatial and expectancy components of endogenous and stimulus-driven orienting of attention in the posner task. Cereb Cortex. 2010;20: 1574–1585. doi:10.1093/cercor/bhp215
- 203. Corbetta M, Shulman GL. Control of Goal-Directed and Stimulus-Driven Attention in the Brain. Nat Rev Neurosci. 2002;3: 215–229. doi:10.1038/nrn755
- 204. Corbetta M, Patel G, Shulman GL. The Reorienting System of the Human Brain: From Environment to Theory of Mind. Neuron. 2008;58: 306–324. doi:10.1016/j.neuron.2008.04.017
- 205. Smith SM, Fox PT, Miller KL, Glahn DC, Fox PM, Mackay CE, et al. Correspondence of the brain's functional architecture during activation and rest. Proc Natl Acad Sci U S A. 2009;106: 13040–5. doi:10.1073/pnas.0905267106
- 206. Verhagen J V, Kadohisa M, Rolls ET. Primate insular/opercular taste cortex: neuronal representations of the viscosity, fat texture, grittiness, temperature, and taste of foods. J Neurophysiol. 2004;92: 1685–1699.
- 207. Rolls ET. Brain mechanisms underlying flavour and appetite. Philos Trans R Soc Lond B Biol Sci. 2006;361: 1123–36. doi:10.1098/rstb.2006.1852
- 208. Kelly C, Toro R, Di Martino A, Cox CL, Bellec P, Castellanos FX, et al. A convergent functional architecture of the insula emerges across imaging modalities. Neuroimage. 2012;61: 1129–1142. doi:10.1016/j.neuroimage.2012.03.021
- 209. Charbonnier L, Van Der Laan LN, Viergever MA, Smeets PAM, Tregellas JR. Functional MRI of challenging food choices: Forced choice between equally liked high-and low-calorie foods in the absence of hunger. PLoS

- One. 2015;10. doi:10.1371/journal.pone.0131727
- 210. Buckner RL, Carroll DC. Self-projection and the brain. Trends Cogn Sci. 2007;11: 49–57. doi:10.1016/j.tics.2006.11.004
- 211. Cavanna AE, Trimble MR. The precuneus: A review of its functional anatomy and behavioural correlates. Brain. 2006;129: 564–583. doi:10.1093/brain/awl004
- 212. Tataranni PA, Gautier J-F, Chen K, Uecker A, Bandy D, Salbe AD, et al. Neuroanatomical correlates of hunger and satiation in humans using positron emission tomography. Proc Natl Acad Sci. 1999;96: 4569–4574. doi:10.1073/pnas.96.8.4569
- 213. Zhao J, Li M, Zhang Y, Song H, von Deneen KM, Shi Y, et al. Intrinsic brain subsystem associated with dietary restraint, disinhibition and hunger: an fMRI study. Brain Imaging and Behavior. 2016: 1–14. doi:10.1007/s11682-015-9491-4
- 214. Higgins SC, Gueorguiev M, Korbonits M. Ghrelin, the peripheral hunger hormone. Ann Med. 2007;39: 116–136. doi:10.1080/07853890601149179
- 215. Jones RB, McKie S, Astbury N, Little TJ, Tivey S, Lassman DJ, et al. Functional neuroimaging demonstrates that ghrelin inhibits the central nervous system response to ingested lipid. Gut. 2012;61: 1543–1551. doi:10.1136/gutjnl-2011-301323
- 216. Kelley AE, Baldo BA, Pratt WE, Will MJ. Corticostriatal-hypothalamic circuitry and food motivation: Integration of energy, action and reward. Physiology and Behavior. 2005. pp. 773–795. doi:10.1016/j.physbeh.2005.08.066
- 217. Coss-Adame E, Rao SSC. Brain and gut interactions in irritable bowel syndrome: New paradigms and new understandings. Curr Gastroenterol Rep. 2014;16. doi:10.1007/s11894-014-0379-z
- 218. Rolls ET. Taste, olfactory, and food texture processing in the brain, and the control of food intake. Physiol Behav. 2005;85: 45–56. doi:10.1016/j.physbeh.2005.04.012
- 219. Biswal BB, Mennes M, Zuo X-N, Gohel S, Kelly C, Smith SM, et al. Toward discovery science of human brain function. Supporting Information. Proc Natl Acad Sci U S A. 2010;107: 4734–9. doi:10.1073/pnas.0911855107
- 220. Sporns O. The human connectome: A complex network. Annals of the New York Academy of Sciences. 2011. doi:10.1111/j.1749-6632.2010.05888.x
- 221. Wee C-Y, Yap P-T, Zhang D, Wang L, Shen D. Constrained sparse functional connectivity networks for MCI classification. Med Image Comput Comput Assist Interv. 2012; doi:10.1016/j.micinf.2011.07.011.Innate
- 222. Jie B, Shen D, Zhang D. Brain connectivity hyper-network for MCI classification. Lecture Notes in Computer Science (including subseries Lecture Notes in Artificial Intelligence and Lecture Notes in Bioinformatics). 2014. doi:10.1007/978-3-319-10470-6_90
- 223. Marrelec G, Horwitz B, Kim J, Pélégrini-Issac M, Benali H, Doyon J. Using partial correlation to enhance structural equation modeling of functional MRI data. Magn Reson Imaging. Elsevier; 2007;25: 1181–1189.
- 224. Marrelec G, Krainik A, Duffau H, Pélégrini-Issac M, Lehéricy S, Doyon J, et al. Partial correlation for functional brain interactivity investigation in functional MRI. Neuroimage. Elsevier; 2006;32: 228–237.
- 225. Salvador R, Suckling J, Coleman MR, Pickard JD, Menon D, Bullmore E. Neurophysiological architecture of functional magnetic resonance images of human brain. Cereb Cortex. 2005; doi:10.1093/cercor/bhi016
- 226. Chen R, Herskovits EH. Clinical diagnosis based on bayesian classification of functional magnetic-resonance data. Neuroinformatics. Springer; 2007;5: 178–188.
- 227. Lee K, Tak S, Ye JC. A data-driven sparse GLM for fMRI analysis using sparse dictionary learning with MDL criterion. IEEE Trans Med Imaging. 2011; doi:10.1109/TMI.2010.2097275
- Wee CY, Yap PT, Zhang D, Wang L, Shen D. Group-constrained sparse fMRI connectivity modeling for mild cognitive impairment identification. Brain Struct Funct. 2014; doi:10.1007/s00429-013-0524-8
- 229. Tahmasian M, Bettray LM, van Eimeren T, Drzezga A, Timmermann L, Eickhoff CR, et al. A systematic review on the applications of resting-state fMRI in Parkinson's disease: Does dopamine replacement therapy play a role? Cortex. 2015. doi:10.1016/j.cortex.2015.08.005
- 230. Sheline YI, Raichle ME. Resting state functional connectivity in preclinical Alzheimer's disease. Biol Psychiatry. Elsevier; 2013;74: 340–347.
- 231. Dennis EL, Thompson PM. Functional brain connectivity using fMRI in aging and Alzheimer's disease. Neuropsychol Rev. Springer; 2014;24: 49–62.
- 232. Göttlich M, Jandl NM, Wojak JF, Sprenger A, Der Gablentz J Von, Münte TF, et al. Altered resting-state functional connectivity in patients with chronic bilateral vestibular failure. NeuroImage Clin. 2014; doi:10.1016/j.nicl.2014.03.003
- 233. Alderson-Day B, Diederen K, Fernyhough C, Ford JM, Horga G, Margulies DS, et al. Auditory hallucinations

- and the brain's resting-state networks: findings and methodological observations. Schizophr Bull. Oxford University Press US; 2016;42: 1110–1123.
- 234. Hu M-L, Zong X-F, Mann JJ, Zheng J-J, Liao Y-H, Li Z-C, et al. A review of the functional and anatomical default mode network in schizophrenia. Neurosci Bull. Springer; 2017;33: 73–84.
- 235. Göttlich M, Krämer UM, Kordon A, Hohagen F, Zurowski B. Decreased limbic and increased fronto-parietal connectivity in unmedicated patients with obsessive-compulsive disorder. Hum Brain Mapp. Wiley Online Library; 2014;35: 5617–5632.
- 236. Gürsel DA, Avram M, Sorg C, Brandl F, Koch K. Frontoparietal areas link impairments of large-scale intrinsic brain networks with aberrant fronto-striatal interactions in OCD: a meta-analysis of resting-state functional connectivity. Neurosci Biobehav Rev. Elsevier; 2018;
- 237. Cox DD, Savoy RL. Functional magnetic resonance imaging (fMRI) "brain reading": detecting and classifying distributed patterns of fMRI activity in human visual cortex. Neuroimage. Elsevier; 2003;19: 261–270.
- 238. Pereira F, Mitchell T, Botvinick M. Machine learning classifiers and fMRI: a tutorial overview. Neuroimage. Elsevier Inc.; 2009;45: S199–S209. doi:10.1016/j.neuroimage.2008.11.007
- 239. Norman KA, Polyn SM, Detre GJ, Haxby J V. Beyond mind-reading: multi-voxel pattern analysis of fMRI data. Trends Cogn Sci. Elsevier; 2006;10: 424–430.
- 240. Haynes J-D, Rees G. Neuroimaging: decoding mental states from brain activity in humans. Nat Rev Neurosci. Nature Publishing Group; 2006;7: 523.
- 241. Mahmoudi A, Takerkart S, Regragui F, Boussaoud D, Brovelli A. Multivoxel pattern analysis for fMRI data: A review. Comput Math Methods Med. 2012;2012. doi:10.1155/2012/961257
- 242. Cortes C, Vapnik V. Support-vector networks. Mach Learn. Springer; 1995;20: 273–297.
- 243. Vapnik V. The nature of statistical learning theory. Springer science & business media; 2013.
- 244. O'Toole AJ, Jiang F, Abdi H, Pénard N, Dunlop JP, Parent MA. Theoretical, statistical, and practical perspectives on pattern-based classification approaches to the analysis of functional neuroimaging data. J Cogn Neurosci. MIT Press; 2007;19: 1735–1752.
- 245. Mountrakis G, Im J, Ogole C. Support vector machines in remote sensing: A review. ISPRS J Photogramm Remote Sens. Elsevier; 2011;66: 247–259.
- 246. Meier TB, Desphande AS, Vergun S, Nair VA, Song J, Biswal BB, et al. Support vector machine classification and characterization of age-related reorganization of functional brain networks. Neuroimage. Elsevier; 2012;60: 601–613.
- 247. Orru G, Pettersson-Yeo W, Marquand AF, Sartori G, Mechelli A. Using support vector machine to identify imaging biomarkers of neurological and psychiatric disease: a critical review. Neurosci Biobehav Rev. Elsevier; 2012;36: 1140–1152.
- 248. Wang Z. A hybrid SVM-GLM approach for fMRI data analysis. Neuroimage. Elsevier; 2009;46: 608-615.
- 249. Zhang L, Samaras D, Tomasi D, Volkow N, Goldstein R. Machine learning for clinical diagnosis from functional magnetic resonance imaging. IEEE; 2005.
- 250. Kamitani Y, Tong F. Decoding the visual and subjective contents of the human brain. Nat Neurosci. Nature Publishing Group; 2005;8: 679.
- 251. Mitchell TM, Hutchinson R, Niculescu RS, Pereira F, Wang X, Just M, et al. Learning to decode cognitive states from brain images. Mach Learn. Springer; 2004;57: 145–175.
- 252. Abós A, Baggio HC, Segura B, García-Díaz AI, Compta Y, Martí MJ, et al. Discriminating cognitive status in Parkinson's disease through functional connectomics and machine learning. Sci Rep. 2017; doi:10.1038/srep45347
- 253. Khazaee A, Ebrahimzadeh A, Babajani-Feremi A. Identifying patients with Alzheimer's disease using resting-state fMRI and graph theory. Clin Neurophysiol. Elsevier; 2015;126: 2132–2141.
- 254. Hojjati SH, Ebrahimzadeh A, Khazaee A, Babajani-Feremi A. Predicting conversion from MCI to AD using resting-state fMRI, graph theoretical approach and SVM. J Neurosci Methods. 2017; doi:10.1016/j.jneumeth.2017.03.006
- 255. Bi X, Wang Y, Shu Q, Sun Q, Xu Q. Classification of Autism Spectrum Disorder Using Random Support Vector Machine Cluster. Front Genet. Frontiers; 2018;9: 18.
- 256. Cao Q, Zang Y, Sun L, Sui M, Long X, Zou Q, et al. Abnormal neural activity in children with attention deficit hyperactivity disorder: a resting-state functional magnetic resonance imaging study. Neuroreport. 2006;17: 1033–1036. doi:10.1097/01.wnr.0000224769.92454.5d
- 257. Paakki JJ, Rahko J, Long X, Moilanen I, Tervonen O, Nikkinen J, et al. Alterations in regional homogeneity of resting-state brain activity in autism spectrum disorders. Brain Res. Elsevier B.V.; 2010;1321: 169–179. doi:10.1016/j.brainres.2009.12.081

- 258. Jović A, Brkić K, Bogunović N. A review of feature selection methods with applications. Information and Communication Technology, Electronics and Microelectronics (MIPRO), 2015 38th International Convention on. IEEE; 2015. pp. 1200–1205.
- 259. Tang J, Alelyani S, Liu H. Feature selection for classification: A review. Data Classif Algorithms Appl. CRC Press; 2014; 37.
- 260. Mwangi B, Tian TS, Soares JC. A Review of Feature Reduction Techniques in Neuroimaging. 2014; 229–244. doi:10.1007/s12021-013-9204-3
- 261. Burrell L, Smart O, Georgoulas GK, Marsh E, Vachtsevanos GJ. Evaluation of Feature Selection Techniques for Analysis of Functional MRI and EEG. DMIN. 2007. pp. 256–262.
- 262. Guyon I, Elisseeff A. An Introduction to Variable and Feature Selection. J Mach Learn Res. 2003; doi:10.1016/j.aca.2011.07.027
- 263. Maldonado S, Weber R. A wrapper method for feature selection using Support Vector Machines. Inf Sci (Ny). Elsevier Inc.; 2009;179: 2208–2217. doi:10.1016/j.ins.2009.02.014
- 264. Kudo M, Sklansky J. Comparison of algorithms that select features for pattern classifiers. Pattern Recognit. Elsevier; 2000;33: 25–41.
- 265. Chen L, Seidel G, Mertins A. Multiple feature extraction for early Parkinson risk assessment based on transcranial sonography image. 2010 Iinternational conference on image processing. 2010. doi:10.1109/ICIP.2010.5654216
- 266. Pudil P, Novovičová J, Kittler J. Floating search methods in feature selection. Pattern Recognit Lett. 1994; doi:10.1016/0167-8655(94)90127-9
- 267. Al-Zubaidi A, Chen L, Hagenah J, Mertins A. Robust feature for transcranial sonography image classification using rotation-invariant Gabor filter. Informatik aktuell. 2013. doi:10.1007/978-3-642-36480-8_48
- 268. Kohavi R, John GH. Wrappers for feature subset selection. Artif Intell. 1997; doi:10.1016/S0004-3702(97)00043-X
- Jain A, Zongker D. Feature Selection: Evaluation, Application, and Small Sample Performance. IEEE Trans Pattern Anal Mach Intell. 1997; doi:10.1109/34.574797
- 270. Kira K, Rendell LA. A practical approach to feature selection. Proceedings of the ninth international workshop on Machine learning. 1992. doi:10.1016/S0031-3203(01)00046-2
- 271. Almuallim H, Dietterich TG. Learning Boolean concepts in the presence of many irrelevant features. Artif Intell. 1994; doi:10.1016/0004-3702(94)90084-1
- 272. Zhu Z, Ong YS, Dash M. Wrapper-filter feature selection algorithm using a memetic framework. IEEE Trans Syst Man, Cybern Part B Cybern. 2007; doi:10.1109/TSMCB.2006.883267
- 273. Neshatian K, Zhang M. Pareto front feature selection: using genetic programming to explore feature space. GECCO '09: Proceedings of the 11th Annual conference on Genetic and evolutionary computation. 2009. doi:10.1145/1569901.1570040
- 274. Gu S, Cheng R, Jin Y. Feature selection for high-dimensional classification using a competitive swarm optimizer. Soft Comput. Springer; 2018;22: 811–822.
- 275. Stice E, Spoor S, Bohon C, Veldhuizen MG, Small DM. Relation of Reward From Food Intake and Anticipated Food Intake to Obesity: A Functional Magnetic Resonance Imaging Study. J Abnorm Psychol. 2008; doi:10.1037/a0013600
- 276. Stice E, Yokum S. Gain in Body Fat Is Associated with Increased Striatal Response to Palatable Food Cues, whereas Body Fat Stability Is Associated with Decreased Striatal Response. J Neurosci. 2016; doi:10.1523/JNEUROSCI.4365-15.2016
- 277. Stice E, Burger KS, Yokum S. Relative ability of fat and sugar tastes to activate reward, gustatory, and somatosensory regions1-3. Am J Clin Nutr. 2013; doi:10.3945/ajcn.113.069443
- 278. Stice E, Yokum S, Bohon C, Marti N, Smolen A. Reward circuitry responsivity to food predicts future increases in body mass: Moderating effects of DRD2 and DRD4. Neuroimage. 2010; doi:10.1016/j.neuroimage.2010.01.081
- 279. Van Duinkerken E, Schoonheim MM, Sanz-Arigita EJ, IJzerman RG, Moll AC, Snoek FJ, et al. Resting-state brain networks in type 1 diabetic patients with and without microangiopathy and their relation to cognitive functions and disease variables. Diabetes. 2012; doi:10.2337/db11-1358
- 280. Krusemark EA, Novak LR, Gitelman DR, Li W. When the Sense of Smell Meets Emotion: Anxiety-State-Dependent Olfactory Processing and Neural Circuitry Adaptation. J Neurosci. 2013; doi:10.1523/JNEUROSCI.1835-13.2013
- 281. Li J, Yang R, Xia K, Wang T, Nie B, Gao K, et al. Effects of stress on behavior and resting-state fMRI in rats and evaluation of Telmisartan therapy in a stress-induced depression model. BMC Psychiatry. BioMed

- Central; 2018;18: 337. doi:10.1186/s12888-018-1880-y
- 282. Hare TA, Camerer CF, Rangel A. Self-control in decision-Making involves modulation of the vmPFC valuation system. Science (80-). 2009; doi:10.1126/science.1168450
- 283. Sundermann B, Pfleiderer B. Functional connectivity profile of the human inferior frontal junction: Involvement in a cognitive control network. BMC Neurosci. 2012; doi:10.1186/1471-2202-13-119
- 284. Lopez RB, Hofmann W, Wagner DD, Kelley WM, Heatherton TF. Neural Predictors of Giving in to Temptation in Daily Life. Psychol Sci. 2014; doi:10.1177/0956797614531492
- 285. Gabrieli JDE, Ghosh SS, Whitfield-Gabrieli S. Prediction as a humanitarian and pragmatic contribution from human cognitive neuroscience. Neuron. 2015. doi:10.1016/j.neuron.2014.10.047
- 286. Hollmann M, Hellrung L, Pleger B, Schlögl H, Kabisch S, Stumvoll M, et al. Neural correlates of the volitional regulation of the desire for food. Int J Obes. 2012; doi:10.1038/ijo.2011.125
- 287. Sweet LH, Hassenstab JJ, McCaffery JM, Raynor HA, Bond DS, Demos KE, et al. Brain response to food stimulation in obese, normal weight, and successful weight loss maintainers. Obesity. 2012; doi:10.1038/oby.2012.125
- 288. Killgore WDS, Yurgelun-Todd DA. Positive affect modulates activity in the visual cortex to images of high calorie foods. Int J Neurosci. 2007; doi:10.1080/00207450600773848
- van der Laan LN, de Ridder DTD, Viergever MA, Smeets PAM. The first taste is always with the eyes: A meta-analysis on the neural correlates of processing visual food cues. Neuroimage. 2011; doi:10.1016/j.neuroimage.2010.11.055
- 290. Mendez-Torrijos A, Kreitz S, Ivan C, Konerth L, Rösch J, Pischetsrieder M, et al. Snack food as a modulator of human resting-state functional connectivity. CNS Spectr. 2018/04/04. Cambridge University Press; 2018;23: 321–332. doi:DOI: 10.1017/S1092852918000767
- 291. Zhang B, Tian D, Yu C, Zhang J, Tian X, von Deneen KM, et al. Altered baseline brain activities before food intake in obese men: A resting state fMRI study. Neurosci Lett. Elsevier Ireland Ltd; 2015;584: 156–161. doi:10.1016/j.neulet.2014.10.020
- 292. Arbabshirani MR, Plis S, Sui J, Calhoun VD. Single subject prediction of brain disorders in neuroimaging: Promises and pitfalls. Neuroimage. 2017;145: 137–165. doi:https://doi.org/10.1016/j.neuroimage.2016.02.079
- 293. Lo A, Chernoff H, Zheng T, Lo S-H. Why significant variables aren't automatically good predictors. Proc Natl Acad Sci. 2015; doi:10.1073/pnas.1518285112
- 294. Baker MC, Kerr AS, Hames E, Akrofi K. An SFFS technique for EEG feature classification to identify subgroups. Computer-Based Medical Systems (CBMS), 2012 25th International Symposium on. IEEE; 2012. pp. 1–4.
- 295. Poldrack RA, Baker CI, Durnez J, Gorgolewski KJ, Matthews PM, Munafò MR, et al. Scanning the horizon: towards transparent and reproducible neuroimaging research. Nat Rev Neurosci. Nature Publishing Group; 2017;18: 115.
- 296. Schnack HG, Kahn RS. Detecting neuroimaging biomarkers for psychiatric disorders: sample size matters. Front psychiatry. Frontiers; 2016;7: 50.
- 297. Lord A, Horn D, Breakspear M, Walter M. Changes in community structure of resting state functional connectivity in unipolar depression. PLoS One. Public Library of Science; 2012;7: e41282.
- Wei M, Qin J, Yan R, Li H, Yao Z, Lu Q. Identifying major depressive disorder using Hurst exponent of resting-state brain networks. Psychiatry Res Neuroimaging. Elsevier; 2013;214: 306–312.
- 299. Cheng H, Newman S, Goñi J, Kent JS, Howell J, Bolbecker A, et al. Nodal centrality of functional network in the differentiation of schizophrenia. Schizophr Res. Elsevier; 2015;168: 345–352.
- 300. Wang X, Jiao Y, Tang T, Wang H, Lu Z. Altered regional homogeneity patterns in adults with attention-deficit hyperactivity disorder. Eur J Radiol. Elsevier; 2013;82: 1552–1557.
- 301. Fekete T, Wilf M, Rubin D, Edelman S, Malach R, Mujica-Parodi LR. Combining classification with fMRI-derived complex network measures for potential neurodiagnostics. PLoS One. Public Library of Science; 2013;8: e62867.
- 302. Tang Y, Wang L, Cao F, Tan L. Identify schizophrenia using resting-state functional connectivity: an exploratory research and analysis. Biomed Eng Online. BioMed Central; 2012;11: 50.
- 303. Anderson A, Cohen M. Decreased small-world functional network connectivity and clustering across resting state networks in schizophrenia: an fMRI classification tutorial [Internet]. Frontiers in Human Neuroscience . 2013. p. 520. Available: https://www.frontiersin.org/article/10.3389/fnhum.2013.00520
- 304. Krystal JH, Anticevic A, Savic A, Pearlson GD, Glahn DC, Winkler AM, et al. Characterizing Thalamo-Cortical Disturbances in Schizophrenia and Bipolar Illness. Cereb Cortex. 2013;24: 3116–3130.

- doi:10.1093/cercor/bht165
- Guo W, Su Q, Yao D, Jiang J, Zhang J, Zhang Z, et al. Decreased regional activity of default-mode network in unaffected siblings of schizophrenia patients at rest. Eur Neuropsychopharmacol. Elsevier; 2014;24: 545– 552.
- 306. Tang CC, Poston KL, Eckert T, Feigin A, Frucht S, Gudesblatt M, et al. Differential diagnosis of parkinsonism: a metabolic imaging study using pattern analysis. Lancet Neurol. 2010; doi:10.1016/S1474-4422(10)70002-8
- 307. Schwartz MW, Porte D. Diabetes, obesity, and the brain. Science (80-). American Association for the Advancement of Science; 2005;307: 375–379.
- 308. Lam TKT. Neuronal regulation of homeostasis by nutrient sensing. Nat Med. Nature Research; 2010;16: 392–395.
- 309. Suzuki K, Simpson KA, Minnion JS, Shillito JC, Bloom SR. The role of gut hormones and the hypothalamus in appetite regulation. Endocr J. The Japan Endocrine Society; 2010;57: 359–372.
- 310. Gao Q, Horvath TL. Neuronal control of energy homeostasis. FEBS Lett. Wiley Online Library; 2008;582: 132–141.
- 311. Schwartz MW, Woods SC, Porte Jr D, Seeley RJ, Baskin DG. Central nervous system control of food intake. Nature. Nature Publishing Group; 2000;404: 661.
- Woods SC, Seeley RJ, Porte D, Schwartz MW. Signals that regulate food intake and energy homeostasis. Science (80-). American Association for the Advancement of Science; 1998;280: 1378–1383.
- 313. Liu Y, Gao JH, Liu HL, Fox PT. The temporal response of the brain after eating revealed by functional MRI. Nature. 2000;405: 1058–1062. doi:10.1038/35016590
- 314. Wallner-Liebmann S, Koschutnig K, Reishofer G, Sorantin E, Blaschitz B, Kruschitz R, et al. Insulin and hippocampus activation in response to images of high-calorie food in normal weight and obese adolescents. Obesity. Wiley Online Library; 2010;18: 1552–1557.
- 315. Kullmann S, Frank S, Ketterer C. Intranasal Insulin Modulates Intrinsic Reward and Prefrontal Circuitry of the Human Brain in Lean Women. 2012; doi:10.1159/000341406
- 316. Heuvel MP va. den, Pol HEH. Exploring the brain network: a review on resting-state fMRI functional connectivity. Eur 2010; Available: http://www.ncbi.nlm.nih.gov/entrez/query.fcgi?db=pubmed&cmd=Retrieve&dopt=AbstractPlus&list_uids= 10605483311326741661related:ncT2ouE-LpMJ%5Cnpapers://3fee8da1-24f9-490b-9ed9-3b7bcb767493/Paper/p304
- 317. Lee MH, Smyser CD, Shimony JS. Resting-State fMRI: A Review of Methods and Clinical Applications. 2013:
- 318. Kullmann S, Heni M, Veit R, Ketterer C, Schick F, Häring HU, et al. The obese brain: Association of body mass index and insulin sensitivity with resting state network functional connectivity. Hum Brain Mapp. 2012;33: 1052–1061. doi:10.1002/hbm.21268
- 319. Egorova N, Veldsman M, Cumming T, Brodtmann A. Fractional amplitude of low-frequency fluctuations (fALFF) in post-stroke depression. NeuroImage Clin. 2017; doi:10.1016/j.nicl.2017.07.014
- 320. Williams G, Harrold JA, Cutler DJ. The hypothalamus and the regulation of energy homeostasis: lifting the lid on a black box. Proc Nutr Soc. Cambridge University Press; 2000;59: 385–396.
- 321. Figlewicz DP. Adiposity signals and food reward: expanding the CNS roles of insulin and leptin. Am J Physiol Integr Comp Physiol. Am Physiological Soc; 2003;284: R882–R892.
- 322. Nathans LL, Oswald FL, Nimon K. Interpreting Multiple Linear Regression: A Guidebook of Variable Importance. Pract Assessment, Res Eval. 2012; doi:10.3102/00346543074004525
- 323. Friston K. Statistical Parametric Mapping. Statistical Parametric Mapping: The Analysis of Functional Brain Images. 2007. pp. 101–125. doi:10.1016/B978-012372560-8/50002-4
- 324. Field A. Discovering Statistics using IBM SPSS Statistics. 4th ed. Sage Publications Ltd. ©2013; 2014.
- 325. Chumbley J, Worsley K, Flandin G, Friston K. Topological FDR for neuroimaging. Neuroimage. Elsevier Inc.; 2010;49: 3057–3064. doi:10.1016/j.neuroimage.2009.10.090
- 326. Tzagournis M, Skillman TG. Glucose intolerance mechanism after starvation. Metabolism. Elsevier; 1970;19: 170–178.
- 327. Owen L, Scholey AB, Finnegan Y, Hu H, Sünram-Lea SI. The effect of glucose dose and fasting interval on cognitive function: A double-blind, placebo-controlled, six-way crossover study. Psychopharmacology (Berl). 2012;220: 577–589. doi:10.1007/s00213-011-2510-2
- 328. Pruessner JC, Kirschbaum C, Meinlschmid G, Hellhammer DH. Two formulas for computation of the area under the curve represent measures of total hormone concentration versus time-dependent change.

- Psychoneuroendocrinology. 2003;28: 916-931. doi:10.1016/S0306-4530(02)00108-7
- 329. Esterman M, Tamber-Rosenau BJ, Chiu Y-C, Yantis S. Avoiding non-independence in fMRI data analysis: leave one subject out. Neuroimage. Elsevier; 2010;50: 572–576.
- 330. Führer D, Zysset S, Stumvoll M. Brain activity in hunger and satiety: an exploratory visually stimulated FMRI study. Obesity (Silver Spring). 2008;16: 945–50. doi:10.1038/oby.2008.33
- 331. Gerozissis K. Brain insulin: regulation, mechanisms of action and functions. Cell Mol Neurobiol. Springer; 2003;23: 1–25.
- 332. Kurth F, Zilles K, Fox PT, Laird AR, Eickhoff SB. A link between the systems: functional differentiation and integration within the human insula revealed by meta-analysis. Brain Struct Funct. 2010;214: 1–16. doi:10.1007/s00429-010-0255-z
- 333. Nieuwenhuys R. The insular cortex: A review [Internet]. 1st ed. Evolution of the Primate Brain. Elsevier B.V.; 2012. doi:10.1016/B978-0-444-53860-4.00007-6
- 334. Tang DW, Fellows LK, Small DM, Dagher A. Food and drug cues activate similar brain regions: A meta-analysis of functional MRI studies. Physiol Behav. Elsevier Inc.; 2012;106: 317–324. doi:10.1016/j.physbeh.2012.03.009
- 335. Siep N, Roefs A, Roebroeck A, Havermans R, Bonte M, Jansen A. Fighting food temptations: The modulating effects of short-term cognitive reappraisal, suppression and up-regulation on mesocorticolimbic activity related to appetitive motivation. Neuroimage. 2012;60: 213–220. doi:https://doi.org/10.1016/j.neuroimage.2011.12.067
- 336. Bohon C, Stice E. Reward abnormalities among women with full and subthreshold bulimia nervosa: a functional magnetic resonance imaging study. Int J Eat Disord. Wiley Online Library; 2011;44: 585–595.
- 337. Gautier JF, Chen K, Salbe AD, Bandy D, Pratley RE, Heiman M, et al. Differential brain responses to satiation in obese and lean men. Diabetes. 2000;49: 838–846. doi:10.2337/diabetes.49.5.838
- 338. McCaffery JM, Haley AP, Sweet LH, Phelan S, Raynor HA, Del Parigi A, et al. Differential functional magnetic resonance imaging response to food pictures in successful weight-loss maintainers relative to normal-weight and obese controls. Am J Clin Nutr. Am Soc Nutrition; 2009;90: 928–934.
- 339. Batterink L, Yokum S, Stice E. Body mass correlates inversely with inhibitory control in response to food among adolescent girls: an fMRI study. Neuroimage. Elsevier; 2010;52: 1696–1703.
- 340. Hadjikhani N, Joseph RM, Snyder J, Chabris CF, Clark J, Steele S, et al. Activation of the fusiform gyrus when individuals with autism spectrum disorder view faces. Neuroimage. 2004;22: 1141–1150. doi:http://dx.doi.org/10.1016/j.neuroimage.2004.03.025
- 341. Heni M, Kullmann S, Ketterer C, Guthoff M, Bayer M, Staiger H, et al. Differential effect of glucose ingestion on the neural processing of food stimuli in lean and overweight adults. Hum Brain Mapp. 2014;35: 918–928. doi:10.1002/hbm.22223
- 342. Woods SC. The Control of Food Intake: Behavioral versus Molecular Perspectives. Cell Metabolism. 2009. doi:10.1016/j.cmet.2009.04.007
- 343. Woods SC, Ramsay DS. Food intake, metabolism and homeostasis. Physiol Behav. 2011; doi:10.1016/j.physbeh.2011.04.026
- 344. Val-Laillet D, Aarts E, Weber B, Ferrari M, Quaresima V, Stoeckel LE, et al. Neuroimaging and neuromodulation approaches to study eating behavior and prevent and treat eating disorders and obesity. NeuroImage Clin. 2015; doi:10.1016/j.nicl.2015.03.016
- 345. Bowen DJ, Barrington WE, Beresford S a. a., De Jong JW, Vanderschuren LJMJ, Adan R a H, et al. Hormonal and neural mechanisms of food reward, eating behaviour and obesity. Obes Facts. Nature Publishing Group; 2014;5: 1–51. doi:10.1159/000338292
- 346. Morton GJ, Meek TH, Schwartz MW. Neurobiology of food intake in health and disease. Nat Rev Neurosci. Nature Publishing Group; 2014;15: 367–78. doi:10.1038/nrn3745
- 347. Chodkowski BAA, Cowan RL, Niswender KD. Imbalance in resting state functional connectivity is associated with eating behaviors and adiposity in children. Heliyon. 2016; doi:10.1016/j.heliyon.2015.e00058
- 348. Teitelbaum P, Stellar E. Recovery from the failure to eat produced by hypothalamic lesions. Science (80-). 1954; doi:10.1126/science.120.3126.894
- 349. Graff H, Stellar E. Hyperphagia, obesity, and finickiness. J Comp Physiol Psychol. American Psychological Association; 1962;55: 418.
- 350. Stellar E, Corbit JD. Neural control of motivated behavior. Neurosci Res Program Bull. The MIT Press; 1973;
- 351. Grijalva C V, Kiefer SW, Gunion MW, Cooper PH, Novin D. Ingestive responses to homeostatic challenges in rats with ablations of the anterolateral neocortex. Behav Neurosci. American Psychological Association; 1985;99: 162.

- 352. Barbas H, Saha S, Rempel-Clower N, Ghashghaei T. Serial pathways from primate prefrontal cortex to autonomic areas may influence emotional expression. BMC Neurosci. 2003; doi:10.1186/1471-2202-4-25
- 353. Kullmann S, Heni M, Linder K, Zipfel S, Häring H, Veit R, et al. Resting-state functional connectivity of the human hypothalamus. Hum Brain Mapp. Wiley Online Library; 2014;35: 6088–6096.
- 354. Lemaire J-J, Frew AJ, McArthur D, Gorgulho AA, Alger JR, Salomon N, et al. White matter connectivity of human hypothalamus. Brain Res. Elsevier; 2011;1371: 43–64.
- 355. Lips MA, Wijngaarden MA, Van Der Grond J, Van Buchem MA, De Groot GH, Rombouts SARB, et al. Resting-state functional connectivity of brain regions involved in cognitive control, motivation, and reward is enhanced in obese females. Am J Clin Nutr. 2014;100: 524–531. doi:10.3945/ajcn.113.080671
- 356. Purnell JQ, Lahna DL, Samuels MH, Rooney WD, Hoffman WF. Loss of pons-to-hypothalamic white matter tracks in brainstem obesity. Int J Obes. 2014; doi:10.1038/ijo.2014.57
- 357. Wijngaarden MA, Veer IM, Rombouts SARB, Buchem MA Van, Dijk KW Van, Pijl H, et al. Obesity is marked by distinct functional connectivity in brain networks involved in food reward and salience. Behav Brain Res. Elsevier B.V.; 2015; 1–8. doi:10.1016/j.bbr.2015.03.016
- 358. Gogolla N. The insular cortex. Curr Biol. Elsevier; 2017;27: R580–R586.
- 359. Uddin LQ, Nomi JS, Hébert-Seropian B, Ghaziri J, Boucher O. Structure and function of the human insula. J Clin Neurophysiol. LWW; 2017;34: 300–306.
- 360. Veldhuizen MG, Albrecht J, Zelano C, Boesveldt S, Breslin P, Lundström JN. Identification of human gustatory cortex by activation likelihood estimation. Hum Brain Mapp. 2011; doi:10.1002/hbm.21188
- 361. Small DM, Gregory MD, Mak YE, Gitelman D, Mesulam MM, Parrish T. Dissociation of neural representation of intensity and affective valuation in human gustation. Neuron. 2003; doi:10.1016/j.porgcoat.2018.08.012
- 362. Berthoud HR. Metabolic and hedonic drives in the neural control of appetite: Who is the boss? Current Opinion in Neurobiology. 2011. doi:10.1016/j.conb.2011.09.004
- 363. Livneh Y, Ramesh RN, Burgess CR, Levandowski KM, Madara JC, Fenselau H, et al. Homeostatic circuits selectively gate food cue responses in insular cortex. Nature. 2017; doi:10.1038/nature22375
- 364. Bonthius DJ, Solodkin A, Van Hoesen GW. Pathology of the insular cortex in Alzheimer disease depends on cortical architecture. J Neuropathol Exp Neurol. 2005; doi:10.1097/01.jnen.0000182983.87106.d1
- 365. Aleksandrov VG, Fedorova KP. Structure of the insular region of the rat neocortex. Neurosci Behav Physiol. Springer; 2003;33: 199–202.
- 366. Mesulam M-M, Mufson EJ. The insula of Reil in man and monkey. Association and auditory cortices. Springer; 1985. pp. 179–226.
- 367. Mufson EJ, Sobreviela T, Kordower JH. Chapter VII Chemical neuroanatomy of the primate insula cortex: Relationship to cytoarchitectonics, connectivity, function and neurodegeneration. Handbook of chemical neuroanatomy. Elsevier; 1997. pp. 377–454.
- 368. Cauda F, D'Agata F, Sacco K, Duca S, Geminiani G, Vercelli A. Functional connectivity of the insula in the resting brain. Neuroimage. 2011; doi:10.1016/j.neuroimage.2010.11.049
- 369. Moreno-Lopez L, Contreras-Rodriguez O, Soriano-Mas C, Stamatakis EA, Verdejo-Garcia A. Disrupted functional connectivity in adolescent obesity. NeuroImage Clin. 2016; doi:10.1016/j.nicl.2016.07.005
- 370. Timper K, Brüning JC. Hypothalamic circuits regulating appetite and energy homeostasis: Pathways to obesity. DMM Dis Model Mech. 2017; doi:10.1242/dmm.026609
- 371. Sun T, Hevner RF. Growth and folding of the mammalian cerebral cortex: from molecules to malformations. Nature Reviews Neuroscience. 2014. doi:10.1038/nrn3707
- 372. DelParigi A, Chen K, Salbe AD, Reiman EM, Tataranni PA. Sensory experience of food and obesity: A positron emission tomography study of the brain regions affected by tasting a liquid meal after a prolonged fast. Neuroimage. 2005; doi:10.1016/j.neuroimage.2004.08.035
- 373. Pelchat ML, Johnson A, Chan R, Valdez J, Ragland JD. Images of desire: Food-craving activation during fMRI. Neuroimage. 2004;23: 1486–1493. doi:10.1016/j.neuroimage.2004.08.023
- 374. Craig ADB. Forebrain emotional asymmetry: a neuroanatomical basis? 2005;9. doi:10.1016/j.tics.2005.10.005
- 375. Craig AD. How do you feel?: an interoceptive moment with your neurobiological self. 2014.
- Dagher A, Han J-E, Neseliler S. The use of functional magnetic resonance imaging in the study of appetite and obesity. Appetite and Food Intake. CRC Press; 2017. pp. 117–134.
- 377. Rilling JK. Human and NonHuman primate brains: Are they allometrically scaled versions of the same design? Evol Anthropol. 2006; doi:10.1002/evan.20095
- 378. Panksepp J. Cross-Species affective neuroscience decoding of the primal affective experiences of humans and

- related animals. PLoS One. 2011; doi:10.1371/journal.pone.0021236
- 379. Sladky R, Friston KJ, Tr??stl J, Cunnington R, Moser E, Windischberger C. Slice-timing effects and their correction in functional MRI. Neuroimage. Elsevier Inc.; 2011;58: 588–594. doi:10.1016/j.neuroimage.2011.06.078
- 380. Ashburner J, Friston KJ. Unified segmentation. Neuroimage. 2005;26: 839–851. doi:10.1016/j.neuroimage.2005.02.018
- 381. Maldjian JA, Laurienti PJ, Kraft RA, Burdette JH. An automated method for neuroanatomic and cytoarchitectonic atlas-based interrogation of fMRI data sets. Neuroimage. Elsevier; 2003;19: 1233–1239.
- 382. Friston KJ, Williams S, Howard R, Frackowiak RSJ, Turner R. Movement-related effects in fMRI time-series. Magn Reson Med. Wiley Online Library; 1996;35: 346–355.
- 383. Cauda F, Costa T, Torta DME, Sacco K, D'agata F, Duca S, et al. Meta-analytic clustering of the insular cortex: characterizing the meta-analytic connectivity of the insula when involved in active tasks. Neuroimage. Elsevier; 2012;62: 343–355.
- 384. Druce MR, Small CJ, Bloom SR. Minireview: Gut peptides regulating satiety. Endocrinology. 2004. doi:10.1210/en.2004-0089
- 385. Marić G, Gazibara T, Zaletel I, Borović ML, Tomanović N. The role of gut hormones in appetite regulation (Review). 2014;101: 395–407. doi:10.1556/APhysiol.101.2014.4.1
- 386. Penny WD, Stephan KE, Mechelli A, Friston KJ. Comparing dynamic causal models. Neuroimage. 2004; doi:10.1016/j.neuroimage.2004.03.026
- 387. Stephan KE, Penny WD, Moran RJ, den Ouden HEM, Daunizeau J, Friston KJ. Ten simple rules for dynamic causal modeling. Neuroimage. Elsevier Inc.; 2010;49: 3099–3109. doi:10.1016/j.neuroimage.2009.11.015
- 388. Pires JCM, Martins FG, Sousa SIV, Alvim-Ferraz MCM, Pereira MC. Selection and validation of parameters in multiple linear and principal component regressions. Environ Model Softw. 2008; doi:10.1016/j.envsoft.2007.04.012
- 389. Gałecki A, Burzykowski T. Linear Mixed-Effects Models Using R: A Step-by-Step Approach. New York: Springer Texts in Statistics; 2013. doi:10.1007/978-1-4614-3900-4
- 390. Bates DM, Maechler M, Bolker B, Walker S. lme4: linear mixed-effects models using S4 classes. J Stat Softw. 2015; doi:10.1088/1742-6596/43/1/292
- 391. Pinheiro J, Bates D, DebRoy S, Sarkar D. R Core Team (2017) nlme: linear and nonlinear mixed effects models. R package version 3.1-131. Comput software] Retrieved from https://CRAN R-project org/package=nlme. 2017;
- 392. Lüdecke D. sjPlot: Data visualization for statistics in social science. R package version 2.6.1 [Internet]. 2018. Available: https://cran.r-project.org/web/packages/sjPlot/index.html
- 393. Pitt MA, Myung IJ. When a good fit can be bad. Trends in Cognitive Sciences. 2002. doi:10.1016/S1364-6613(02)01964-2
- 394. Stephan KE, Friston KJ. Analyzing effective connectivity with functional magnetic resonance imaging. Wiley Interdiscip Rev Cogn Sci. 2010;1: 446–459. doi:10.1002/wcs.58
- 395. Craig AD. How do you feel? Interoception: the sense of the physiological condition of the body. Nat Rev Neurosci. Nature Publishing Group; 2002;3: 655.
- 396. Duerden EG, Arsalidou M, Lee M, Taylor MJ. Lateralization of affective processing in the insula. Neuroimage. Elsevier Inc.; 2013;78: 159–175. doi:10.1016/j.neuroimage.2013.04.014
- 397. Kann S, Zhang S, Manza P, Leung H-C, Li C-SR. Hemispheric Lateralization of Resting-State Functional Connectivity of the Anterior Insula: Association with Age, Gender, and a Novelty-Seeking Trait. Brain Connect. 2016;6: 724–734. doi:10.1089/brain.2016.0443
- 398. Oppenheimer SM, Gelb A, Girvin JP, Hachinski VC. Cardiovascular effects of human insular cortex stimulation. Neurology. AAN Enterprises; 1992;42: 1727.
- 399. Devoto F, Zapparoli L, Bonandrini R, Berlingeri M, Ferrulli A, Luzi L, et al. Hungry Brains: A Meta-Analytical Review of Brain Activation Imaging Studies On Food Perception and Appetite in Obese Individuals. Neurosci Biobehav Rev. Elsevier; 2018;
- 400. Penfield W, Faulk ME. The insula: Further observations on its function. Brain. 1955; doi:10.1093/brain/78.4.445
- Wang GJ, Tomasi D, Backus W, Wang R, Telang F, Geliebter A, et al. Gastric distention activates satiety circuitry in the human brain. Neuroimage. 2008; doi:10.1016/j.neuroimage.2007.11.008
- 402. Chang LJ, Yarkoni T, Khaw MW, Sanfey AG. Decoding the role of the insula in human cognition: Functional parcellation and large-scale reverse inference. Cereb Cortex. 2013;23: 739–749. doi:10.1093/cercor/bhs065
- 403. Schulz SM. Neural correlates of heart-focused interoception: A functional magnetic resonance imaging meta-

- analysis. Philosophical Transactions of the Royal Society B: Biological Sciences. 2016. doi:10.1098/rstb.2016.0018
- 404. Wager TD, Barrett LF. From affect to control: Functional specialization of the insula in motivation and regulation. Emotion. 2004; doi:http://dx.doi.org/10.1101/102368
- 405. Kurth F, Eickhoff SB, Schleicher A, Hoemke L, Zilles K, Amunts K. Cytoarchitecture and probabilistic maps of the human posterior insular cortex. Cereb Cortex. 2010; doi:10.1093/cercor/bhp208
- 406. Augustine JR. Circuitry and functional aspects of the insular lobe in primates including humans. Brain Research Reviews. 1996. doi:10.1016/S0165-0173(96)00011-2
- 407. Brooks JCW, Zambreanu L, Godinez A, Craig AD, Tracey I. Somatotopic organisation of the human insula to painful heat studied with high resolution functional imaging. Neuroimage. 2005; doi:10.1016/j.neuroimage.2005.03.041
- 408. Cole J, Bushnell MC, McGlone F, Elam M, Lamarre Y, Vallbo Å, et al. Unmyelinated tactile afferents underpin detection of low-force monofilaments. Muscle and Nerve. 2006; doi:10.1002/mus.20534
- 409. Craig A. Pain mechanisms: labeled lines vs. convergence in central processing. Annu Rev Neurosci. 2003; doi:10.1146/annurev.neuro.26.041002.131022
- 410. Ostrowsky K. Representation of Pain and Somatic Sensation in the Human Insula: a Study of Responses to Direct Electrical Cortical Stimulation. Cereb Cortex. 2002; doi:10.1093/cercor/12.4.376
- 411. Schweinhardt P, Glynn C, Brooks J, McQuay H, Jack T, Chessell I, et al. An fMRI study of cerebral processing of brush-evoked allodynia in neuropathic pain patients. Neuroimage. 2006; doi:10.1016/j.neuroimage.2006.03.024
- 412. Flynn FG, Benson DF, Ardila A. Anatomy of the insula Functional and clinical correlates. Aphasiology. 1999. doi:10.1080/026870399402325
- 413. Craig AD. Interoception and emotion: a neuroanatomical perspective. Handb Emot. Guilford Press New York; 2008;3: 272–288.
- 414. Taylor KS, Seminowicz DA, Davis KD. Two systems of resting state connectivity between the insula and cingulate cortex. Hum Brain Mapp. 2009; doi:10.1002/hbm.20705
- 415. Kuehn E, Mueller K, Lohmann G, Schuetz-Bosbach S. Interoceptive awareness changes the posterior insula functional connectivity profile. Brain Struct Funct. 2016; doi:10.1007/s00429-015-0989-8
- 416. Craig a D, Chen K, Bandy D, Reiman EM. Thermosensory activation of insular cortex. Nat Neurosci. 2000;3: 184–190. doi:10.1038/72131
- 417. Verhagen J V, Kadohisa M, Rolls ET. Primate insular/opercular taste cortex: neuronal representations of the viscosity, fat texture, grittiness, temperature, and taste of foods. J Neurophysiol. American Physiological Society; 2004;92: 1685–1699.
- 418. Lamm C, Decety J, Singer T. Meta-analytic evidence for common and distinct neural networks associated with directly experienced pain and empathy for pain. Neuroimage. 2011; doi:10.1016/j.neuroimage.2010.10.014
- 419. Harrison NA, Gray MA, Gianaros PJ, Critchley HD. The Embodiment of Emotional Feelings in the Brain. J Neurosci. 2010; doi:10.1523/JNEUROSCI.1725-10.2010
- 420. Pollatos O, Schandry R, Auer DP, Kaufmann C. Brain structures mediating cardiovascular arousal and interoceptive awareness. Brain Res. 2007; doi:10.1016/j.brainres.2007.01.026
- 421. Herbert BM, Pollatos O, Schandry R. Interoceptive sensitivity and emotion processing: An EEG study. Int J Psychophysiol. 2007; doi:10.1016/j.ijpsycho.2007.04.007
- 422. Critchley HD, Wiens S, Rotshtein P, Ohman A, Dolan RJ, Öhman A, et al. Neural systems supporting interoceptive awareness. Nat Neurosci. 2004; doi:10.1038/nn1176
- 423. Brooks JCW, Nurmikko TJ, Bimson WE, Singh KD, Roberts N. fMRI of thermal pain: Effects of stimulus laterality and attention. Neuroimage. 2002; doi:10.1006/nimg.2001.0974
- 424. Corbetta M, Shulman GL. Control of goal-directed and stimulus-driven attention in the brain. Nat Rev Neurosci. 2002; doi:10.1038/nrn755
- 425. Fox MD, Corbetta M, Snyder AZ, Vincent JL, Raichle ME. Spontaneous neuronal activity distinguishes human dorsal and ventral attention systems. Proc Natl Acad Sci. 2006; doi:10.1073/pnas.0604187103
- 426. Dosenbach NUF, Visscher KM, Palmer ED, Miezin FM, Wenger KK, Kang HC, et al. A Core System for the Implementation of Task Sets. Neuron. 2006; doi:10.1016/j.neuron.2006.04.031
- 427. Ploran EJ, Nelson SM, Velanova K, Donaldson DI, Petersen SE, Wheeler ME. Evidence Accumulation and the Moment of Recognition: Dissociating Perceptual Recognition Processes Using fMRI. J Neurosci. 2007; doi:10.1523/JNEUROSCI.3522-07.2007
- 428. Seeley WW, Menon V, Schatzberg AF, Keller J, Glover GH, Kenna H, et al. Dissociable Intrinsic

- Connectivity Networks for Salience Processing and Executive Control. J Neurosci. 2007; doi:10.1523/JNEUROSCI.5587-06.2007
- 429. Tops M, Boksem MAS. A Potential Role of the Inferior Frontal Gyrus and Anterior Insula in Cognitive Control, Brain Rhythms, and Event-Related Potentials. Front Psychol. 2011; doi:10.3389/fpsyg.2011.00330
- 430. Craig AD. How do you feel now? The anterior insula and human awareness. Nat Rev Neurosci. 2009;10: 59–70. doi:10.1038/nrn2555
- 431. Stephan KE, Manjaly ZM, Mathys CD, Weber LAE, Paliwal S, Gard T, et al. Allostatic Self-efficacy: A Metacognitive Theory of Dyshomeostasis-Induced Fatigue and Depression. Front Hum Neurosci. 2016; doi:10.3389/fnhum.2016.00550
- 432. Seth AK, Suzuki K, Critchley HD. An interoceptive predictive coding model of conscious presence. Front Psychol. 2012; doi:10.3389/fpsyg.2011.00395
- 433. Friston K. A theory of cortical responses. Philos Trans R Soc B Biol Sci. 2005; doi:10.1098/rstb.2005.1622
- 434. Rao RPN, Ballard DH. Predictive coding in the visual cortex: A functional interpretation of some extraclassical receptive-field effects. Nat Neurosci. 1999; doi:10.1038/4580
- 435. Pezzulo G, Rigoli F, Friston K. Active Inference, homeostatic regulation and adaptive behavioural control. Progress in Neurobiology. 2015. doi:10.1016/j.pneurobio.2015.09.001
- 436. Lundbaek K. Metabolic abnormalities in starvation diabetes. Yale J Biol Med. Yale Journal of Biology and Medicine; 1948;20: 533.
- Bergman BC, Cornier M-A, Horton TJ, Bessesen DH. Effects of fasting on insulin action and glucose kinetics in lean and obese men and women. Am J Physiol Metab. American Physiological Society; 2007;293: E1103– E1111.
- 438. Friston KJ, Holmes a. P, Worsley KJ, Poline J-P, Frith CD, Frackowiak RSJ. Statistical parametric maps in functional imaging: A general linear approach. Hum Brain Mapp. 1995;2: 189–210. doi:10.1002/hbm.460020402
- 439. Rencher AC. Methods of Multivariate Analysis. Second. Canada: John Wiley & Sons, Inc; 2002.
- 440. Tabachnik BG, Fidell LS. Using Multivariate Statistics: Pearson New International Edition. Using Multivariate Statistics. 2013. doi:10.1037/022267
- 441. Takerkart S, Auzias G, Thirion B, Ralaivola L. Graph-based inter-subject pattern analysis of fMRI data. PLoS One. 2014; doi:10.1371/journal.pone.0104586
- 442. Reno CM, Puente EC, Sheng Z, Daphna-Iken D, Bree AJ, Routh VH, et al. Brain GLUT4 Knockout Mice Have Impaired Glucose Tolerance, Decreased Insulin Sensitivity, and Impaired Hypoglycemic Counterregulation. Diabetes. Am Diabetes Assoc; 2016; db160917.
- 443. Rosario W, Singh I, Wautlet A, Patterson C, Flak J, Becker TC, et al. The Brain to Pancreatic Islet Neuronal Map Reveals Differential Glucose Regulation from Distinct Hypothalamic Regions. Diabetes. Am Diabetes Assoc; 2016; db150629.
- 444. Gamer M, Zurowski B, Buchel C. Different amygdala subregions mediate valence-related and attentional effects of oxytocin in humans. Proc Natl Acad Sci. 2010; doi:10.1073/pnas.1000985107
- 445. Mayer J, Thomas DW. Regulation of Food Intake and Obesity. Science (80-). 1967; doi:10.1126/science.156.3773.328
- 446. Suzuki K, Simpson KA, Minnion JS, Shillito JC, Bloom SR. The role of gut hormones and the hypothalamus in appetite regulation. 2010;57: 359–372.
- 447. Bragulat V, Dzemidzic M, Bruno C, Cox CA, Talavage T, Considine R V., et al. Food-related odor probes of brain reward circuits during hunger: a pilot FMRI study. Obesity (Silver Spring). 2010; doi:10.1038/oby.2010.57
- Haase L, Green E, Murphy C. Males and females show differential brain activation to taste when hungry and sated in gustatory and reward areas. Appetite. 2011;57: 421–434. doi:10.1016/j.appet.2011.06.009
- 449. Carnell S, Gibson C, Benson L, Ochner CN, Geliebter A. Neuroimaging and obesity: Current knowledge and future directions. Obes Rev. 2012;13: 43–56. doi:10.1111/j.1467-789X.2011.00927.x
- 450. Ghasemi R, Haeri A, Dargahi L, Mohamed Z, Ahmadiani A. Insulin in the brain: sources, localization and functions. Mol Neurobiol. Springer; 2013;47: 145–171.
- 451. Daunizeau J, David O, Stephan KE. Dynamic causal modelling: A critical review of the biophysical and statistical foundations. NeuroImage. 2011. doi:10.1016/j.neuroimage.2009.11.062
- 452. Liu J, Pearlson G, Windemuth A, Ruano G, Perrone-Bizzozero NI, Calhoun V. Combining fMRI and SNP data to investigate connections between brain function and genetics using parallel ICA. Hum Brain Mapp. 2009;30: 241–255.
- 453. Meier TB, Wildenberg JC, Liu J, Chen J, Calhoun VD, Biswal BB, et al. Parallel ICA identifies sub-

- components of resting state networks that covary with behavioral indices. Front Hum Neurosci. 2012;6: 1–14. doi:10.3389/fnhum.2012.00281
- 454. Pearlson GD, Liu J, Calhoun VD. An introductory review of parallel independent component analysis (p-ICA) and a guide to applying p-ICA to genetic data and imaging phenotypes to identify disease-associated biological pathways and systems in common complex disorders. Front Genet. 2015;6: 1–13. doi:10.3389/fgene.2015.00276
- 455. Kinzie JD. Post-Traumatic Stress Disorder. International Encyclopedia of the Social & Behavioral Sciences: Second Edition. 2015. doi:10.1016/B978-0-08-097086-8.27051-7
- 456. Zhou Y, Friston KJ, Zeidman P, Chen J, Li S, Razi A. The Hierarchical Organization of the Default, Dorsal Attention and Salience Networks in Adolescents and Young Adults. Cereb Cortex. 2018; doi:10.1093/cercor/bhx307

Curriculum Vitae

ARKAN AL-ZUBAIDI

T7.14*1	Δ	• 6• - 4 •
Educational	Onai	incation

08/2014 - 09/2019

Ph.D. candidate at Adipocyte-Brain Crosstalk program

University of Luebeck

Focus: Cognitive neuroscience, Analysing brain imaging data

• Ph.D. Thesis: "Modulatory impact of metabolic states on the connectivity of the resting human brain", supervisor: Prof. Dr. Thomas F. Münte

01/2017 - 04/2017

Internship at Translational Neuromodeling Unit / ETH Zurich

- Using different algorithms to extract brain networks
- Investigating effective brain connectivity from resting-state fMRI, supervisor: Prof. Dr. Klaas Enno Stephan

09/2010 - 03/2013

International Master Program Biomedical Engineering

University of Luebeck/ University of Applied Science Luebeck Focus: Medical electronic, Signal processing (Final Grade: 1.8)

 Master Thesis: "Rotation-invariant Gabor features for robust Transactional image classification", supervisor: Prof. Dr.-Ing. Alfred Mertins (Grade: 1.3)

10/2012 - 02/2012

Internship at Institute of Medical Robotics/ University of Luebeck

- Simulation of the aortic valve leaflets deformation by using the finite element method (FEM) with ANSYS program
- Evaluation of different strategies to model the contact between flexible bodies, supervisor: Prof. Dr.-Ing. Achim Schweikard

09/2002 - 07/2007

Bachelor of Biomedical Engineering

University of Baghdad /Iraq

Focus: Medical Instruments, Biomechanics (Final Grade: 1.3)

• Bachelor Thesis: "Design a medical device for ECG measurement", supervisor: Dr. Nebras Hussein (Grade:1.2)

Publications

Al-Zubaidi, A., Chen, L., Hagenah, J. and Mertins, A., (2013). *Robust feature for transcranial sonography image classification using rotation-invariant Gabor filter*. In Bildverarbeitung für die Medizin 2013 (pp. 271-276). Springer, Berlin, Heidelberg.

Al-Zubaidi, A., Heldmann, M., Mertins, A., Jauch-Chara, K., & Münte, T. F. (2018). *Influences of Hunger, Satiety and Oral Glucose on Functional Brain Connectivity: A Multimethod Resting-State fMRI Study.* Neuroscience, 382, 80-92.

Al-Zubaidi A., Mertins A., Heldmann M., Jauch-Chara K., Münte T.F. (2018). *Amplitude of brain signals classify hunger status based on machine learning in resting-state fMRI*. Bildverarbeitung für die Medizin 2018. Springer Vieweg, Berlin, Heidelberg.

Nolde, J., Laupenmühlen J., **Al-Zubaidi, A.,** Heldmann, M., Münte T. F., Kamila Jauch-Chara, K (2019). *Endocrine responses and food intake in fasted individuals under the influence of glucose ingestion*. PLOS ONE ;14(1):e0211514.

Al-Zubaidi, A., Heldmann, M., Mertins, A., Brabant, G., Nolde J., Jauch-Chara, K., & Münte, T. F. (2019) *Impact of hunger, satiety, and oral glucose on the association between insulin and resting-state human brain activity*. In revision. Frontiers in human neuroscience, 13, 162.

Al-Zubaidi, A., Mertins, A., Heldmann, M., Jauch-Chara, K., & Münte, T. F. (2019) *Machine learning based classification of resting-state fMRI features exemplified by metabolic state (hunger/satiety)*. Frontiers in human neuroscience, 13, 164

Hanßen, H., Steinhardt, J., Münchau, A., **Al-Zubaidi, A.,** et al (2019). *Cerebello-striatal interaction mediates clinical effects of deep brain stimulation in Parkinson's disease*. Parkinsonism & Related Disorders.

Al-Zubaidi, A., Iglesias, S., Stephan, K. E., et al. *Effects of hunger,* satiety and oral glucose on effective connectivity between hypothalamus and insular cortex. In revision.

Noldea, NM., Laupenmühlenb, J., **Al-Zubaidi, A**., Heldmanna, M., Jauch-Charac, K., Müntea, T.F. (2019) *Modulation of brain activity by hormonal factors in the context of ingestive behaviour*. Metabolism, 99, .11-18

Scholarship

German Academic Exchange Service (DAAD) (2010-2013)

Conferences

5th Biennial Conference on Resting State and Brain Connectivity, Vienna, Austria, September 2016. Abstract and Poster. *Influence of oral glucose tolerance test on multimethod brain functional connectivity for resting state fMRI data*.

1st Adipocyte-Brain Crosstalk Symposium, Luebeck, Germany, March 2017. Abstract and Talk. *Impact of hunger, satiety, and oral glucose on the association of insulin with human brain network.*

Bildverarbeitung für die Medizin, Clinical Track, Erlangen, Germany, March 2018. Abstract and Talk. *Amplitude of brain signals classify hunger status based on machine learning in resting-state fMRI*.

2nd Adipocyte-Brain Crosstalk Symposium, Luebeck, Germany, March 2019. Abstract and Poster. *Evaluation of resting-state fMRI features to classify hunger/satiety status based on machine learning.*

Organization for Human Brain Mapping (OHBM) Annual Meeting, Rome, Italy, June 2019. Abstract and Poster. *Hunger status, not oral glucose, affects posterior-anterior insula connectivity: A spectral DCM study.*

Workshops

Brain imaging analyzes using SPM toolbox, University of Edinburg, UK, March 2015.

Brain connectivity analyze, Vienna, Austria, September 2016.

• Summer School

Medical Image Computing, University College London, UK, July 2017.